THE ELECTROCHEMISTRY OF ZINC DEPOSITION

Thesis submitted to the University of Newcastle upon Tyne for the degree of Doctor of Philosophy

H.B. Sierra Alcazar M.Sc.

November 1977

Dedicated to

Sr. Agr. Manuel Alcazar

and

Sra. Aurora E. vda de Alcazar

for their vision of the future and

effective stimulus

Sr. Agr. Biviano H. Sierra

and

Sra. Ofelia A. de Sierra

for their generosity and encouragement

Sra. Margarita T. de Sierra

for her continued love and support

ABSTRACT

Two topics have been carried out in the thesis; a development of an on-line computing method for the investigation of electrode reactions and an investigation of the kinetics of zinc deposition from aqueous chloride solutions at pH 3. The first topic was to assess the possibility of analysing a current time response to a small amplitude potential using a Laplace transform and Fourier transform method. The development work was successful, and the system was experimentally tested on the lead ion reduction. This is a stringent test for the method as the reaction is fast compared to diffusion of lead ions in the solution. The method was then applied to the zinc ion reduction on mercury. Further measurements were carried out on the zinc ion reduction on Hg and zinc amalgams by impedance and other electrochemical methods. Finally the reduction of zinc ions on solid zinc was investigated. A mechanism for the zinc ion reduction is proposed.

CONTENTS

CHAPTER I

ELECTRODE KINETICS AND ELECTROCHEMICAL METHODS

I.1. i-E curves and the calculation of C_O^s, C_R^s

I.1.1. Rate Equation

The rate of an electrochemical reaction can be expressed, as in chemical kinetics by an expression of the form

$$\frac{i}{A} = nF(k_f C_o^s - k_b C_R^s) \tag{1.1}$$

where the rates k_f, k_b are potential dependent and can be defined by the relation

$$k_f = k_1 \exp \alpha_1 E \tag{1.2}$$

$$k_b = k_{-1} \exp -\beta_1 E \tag{1.3}$$

Cathodic current is a positive quantity. α_1, β_1 represent experimental quantities related to the cathodic, a, and anodic, b, Tafel slopes by

$$\frac{1}{a} = \frac{\alpha_1}{2.303} \tag{1.4}$$

$$\frac{1}{b} = \frac{-\beta_1}{2.303} \tag{1.5}$$

Potential, E, is considered to be positive going for k_f increasing. It is very convenient to use this nomenclature which can also be used for anodic reactions (i positive, E positive going).

At equilibrium

$$C_o^* k_1 \exp \alpha_1 E_e = C_R^* k_{-1} \exp -\beta_1 E_e \tag{1.6}$$

$$\frac{C_o^*}{C_R^*} = \frac{k_{-1}}{k_1} \exp\left[-(\alpha_1 + \beta_1) E_e\right] \tag{1.7}$$

which can be compared with the Nernst equation

$$\frac{C_o^*}{C_R^*} = \exp -\left(\frac{E_e n F}{RT}\right) \exp\left(-\frac{E_o n F}{RT}\right) \tag{1.8}$$

therefore

$$\alpha_1 + \beta_1 = \frac{nF}{RT} \tag{1.9}$$

gives the equilibrium condition for any reaction, no matter how many electrons, n, are involved in the overall reaction.

$$\frac{1}{a} + \frac{1}{b} = \frac{nF}{2.303RT} \tag{1.10}$$

As $k_1/k\text{-}1$ can be identified with

$$\frac{k_{-1}}{k_1} = \exp\left(\frac{-E_o n F}{RT}\right) \tag{1.11}$$

then an alternative to the definitions (1.2) and (1.3) is

$$k_f = k_{SH} \exp\left[\alpha_1 (E - E_o)\right] = k_{SH} \exp \alpha_1 \phi \tag{1.12}$$

$$k_b = k_{SH} \exp\left[-\beta_1 (E - E_o)\right] = k_{SH} \exp -\beta_1 \phi \tag{1.13}$$

with k_{SH} a standard rate given by

$$k_{SH} = k_1\left(\frac{k_1}{k_{-1}}\right)^{\frac{-\alpha_1 RT}{nF}} = k_{-1}\left(\frac{k_1}{k_{-1}}\right)^{\frac{\beta_1 RT}{nF}} \qquad (1.14)$$

It is convenient in many experimental situations to use E_e as a reference point then if a new rate i_o is defined, at equilibrium

$$nF C_o^* k_1 \exp \alpha_1 E_e = nF C_R^* k_{-1} \exp -\beta_1 E_e = i_o \qquad (1.15)$$

then

$$k_f = \frac{i_o}{nF C_o^*} \exp\left[\alpha_1 (E - E_e)\right] = \frac{i_o}{nF C_o^*} \exp \alpha_1 \eta \qquad (1.16)$$

$$k_b = \frac{i_o}{nF C_R^*} \exp\left[-\beta_1 (E - E_e)\right] = \frac{i_o}{nF C_R^*} \exp -\beta_1 \eta \qquad (1.17)$$

It now follows that as

$$i_o = nF C_R^* k_{-1} \exp -\beta_1 E_e \qquad (1.18)$$

and

$$\frac{k_1}{k_{-1}} = \frac{C_R^*}{C_o^*} \exp\left[-(\alpha_1 + \beta_1) E_e\right] \qquad (1.19)$$

$$k_{SH} = k_1\left(\frac{k_1}{k_{-1}}\right)^{-\alpha_1 RT/nF} = k_{-1}\left(\frac{k_1}{k_{-1}}\right)^{\beta_1 RT/nF} \qquad (1.20)$$

then the relation between k_{SH} and i_o is

$$i_o = nF k_{SH}\left(C_R^*\right)^{\alpha_1 RT/nF}\left(C_o^*\right)^{\beta_1 RT/nF} \qquad (1.21)$$

or alternatives derived by writing

$$\alpha_1 + \beta_1 = \frac{nF}{RT} \qquad (1.22)$$

Also used in the literature is the form

$$\frac{C_o^*}{C_R^*} = \frac{k_{-1}}{k_1}\left(\frac{l_o}{nFC_o^* k_1}\right)^{\frac{-\alpha_1+\beta_1}{\alpha_1}} \tag{1.23}$$

$$\log\frac{C_o^*}{C_R^*} = \log\frac{k_{-1}}{k_1} - \frac{\alpha_1+\beta_1}{\alpha_1}\log\frac{i_o}{nFC_o^* k_1} \tag{1.24}$$

I.1.2. Interpretation of a and b

It is usual to interpret the measured α_1, β_1 or a and b in terms of combination of 1 electron reactions. For example if the overall reaction is

$$O + 2e \rightleftharpoons R \tag{1.25}$$

then for

$$O + e \rightleftharpoons O_1 \tag{1.26}$$

$$O_1 + e \xrightarrow{(k_1)_2} R \tag{1.27}$$

$$\frac{i}{A} = nF\,(C_o^s)_1\,(k_1)_2\,exp(\alpha FE/RT) \tag{1.28}$$

where α (= ½) is a one electron transfer coefficient.

Also

$$\frac{(C_o^s)_1}{C_o^s} = exp\left(\frac{EF}{RT}\right)exp\left(\frac{(E_o)F}{RT}\right) = K \tag{1.29}$$

and by equating the fluxes in equation (1.26)

$$\frac{D_o(C_o^* - C_o^s)}{\delta} = - D_R (C_o^s)_1 \qquad (1.30)$$

It is assumed for simplicity that $(C_o^*)_1 = 0$

From (1.29) and (1.30)

$$(C_o^s)_1 = \frac{C_o^*}{\left(1/K - D_R/D_o \right)} \qquad (1.31)$$

at low overpotentials η

$$(C_o^s)_1 = K C_o^* \qquad (1.32)$$

therefore

$$\frac{i}{A} = nF (k_1)_2 C_o^* \exp\left(\frac{EF}{RT}\right) \exp\left[\frac{(E_o)_1 F}{RT}\right] \exp(\alpha F E/RT) \qquad (1.33)$$

and

$$\frac{i}{A} = (\text{constant}) \exp \frac{(1+\alpha) FE}{RT} \qquad (1.34)$$

The Tafel slope, a, is hence 40 mV according to the thermodynamic equation (1.10) this must be coupled with a 120 mV anodic Tafel slope, b. The complete i-E relation for the model of equations (1.26), (1.27) could of course be written down to predict the complete i-E curve for this reaction scheme.

I.1.3. Correction of the i-E curve for diffusion

A useful procedure is to predict part of the wave shape, so that diffusion can be eliminated. The procedure is based on

$$i = nFA C_o^s \exp \alpha_1 E \qquad (1.35)$$

$$i = \frac{n F A D_o (C_o^* - C_o^s)}{\delta} \tag{1.36}$$

$$i - i_L = \frac{-n F A D_o C_o^s}{\delta} \tag{1.37}$$

$$\frac{i_L - i}{i} = \frac{D_o \exp - \alpha_1 E}{\delta} \tag{1.38}$$

and for a metal deposition reaction for a reversible reaction

$$i = \frac{n F A D_o C_o^*}{\delta} \left(1 - \exp \frac{-nF}{RT} \eta\right) \tag{1.39}$$

$$\frac{i_L - i}{i_L} = \exp - \frac{nF}{RT} \eta \tag{1.40}$$

These equations allow the two important cases to be distinguished from i-E curves and allow correction of the i-E curve for diffusion so that α_1 or η can be obtained.

I.1.4. Calculation of C_o^s, C_R^s

It is convenient to express the surface concentrations C_o^s, C_R^s specifically for use in the a.c. theory presented later. This procedure follows the Sluyters method.

For the reaction

$$O + ne \rightleftharpoons R \tag{1.41}$$

the faradaic current i, positive for a cathodic process, is given by

$$i = nF k_{SH} \left\{C_o \exp(\alpha_1 \phi) - C_R \exp(-\beta_1 \phi)\right\} \tag{1.42}$$

where $\phi = (E - E_o)$ and goes positive for increasing positive cathodic

current.

According to the "diffusion layer theory"

$$\frac{i}{A} = \frac{n F D_o \left(C_o^* - C_o^s \right)}{\delta_o} = \frac{- n F D_R \left(C_R^* - C_R^s \right)}{\delta_R} \qquad (1.43)$$

According to (1.43) the cathodic limiting current $(i_L)_o$ is positive and the anodic limiting current $(i_L)_R$ is negative. From (1.43)

$$C_o^s = C_o^* - \frac{i \delta_o}{n F A D_o} \qquad (1.44a)$$

$$C_R^s = C_R^* + \frac{i \delta_R}{n F A D_R} \qquad (1.44b)$$

Substitution of i from equation (1.42) into (1.44a) and equation (1.44b) gives

$$C_o^s = C_o^* - \frac{\delta_o}{D_o} k_{SH} \left\{ C_o^s \exp \alpha_1 \phi - C_R^s \exp -\beta_1 \phi \right\} \qquad (1.45a)$$

$$C_R^s = C_R^* + \frac{\delta_R}{D_R} k_{SH} \left\{ C_o^s \exp \alpha_1 \phi - C_R^s \exp -\beta_1 \phi \right\} \qquad (1.45b)$$

which can be expressed in the equivalent form

$$a_o C_o^s = C_o^* a_o - \left(C_o^s \exp \alpha_1 \phi - C_R^s \exp -\beta_1 \phi \right) \qquad (1.46a)$$

$$a_R C_R^s = C_R^* a_R + \left(C_o^s \exp \alpha_1 \phi - C_R^s \exp -\beta_1 \phi \right) \qquad (1.46b)$$

where by definition

$$a_o = \frac{D_o}{k_{SH} \delta_o} \qquad (1.47a)$$

$$a_R = \frac{D_R}{k_{SH} \delta_R} \qquad (1.47b)$$

Rearranging equation (1.46a) gives

$$C_o^s = \frac{C_o^* a_o + C_R^s \exp(-\beta_1 \phi)}{a_o + \exp \alpha_1 \phi} \qquad (1.48)$$

Substituting equation (1.48) into (1.46b) gives

$$C_R^s \left(a_R + \exp(-\beta_1 \phi) - \frac{\exp\left[\frac{(\alpha_1 - \beta_1)\phi}{}\right]}{a_o + \exp \alpha_1 \phi} \right)$$

$$= C_R^* a_R + \frac{\left(\exp(\alpha_1 \phi)\right) C_o^* a_o}{a_o + \exp \alpha_1 \phi} \qquad (1.49)$$

which on rearranging yields

$$C_R^s = \frac{\left[a_o + (\exp \alpha_1 \phi)\left(1 + \frac{C_o^*}{C_R^*} \frac{a_o}{a_R}\right)\right] C_R^*}{a_o + \frac{a_o}{a_R} \exp(-\beta_1 \phi) + \exp \alpha_1 \phi} \qquad (1.50)$$

This equation gives the surface concentration C_R^s in terms of accessible parameters. To obtain C_o^s a similar procedure is followed. Rearranging equation (1.45b) gives

$$C_R^s = \frac{C_R^* a_R + C_o^s \exp \alpha_1 \phi}{a_R + \exp -\beta_1 \phi} \qquad (1.51)$$

Substituting equation (1.51) into (1.46a) and rearranging yields

$$C_o^s = C_o^* \left\{ \frac{a_o + \left(\frac{a_o}{a_R} + \frac{C_R^*}{C_o^*}\right) \exp -\beta_1 \phi}{a_o + \frac{a_o}{a_R} \exp -\beta_1 \phi + \exp \alpha_1 \phi} \right\} \qquad (1.52)$$

Equations (1.50) and (1.52) are equivalent to equations 37a and 37b in Sluyters et al[1], where $\alpha_1 \phi$ and $-\beta_1 \phi$ are equivalent to $-\beta\varphi$ and $\alpha\varphi$ respectively. The only remaining difference of nomenclature, of any significance, is the reversal of the sign of the current (Sluyters et al[1] define the cathodic current as negative). Other differences of

nomenclature are trivial.

I.2. Impedance at various potentials on an i-E curve

I.2.1. The general Faradaic response for a small amplitude a.c. potential signal superimposed on d.c. can be derived as follows. Given a redox reaction where 1 and 2 are electrochemically active species, i.e.

$$1 \underset{\longleftarrow}{\overset{e}{\longrightarrow}} 2 \tag{1.53}$$

then in general

$$\overline{di} = \overline{dE}\left(\frac{\partial i}{\partial E}\right)_{C_1^s, C_2^s} + \overline{dC_1^s}\left(\frac{\partial i}{\partial C_1^s}\right)_{E, C_2^s} - \overline{dC_2^s}\left(\frac{\partial i}{\partial C_2^s}\right)_{E, C_1^s} \tag{1.54}$$

for a perturbation $\overline{dE}$ and its response $\overline{di}$. The quantities $\overline{di}$, $\overline{dE}$, $\overline{dC_1}^s$ and $\overline{dC_2}^s$ are Laplace transforms.

Solution of the Laplace transforms of Ficks second law

$$\frac{\partial C}{\partial t} = D\left(\frac{\partial^2 C}{\partial x}\right) \tag{1.55}$$

gives

$$\overline{dC_2^s} = \frac{\overline{di}}{nF\sqrt{s\,D_2}} \quad \text{and} \quad \overline{dC_1^s} = \frac{-\overline{di}}{nF\sqrt{s\,D_1}} \tag{1.56}$$

Hence

$$\frac{di}{dE} = \frac{1}{Z(s)} = \frac{\left(\frac{\partial i}{\partial E}\right)_{C_1^s, C_2^s}}{1 + \frac{1}{nF\sqrt{s\,D_2}}\left(\frac{di}{\partial C_2^s}\right)_{E, C_1^s} + \frac{1}{nF\sqrt{s\,D_1}}\left(\frac{\partial i}{\partial C_1^s}\right)_{E, C_2^s}} \tag{1.57}$$

which on substituting $s = jw$ gives the familiar Faradaic a.c. impedance

$$Z(jw) = \frac{1}{\left(\frac{\partial i}{\partial E}\right)_{C_1^s, C_2^s}} + \frac{1}{nF\sqrt{jw\,D_2}} \frac{\left(\frac{\partial i}{\partial C_2^s}\right)_{C_1^s, E}}{\left(\frac{\partial i}{\partial E}\right)_{C_1^s, C_2^s}} + \frac{1}{nF\sqrt{jw\,D_1}} \frac{\left(\frac{\partial i}{\partial C_1^s}\right)_{E, C_2^s}}{\left(\frac{\partial i}{\partial E}\right)_{C_1^s, C_2^s}} \tag{1.58}$$

TABLE 2.1. Fourier coefficients of the exponential transient described by equation C.2, with R = 0.01, N = 1024, k_1 = k2 = 1

r	OBTAINED WITH THE FFT SOFTWARE Ar	OBTAINED FROM EQ. 6.2 Ar	% ERROR
1	0.0871	0.0890	2.6
2	-0.0956	-0.0965	0.9
3	0.0819	0.0836	2.0
5	0.0575	0.0586	1.9
9	0.0342	0.0348	1.8
17	0.0186	0.0186	0
29	0.0109	0.0106	2.9
35	0.00908	0.00883	2.8
51	0.00623	0.00563	9.6
55	0.00578	0.00512	11
71	0.00448	0.00358	20
161	0.000128	0.00198	93.5
301	-0.00128	0.00106	220

r	OBTAINED WITH THE FFT SOFTWARE Br	OBTAINED FROM EQ. 6.3 Br	% ERROR
1	-0.1477	-0.1419	3.9
2	+0.0814	+0.0779	4.3
3	-0.0485	-0.0445	8.2
5	-0.0223	-0.0187	16.1
7	-0.0133	-0.0100	24.9
9	-0.0095	-0.0062	34.5
19	-0.00473	-0.00143	69.8
41	-0.00346	-0.000308	91
301	-0.00051	-0.0000057	98.9

and for the diffusion of a single species

$$Z(jw) = \frac{1}{\left(\partial i/\partial E\right)_{C_1^s, C_2^s}} + \frac{1}{nF\sqrt{j w D_2}} \frac{\left(\partial i/\partial C_2^s\right)_{E, C_1^s}}{\left(\partial i/\partial E\right)_{C_1^s, C_2^s}} \tag{1.59}$$

$$= \theta + \left(\sigma_2 \omega^{-1/2} - j\sigma_2 \omega^{-1/2}\right) \tag{1.60}$$

This equation defines the Warburg coefficient σ and charge transfer resistance θ.

Specific expressions $\left(\frac{\partial i}{\partial C_2^s}\right)_{E, C_1^s}$, $\left(\frac{\partial i}{\partial E}\right)_{C_1^s, C_2^s}$ must now be given, these are, if

$$i = nF k_{SH} \left(C_o^s \exp \alpha_1 \phi - C_R^s \exp -\beta_1 \phi\right) \tag{1.61}$$

$$\left(\partial i/\partial C_2^s\right)_{E, C_1^s} = nF\ k_{SH}\ \beta_1 \exp -\beta_1 \phi \tag{1.62}$$

$$\left(\partial i/\partial E\right)_{C_1^s, C_2^s} = nF\ k_{SH} \left(\alpha_1 C_o^s \exp \alpha_1 \phi + C_R^s \beta_1 \exp -\beta_1 \phi\right) \tag{1.63}$$

The insertion of the equation (1.51), (1.52), (1.62), (1.63) into (1.59) then gives the final result. The actual equations are compared with the experimental results in Chapter V, see for example equation (5.3).

I.3. a.c. Impedance for two consecutive le transfers

Similar considerations can be applied to a 2e reaction, which is more appropriate for the case of Zn^{2+} reduction. If

$$1 \underset{i_1}{\overset{n_1 e}{\rightleftharpoons}} 2 \underset{i_2}{\overset{n_2 e}{\rightleftharpoons}} 3 \tag{1.64}$$

then

$$\overline{di_1} = \overline{dE}\left(\partial i_1/\partial E\right)_{C_1^s, C_2^s} + \overline{dC_1^s}\left(\partial i_1/\partial C_1^s\right)_{E, C_2^s} - \overline{dC_2^s}\left(\frac{\partial i_1}{\partial C_2^s}\right)_{E, C_1^s} \tag{1.65}$$

$$\overline{di_2} = \overline{dE}\left(\partial i_2/\partial E\right)_{C_2^s, C_3^s} + \overline{dC_2^s}\left(\partial i_2/\partial C_2^s\right)_{E, C_3^s} - \overline{dC_3^s}\left(\partial i_2/\partial C_3^s\right)_{E, C_2^s} \quad (1.66)$$

and the solution of Fick's second law gives

$$\overline{dC_1^s} = -\frac{\overline{di_1}}{nF\sqrt{s\,D_1}} \quad (1.67)$$

$$\overline{dC_2^s} = \overline{d\left(i/n_1 - i/n_2\right)} \Big/ F\sqrt{s\,D_2} \quad (1.68)$$

$$\overline{dC_3^s} = \frac{\overline{di_2}}{n_2 F\sqrt{s\,D_3}} \quad (1.69)$$

Hence

$$Y_1 = \frac{\overline{di_1}}{\overline{dE}} = \frac{1}{\alpha_1}\left(\frac{\partial i_1}{\partial E}\right)_{C_1^s, C_2^s} - \frac{1}{\alpha_1}\left(\frac{\partial i_1}{\partial C_2^s}\right)_{E, C_1^s} V \quad (1.70)$$

$$Y_2 = \frac{\overline{di_2}}{\overline{dE}} \quad \frac{1}{\alpha_2}\left(\frac{\partial i_2}{\partial E}\right)_{C_2^s, C_3^s} + \frac{1}{\alpha_2}\left(\frac{\partial i_2}{\partial C_2^s}\right)_{E, C_3^s} \quad (1.71)$$

where

$$\alpha_1 = \left[1 + \frac{1}{n_1 F\sqrt{D_1 s}}\left(\frac{\partial i_1}{\partial C_1^s}\right)_{E, C_2^s}\right] \quad (1.72)$$

$$\alpha_2 = \left[1 + \frac{1}{n_2 F\sqrt{D_3 s}}\left(\frac{\partial i_2}{\partial C_3^s}\right)_{E, C_2^s}\right] \quad (1.73)$$

$$V = \frac{\frac{1}{n_1 F \alpha_1}\left(\frac{\partial i_1}{\partial E}\right)_{C_1^s, C_2^s} - \frac{1}{n_2 F \alpha_2}\left(\frac{\partial i_2}{\partial E}\right)_{C_2^s, C_3^s}}{\sqrt{s\,D_2} + \frac{1}{n_1 F \alpha_1}\left(\frac{\partial i_1}{\partial C_2^s}\right)_{E, C_1^s} + \frac{1}{n_2 F \alpha_2}\left(\frac{\partial i_2}{\partial C_2^s}\right)_{E, C_3^s}} \quad (1.74)$$

The impedance is then given by

$$Z(s) = \frac{1}{Y_{(s)}} = \frac{1}{Y_2} + \frac{1}{Y_1} \qquad (1.75)$$

Some authors have followed Smith[3] and earlier workers in incorrectly adding the individual admittances for the case where species 2 is an intermediate.

I.4. Electrochemical Methods

I.4.1. Stationary methods

The theory behind the stationary i-E curve and the impedance $Z_{(jw)}$ at E has been given in the last section. In order to put these into effect it is necessary to have at the electrode a fixed diffusion distance δ. In general this can be accomplished at Hg by natural convection or stirring of the solution, by polarography or by the use of a streaming electrode. For solids this is most satisfactorily accomplished by means of the rotating disc. It can be shown from a consideration of the hydrodynamics[4,5]

$$\delta = 1.61\, D^{1/3}\, \nu^{1/6}\, \omega_R^{-1/2} \qquad (1.76)$$

where W_R is the rotation speed in radians per sec. If this value is inserted in the equations of the last section then the behaviour of the rotating disc system is described.

I.4.2. Non-stationary methods

In order to convert the a.c. theory of the last section into the basis for an electrochemical method it is necessary to take account of the fact that a double layer capacity is always present at an interface.

The equivalent electrochemical circuit of an interface is then

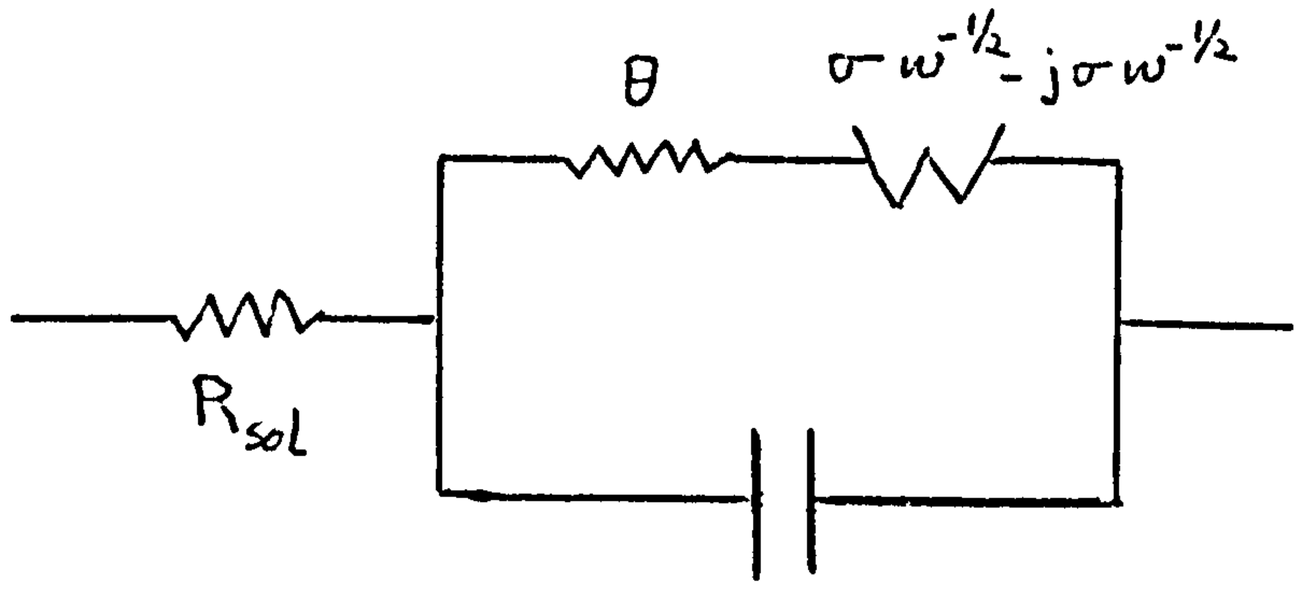

where θ and σ are given by the equations of the last section. At high frequencies the Warburg impedance, W, is negligible.

The linear potential sweep measurement[6] generates an i-E curve which first of all rises exponentially with E and then falls due to the onset of diffusion. The peak current i_p depends on $V^{\frac{1}{2}}$ as the characteristic diffusion parameter. The equations which determine the behaviour of i_p and E_p for irreversible and reversible electrode reactions coupled to diffusion are equations (5.28, (5.29), (5.30), (5.31). There are disadvantages in this method for quantitative analysis as is apparent in the experimental Chapter V. These are that the ohmic resistance R_{sol} must (experimental) be small and also the C_{dl} charging current. This can be checked by carrying out sweeps in the base electrolyte alone. The advantage of this method is that reactions of different rates which occur simultaneously can be detected by variation of the sweep rate.

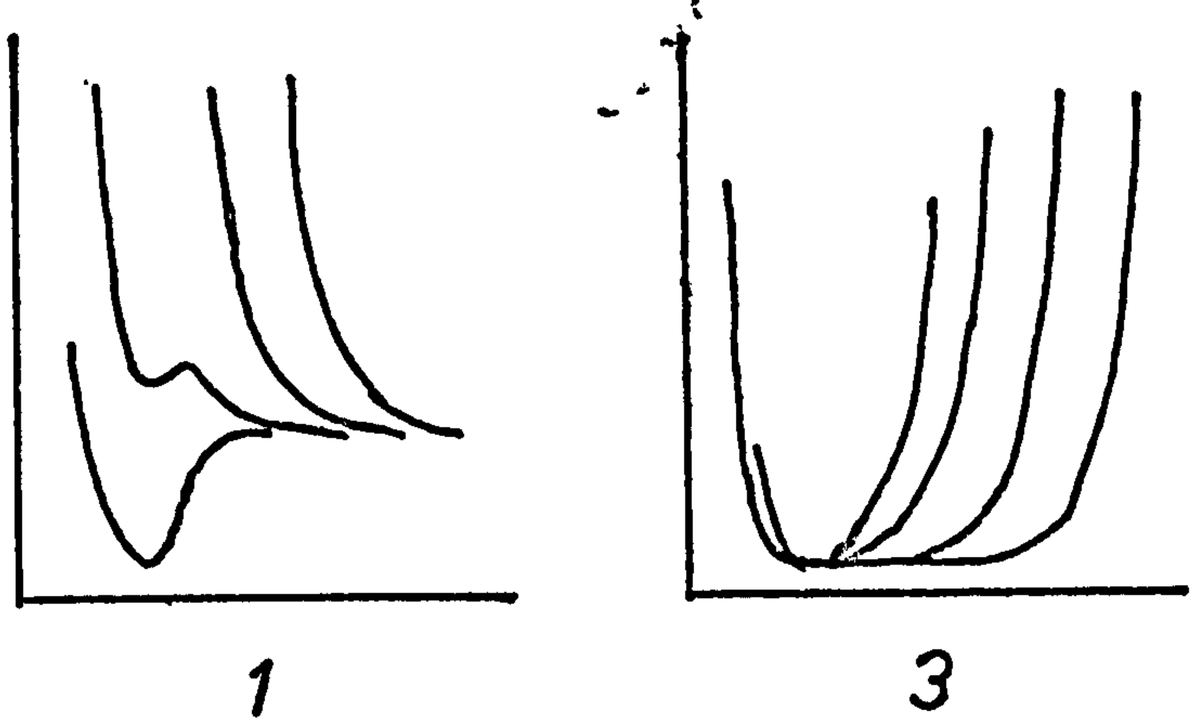

Diagrammatic representation of (1), (2) θ VS $(E-E_o)$ and (3), (4) $6w_*^{-\frac{1}{2}}$ VS $(E-E_o)$ as a function of K_{SH}. (1), (3) $C_R^{o*} = 0$ (2), (4) $Co = C_R^*$. K_{SH} increases from R to L. For details see ref.1.

REFERENCES

1. M. Sluyters-Rehbach, J.H. Sluyters in Electroanal. Chem. (ed. A.J. Bard) Vol. V, p.1.

2. J.A. Harrison, P.J. Stronach Surf. Techn. (in press).

3. D.E. Smith in Electroanal. Chem. (ed. A.J. Bard) Vol. 1, p.1. Dekker 1966.

4. V.G. Levich, Physicochemical Hydrodynamics, Prentice Hall, 1962.

5. W.J..Albery, M.L. Hitchman, Claredon Press, 1971.

6. R.S. Nicholson, I. Shain, Anal. Chem. 36 (1964) 706.

CHAPTER II

METHOD OF IMPEDANCE DETERMINATION FROM PULSE ANALYSIS BY ON-LINE COMPUTER

II.1. Introduction

The availability of mini-computers has introduced a new and powerful element into the measurement of electrode kinetics. A comprehensive review of the present situation has been given by Smith[1]. The computer can be used to evaluate data from analogue or digital devices or to process i(t) and E(t) data directly by means of analogue to digital conversion. In this respect the computer can be compared with other experimental dedicated methods for example the automatic pulse polarograph (e.g. the Tacussel and Princeton Applied Research models) and the automatic frequency bridge (e.g. the Solartron transfer function analysers). Another alternative is the a.c. polarograph controlled by on-line computer. However these systems have significant limitations for the investigation of electrode kinetics. The pulse polarograph applies a single or double pulse and produces, from successive pulses i - E or $\frac{i}{E}$ - E curves as a function of time from the start of the pulse. Analysis of the family of i - E curves and their display is cumbersome. The ohmic drop must be compensated or the current limited to low values. However the method has the advantage of pulsing from a fixed potential, which can eliminate d.c. time effects. The automatic bridge, developed by Epelboin and co-workers[2] for use in electrochemistry, produces $Z(\omega)$ - ω curves as a function of E. Analysis of the data in terms of electrode kinetics is easier than in the case of the pulse polarograph but the time to take a $Z(\omega)$ - ω set at a fixed potential is long. The ohmic drop is a lesser problem in this method. Measurements of this type can easily be falsified, especially in solid metal electrode systems, by slow changes in the d.c. state. The

computer controlled a.c. polarograph[3] is probably better than the automatic bridge, but scans the potentials one frequency at a time, so is rather slow.

An ideal electrode kinetic investigation system would be a combination of these methods taking only the advantages. Fortunately such a method is possible, that is to calculate the Z(w) - w response of the system from a pulse measurement.

II.2. Principle of the Method

The purpose of this method[11,16] is to use a very small amplitude potential step or sweep (second pulse), superimposed on a first potential step, from equilibrium to a particular level, to determine the impedance spectrum Z(w), pertaining to the potential of that level. By varying the level of the first pulse, a set of impedance spectra at various potentials (including the equilibrium potential) can be obtained. With the use of an on-line minicomputer, the time domain measurements are recorded in a very short time, reducing time effects inherent in the system. The time domain data is subsequently transformed into the frequency domain and reduced to an impedance spectrum Z(w) for each potential, as it is well known, the kinetic parameters characterising an electrochemical reaction are more easily determined in the frequency domain.

The theory on which the small amplitude potential pulse method is based is as follows[17]

For the redox reaction

$$O + ne \rightleftharpoons R \tag{2.1}$$

where

$$i = nF(k_f C_o^s - k_b C_R^s) \tag{2.2}$$

then after a pulse from a particular potential and expanding the exponentials

$$i = nFk_{SH}\left\{(1+\alpha_1\Delta E)C_o^s \exp[\alpha_1(E-E_o)] - (1-\beta_1\Delta E)C_R^s \exp[-\beta_1(E-E_o)]\right\} \tag{2.3}$$

Assuming that at $E-E_o$ the surface concentrations in the steady state are $(C_O^S)_{E-E_o}$ and $(C_R^S)_{E-E_o}$, then approximately for small t

$$\overline{(C_O^S)}_{E-E_o+\Delta E} = \frac{\overline{(C_O^S)}_{E-E_o}}{S} - \frac{\overline{i(s)}}{nF\sqrt{s\,D_o}} \tag{2.4}$$

$$\overline{(C_R^O)}_{E-E_o+\Delta E} = \frac{(C_R^S)_{t-E_o}}{S} - \frac{\overline{i(s)}}{nF\sqrt{s\,D_R}} \tag{2.5}$$

where the quantities $\overline{C_O^S}$ and $\overline{i(s)}$ are Laplace Transforms (LT).

If the complete differential of the LT of the current i(s) is written as

$$d\overline{i(s)} = \left(\frac{\partial i}{\partial E}\right)_{C_o^s, C_R^s} \overline{dE(s)} + \left(\frac{\partial i}{\partial C_o^s}\right)_{E, C_R^s} \overline{dC_o^s} - \left(\frac{\partial i}{\partial C_R^s}\right)_{E, C_o^s} \overline{dC_R^s} \tag{2.6}$$

then

$$\frac{d\overline{i(s)}}{dE} = \frac{1}{Z(s)} \frac{\left(\frac{\partial i}{\partial E}\right)_{C_o^s, C_R^s}}{1 + \frac{1}{nF\sqrt{s\,D_o}}\left(\frac{\partial i}{\partial C_o^s}\right)_{E,C_R^s} + \frac{1}{nF\sqrt{s\,D_R}}\left(\frac{\partial i}{\partial C_R^s}\right)_{E, C_o^s}} \tag{2.7}$$

which on substituting s = jw gives the familiar a.c. impedance

$$Z(jw) = \frac{1}{\left(\frac{\partial i}{\partial E}\right)_{C_o^s}} + \frac{1}{nF\sqrt{jw\,D_R}} \frac{\left(\frac{\partial i}{\partial C_R^s}\right)_{E, C_o^s}}{\left(\frac{\partial i}{\partial E}\right)_{C_o^s, C_R^s}} + \frac{1}{nF\sqrt{jw\,D_o}} \frac{\left(\frac{\partial i}{\partial C_R}\right)_{E, C_o^s}}{\left(\frac{\partial i}{\partial E}\right)_{C_o^s, C_R^s}} \tag{2.8}$$

and for the diffusion of a single species

$$Z(j\omega) = \frac{1}{\left(\frac{\partial i}{\partial E}\right)_{C_O^S, C_R^S}} + \frac{1}{nF\sqrt{j\omega D_R}} \cdot \frac{\left(\frac{\partial i}{\partial C_R}\right)_{E, C_O^S}}{\left(\frac{\partial i}{\partial E}\right)_{C_O^S, C_R^S}} \tag{2.9}$$

$$= \theta + \sigma_R \omega^{-1/2} - j\sigma_R \omega^{-1/2} \tag{2.10}$$

The analysis of Z(jw) is simpler than a direct analysis of the i-t transient and has the advantage that it is not limited to a square wave exciting function.

The principle of the method as used in electrochemistry[1,4,5,13,14,15,16,18] is well known and only a sketch will be given here. For a linear system the frequency spectrum of the impedance is given by

$$Z(\omega_j) = \frac{\overline{E(\omega)}\ \overline{E^*(\omega)}}{\overline{i(\omega)}\ \overline{E^*(\omega)}} = Z(Re) + j\,Z(Im) \tag{2.11}$$

where $\overline{E^*(w)}$ is the complex conjugate of $\overline{E(w)}$ and Z(Re) and Z(Im) are defined as the real and imaginary parts of Z(w). The functions $\overline{i(w)}$ and $\overline{E(w)}$ can be derived from i(t) and E(t) for example, by the imaginary axis LT of the current transient

$$\overline{i(jw)} = \int_0^\infty e^{-j\omega t}\, i(t)\, dt \tag{2.12}$$

In practice this integral must be numerically evaluated in the finite interval (O,T). An alternative is to use the Fourier transform,

$$\overline{i(\omega)} = \frac{2}{T} \int_0^T e^{-j\omega t}\, i(t)\, dt \tag{2.13}$$

in the interval (O,T). This definition allows the integral to be replaced by a series identity and allows access to the fast Fourier transform (FFT)

method[20]. Another alternative which will not be considered here is the so-called Z transform.

In principle the applied potential profile E(t) and its transform $\overline{E(w)}$, can have any form. However it has been found necessary to select only suitable functions. These include various kinds of noise[7], a rectangular pulse[7] and a collection of sine waves[8]. Creason et al[7] and Smith report that the Fourier transform will not work satisfactorily for a potentiostatic pulse. Pilla[4], using a Laplace transform approach reports a successful trial using test data and Doblhofer and Pilla[18] experimental data. However on this evidence it is not obvious that these methods can be successfully and simply automated. In addition a cumbersome method of experimental investigation has been used in which the responses from two cells are compared in order to eliminate double layer and ohmic contributions. The method used here is simpler. Only the current transient needed sampling, since the potential signal generated and input was close enough to the ideal, as shown in fig. 2.1, and therefore the height of the potential step was considered a constant in the impedance spectra determinations.

II.2.1. Laplace and Fourier transform theory

Linear integral transformations are particularly useful to perform the transformation from the time domain to the frequency domain, of a function F(t) defined on a finite interval $a < t < b$.

Let K(t,s) denote some prescribed function of the variable t and parameter s. A general linear integral transformation of functions F(t) with respect to the kernel K (t,s) is represented by the equation[21]

$$\overline{f(s)} = \int_a^b K(t,s)\, F(t)\, dt \qquad (2.14)$$

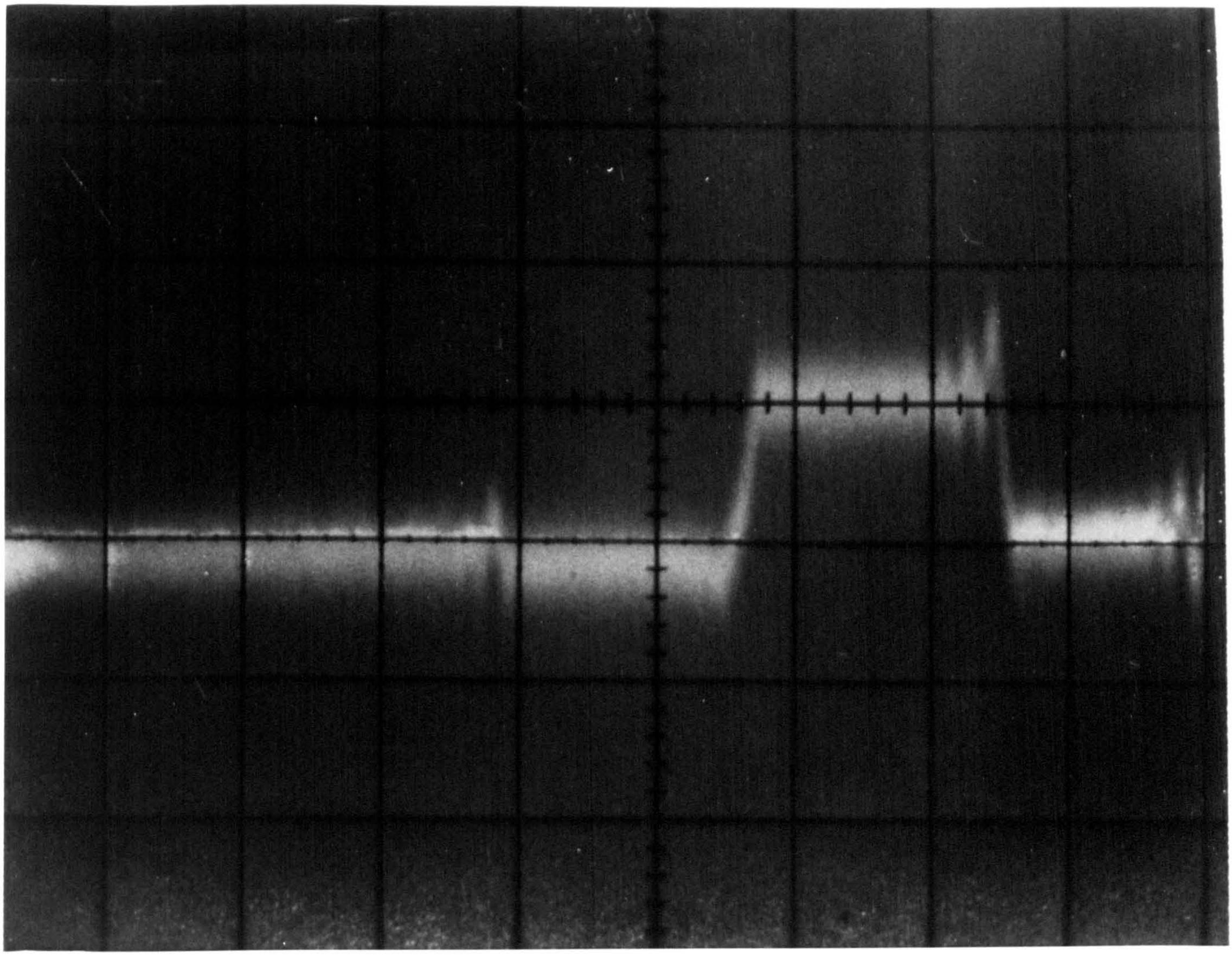

Fig. 2.1

It represents a function $\overline{F(s)}$, the image, or transform, of the function F(t). The class of functions to which F(t) may belong and the range of the parameter s, are to be prescribed in each case. In particular, they must be prescribed so that the integral (2.14) exists.

II.2.1.a. Laplace Transform

When a = 0 and b = ∞ and $K(t,s) = e^{-st}$ the transformation (2.14) becomes the Laplace transformation (LT)

$$\overline{f(s)} = \int_0^\infty e^{-st} F(t)\, dt \qquad (2.15)$$

the transform $\overline{f(s)}$ can assume complex values, when s is the complex variable

$$s = \sigma + j\omega \qquad (2.16)$$

the LT of the real-valued function F(t),

$$\overline{f(s)} = \int_0^\infty e^{-\sigma t}\ e^{-j\omega t} F(t)\, dt \qquad (2.17)$$

can be written in the form

$$\overline{f(s)} = f(\sigma) + f(j\omega) \qquad (2.18)$$

where $f(\sigma)$ is the real axis LT

$$\overline{f(\sigma)} = \int_0^\infty e^{-\sigma t} F(t)\, dt \qquad (2.19)$$

and f(jw) is the imaginary axis LT

$$\overline{f(j\omega)} = \int_0^\infty e^{-j\omega t} F(t)\, dt \qquad (2.20)$$

If the integral in Equation (2.17) exists and converges, Equation (2.19) or (2.20) can be used to perform the transformation of time domain data into frequency domain. The imaginary axis LT is preferred as the real and imaginary parts of the impedance can be calculated directly from it.

The function F(t) can be a suitable potential perturbation E(t), or its corresponding current response i(t). Both transients should be experimentally known, although the potential perturbation can sometimes be represented by a known function of time.

For a digital computer F(t) is known only as a succession of appropriately spaced experimental points. In order to take the integration necessary to perform the Laplace transformation, some assumption is made about the way two or three successive points are joined to each other analytically. In Appendix A the derivations of integration algorithms to perform the LT are given for several assumptions for the case of a potential step perturbation. Essentially, with the assumption of how two points limiting a segment of the transient are analytically joined, we are able to calculate integrals 2.19 or 2.20 limited to that segment. The summation of the segment integrals for all segments of the transient will be the real $\overline{f(\sigma)}$ or imaginary axis $\overline{f(jw)}$ Laplace transform at a particular frequency.

The segment by segment integration and summation need be only performed upon the time varying portion of the signal since the transform of the constant portion is known a priori and need only be added to the result. The digital computer program utilized to do the LT is JAH described in Section 5.

In Appendix B an algorithm is calculated for the case of a potential sweep perturbation.

II.2.1.b. Fourier Transform

Another useful case of the linear integral transformation represented by Equation (2.14) is the Fourier transform. Since substitution of various kernels k(t,s) in Equation (2.14) give rise to a Fourier Transform, there is no universally accepted convention as to what is meant by this title. In order to agree with the commercial computer program DAQUAD (see Section II.4) we define the Fourier Transform as

$$\overline{f(s)} = \frac{2}{T}\int_0^T e^{-jst}\, F(t)\, dt \qquad (2.21)$$

However, if F(t) consists of a set of N equally spaced time samples $X_0, X_I \ldots, X_{n-I}$ the equivalent discrete Fourier Transform is defined as

$$S_r = \frac{1}{N}\sum_{k=0}^{N-1} X_k W^{kr} \qquad (2.22)$$

where $W = e^{-2\pi j/N}$ and $j = \sqrt{-1}$. The collection $S_0, S_1 \ldots S_{N-1}$ is called the frequency spectrum of the data set $\{X_r\}$. It would seem that computation of the complete spectrum S_r would require N^2 complex multiplications. But if N is an integer power of 2, then the algorithm devloped by Cooley and Tukey[23] called the Fast Fourier Transform (FFT) enables computation of the spectrum with only $N \log_2 N$ complex multiples. In essence the algorithm makes use of the fact that

$$W^K = W^{(K \bmod N)} \qquad (2.23)$$

to reduce the number of multiplications necessary for a transformation. This important development can reduce computation time by as much as 99%.

From Equation (2.11) the frequency spectrum of the impedance in terms of the current and potential frequency spectra is

Hardware for on line measurements and LT and FFT analysis of transients

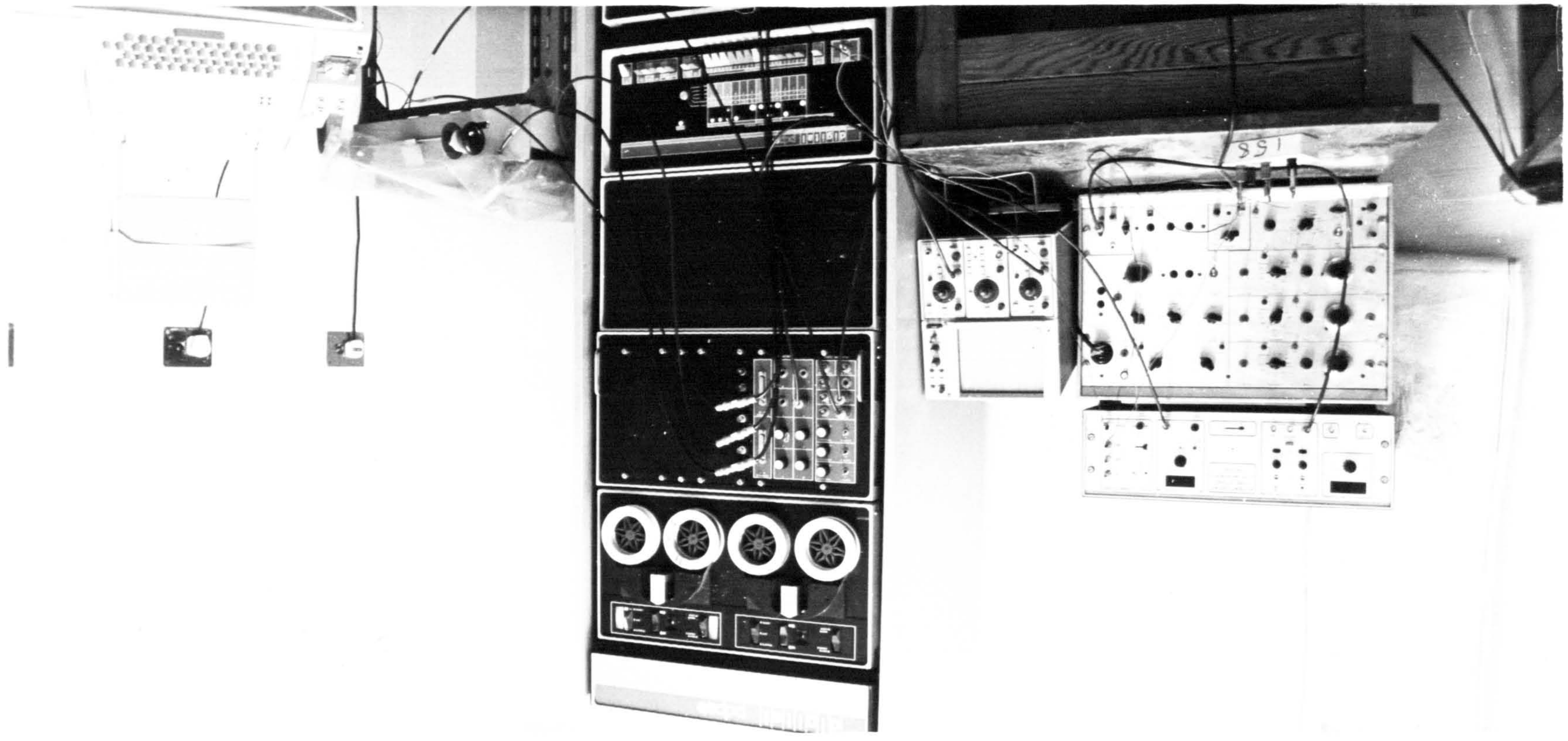
SSI

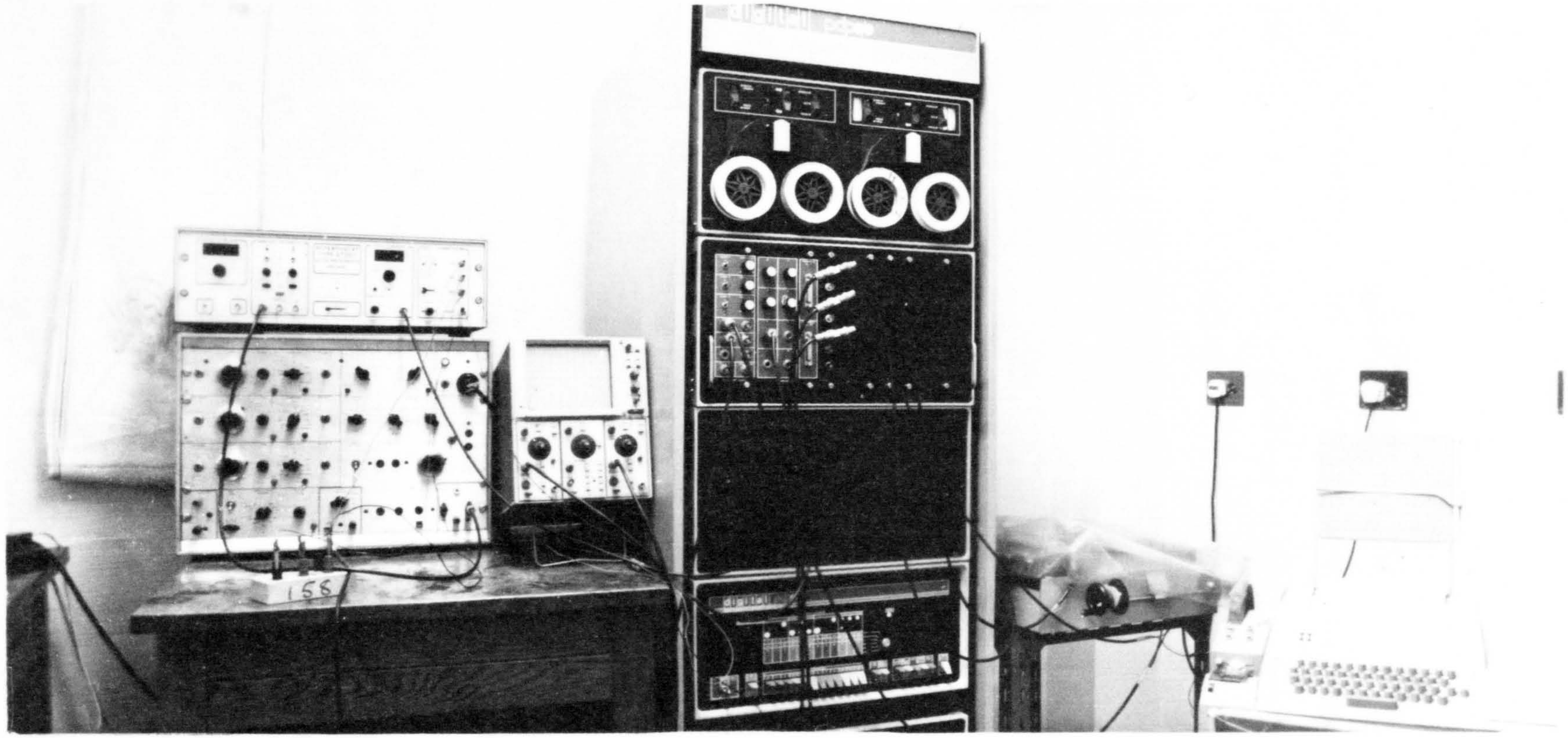

Hardware for on line measurements and LT and FFT analysis of transients

$$Z(Re) = \frac{C_r A_r + D_r B_r}{A_r^2 + B_r^2} \qquad (2.24)$$

$$Z(Im) = -\left(\frac{A_r D_r - C_r B_r}{A_r^2 - B_r^2}\right) \qquad (2.25)$$

where A_r and B_r are respectively the real and imaginary Fourier coefficients of the potential. The subscript r refers to the frequency (w) in radians set by the DAQUAD program and given by $w = 2\pi r/T$.

II.3. Hardware

II.3.1. Waveform generator and Potentiostat

Fig. 2.2 shows schematically the arrangement of hardware used for on line measurements. The waveform generator was constructed in these laboratories by J. Dawson from a design by O.R. Brown and is capable of pulsing or linearly sweeping the potential at three consecutive epochs with simultaneous triggering at the start of each. A repetition period can be set for signal averaging. Controls are provided to set the potential, duration, sweep rate, polarity etc. for each epoch.

A potentiostat type DT 2101, (HI-TEK INSTRUMENTS, ENGLAND) which has a fast rise time (see Fig. 2.1) and an analogue current output signal centred about earth, as required by the minicomputer,was used.

II.3.2. LAB-8/E System

The hardware associated with the minicomputer is called LAB-8/E SYSTEM and comprises:[24]

a) A PDP-8/E General Purpose, 12 bit Digital Computer with 16K of memory and 1.2μs cycle time.

Fig. 2.2 Hardware arrangement for on-line measurements.

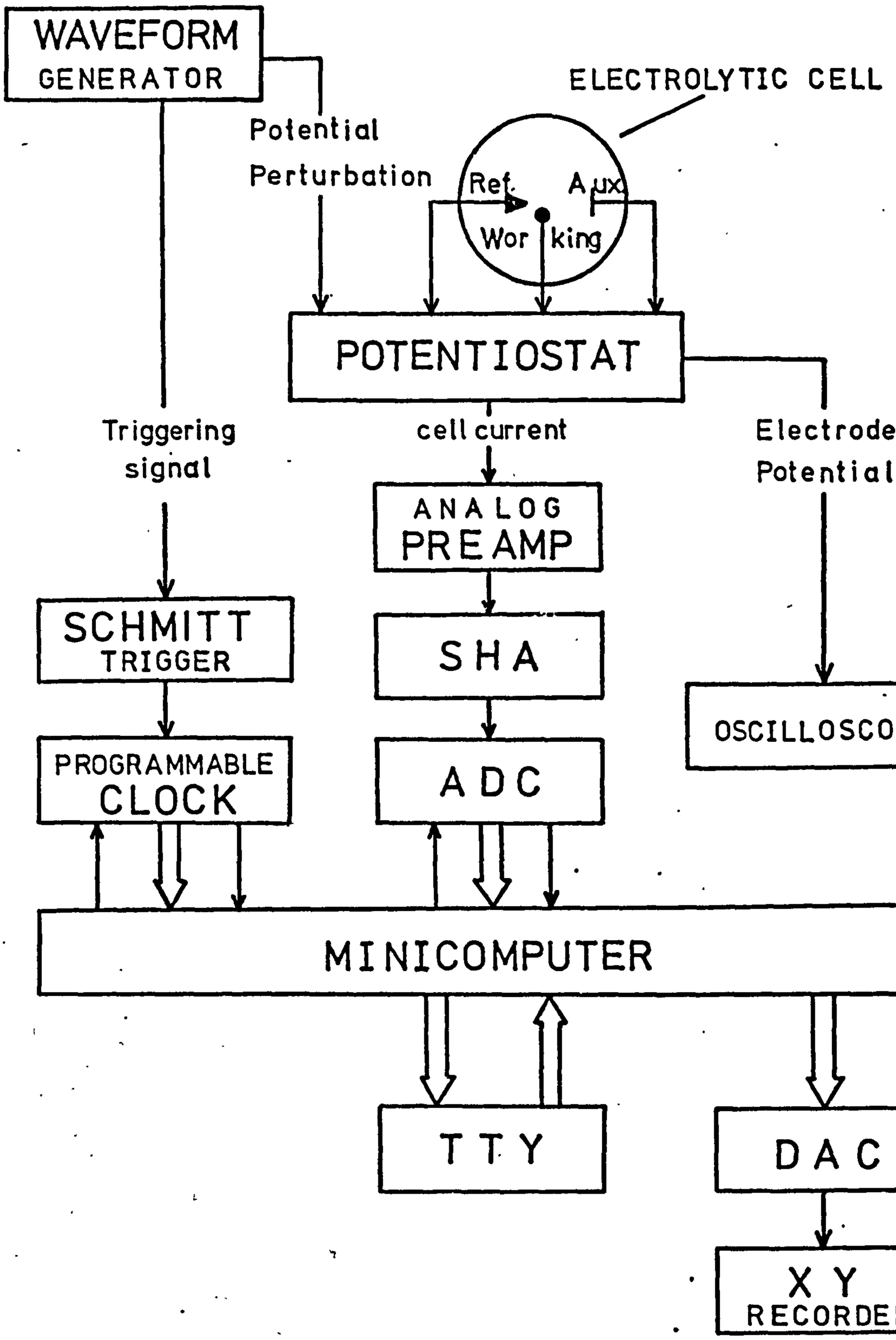

b) A Teletype Model ASR 33, 10 bit input/output device with paper-tape reader and punch.

c) A laboratory mounting panel with precision power supply for use with LAB-8/E peripherals.

d) A 10 bit Analog to Digital Converter with sample and hold circuitry and 8 channel analog multiplexer (expandable to 16 channels).

e) A 10 bit Point Plot Display Control for the graphic display of data on an oscilloscope.

f) A Real-Time Clock with five programmable ranges from 1μs per count to 10 ms per count, plus three Schmitt triggers.

g) A 510 3N TEKTRONIX Oscilloscope with D13 Dual Beam storage and 5020N Differential amplifiers was used both as measuring and display unit of the analog signals, as well as output peripheral to display data, instructions etc. The board controlling the display of visual data was specially modified to allow this oscilloscope to interface with the computer.

h) A BRYANS X-Y Recorder 26000 A4 with an adapted null detector.

II.3.3. Analogue-to-Digital Converter (ADC) System

The ADC is a 10 bit successive-approximation converter with a 50 Khz maximum conversion rate and 0.1% accuracy. Its operation is program controlled with the aid of the programmable Real Time Clock. The ADC system enables the user to sample analogue data at specified rates and to store the equivalent digital value in the memory of the PDP-8/E for subsequent processing or mass storage.

The input range for the analogue signal from the experiment is $\pm$ 1V differential, which is amplified to $\pm$ 5V for input to an analogue buffer that feeds a sample and hold amplifier (SHA). The SHA permits the sampling of rapidly changing signals, by holding the voltage at the input constant,

until the conversion process is complete.

II.4. Fourier Transform Software

II.4.1. Introduction

A flow diagram indicating the software used to calculate the impedance from transient analysis via Fourier Transformation is shown in Fig. 2.3.

Any one of the three following commercial programs supplied by DECUS for the Lab 8/E Software System, could be used for sampling the experimental signal:

a) DAQUAN MS for OS/8 with
   DAFFT OVERLAY (DAQUAD)

b) ADVANCED AVERAGER (AAVG)

c) BASIC AVERAGER (BASAV)

The DAQUAD program is used to perform the Fast Fourier Transformation via command FFT:. It also has a section dedicated to sample and average data on line, but unfortunately some editing has to be done manually, as explained later, therefore although the sampling and transformation may be done by the same DAQUAD program, the processing is not straightforward and the use of the ADVANCED or BASIC AVERAGER is more advantageous, even though it might look more cumbersome in the flow diagram of Fig. 2.2 since it takes more steps, (but in reality is faster than the manual editing involved when DAQUAD is used to acquire the data).

The following programs were used to edit the data sampled by any of the ADVANCED or BASIC AVERAGERS, and to cope with the change of format and transference necessities.

d) CONVERT (CONVRT. SV)

Fig. 2.3 FT software flow diagram.

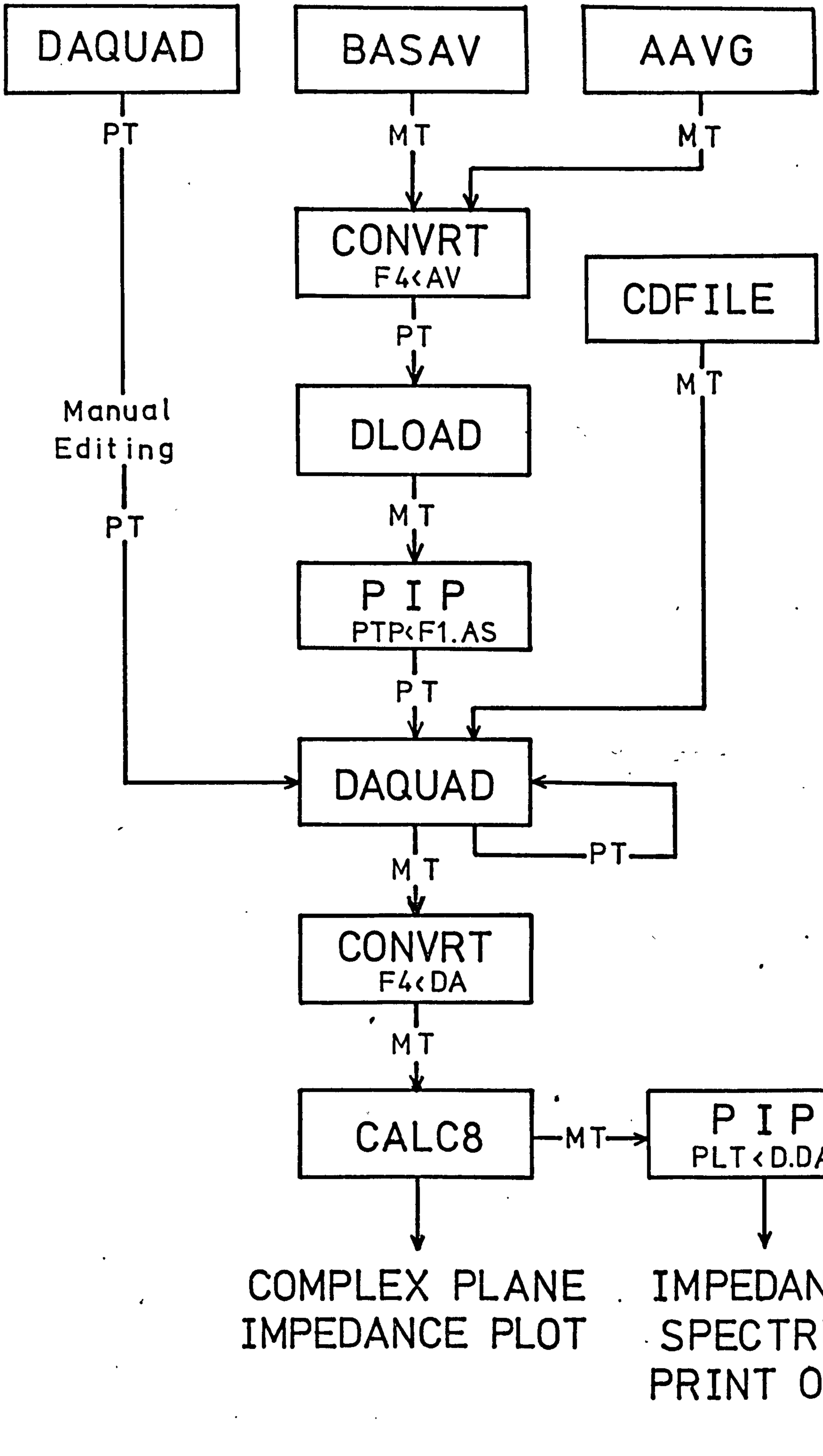

e) DLOAD BA (DLOAD. SV)

f) PERIPHERAL INTERCHANGE

PROGRAM (PIP)

Program d) forms part of the LAB 8/E SYSTEM, it was used to convert data from AV format (output of programms b) and c)) into F4, the format used by BASIC, since the editing program DLOAD was written in that language.

The output from DLOAD is a magnetic tape (MT) file-in DA (or ASCII) format. In order to transfer it to paper tape (PT), the OS/8 Operating System program PIP was used. The punching and reading of paper tape is slow and cumbersome, but had to be done in this way since there is an error in the program a) supplied by DECUS. The command MA: of this program, used to input or output data from or to mass storage (MT), could only be used once within the DAQUAD program. We preferred, then, to use paper tape to input the edited data via the PA: command in order to use the MA: command only once to output the calculated Fourier coefficients Y_r onto magnetic tape files.

The BASIC language program

g) CALC8.BA (or FT8.SV)

was written in order to calculate the real and imaginary components of the complex impedance, according to Equations (2.24), (2.25) and (2.26) from the real and imaginary Fourier coefficients A_r, B_r, C_r, D_r of current and potential, output by DAQUAD, and CONVERTED from DA into F4 format for adequate input into the CALC8 program.

For the case of the potential square pulse, a BASIC language program

h) CDFILE

was written to calculate the Fourier coefficients C_r and D_r according to Equations (C.18) and (C.19). The resulting double precision values give

a more accurate impedance spectrum when processed by CALC8 than the single precision coefficients resulting from the FFT obtained by DAQUAD on the experimental or simulated potential step data.

The CALC8 program gives a TELETYPE printout of the real and imaginary components of the complex impedance at frequencies conveniently distributed to cover the complete transient sampled. It also creates a MT file used to plot the impedance spectra in the complex plane. The transference of this file onto an XY recorder adapted as peripheral device was made with the PIP program, using a "handler" adapted by Alan Cleary of the Psychology Department, University of Newcastle upon Tyne.

II.4.2. ADVANCED AVERAGER MS

The LAB 8/E Advanced Averager MS Program (AAVG), displays and averages analog signals at rates from 175 μs to 4 s/point. It is very versatile, with many features that are not very useful to our purposes, such as on line computation of 95% confidence limits and trend, some signal editing etc. It has a conversational compiler for selecting the parameters of an average and a pre-stimulus (triggering) averaging feature which could be of some use. However the main reason to consider AAVG as an alternative program for data sampling is its capacity to digitise and average signals in two different time intervals at two different sampling rates, i.e. standard or high resolution. This permits the sampling of long time intervals at the standard rate, simultaneously with high resolution sampling at the beginning of the signal of interest, i.e. just before the start of the second perturbation. The epochs corresponding to the high and standard resolutions are positioned with respect to the triggering pulse by chosing the adequate delays in the conversational compiler section I.

A magnetic or paper control tape can be created to contain the average parameters compiled in section I, so that consecutive transient

recordings can be made more rapidly at various potentials without the need to type in the parameters each time an average is to be taken.

Another advantage derived from the double sampling rate facility of the AAVG program is the ability to digitise the start of the second pulse (see Fig. 2.9) at the fastest sample rate available (175μs/point) allowing reasonable precision at the high frequency extreme of the calculated impedance spectra, while sampling the whole of the second pulse at a slower standard resolution (up to 4 s/point) thus extending the impedance spectra to very low frequencies as well as keeping the number of sampled points and the computation time down. It has to be noted here that only the LT program can deal with two or more sampling rates, since it integrates consecutive points which can be at different distances from each other, as long as they are defined. The FFT program requires data with equidistantly sampled points, therefore data sampled at two different rates has to be interpolated.

II.4.3. Basic Averager

The LAB 8/E Basic Averager Program, BASAV, digitises, displays and averages analogue signals at rates from 25μs per point for one channel or from 33μs per point per channel when multiple channels are used.

For our purposes BASAV has two advantages over the AAVG program; one is its fastest sampling rate, and the other its sampler parameter compilation section. As in AAVG, a control tape can be formed to speed up the time taken to record the averages of transients at consecutive potentials.

This program, as we used it, sampled 1000 points in one channel only. Nevertheless modification tapes are supplied to sample 2 channels at 500 points each, 2 channels at 150 points each giving average, confidence limits, trend and other features irrelevant to our purposes.

When using the fastest rate available to obtain good accuracy at the high frequency end of the impedance spectra, the low frequency end may be insufficiently covered with only 1000 points sampled, for the case of certain irreversible systems. However it is possible to augment the number of points sampled to more than a thousand if the computer has more than 4K of memory. A 16K computer was used but it was not found necessary to investigate very low frequencies and a thousand points were sufficient. Even so, a piece of software was written to skip data points at the low frequency end, (see program JAH) in order to speed up the calculations. This procedure is equivalent to having two or more sampling rates, therefore only the LT program can be used, for the FFT program, the whole set of data, without skipping, has to be used.

II.4.4. DLOAD

In order to edit the experimental data and LOAD it to DAQUAN, the program DLOAD has been written in BASIC language. It lists selective parts of the data, to determine by inspection where the first point of the second perturbation is. When the position of this point is entered, the program substitutes the first pulse with a horizontal base line, and positions the second as required, usually at the centre of the total time interval.

This program accepts any file with data in F4 format. The edited signal is output onto the magnetic tape files F1.AS in ASC11 and F2.DA in F4 format.

A listing of DLOAD is given on this section. The object of line 330 is to scale the data up in the range 0 to 1000; the number 1/0.209715 E + 7 corrects a factor left by the CONVRT program and converts back to real numbers. The minus sign renders cathodic currents positive.

OPERATION - Call and run DLOAD. BA or DLOAD.SV., the program prints:

F. NAME ? Enter the name of the file to be edited.

```
DLOAD   BA     3.0

100 REM-DAQUAD PTP LOADER
193 DIM A$(13)
200 DIM C(1024)
210 PRINT "F. NAME"
220  INPUT A$
230 PRINT "POINTS"
240  INPUT P1
300 FILEN#1:A$
310 FOR I=1 TO P1
320  INPUT#1:C(I)
330 C(I)=-1000*C(I)/0.209715E+7
340 NEXT I
350 CLOSE#1
400 PRINT "S/F LIST"
410  INPUT Z3,Z4
420 FOR I=Z3 TO Z4
430 PRINT"C";I;"=";C(I)
440 NEXT I
550 PRINT "MORE"
560  INPUT B$
570  IF B$="Y" THEN 400
600 PRINT "S. PERTURBATION"
610  INPUT Z8
650 PRINT"F1 POINTS,ADD. P,BASE"
660  INPUT P,N,A3
700 FILEV#2:"DTA1:F1.AS"
720 FOR I=1 TO N
730 PRINT#2:A3
740 NEXT I
800 FOR I=Z8 TO INT(Z8+P-N+0.3)
810 PRINT#2:C(I)
820 NEXT I
830 CLOSE#2
900 FILEVN#3:"DTA1:F2.DA"
910 FOR I=1 TO N
920 PRINT#3:A3
930 NEXT I
940 FOR I=Z8 TO INT(Z8+P-N+0.3)
950 PRINT#3:C(I)
960 NEXT I
970 CLOSE#3
1000 END

READY.
```

```
CDFILE  BA     3.Ø     30-MAY-77

10 REM- C AND D FOURIER COEFF. FOR SQUARE PULSE
20 DIM C(513),D(1025)
24 PRINT "K="
25 INPUT G
30 FILEVN#1:"DTA1:D.DD"
40 FOR K=Ø TO 1024 STEP 2
50 D(K)=Ø
60 NEXT K
70 FOR K=1 TO 1023 STEP 2
80 D(K)=1.273239545*G/K
90 NEXT K
100 FOR K=Ø TO 1024
110 PRINT#1:D(K)
120 NEXT K
130 CLOSE#1
140 FILEVN#2:"C.DD"
150 FOR K=Ø TO 511
160 PRINT#2:Ø
170 NEXT K
180 CLOSE#2
190 PRINT "HI SAILOR"
200 END

READY
```

```
TEST8   BA     3.Ø      30-MAY-77

10 REM
15 PRINT DAT$(X)
20 DIM C(1100)
25 PRINT "RATE"
26 INPUT O
30 FOR I=1 TO 30
40 C(I)=-Ø.1*Ø.209715E+7
50 NEXT I
60 FOR I=31 TO 1006
70 C(I)=-Ø.1-Ø.ØØ1*((I-30.5)*O)**-Ø.5
75 C(I)=C(I)*Ø.209715E+7
80 NEXT I
90 FILEVN#1:"DTA1:AL2.DA"
100 FOR I=1 TO 1006
110 PRINT#1:C(I)
120 NEXT I
130 CLOSE #1
140 END

READY
```

POINTS ? Enter the number of data points of the file to be edited. Less points than the total could be entered for convenience.

S/F LIST ? Enter the starting and finishing points of the segment of data that the user wants to inspect, they will be listed on the teletype. The main purpose of the inspection is to determine the position of the first point of the second perturbation.

MORE ? Enter Y if more inspection is desired.

S. PERTURBATION ? Enter the position (number) of the first point of the second perturbation.

F1 POINTS Enter the total number of points to be contained in the output file, including base line. This number has to be a power of two, in order to calculate the FFT.

ADD. POINTS Enter the base line points to be added to the second perturbation, replacing the first pulse. With a suitable manipulation of the last two parameters the second perturbation signal can be positioned anywhere along the total time interval. In order to position it in the centre ADD. POINTS has to be a half of the number entered in F1 POINTS.

BASE ? Enter the value to set the level of the base line, usually determined by the steady state level of the first perturbation.

The program will now execute.

II.4.5. DAQUAD

DAQUAD is the name given to the DAQUAN MS program with DAFFT overlay, provided by the LAB-8/E Software System[25]. It can be used to acquire data by boxcar, multi-sweep time averaging from one instrument at a time, at a sampling rate from 123 μs/point to 30 s/point, and to display the results. A wide variety of subsequent processing techniques, such as smoothing, integration, scaling, deconvolution of fused peaks, Fast Fourier

transform (FFT), Inversed Fast Fourier Transform (IT), etc. can be used to reduce the data.

As a program to acquire on-line data, DAQUAD is inferior to both the AAVG and BASAV programs because of the longer time required to record consecutive signals at various potentials due to the longer initialising procedure. The maximum sampling rate of 123μs/point may not be fast enough for many applications and its only possible advantage of sampling and processing (FFT) the data immediately is curtailed by the fact that the raw data needs editing (to set a base line and position the signal). Unfortunately DAQUAD does not provide the facilities to do this automatically, instead a laborious process of manipulation of output paper tapes has to be used, employing the skip facility of the PA: command to cut out the first pulse and then enter the base line points manually via the teletype. This procedure may be followed when only one impedance spectrum is to be calculated. The experimental signal is digitised from -1V to +1V by the ADC. This range is automatically compressed by the averaging section of DAQUAD into a range from 0 to 1000. Zero in this case is equivalent to 1V of cathodic signal, and 1000 is equivalent to 1V of anodic signal.

The main use of DAQUAD is the calculation of the FFT of the real time domain data F(t) via the command ZT: . The calculations are made by employing single precision numbers. In order to utilize the maximum number of bits in the transformation, it is sometimes necessary to divide by 2 in a computation. As a result of this a pseudo-floating point format has been adopted in which a variable scale FACTOR (or exponent) is imposed on all the frequency spectra. The value of FACTOR is printed out by DAQUAD together with the pseudo-Fourier coefficients Y_r . The true Fourier coefficients S_r are given by

$$S_r = \frac{Y_r \times 2.048 \times G \times AMPL.}{2^{FACTOR} \times 1000} \qquad (2.26)$$

where AMPL is an external scaling factor that can be applied to the time domain data when it is very small, as is the case of the potential perturbing signal which departs only a few milivolts from the level of the first pulse. This level is considered as zero. G is a factor related to the way the analogue data is digitised. For a range of -1V to +1V of signal digitised into 0 to 1000, G = 2, but if 0 to $\pm$ 1V is digitised into 0 to 1000 then G = 1. All these scaling factors are intended to avoid rounding off errors associated with small figures when calculations are made with single precision numbers. The actual calculation of S_r according to Equation (2.26) is made in the program CALC8.BA.

OPERATION

In order to output the real coefficients A_r of the current signal, the user has to proceed as follows

1) Call and run DAQUAD. SV

2) Use the 1PA: command to input the paper tape edited data into Buffer 1. It is within this command that the AMPL factor can be applied to the time domain data by assigning suitable range parameters. The minimum will be set to zero and the maximum to 1000.

3) Use the ZT: command to perform the FFT on the data (zeroing the imaginary values since the data is real valued).

4) Use the MA: command to output the real A_r contained in Buffer 1 into a file called A.DD.

5) CONTROL C it is necessary to restart the program again to be able to use the MA: command.

In order to output the imaginary Fourier coefficient of the current B_r , repeat steps 1) to 3) as before and then

4) Use the SH: command to shift the B_r from Buffer 2 to Buffer 1.

5) Use the 1 MA: command to output the B_r coefficients in Buffer 1 into the file B.DD.

6) CONTROL C.

The Fourier coefficients of the potential step signal can be accurately calculated by the CDFILE program and therefore there is no need to use DAQUAD for that. However if it is desired to transform the experimental potential signal the procedure outlined for the current can be used, the real and imaginary Fourier coefficient C_r and D_r, should be stored in files C.DD and D.DD respectively.

II.4.6. CALC8

This program written in BASIC language fetches the files A.DA, B.DA, D.DA which contain the real and imaginary Fourier coefficients Y_r of the current and potential signals. These files are the F4 CONVERTed versions of files A.DD, B.DD, C.DD and D.DD.

CALC8 calculates the impedance spectrum according to Equations (2.24), (2.25) and (2.26).

OPERATION

Call and run CALC8. BA or CALC8. SV, the program will print.

FACTORS C,V ? Enter the FACTORs associated with the Y_r of the current and potential as given by DAQUAD.

V AMPL ? Enter the AMP factor used to scale up the potential time domain data.

RATE (SEC) ? Enter the sampling rate in sec.

P, Enter the number of Y_r to be processed. This number is half of the time domain data points.

STEP, Enter number 2 for central signal positioning, this will skip alternate Y_r which are equal to zero.

R ? Enter the value of the current measuring resistor in ohms.

```
CALC8   BA     3.Ø       3Ø-MAY-77

Ø REM
1Ø DIM A(513),B(513),C(513)
11 K2=Ø.8975
12 Z9=1.Ø45
13 Q4=INT(2ØØ*Z9+Ø.5)
14 Q5=INT(4ØØ*K2+Ø.5)
2Ø DIM D(513),R(513),I(513)
35 PRINT "FACTORS C,V"
36 INPUT C,V
37 PRINT "V AMPL.,RATE(SEC)"
38 INPUT L,O
39 PRINT "P,STEP"
4Ø INPUT N,B
45 PRINT "R="
46 INPUT M
47 C=(2**(1-C))/1ØØØ
48 V=(2**(1-V))/(1ØØØ*L)
5Ø FILEN#1:"DTA1:A.DD"
52 C=C*2
54 V=V*2
6Ø FOR K=Ø TO N-1
7Ø INPUT#1:A(K)
75 A(K)=C*A(K)
1ØØ NEXT K
1Ø5 CLOSE#1
11Ø FILEN#2:"DTA1:B.DD"
12Ø FOR K=Ø TO N-1
13Ø INPUT#2:B(K)
135 B(K)=B(K)*C
14Ø NEXT K
15Ø CLOSE#2
2ØØ FILEN#3:"DTA1:C.DD"
21Ø FOR K=Ø TO N-1
22Ø INPUT#3:C(K)
225 C(K)=V*C(K)
23Ø NEXT K
24Ø CLOSE#3
25Ø FILEN#4:"DTA1:D.DD"
26Ø FOR K=Ø TO N-1
27Ø INPUT#4:D(K)
275 D(K)=V*D(K)
28Ø NEXT K
29Ø CLOSE#4
294 PRINT "FREQ=R/L"
295 PRINT "  R","   Z(RE)","    Z(IM)","HZ","  1/HZ**Ø.5"
296 PRINT
299 R=M
3ØØ FOR K=1 TO (N-1) STEP B
31Ø S=A(K)**2+B(K)**2
32Ø R(K)=(A(K)*C(K)+B(K)*D(K))/S
325 R(K)=R(K)*M
33Ø I(K)=(A(K)*D(K)-B(K)*C(K))/S
335 I(K)=I(K)*M
336
```

```
336 NEXT K
337 FOR K=1 TO 31 STEP B
338 F=K/(2*N*0)
339 PRINT K,R(K),I(K),F,1/SQR(F)
340 PRINT "Z(T)=";R/(6.28319*SQR(F))
341 NEXT K
342 IF N<32 THEN 361
343 FOR K=33 TO 63 STEP 4
344 F=K/(2*N*0)
345 PRINT K,R(K),I(K),F,1/SQR(F)
346 PRINT "Z(T)=";R/(6.2832*SQR(F))
347 NEXT K
348 IF N<64 THEN 361
349 FOR K=65 TO 255 STEP 8
350 F=K/(2*N*0)
351 PRINT K,R(K),I(K),F,1/SQR(F),"Z(T)=";R/(6.2832*SQR(F))
352 IF K>N THEN 361
353 NEXT K
354 IF N<256 THEN 361
355 FOR K=257 TO (N-1) STEP 12
356 F=K/(2*N*0)
357 PRINT K,R(K),I(K),F
358 PRINT "Z(T)=";R/(6.2832*SQR(F))
359 NEXT K
361 PRINT "AMPL.PLOT"
362 INPUT B1
363 FILEV#1:"DTA1:D.DA"
364 FOR K=1 TO N STEP B
365 R(K)=INT(R(K)*K2*B1+0.5)
366 I(K)=INT(I(K)*Z9*B1*-1+0.5)
367 PRINT#1:R(K);PNT(44);I(K)
368 NEXT K
370 FOR X=0 TO 400 STEP 5
380 PRINT#1:X;PNT(44);0
390 NEXT X
400 FOR Y=0 TO 9
410 PRINT#1:Q5;PNT(44);Y
420 NEXT Y
430 FOR Y=0 TO 200 STEP 2
440 PRINT#1:0;PNT(44);Y
450 NEXT Y
460 FOR X=0 TO 9
470 PRINT#1:X;PNT(44);Q4
480 NEXT X
490 CLOSE#1
495 CHAIN"SYS:PIP.SV"
500 END

READY
```

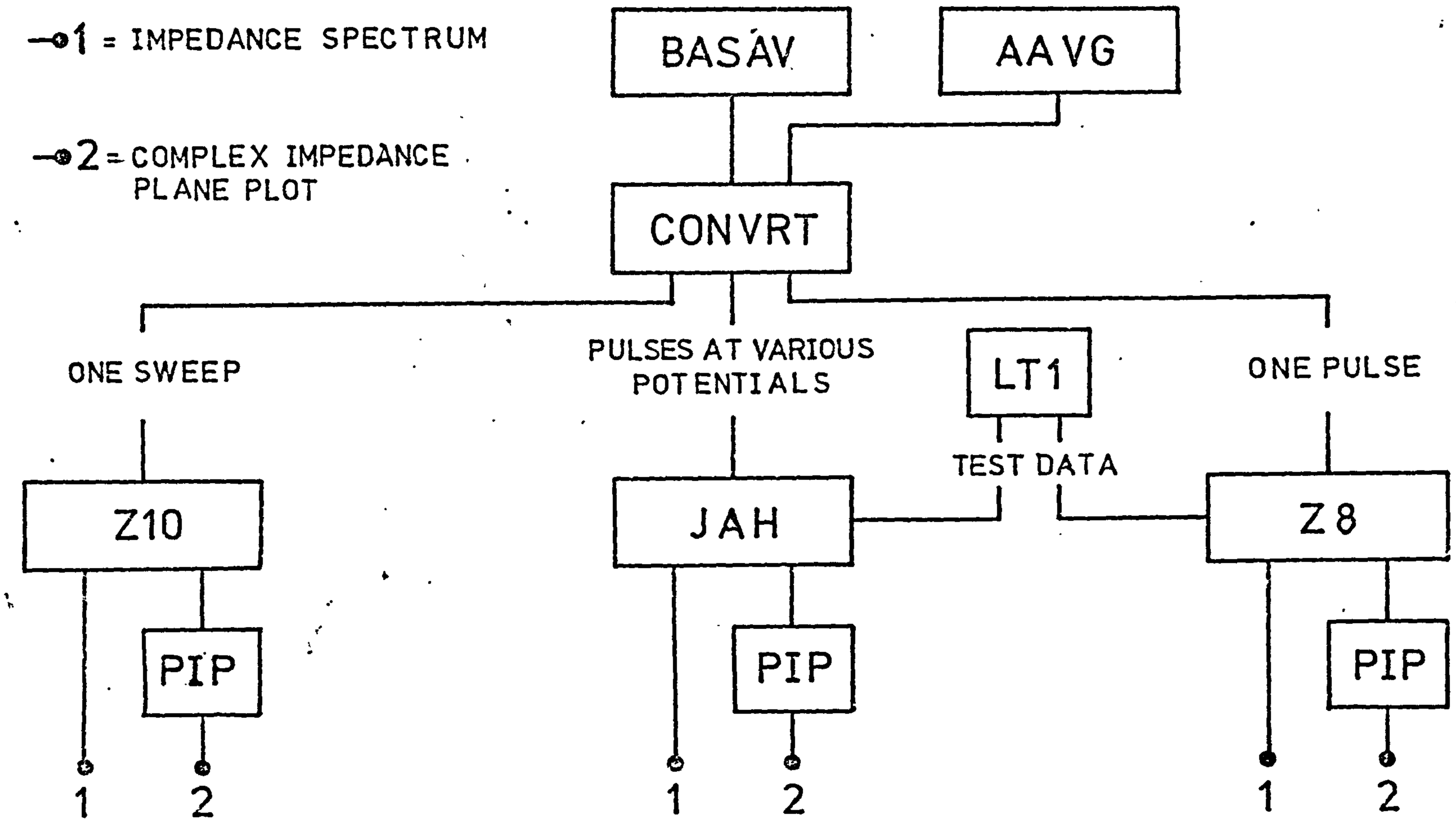

Fig. 2.4 LT Software Flow Diagram.

The impedance spectrum will be printed out via the teletype.

* Enter PLT: D.DA to plot the impedance spectrum on the complex plane via the X-Y plotter.

II.5. Laplace Transform Software

II.5.1. Introduction

A flow diagram indicating the software used to calculate the impedance spectrum from pulse or sweep analysis via Laplace Transform (LT) is shown in Fig. 2.4. A choice of two signal samplers and averagers can be used: BASAV and AAVG, the characteristics of which have been already described. When sampling at consecutive potentials the files should be named RUN1. DA, RUN2.DA, RUN3.DA ... and then CONVERTed to RUN1.CO, RUN2. CO, RUN3.CO ... up to RUN20.CO since those are the files names accepted by the JAH program for automatic consecutive processing.

The object of the CONVERT program is to change the format of the data coming from BASAV or AAVG into F4, the format accepted by BASIC, since both JAH and Z8 are written in that language. When intending to use Z8 the CONVERTed file should be called AL2.DA.

The Z8 program calculates the impedance spectrum via Laplace Transformation for single potential step data. The JAH program is the automated version of Z8 to process transient data for successive pulses to various potentials under given experimental conditions.

The Z10 program calculates the impedance spectrum from potential sweeps using Laplace Transformation Analysis.

The LT1 program generates artificial data to test the performance of the Laplace Transformation program.

II.5.2. JAH

This program processes data from consecutive time domain pulses and calculates the associated impedances spectra via LT. It has an inspection section and a parameter input section at the beginning. The idea is to fix the experimental parameters such as second pulse height, length, sampling rate, measuring resistor and triggering. Then only the level of the first pulse varies. By inspection of one or two pulses the position of the relevant second pulse can be determined for all runs. Therefore the parameters for all runs can be entered at the beginning, the computer processing consecutively a series of runs, with no need for human intervention.

A description and operation of the program follows.

OPERATION

1) Call and run JAH.BA or JAH.SV the program will print on the teletype the DATE, and then

2) INSPECTION ? Enter Y if inspection of a file is desired. If any other or no character is entered the program will continue to 6).

3) FILE ? Enter the name of the F4 format file that the user wants to inspect. It will be fetched from the specified magnetic tape.

4) S/F LIST ? Enter the starting and finishing point delimiting the segment of data that the user wants to list.

5) MORE ? Enter Y and the program will return to 4), other or no character will cause the program to continue.

6) S/F RUN ? Enter two numbers specifying the initial and final RUN that the user wants to process. For example 2, 10 will cause files RUN2.CO to RUN10.CO to be processed batch wise.

7) Starting with the initial run, the following parameters have to be entered for each RUN.

E/V second pulse height with respect to the first pulse, in Volts.

SAMPL.R/S sampling rate in seconds.

MEAS.R/OHMS value of measuring resistor.

S. POINT ? position number of the first point of the second pulse.

LENGTH (UP TO XXX) ? the number of working points that will determine the real length of the second pulse processed, according to the following equivalence table

WORKING POINTS	REAL LENGTH
0 to 200	0 to 200
201 to 400	202 to 600
401 to 500	604 to 1000

The number XXX in parenthesis specifies the maximum number of working points.

PLOT (1=YES) Entering number 1 will cause the program to create a file DP#.AS (where # is the RUN number) containing the time domain current data ready to be plotted via XY recorder and PIP as explained later.

8) AGAIN ? Entering Y will return the program to 7) so that all parameters can be re-entered. Any other input will cause the program to continue.

9) The program is executed: a) the time domain data file is created, if so specified. b) The teletype prints RUN to indicate to what RUN the following listing refers. c) Three columns are printed which refer to:

F/HZ The frequency in hertz at which the impedance is calculated. The frequency spectrum is computed so that it corresponds exactly to the time domain data considered.

Z(RE) This is the real impedance component of the imaginary axis LT.

Z(1M) This is the imaginary impedance component in ohms of the imaginary axis LT.

d) The program will create a file Z#.AS, (where # is the run number)

containing ordered pairs of Z(RE) and Z(1M) ready to be plotted via PIP and XY recorder. The program then prints as a remainder:

Z##.AS Y = XX ohms

The number XX gives the value of the scaling mark on the ordinate of the plot frame approximately 10 cm away from the origin. The scaling of the data for plotting purposes is done automatically according to the following criteria

Z (IM)/OHMS	Y AXIS SCALING MARK/OHMS
0 to 1	1
2.5 to 14	10
14 to 28	20
28 to 70	50
70 to 140	100
140 to 280	200
280 to 700	500
700 to 2800	2000
2800 to 20000	10000

10) The processing of the particular run is finished, the program now fetches the next RUN#.CO file to process and returns to 9) until all runs are processed. End of program.

11) Call and run PIP.SV. To facilitate the interfacing between the computer and the pen recorder, a "handler" PLT has been written[25]. To plot the impedance spectrum enter

* PLT: < Z#.AS

When a pair of imaginary (Y axis) and real (X axis) impedance data is output, the pen of the X-Y recorder moves to the co-ordinate specified, puts the pen down, raises it and a potential pulse is sent back to the computer to tell it to output the next pair of coordinates.

To plot the time domain data enter

* PLT: < P#.DA

if desired a frame with the Y axis mark referred to in 9) d) can be plotted

on the Z#.AS or P#.DA plots by entering

PLT:FRAME.AS

the X axis mark of this frame corresponds to twice the Y axis mark value.

Description of the JAH program

The program is listed at the end of this section, and in Fig.2.5 some of the variables used in the program are shown. The control section is enclosed between lines 0 to 490. Lines 0 to 50 define arrays dimensions and print out the data. From lines 100 to 320 the program permits access and inspection of CONVERTed data files. From lines 340 to 490 the parameters defining the consecutive runs are compiled interactively and stored in arrays. Please refer to OPERATION for a definition of these parameters.

A big loop containing all the processing done to a run is enclosed between lines 700 and 13710. Subsequent runs are subject to the same processing. In the first part of the loop, from line 720 to 980, the current transient data corresponding to the given run is retrieved and stored in the array C(I). The factor -1/0.209715E+7 in lines 207 and 940 is included to compensate for the factor 0.209715E+7 which has been carried by the data after being sampled by the AAVG or BASAV programs. The CONVRT program does not rescale the data passing through it. The minus sign ensures that the cathodic currents are positive in sign.

From line 1000 to 1120 a Plot Section has been written to allow for the plotting of the current transient via the PIP program (if so specified in the Control Section). The factors K2 and Z9 correct the sensitivity of the X and Y axis pen recorder preamplifiers, presumably affected by transmission and connections potential drops. When the sensitivity of both amplifiers is set at 0.2V/cm, 10 cm of the Y axis is equivalent to the full 1V signal accepted by the ADC, and 10 cm of the X axis is equivalent to 500 sampled points. By knowing the current measuring

resistor and the sampling rate, the plot coordinates can be determined in terms of current vs time.

Lines 2000 to 3305 form the Array Section. Here, the parameters entered at the Control Section, which are relevant to the run being processed, are retrieved and assigned to the variables used in the LT calculation. Also the current and time arrays are formed as described below. Q1 in line 2010 is a delay to skip a number of points at the beginning of the second pulse to allow for potentiostat rise time. It is set to zero here, but is kept in the time array forming algorithm of line 3010, and in the various algorithms that form current arrays, in order to make its use possible for the case of very fast sampling rates. The meaning of parameters P1, V9, Z2 and Q2 in lines 2015, 2020, 2030 and 2040 is best illustrated by Fig. 2.5.

P2 in line 2050, the same as P3 in line 2684 and P4 in line 2710 give the position of the last point considered in the current array. Correspondingly, C1, in line 2060, or in lines 2687 and 2688, or in line 2715, represents the level of the current at the end of the segment of second pulse considered, with respect to the current level Z2 at the end of the first pulse. The Z2 level is considered as zero by subtracting Z2 from the current array (see lines 2060, 2688, 2715, 2720, 3210, 3265 and 3303).

The variable O in line 2070 is the sampling rate, and the quantity T1 in line 2080 is just an internal scaling factor used to improve calculations accuracy. The plotting factor Z9 in line 2170 has a negative sign in order to plot the negative imaginary impedances in the first quadrant of the complex plane later. The quantity T in lines 2650 and 3235, determines the highest frequency at which the impedance will be calculated. Similarly, B in lines 2660, 2680 and 2700 gives the lowest possible frequency that corresponds to the time domain data considered.

The number of time domain points in the second pulse, when bigger than 200, was condensed in order to diminish the array size. This optimizes the use of available core and also reduces computation time. Between time domain points 200 and 600 only each alternative point was considered and the skipped point averaged with it (lines 3260 and 3265). Between time domain points 600 and 1000, only each fourth point was considered, although the adjacent skipped points were blended into an average (lines 3295, 3300 and 3303) to smooth out any noise. The result is a condensed current array where the first 200 points sustain a point to point equivalence; condensed points 201 to 400 correspond to time domain points 202 to 600, and finally, points 401 to 500 of the condensed array correspond to points 604 to 1000 of the current time domain array.

The current array in all cases was formed by subtracting the level C1 in order to cause the signal to converge, (lines 2720, 3210, 3223, 3265, 3303), as seen in Fig. 2.5, where the vertically hatched area represents the final current array as fed to the LT Calculation Section. The LT of the area with the oblique hatching is taken into consideration later, as explained in Section II.2.

The time array is formed in lines 3010, 3255 and 3290 to match the current array. For a delay Q1 = 0 it is assumed that the first sampled point of the second pulse is C(2) sampled at a time T(2)=0/2, where 0 is the sampling rate, see line 3010. The first point C(1) of the second pulse is extrapolated (line 3223) and is assumed to be sampled exactly at the time T(1)=0, i.e. the time at which the second potential pulse is triggered. The extrapolation, performed in line 3223 was found by trial and error, to give better results for artificial data described by Equations C.31 and C.49.

The Frequency Distribution Section is comprised between lines 3310 and 6310. Its object is to form a frequency spectrum corresponding

to the time interval of the current transient. In lines 4210 to 4410 the maximum frequency W(1) and the minimum frequency W2 are retrieved. In lines 4510 and 4610 the number of decades of frequency A is determined. In line 4710, the total number of frequencies N1 is determined, and in lines 4810 to 6310 a distribution of 20 frequencies per decade is assigned to the frequency array W(K).

The LT Calculation Section is comprised between lines 6510 and 13710. In this section the impedance spectrum for the run is calculated and output into a teletype print out and a file for plotting purposes.

For each calculated frequency W(K), the program calculates SIN(WT) (line 7010) and COS(WT) (line 7110) for each time point used in the transform. The SIN(WT) and the COS(WT) values corresponding to all time points T(M) and one frequency W(K) are stored in arrays S(M) and O(M) respectively. With these two arrays used in the following calculation, the program enters the LT subroutine in line 10410. Both the real part of the imaginary axis transform (calculated in line 11810) and the imaginary part (calculated in line 11710) are generated over all defined points in the current arrays according to Equations A.54 (without the steady state transform) and A.55 and then the program returns to form new S(M) and O(M) arrays at another time point T(M) until the imaginary and real parts of the imaginary axis LT are generated over all defined points in the current and time arrays. After this numerical integration is complete, the values of the real (C5) and imaginary (C3) coefficients (at the defined frequency) are returned to the main program where the transform (C2), of the last current data point C1 (assumed to be the steady state current value) is added onto the imaginary coefficient (lines 7410, 7510).

The imaginary part of the constant potential profile is calculated in lines 7610 and 7710; the real part, V4 is zero (line 7810). The constancy of this theoretical profile can be shown to be valid in practice,

```
JAH     BA     3.0

0 REM CONTROL SECTION
10 DIM C(1025)
20 DIM S(500),T(500),O(500)
25 DIM D(25)
30 DIN W(55),R(55),I(55)
35 PRINT DAT$(X)
40 DIM E(25),B(25),A(25),J(25),P(25)
50 DIM I$(19)
100 PRINT "INSPECTION"
120 INPUT I$
140 IF I$><"Y" THEN 340
160 PRINT "FILE"
180 INPUT I$
200 FILEN#1:I$
203 FOR I=1 TO 1006
205 INPUT#1:C(I)
207 C(I)=C(I)/-0.209715E+7
206 NEXT I
209 CLOSE#1
210 PRINT "S/F LIST"
220 INPUT A1,A2
230 FOR I=A1 TO A2
240 PRINT "C";I;"=";C(I)
250 NEXT I
280 PRINT "MORE"
300 INPUT I$
310 IF I$="Y" THEN 210
320 GO TO 100
340 PRINT "S/F RUN"
360 INPUT B1,B2
380 PRINT "E/V","SAMPL.R./S","MEAS. R/OHMS"," S.POINT"
400 FOR N=B1 TO B2
410 PRINT "RUN";N
420 INPUT E(N),B(N),A(N),J(N)
430 PRINT"LENGHT (UP TO";INT(501-J(N)/4);")"
435 INPUT P(N)
436 PRINT "PLOT? (1=YES)"
437 INPUT D(N)
440 NEXT N
480 PRINT "AGAIN"
485 INPUT A$
490 IF A$="Y" THEN 100
700 FOR N=B1 TO B2
720 I$="DTA1:RUN"&STR$(N)&".CO"
740 FILEN#1:I$
900 FOR I=1 TO 1006
920 INPUT#1:C(I)
940 C(I)=C(I)/-0.209715E+7
960 NEXT I
980 CLOSE#1
1000 REM PLOT SECTION
1005 K2=0.8975
1007 Z9=1.045
1010 IF D(N)<>1 THEN 2010
1045 I$="DTA1:DP"&STR$(N)&".AS"
1050 FILEV#2:I$
1060 FOR I=7 TO 1006
1070 P=INT((I-6)*K2/2.5+0.5)
```

```
1075 L1=INT(C(I)*Z9*200+0.5)
1080 PRINT#2:P;PNT(44);L1
1100 NEXT I
1120 CLOSE#2
2000 REM I/E ARRAY SECTION
2010 Q1=0
2015 P1=P(N)
2020 V9=E(N)
2030 Z2=(C(J(N)-1)+C(J(N)-2)+C(J(N)-3))/3
2040 Q2=J(N)+Q1
2050 P2=P(N)+Q2
2060 C1=(C(P2)+C(P2-1)+C(P2+1))/3-Z2
2070 O=B(N)
2080 T1=1/O
2090 Q2=J(N)+Q1
2170 Z9=-Z9
2650 T=6.2832/O
2660 B=6.2832/(P1*B(N))
2670 IF P1=<200 THEN 2720
2680 B=6.2832/((2*P1-200)*O)
2684 P3=2*P1+Q2-200
2687 C1=0.5*C(P3)+0.25*(C(P3-1))+0.25*C(P3+1)
2688 C1=C1-Z2
2690 IF P1=<400 THEN 2720
2700 B=6.2832/((4*P1-1000)*O)
2710 P4=4*P1+Q2-1200
2715 C1=(C(P4)+C(P4-1)+C(P4-2))/3-Z2
2720 C(1)=C(Q2)-Z2-C1
2730 T(1)=0
2800 A3=200
2810 IF P1>A3 THEN 2910
2840 A3=P1
2910 FOR K=2 TO A3
3010 T(K)=Q1*O+O/2+(K-2)*O
3110 T(K)=T(K)*T1
3210 C(K)=C(Q2+K-2)-Z2-C1
3220 NEXT K
3223 C(1)=3.333*(C(1)**2)/C(2)
3230 IF P1<=200 THEN 3310
3235 T=3.1416/O
3240 A3=400
3245 IF P1>A3 THEN 3250
3247 A3=P1
3250 FOR K=201 TO A3
3255 T(K)=T(200)+(K-200)*2
3260 A4=Q2+2*K-200
3265 C(K)=0.5*C(A4)+0.25*C(A4-1)+C(A4+1)*0.25-Z2-C1
3270 NEXT K
3280 IF P1<=400 THEN 3310
3283 1.25664/O
3285 FOR K=401 TO P1
3290 T(K)=T(400)+(K-200)*4
3295 A4=Q2+4*K-1000
3300 C(K)=(C(A4)+C(A4-1)+C(A4+1))/3
3303 C(K)=C(K)-C1-Z2
3305 NEXT K
3310 REM FREQ. DISTR. SECTION
4210 W1=T*!.0/T1
4310 W2=B*1.0/T1
4410 W(1)=W1
4510 A=(LOG(W2/W(1)))/2.303
```

```
4610  I=ABS(A)
4710  N1=I*20
4810  F5=1
4910  W3=0.1*W(1)
5010  FOR K=2 TO N1
5110  W(K)=W(K-1)-W3
5210  F5=F5+1
5310  IF INT(F5+0.3)=5 THEN 5710
5340  IF INT(F5+0.3)=11 THEN 5710
5350  IF INT (F5+0.3)=15 THEN 5740
5370  IF INT (F5+0.3)=20 THEN 5760
5390  GO TO 6310
5710  W3=0.5*W3
5730  GO TO 6310
5740  W3=0.8*W3
5750  GO TO 6310
5760  W3=.5*W3
5780  F5=1
6310  NEXT K
6510  PRINT
6515  PRINT "RUN";N
6520  PRINT " F/HZ","  Z(RE)","  Z(IM)"
6610  PRINT
6710  FOR K=1 TO INT(N1)
6810  FOR M=1 TO INT(P1+0.3)
6910  W4=(W(K)*T(M))
7010  S(M)=SIN(W4)
7110  O(M)=COS(W4)
7210  NEXT M
7310  GOSUB 10410
7410  C2=-C1/W(K)
7510  C3=C3+C2
7610  V2=-V9/W(K)
7710  V3=0.0+V2
7810  V4=0.0
7910  C4=C5*C5+C3*C3
8010  R(K)=(V4*C5+V3*C3)/C4
8110  I(K)=(C5*V3-V4*C3)/C4
8310  L1=W(K)*T1
8510  L3=R(K)*A(N)
8710  L4=I(K)*A(N)
8720  L5=L1/6.2832
9010  PRINT L5,L3,L4
9020  NEXT K
9025  L4=ABS(L4)
9030  IF L4<2.5 THEN 9100
9040  IF L4=<14 THEN 9105
9060  IF L4<28 THEN 9110
9070  IF L4=<70 THEN 9115
9075  IF L4=<140 THEN 9120
9080  IF L4=<280 THEN 9125
9085  IF L4=<700 THEN 9127
9090  IF L4=<2800 THEN 9129
9095  Z6=0.02
9097  GO TO 9130
9100  Z6=100
9102  GO TO 9130
9105  Z6=20
9107  GO TO 9130
9110  Z6=10
9112  GO TO 9130
```

```
9115  Z6=4
9117 GO TO 9130
9120  Z6 =2
9122 GO TO 9130
9125  Z6=1
9126 GO TO 9130
9127  Z6=0.4
9128 GO TO 9130
9129  Z6=0.1
9130 PRINT "Z";N;".AS","Y=";200/Z6;"OHMS"
9140  Z6=Z6*A(N)
9200  I$="DTA1:Z"&STR$(N)&".AS"
9210 FILEV#2:I$
9310 FOR K=1 TO INT(N1)
9410 PRINT#2:INT(R(K)*Z6*K2+0.5);PNT(44);INT(I(K)*Z6*Z9+.5)
9510 NEXT K
10210 CLOSE#2
10310 GO TO 13710
10410  H5=0.0
10510  H6=0.0
10610  H7=0.0
10710 FOR J=2 TO P1
10810  B8=C(J)
10910  B9=C(J-1)
11010  X1=W(K)
11110  X2=X1*X1
11210  D6=S(J)
11310  D7=S(J-1)
11410  D8=O(J)
11510  D9=O(J-1)
11610  E1=(B8-B9)/(X2*(T(J)-T(J-1)))
11710  E2=E1*D6-B8*D8/X1-E1*D7+B9*D9/X1
11810  E3=E1*D8+B8*D6/X1-E1*D9-B9*D7/X1
11910  E2=-E2
12010  H5=H5+E3
12110  H6=H6+E2
12210 NEXT J
13310 C5=H5
13410 C3=H6
13610 RETURN
13710 NEXT N
13800 END
```

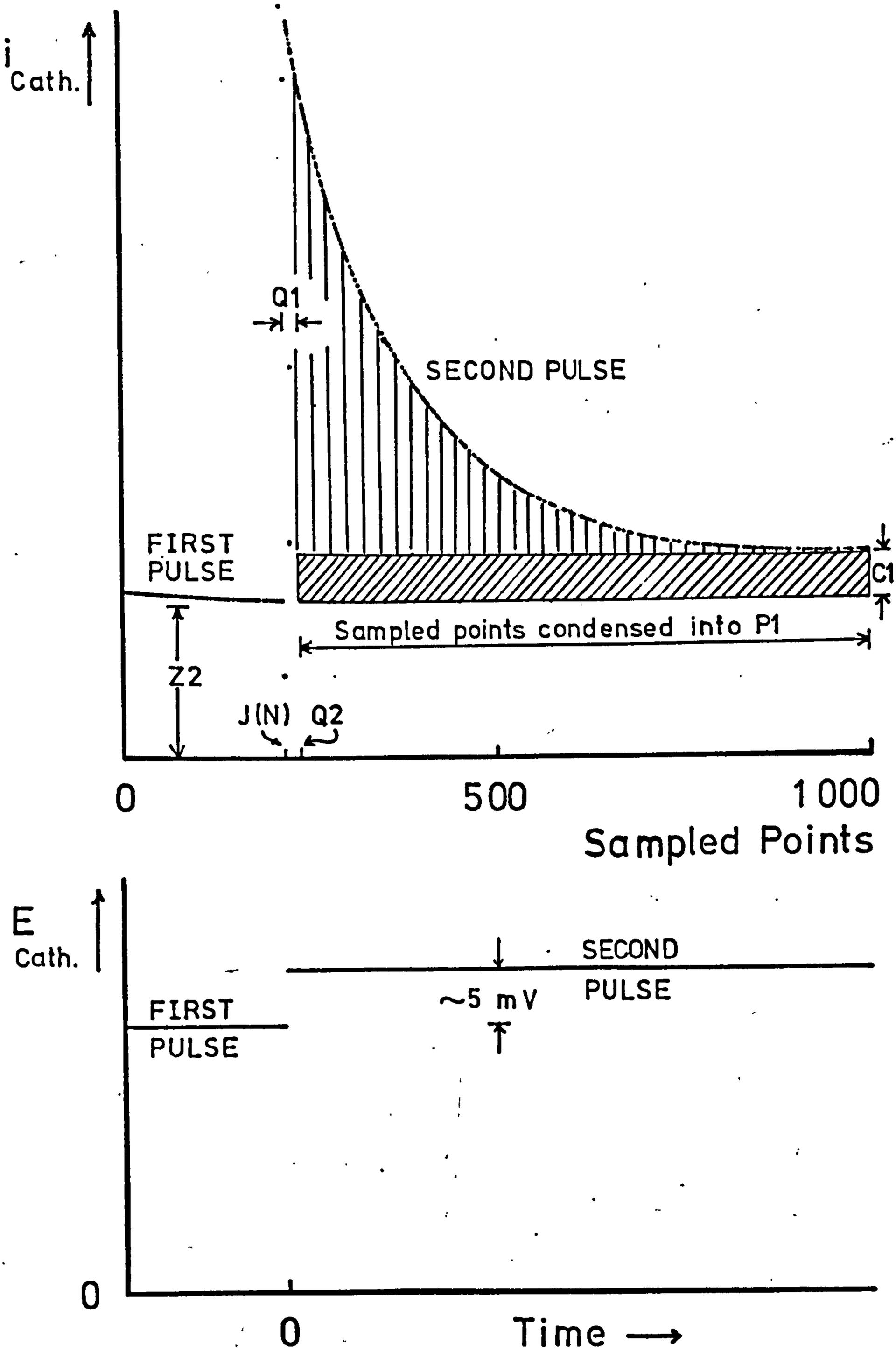

Fig. 2.5 Potential profile (bottom) and current response (top) as used to calculate the impedance spectrum from a double pulse. Some variables used in the JAH and Z8 programmes are indicated.

```
Z9Q      BA     3.Ø      3Ø-MAY-77

Ø REM-IMAG. AXIS LAPLACE TRANSFORM
1Ø DIM C(1ØØ6)
2Ø DIM S(55Ø),T(55Ø),O(55Ø)
3Ø DIM W(62),R(62),I(62)
21Ø FILEN#1:"DTA1:AL2.DA"
31Ø FOR I=1 TO 1ØØ6
41Ø INPUT#1:C(I)
51Ø C(I)=-1*C(I)/Ø.2Ø9715E+7
61Ø NEXT I
71Ø CLOSE#1
72Ø K2=.8975
73Ø Z9=1.Ø45
74Ø Q4=INT(2ØØ*Z9+Ø.5)
75Ø Q5=INT(4ØØ*K2+Ø.5)
81Ø PRINT"ENTER START AND FINAL POINT FOR LISTING"
91Ø INPUT Z3,Z4
1Ø1Ø FOR I=Z3 TO Z4
111Ø PRINT "C";I;"=";C(I)
121Ø NEXT I
131Ø PRINT "MORE INSPECTION? (Y FOR YES)"
132Ø INPUT Z$
133Ø IF Z$="Y" THEN 81Ø
134Ø PRINT "PLOT PULSE? (Y OR N)"
1345 INPUT K$
135Ø IF K$="N" THEN 178Ø
1512 Z5=2ØØ
1513 Z6=2
1514 REM" C FACTOR AND POINT DIV."
153Ø K5=7
1535 K6=8Ø6
1545 FILEV#3:"DTA1:DP"
155Ø FOR K=K5 TO K6
1552 L1=C(K)
1555 C(K)=INT(C(K)*Z9*Z5+Ø.5)
156Ø P=INT((K-K5)*K2/Z6+Ø.5)
1565 PRINT#3:P;PNT(44);C(K)
1567 C(K)=L1
157Ø NEXT K
1575 FOR K=Ø TO 2ØØ STEP 2
158Ø PRINT#3:Ø;PNT(44);K
1585 NEXT K
159Ø FOR X=Ø TO 5
1595 PRINT#3:X;PNT(44);Q4
16ØØ NEXT X
1605 FOR T=Ø TO 4ØØ STEP 5
1610 PRINT#3:T;PNT(44);Ø
1615 NEXT T
1620 FOR Y=Ø TO 5
1625 PRINT#3:Q5;PNT(44);Y
163Ø NEXT Y
1635 CLOSE#3
1636 PRINT "PLOT P?"
1637 INPUT B$
1638 IF B$="N" THEN 178Ø
164Ø G5=813
1645 G6=1ØØ6
165Ø G8=Ø.5
```

```
1655 FILEV#4:"DTA1:P"
1660 FOR I=G5 TO G6
1662 L1=C(I)
1670 C(I)=INT(C(I)*Z5*Z9+0.5)
1675 P=INT((I-G5+1)*(K2/G8)+0.5)
1680 PRINT#4:P;PNT(44);C(I)
1682 C(I)=L1
1685 NEXT I
1690 FOR Y=0 TO 200 STEP 2
1695 PRINT#4:0,PNT(44);Y
1700 NEXT Y
1705 FOR X=0 TO 5
1710 PRINT#4:X;PNT(44);Q4
1715 NEXT X
1720 FOR X=0 TO 400 STEP 5
1725 PRINT#4:X;PNT(44);0
1730 NEXT X
1735 FOR Y=0 TO 5
1740 PRINT#4:Q5;PNT(44);Y
1745 NEXT Y
1750 CLOSE#4
1780 PRINT" S OF SECOND PULSE"
1790 INPUT Z8
1810 PRINT "POINTS OF DELAY"
1910 INPUT Q1
2010 Z2=(C(Z8-1)+C(Z8-2))/2
2110 PRINT "ENTER AMPL.FACTOR"
2115 INPUT Z7
2170 Z9=-Z9
2310 PRINT "RATE IN SEC"
2410 INPUT O
2510 PRINT "POINTS"
2610 INPUT P1
2650 PRINT"WI,WF,JUMP(V)"
2655 INPUT T,B,V9
2700 P2=P1+Q1+Z8
2710 C1=C(P2)
2720 C1=C1-Z2
2810 T1=1/O
2850 T(1)=0
2870 C(1)=C(Z8+Q1)
2871 C(1)= C(1)-Z2-C1
2910 FOR K=2 TO INT(P1+0.3)
3010 T(K)= Q1*O+O/2+(K-2)*O
3110 T(K)=T(K)*T1
3210 C(K)=C(Z8+Q1+K-2)-Z2-C1
3310 NEXT K
3320 C(1)=C(1)**2/C(2)
3810 C=1
3910 V=1
4210 W1=T*1.0/T1
4310 W2=B*1.0/T1
4410 W(1)=W1
4510 A=(LOG(W2/W(1)))/2.303
4610 I=ABS(A)
4710 N1=I*20
4810 N=1
4910 W3=0.1*W(1)
```

```
5010 FOR K=2 TO N1
5110 W(K)=W(K-1)-W3
5210 N=N+1
5310 IF INT(N+0.3)=5 THEN 5710
5340 IF INT(N+0.3)=11 THEN 5710
5350 IF INT(N+0.3)=15 THEN 5740
5370 IF INT(N+3.3)=20 THEN 5760
5390 GO TO 6310
5710 W3=0.5*W3
5730 GO TO 6310
5740 W3=0.8*W3
5750 GO TO 6310
5760 W3=.5*W3
5780 N=1
6310 NEXT K
6410 PRINT DAT$(X)
6510 PRINT "RADIANS","RE(Z)","IM(Z)","HERZ"
6610 PRINT
6710 FOR K=1 TO INT(N1)
6810 FOR M=1 TO INT(P1+0.3)
6910 W4=(W(K)*T(M))
7010 S(M)=SIN(W4)
7110 O(M)=COS(W4)
7210 NEXT M
7310 GOSUB 10410
7410 C2=-C1/W(K)
7510 C3=C3+C2
7610 V2=-V9/W(K)
7710 V3=0.0+V2
7810 V4=0.0
7910 C4=C5*C5+C3*C3
8010 R(K)=(V4*C5+V3*C3)/C4
8110 I(K)=(C5*V3-V4*C3)/C4
8210 F7=C8-C2
8310 L1=W(K)*T1
8510 L3=R(K)*Z7
8710 L4=I(K)*Z7
9010 PRINT INT(L1+0.2),L3,L4,INT(L1/6.2832+0.5)
9110 NEXT K
9120 PRINT"AMPL. FACTOR (PLOT)"
9130 INPUT Z6
9210 FILEV#2:"DTA1:D.DA"
9310 FOR K=1 TO INT(N1)
9410 PRINT#2:INT(R(K)*Z6*K2+0.5);PNT(44);INT(I(K)*Z6*Z9+.5)
9510 NEXT K
9610 FOR X=0 TO 400 STEP 5
9710 PRINT#2:X;PNT(44);0
9810 NEXT X
9820 FOR Y=0 TO 6
9830 PRINT#2:Q5;PNT(44);Y
9840 NEXT Y
9910 FOR Y=0 TO 200 STEP 2
10010 PRINT#2:0;PNT(44);Y
10110 NEXT Y
10120 FOR X=0 TO 6
```

```
10130 PRINT#2:X;PNT(44);Q4
10140 NEXT X
10210 CLOSE#2
10310 GO TO 13710
10410 H5=0.0
10510 H6=0.0
10610 H7=0.0
10690 P1=INT(P1+0.2)
10700 G1=S(P1)
10820 N2=INT(P1-1+0.2)
10821 G2=S(N2)
10822 G3=O(P1)
10823 G4=O(N2)
10824 G5=(C(P1)-C(N2))/(W(K)*W(K)*(T(P1)-T(N2)))
10825 G6=(G5*G1)-(C(P1)*G3/W(K))-(G5*G2)+(C(N2)*G4/W(K))
10826 G7=(G5*G3)-(C(P1)*G1/W(K))-(G5*G4)-(C(N2)*G2/W(K))
10827 G6=-G6
10828 H6=H6+G6
10829 H5=G7+H6
11830 FOR J=3 TO P1 STEP 2
11840 X1=T(J)
11842 X3=T(J-1)
11844 X5=T(J-2)
11846 X7=C(J)
11847 X8=C(J-1)
11848 X9=C(J-2)
11850 D1=(X3-X5)*(X1-X3)*(X5-X1)
11860 D2=((X8-X9)*(X1-X3)-(X7-X8)*(X3-X5))/D1
11870 D3=(X8-X9)/(X3-X5)-D2*(X3+X5)
11890 D5=S(J)
11900 D6=S(J-2)
11910 D8=O(J)
11920 D9=O(J-2)
11930 E1=W(K)*W(K)
11940 E2=W(K)*E1
11950 Y1=X7/W(K)
11955 Y2=X9/W(K)
11960 Y3=(D3+2*D2*X1)/E1
11965 Y4=(D3+2*D2*X5)/E1
11970 Y5=2*D2/E2
11980 E3=Y1*D5+Y3*D8-Y5*D5-Y2*D6-Y4*D9+Y5*D6
11990 H5=H5+E3
12000 E7=-Y1*D8+Y3*D5+Y5*D8+Y2*D9-Y4*D6-Y5*D9
12010 E7=-E7
12020 H6=H6+E7
12021 E8=-2*D2/E2
12022 E9=EXP(-W(K)*X1)
12023 F1=EXP(-W(K)*X5)
12024 F2=-X7/W(K)
12025 F3=-X9/W(K)
12026 F4=-(D3+2*D2*X1)/E1
12027 F5=-(D3+2*D2*X5)/E1
12028 F8=E9*(F2+F4+E8)-F1*(F3+F5+E8)
12029 H7=H7+F8
12210 NEXT J
13310 C5=H5
13410 C3=H6
13510 C8=H7
13610 RETURN
13710 PRINT "AGAIN? (Y FOR YES)"
13720 INPUT A$
13730 IF A$="Y" THEN 210
13800 END

READY
```

see Fig. 2.1, and thus alleviates the necessity of sampling the applied potential profile. The real, R(K), and imaginary, I(K), components of the impedance are then calculated (lines 8010, 8110 respectively) and printed on the teletype (lines 6515, 6520, and 8310 to 9010).

From lines 9025 to 10210 the imaginary and real parts of the calculated impedance are scaled and stored in a file Z#.AS to be plotted via PIP, the PLT: handler and the XY recorder, into a complex impedance plane plot. The value XXX of the ordinate marker (which has been scaled to be 10 cm when the 0.2 V/cm sensitivity in the Y preamplifier is used) is printed out by the teletype as Y=XXX OHMS. The abscissa marker is set to 20 cm when the X preamplifier has 0.2 V/cm sensitivity and has a value of 2Y.

After this, the program returns to line 700 to process the next RUN#.CO file, until all are processed. The plotting procedure under the PIP program is similar to the outlined for the FT program, so it will not be repeated here.

II·5·3

Z8 Program

A version of this program using the quadratic approximation was named Z9Q, a listing is given in this section. The LT subroutine calculates the transforms according to Equations A·56 and A·57. The interactive section gathers information for one run only, including a delay facility for the case that potentiostat rise time is significant.

II.6. Software Accuracy Test

II.6.1. Introduction

Synthetic and experimental data was used to test the FFT or LT software against theoretical results derived in Appendix C. The synthetic

data was chosen to simulate the range of responses expected to occur in typical electrochemical systems, namely an exponential and an inverse square root transient falls. The experiment chosen was the reduction of lead on the HMDE, a reaction known to be reversible.

II.6.2. Exponential Transient

We will here examine the results obtained when applying the FFT or LT programs to the transient fall

$$i(t) = k_1 e^{-k_2 t} = k_1 e^{-k_2 R n} \tag{2.17}$$

as the response to a square pulse i.e. E(t) is a constant E. Where R is the sampling rate and n=0,1,2,...N-1.

II.6.2.a. FFT Impedance

Fig. 2.6 shows a schematic diagram of the current and potential transients as used in the impedance spectrum calculation with the FFT software.

For the current exponential transient outlined in C3 the real and imaginary Fourier coefficients are given by

$$A_r = -\frac{2 k_2 N R \cos \pi r}{k_2^2 N^2 R^2 + 4\pi^2 r^2} \tag{2.18}$$

$$B_r = -j \frac{4\pi r \cos \pi r}{k^2 N^2 R^2 + 4\pi^2 r^2} \tag{2.19}$$

when $T = 2\tau = NR$ and $T - \tau$ is large, (see Appendix C, Equations C12 and C13, for derivation).

In Table 2.1 the accuracy of the FFT performed by the DAQUAD

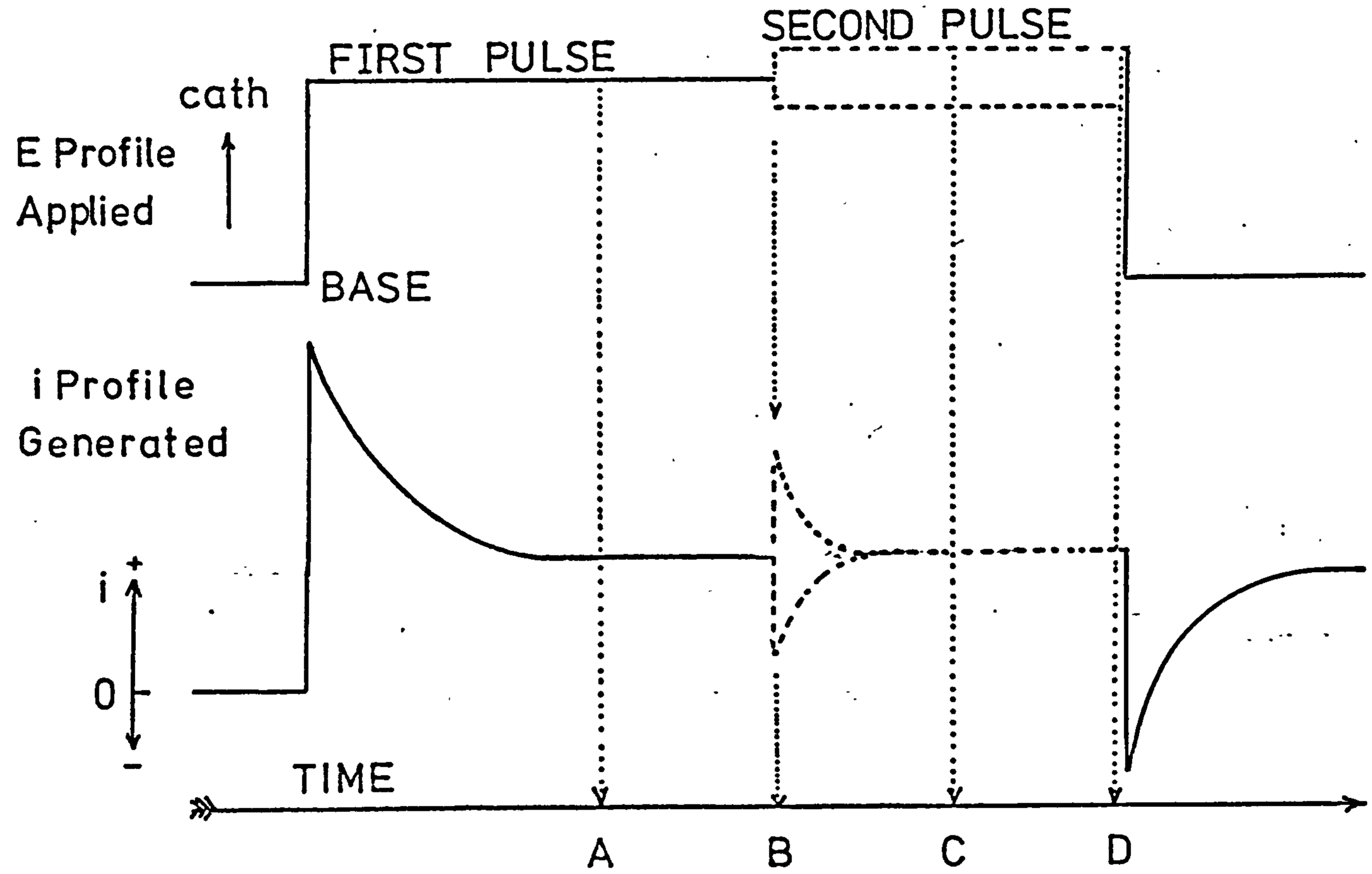

Fig. 2.6. Schematic diagram of the potential and current transients used in the transform method to calculate impedance. Typically the FFT method uses epoch AC, and the LT method uses an epoch starting at B. Time D is the limit for both methods.

TABLE 2.15. Value of deduced from LT impedance determinations from experimental graphs 2.20 and 2.21, according to = $Z(Im)/(2\ f)^{\frac{1}{2}}$

f/Hz	Z(Im)/	/ $s^{-\frac{1}{2}}$
642.8	-8.43	-535
500	-12.7	-711
285.7	-14.9	-631
196.4	-18.67	-656
178.5	-14.67	-491
100	-18.84	-472
71.42	-21.56	-456
50	-28.48	-504
35.7	-32.63	-488
32.14	-35.9	-510
21.42	-43.65	-507
16.0	-51.27	-513
10.7	-55.94	-459
	=	518 AVERAGE

program is evaluated by comparison with the theoretical values. The real and imaginary coefficients Y_r outputted by DAQUAD are converted into the real and imaginary Fourier coefficients A_r and B_r, respectively, according to Equation (2.16), and then compared with the theoretical results given by Equations (2.18) and (2.19). It can be seen that a good accuracy is obtained at low frequencies because the values of Y_r are high for both real and imaginary parts. The accuracy decreases as the values of Y_r become smaller, since the rounding off errors of the single precision calculations of the DAQUAD program become significant. However the imaginary Fourier coefficients B_r show an accuracy within 20% up to a value of r=71. A steeper transient fall ($R > 0.01$) will improve the accuracy in the high frequency region while in the low frequency region the accuracy will decrease. A flatter exponential transient fall ($R < 0.01$) will give the opposite effect.

The general theoretical impedance spectrum for an exponential current transient is derived in Appendix C from Equation (2.10). It is given by

$$Z(2\pi r/T) = \left[\frac{ET(k_2 + j2\pi r/T)\left(e^{-j2\pi r\tau/T} - 1\right)}{e^{-j2\pi r\tau/T} - e^{-k_2(T-\tau)}} \right] \qquad (2.20)$$

Artificial exponential transients with different values of τ/T gave results which behaved as expected from (2.20). However in most of this work a value of $\tau/T=1/2$ was used, since along with the condition $e^{-k_2(T-\tau)} \longrightarrow 0$, lead to a simplification of Equation (2.20), which gives the real and imaginary components of the impedance spectrum as

$$Z(Re) = 2 E k_1^{-1} \qquad (2.21)$$

$$Z(Im) = \frac{2 k_2 E T}{k_1 2\pi r} \qquad (2.22)$$

for r = 1,3,5, ... (N-1)/2 (see Appendix C for derivation).

In order to avoid dependance of the rate of sampling R and magnitude parameters of the transients, complex plane plots were made with the equivalent of Equations (2.21) and (2.22) in the non-dimensional forms

$$Z(Re)^{\circ} = Z(Re)\, k_1 E^{-1} = 2 \tag{2.23}$$

$$Z(Im)^{\circ} = Z(Im)\, k_1 k_2^{-1} E^{-1} R^{-1} = \frac{N}{2\pi r} \tag{2.24}$$

where each point of the plot corresponds to a frequency given by the non-dimensional group fR in which f is the frequency in hertz given by

$$f = \frac{1}{r R} \tag{2.25}$$

One of these plots is shown in Fig. 2.7 for the data generated according to Equations C.1 and C.2 with R=0.01 and N=1024. This data was converted into the frequency domain with the FFT software and the results compared with those obtained from Equations (2.23) and (2.24). A reasonable agreement is observed for frequencies bigger than that given by fR=0.0127. For smaller values of R, i.e. as the current transient gets flatter, the accuracy of the FFT software diminishes in the high frequency region and augments in the low frequency region.

In Fig. 2.8 a value of R=0.1 was used to generate the exponential current transient. There is an acceptable agreement with the theoretical values obtained, for frequency values satisfying fR $>$ 0.036, down to the minimum frequency value corresponding to fR=0.000976. For R $>$ 0.1 values, the accuracy of the FFT software diminishes in the low frequency region, although it improves in the high frequency region of the impedance spectra. These limitations are due to the truncation errors associated with the

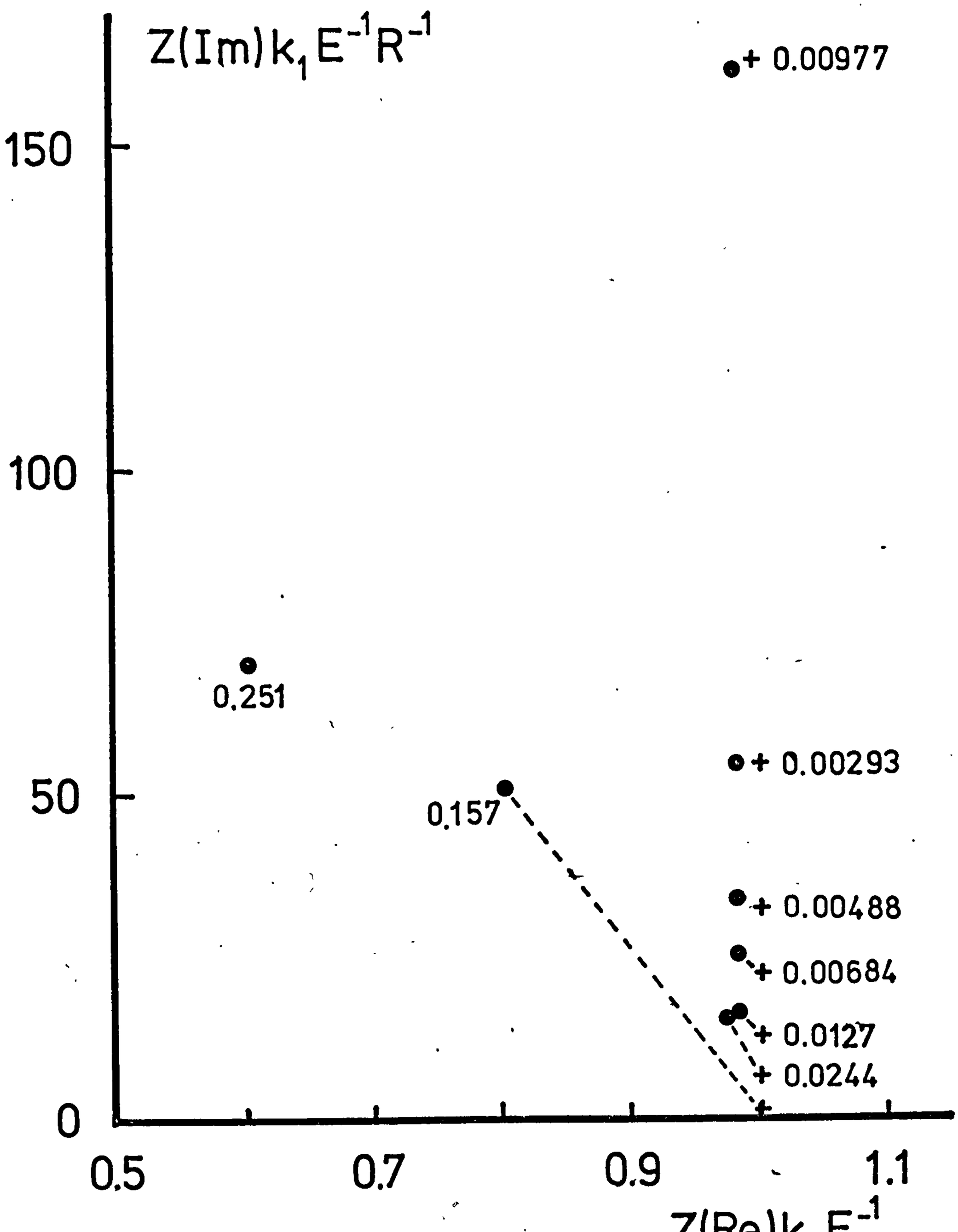

Fig. 2.7 Complex impedance plane plot in non dimensional form for the test data generated according to Eqs. C.1 and C.2 with R = 0.01 and N = 1024. (●) Results obtained with the FFT software. (+) Theoretical results given by Eqs. 2.23 and 2.24. Figures indicate corresponding fR value.

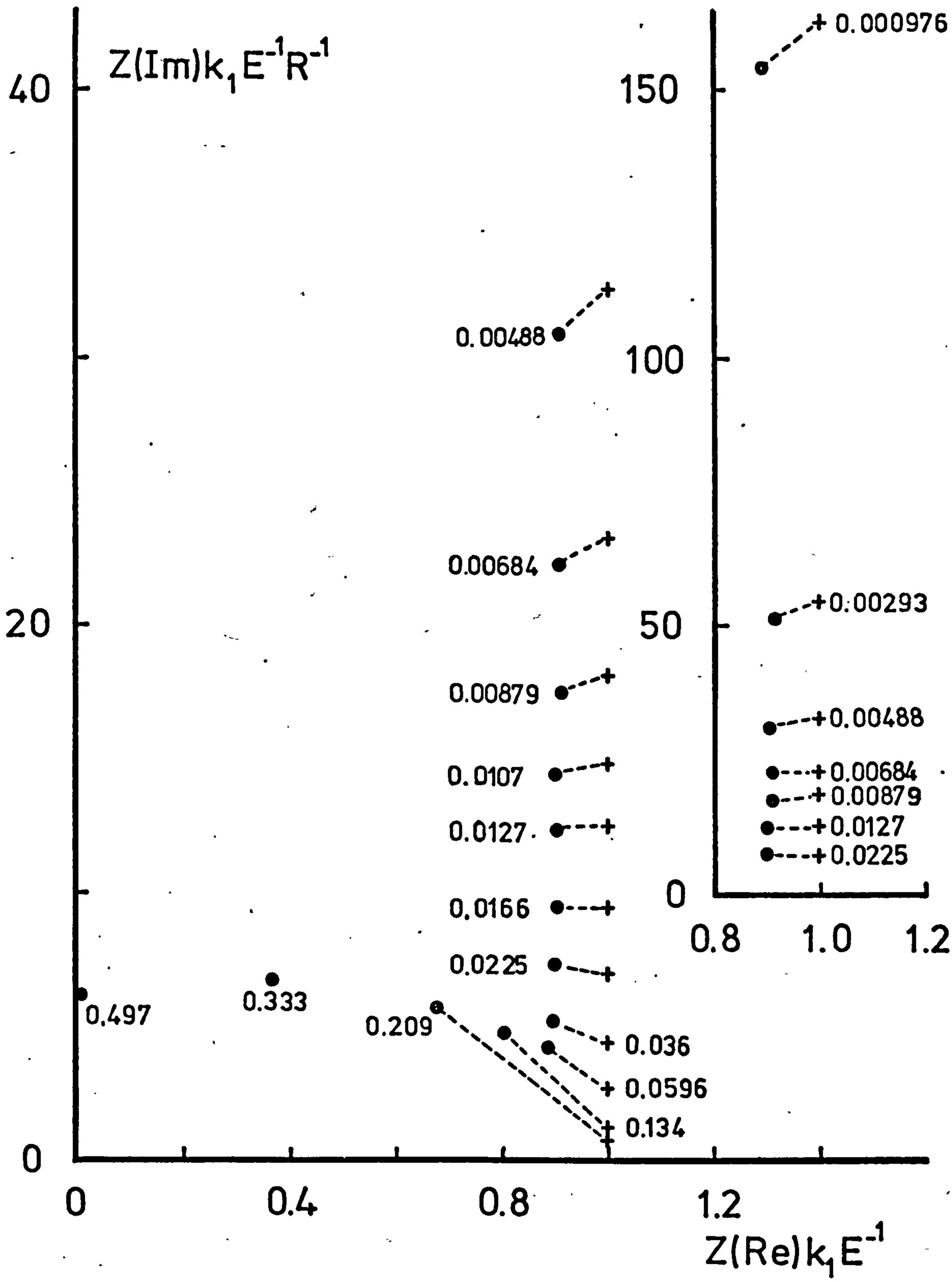

Fig. 2.8 Complex impedance plane plot in non dimensional form for the test data generated according to Eqs. C.1 and C.2 with R = 0.1 and N = 1024. (●) Results obtained from the FFT software. (+) Theoretical values according to Eqs. 2.23 and 2.24. Figures on graph indicate the corresponding fR values.

single precision calculations, as already explained for the Fourier coefficients calculated by DAQUAD.

Since the potential perturbation is a well known function of time, (which modern wave generators can approach very closely), we can use the theoretical coefficients C_r and D_r instead of the less accurate ones obtained with the FFT software, in order to obtain improved accuracy in the impedance spectra, for both the experimental and synthetic current transients. For the case of the step pulse, the Fourier coefficients derived in Appendix C (Equations C.18 and C.19) are

$$C_r = 0 \tag{2.26}$$

$$D_r = j \frac{E(\cos(\pi r) - 1)}{\pi r} \tag{2.27}$$

II.6.2.b. Imaginary Axis LT Impedance

The theoretical impedance spectrum for the exponential current transient described by Equation C.33 resulting from the potential step perturbation at t = 0, as described by Equation C.32, is obtained from the imaginary axis LT in Appendix C, as

$$Z(j\omega) = \frac{E}{k_1} - j \frac{k_2 E}{k_1 \omega} \tag{2.28}$$

The real and imaginary parts of this impedance spectrum are expressed in a non-dimensional form as

$$Z(Re)^\circ = Z(Re)\, k_1 E^{-1} = 1 \tag{2.29}$$

$$Z(Im)^\circ = Z(Im)\, k_1 k_2^{-1} E^{-1} R^{-1} = -\frac{n}{2\pi} \tag{2.30}$$

where the frequency itself is expressed by the non-dimensional group fR.

(see Appendix C).

In Tables 2.2 to 2.7 the theoretical result given by (2.30) is compared with the result obtained with the LT software when using the linear approximation. The real component is compared against unity as prescribed in Equation (2.29). The synthetic exponential transients used were prepared according to Equation C.33 giving different values to R. This means that for a given number of sampled points N, the transient is flatter for small values of R.

The transient examined in Table 2.2 is quite steep, the rapidly falling part is covered by too few points and a slight error in the approximation leads to considerable inaccuracy at high frequencies, since as can be observed from Equations A.54 and A.55, for both the real and imaginary parts, high frequencies tend to emphasize the contribution of short time F(t) data to the transform, while at low frequency the short time F(t) data contribute relatively less to the transform. That is why an improvement in the accuracy is observed at low fR values in Tables 2.2 to 2.7.

The transient examined in Table 2.4 is a flatter one and improved accuracy in the high frequency side is observed by comparison with the results of Table 2.2. However the low frequency accuracy is poor due to the fact that 200 points is an insufficient length to consider the current level there as "steady state" since the variation from one point to the next is still significant. In Table 2.6 the same transient is examined in a more appropriate length of N=978, the results show a definite improvement in accuracy. The most accurate results were obtained, however, with the transient with R=0.1, shown in Table 2.3 for N=200 and Table 2.5 for N=968 points. The transient is not too steep nor too flat and both lengths are appropriate, although the longer length (N=968) gives slightly more accuracy and naturally renders lower frequency results. In Tables 2.3 and 2.5 the imaginary part has an accuracy of 0.1% and the real part 0.08% at fR=0.2

TABLE 2.2. LT impedance results in non-dimensional form for the test data defined by Eqs. C.32 and C.33 (exponential response). Compared with the theoretical $Z(Re)^{o} = 1$ and Z(Im) given by Eq.2.30. R = 1, N = 200.

FR R= 1	Z(RE)Ø	Z(IM)Ø	Z(IM)Ø THEOR.
1	1	.272876E-ØØ7	-Ø.159155
Ø.9	Ø.926257	-3.Ø465Ø43	-Ø.176838
Ø.8	Ø.9Ø9848	-Ø.1Ø9952	-Ø.198943
Ø.699999	Ø.911624	-Ø.161894	-Ø.227364
Ø.599999	Ø.916183	-Ø.212Ø26	-Ø.265258
Ø.549999	Ø.918368	-Ø.23954	-Ø.289372
Ø.499999	Ø.92Ø345	-Ø.27Ø758	-Ø.318309
Ø.449999	Ø.922Ø88	-Ø.3Ø7114	-Ø.353677
Ø.399999	Ø.923601	-Ø.351116	-Ø.397887
Ø.349999	Ø.924893	-Ø.4Ø6394	-Ø.454728
Ø.299999	Ø.925979	-Ø.478879	-Ø.53Ø517
Ø.274999	Ø.926449	-Ø.524583	-Ø.578746
Ø.249999	Ø.926873	-Ø.579151	-Ø.63662
Ø.224999	Ø.927251	-Ø.645564	-Ø.7Ø7357
Ø.199999	Ø.927587	-Ø.728283	-Ø.795776
Ø.179999	Ø.927825	-Ø.81Ø779	-Ø.884197
Ø.159999	Ø.928Ø36	-Ø.913687	-Ø.994722
Ø.139999	Ø.928223	-1.Ø4577	-1.1Ø683
Ø.119999	Ø.928382	-1.22161	-1.3263
Ø.Ø99999	Ø.928515	-1.4675	-1.59156
Ø.Ø89999	Ø.928574	-1.6313	-1.7684
Ø.Ø79999	Ø.928624	-1.83596	-1.98945
Ø.Ø69999	Ø.92867	-2.Ø9899	-2.27367
Ø.Ø59999	Ø.928707	-2.44958	-2.65262
Ø.Ø54999	Ø.928727	-2.67264	-2.89377
Ø.Ø49999	Ø.928744	-2.94Ø27	-3.18315
Ø.Ø44999	Ø.928757	-3.26734	-3.53684
Ø.Ø39999	Ø.928773	-3.67616	-3.97896
Ø.Ø34999	Ø.928789	-4.2Ø172	-4.5474
Ø.Ø29999	Ø.928805	-4.9Ø243	-5.3Ø533
Ø.Ø27499	Ø.928818	-5.34833	-5.78765
Ø.Ø24999	Ø.928824	-5.88339	-6.36643
Ø.Ø22499	Ø.928838	-6.53738	-7.Ø7385
Ø.Ø19999	Ø.928867	-7.3549	-7.95812
Ø.Ø17999	Ø.928897	-8.1725	-8.8424
Ø.Ø15999	Ø.928934	-9.19436	-9.94777
Ø.Ø13999	Ø.928974	-1Ø.5Ø84	-11.369
Ø.Ø11999	Ø.929Ø56	-12.26Ø4	-13.264
Ø.ØØ999991	Ø.929181	-14.7145	-15.917
Ø.ØØ8999	Ø.929317	-16.35Ø6	-17.6858
Ø.ØØ799991	Ø.929554	-18.3968	-19.8968
Ø.ØØ6999	Ø.929736	-21.Ø271	-22.7396
Ø.ØØ5999	Ø.929778	-24.5348	-26.53Ø1
Ø.ØØ549991	Ø.929889	-26.7686	-28.9424
Ø.ØØ4999	Ø.93Ø44	-29.45Ø3	-31.8372
Ø.ØØ4499	Ø.933696	-32.7259	-35.3755

TABLE 2.3. Impedance results in non-dimensional form obtained with the LT software. Test data according to Eqs. C.32 and C.33 with R = 0.1, N = 200. A comparison is made with the theoretical results

FR , R= 0.1	$Z(Re)^o$	$Z(Im)^o$	$Z(Im)^o_{theor.}$
0.99999	0.999987	.935648E-008	0.0159155
0.899999	0.997045	-0.0171624	0.0176838
0.8	0.998241	-0.0197205	0.0198943
0.7	0.998655	-0.0226362	0.0227364
0.6	0.998852	-0.0264522	0.0265258
0.55	0.998921	-0.0288705	0.0289372
0.5	0.998978	-0.0317718	0.0318309
0.45	0.999019	-0.0353088	0.0353677
0.4	0.999055	-0.0397305	0.0397886
0.35	0.999083	-0.0454139	0.0454727
0.3	0.999098	-0.0529884	0.0530515
0.275	0.999109	-0.0578087	0.0578743
0.25	0.999121	-0.0635929	0.0636618
0.225	0.999127	-0.0706607	0.0707353
0.2	0.999135	-0.079497	0.0795772
0.18	0.99914	-0.0883327	0.0884192
0.16	0.999145	-0.0993767	0.0994715
0.14	0.999141	-0.113574	0.11382
0.12	0.999148	-0.132506	0.132629
0.1	0.999155	-0.159011	0.159154
0.0900001	0.999156	-0.17668	0.176838
0.0800001	0.999157	-0.198767	0.198943
0.07	0.999153	-0.227161	0.227363
0.06	0.999157	-0.265022	0.265257
0.055	0.999159	-0.289116	0.289371
0.05	0.999161	-0.318031	0.318309
0.0450001	0.999162	-0.353357	0.353676
0.0400001	0.999166	-0.397541	0.397886
0.035	0.999166	-0.454334	0.454726
0.0300001	0.999168	-0.530051	0.530514
0.0275001	0.99917	-0.578241	0.578742
0.0250001	0.999172	-0.636067	0.636616
0.0225001	0.999174	-0.706746	0.707351
0.0200001	0.999177	-0.795089	0.79577
0.0180001	0.999184	-0.883438	0.884188
0.0160001	0.999189	-0.993873	0.994711
0.0140001	0.999192	-1.13586	1.13681
0.0120001	0.999189	-1.32517	1.32628
0.0100001	0.999195	-1.59021	1.59153
0.00900006	0.999201	-1.76691	1.76837
0.00800006	0.999204	-1.98778	1.98941
0.00700007	0.999212	-2.27176	2.27361
0.00600007	0.999211	-2.6504	2.65254
0.00550007	0.999203	-2.89134	2.89368
0.00500007	0.999227	-3.18051	3.18305
0.00450006	0.999215	-3.5339	3.53671

$Z(Re)^o_{theor} = 1$ and $Z(Im)^o_{theor}$ given by Eq. 2.30.

TABLE 2.4. Non-dimensional impedance spectrum obtained with the LT software. Test data according to Eqs. C.32 and C.33 with R = 0.01, N = 200. Theoretical results $Z(Re)^{\circ}_{theor} = 1$ and $Z(Im)^{\circ}_{theor}$ given by Eqs. 2.29 and 2.30

FR , R= 0.01	$Z(Re)^{\circ}$	$Z(Im)^{\circ}$	$Z(Im)^{\circ}_{theor.}$
0.99999	1.00137	-0.00000339	0.00159155
0.899999	1.00121	-0.00237339	0.00176838
0.799999	1.00065	-0.0031 9592	0.00198943
0.699999	0.999853	-0.00365152	0.00227364
0.599999	0.999095	-0.00372753	0.00265258
0.549999	0.998812	-0.00366855	0.00289372
0.499999	0.998635	-0.00361045	0.0031 8309
0.449999	0.998547	-0.00355208	0.00353677
0.399999	0.998573	-0.00359965	0.00397887
0.349999	0.998698	-0.0037946	0.00454728
0.299999	0.998894	-0.0042172	0.00530517
0.274999	0.99901	-0.00455055	0.00578745
0.249999	0.999134	-0.00499112	0.0063662
0.224999	0.999267	-0.00556507	0.00707356
0.199999	0.999395	-0.00631817	0.00795776
0.179999	0.999499	-0.00708895	0.00884196
0.159999	0.999598	-0.00806453	0.00994722
0.139999	0.99969	-0.00932738	0.0113682
0.119999	0.999775	-0.0110113	0.013263
0.099999	0.999854	-0.0133632	0.0159156
0.089999	0.999894	-0.0149215	0.017684
0.079999	0.999935	-0.01687	0.0198945
0.069999	0.999971	-0.0193659	0.0227367
0.059999	1.00001	-0.0226764	0.0265262
0.054999	1.00004	-0.0247831	0.0289377
0.049999	1.00007	-0.0273046	0.0318315
0.044999	1.00011	-0.030381	0.0353684
0.039999	1.00015	-0.0342262	0.0397896
0.034999	1.00021	-0.0391607	0.045474
0.029999	1.0003	-0.0457333	0.0530532
0.027499	0.99948	-0.0658155	0.0578764
0.024999	1.00046	-0.0549289	0.0636643
0.022499	0.999224	-0.0803924	0.0707384
0.019999	1.00072	-0.0687082	0.0795812
0.017999	0.992025	-0.0973998	0.088424
0.015999	1.01343	-0.09646	0.0994777
0.013999	0.986012	-0.107409	0.11369
0.011999	1.00851	-0.148885	0.13264
0.00999901	1.00294	-0.13751	0.15917
0.008999	0.97889	-0.165835	0.176858
0.007999	0.979751	-0.21691	0.198968
0.006999	1.01193	-0.25725	0.227396
0.005999	1.03839	-0.262698	0.265301
0.005499	1.03207	-0.262707	0.289424
0.004999	1.01179	-0.274733	0.318372
0.004499	0.984136	-0.306985	0.353755

TABLE 2.5. Non-dimensional impedance spectrum obtained with the LT software. Test data according to Eqs. C.32 and C.33 (exponential response) with R = 0.1, N = 968. A comparison is made with $Z(Im)^{o}_{theor}$ given by Eq. 2.30 and $Z(Re)^{o}_{theor} = 1$.

FR R= Ø.1	Z(RE)Ø	Z(IM)Ø	Z(IM)Ø THEOR.
Ø.2	Ø.999119	-Ø.Ø794917	Ø.Ø795773
Ø.18	Ø.999121	-Ø.Ø883267	Ø.Ø884192
Ø.16	Ø.999129	-Ø.Ø993718	Ø.Ø994716
Ø.14	Ø.999112	-Ø.113563	Ø.113682
Ø.12	Ø.999124	-Ø.132496	Ø.132629
Ø.11	Ø.999128	-Ø.144544	Ø.144686
Ø.Ø99999	Ø.999135	-Ø.159002	Ø.159155
Ø.Ø899999	Ø.999139	-Ø.176669	Ø.176838
Ø.Ø799999	Ø.999144	-Ø.198757	Ø.198943
Ø.Ø699999	Ø.999125	-Ø.227143	Ø.227364
Ø.Ø599999	Ø.999137	-Ø.265003	Ø.265258
Ø.Ø549999	Ø.99914	-Ø.289098	Ø.289372
Ø.Ø5	Ø.999146	-Ø.318014	Ø.318309
Ø.Ø449999	Ø.999153	-Ø.353345	Ø.353677
Ø.Ø4	Ø.999158	-Ø.397521	Ø.397887
Ø.Ø359999	Ø.99916	-Ø.441695	Ø.442Ø96
Ø.Ø319999	Ø.999164	-Ø.496912	Ø.497358
Ø.Ø279999	Ø.999166	-Ø.56788	Ø.56841
Ø.Ø239999	Ø.999176	-Ø.662542	Ø.663145
Ø.Ø199999	Ø.999184	-Ø.795Ø64	Ø.795775
Ø.Ø179999	Ø.999208	-Ø.883412	Ø.884194
Ø.Ø159999	Ø.999217	-Ø.993853	Ø.994719
Ø.Ø139999	Ø.999224	-1.13584	1.13682
Ø.Ø119999	Ø.999227	-1.32516	1.32629
Ø.Ø1Ø9999	Ø.99923	-1.44565	1.44687
Ø.ØØ999994	Ø.999236	-1.59Ø22	1.59155
Ø.ØØ899994	Ø.999248	-1.7669 2	1.76839
Ø.ØØ799994	Ø.999255	-1.9878	1.98944
Ø.ØØ699994	Ø.999278	-2.27184	2.27365
Ø.ØØ599994	Ø.999275	-2.6505	2.6526
Ø.ØØ549994	Ø.999275	-2.89147	2.89375
Ø.ØØ499994	Ø.999291	-3.18Ø65	3.18313
Ø.ØØ449994	Ø.999294	-3.53409	3.53681
Ø.ØØ399994	Ø.99933	-3.97592	3.97892
Ø.ØØ359994	Ø.999319	-4.41771	4.42Ø3
Ø.ØØ319994	Ø.9993	-4.96996	4.97367
Ø.ØØ279994	Ø.999337	-5.68ØØ8	5.68421
Ø.ØØ239994	Ø.999372	-6.62694	6.6316
Ø.ØØ199994	Ø.999394	-7.95276	7.95796
Ø.ØØ179994	Ø.999368	-8.83643	8.8422
Ø.ØØ159994	Ø.999447	-9.94153	9.94752
Ø.ØØ139994	Ø.9994	-11.3622	11.3686
Ø.ØØ119994	Ø.999502	-13.2573	13.2635
Ø.ØØ1Ø9994	Ø.999498	-14.4632	14.4693
Ø.ØØØ99994	Ø.999553	-15.9113	15.9164

TABLE 2.6. Non-dimensional impedance spectrum obtained with the LT software. Test data according to Eqs. C.32 and C.33 (exponential response) with R = 0.01, N = 978. A comparison is made against $Z(Im)^{o}_{theor}$ given by Eq. 2.30 and $Z(Re)^{o}_{theor} = 1$.

FR , R=0.01	$Z(Re)^{o}$	$Z(Im)^{o}$	$Z(Im)^{o}_{theor.}$
0.2	1.00087	-0.00756989	0.00795773
0.18	1.00096	-0.0091 8935	0.00884192
0.16	1.00133	-0.00962266	0.00994716
0.14	1.00075	-0.011462	0.0113682
0.12	1.00152	-0.0132839	0.0132629
0.11	1.001	-0.0147847	0.0144686
0.0999999	1.00086	-0.0156457	0.0159155
0.0899999	1.00149	-0.0174167	0.0176838
0.0799999	1.00134	-0.0202234	0.0198943
0.0699999	1.0008	-0.0227699	0.0227364
0.0599999	1.00124	-0.0261288	0.0265258
0.0549999	1.00153	-0.0287328	0.0289372
0.05	1.00156	-0.0319723	0.0318309
0.0449999	1.00131	-0.035741 1	0.0353677
0.04	1.00098	-0.0401059	0.0397886
0.0359999	1.00022	-0.0458526	0.0442096
0.0319999	0.999168	-0.0508445	0.0497358
0.0279999	0.998968	-0.0561581	0.056841
0.0239999	1.0011	-0.0651787	0.0663145
0.0199999	1.00158	-0.0795149	0.0795775
0.0179999	0.998211	-0.0876451	0.0884194
0.0159999	1.00032	-0.100451	0.0994719
0.0139999	1.00072	-0.112861	0.113682
0.0119999	0.999467	-0.13299	0.132629
0.0109999	1.00026	-0.146015	0.144687
0.00999994	1.00119	-0.159705	0.159155
0.00899994	1.00077	-0.175761	0.176839
0.00799994	0.99808	-0.197283	0.198945
0.00699994	1.00012	-0.228075	0.227365
0.00599994	0.999471	-0.266837	0.26526
0.00549994	1.00196	-0.291258	0.289375
0.00499994	1.00083	-0.318751	0.318313
0.00449994	0.999391	-0.35243	0.353681
0.00399994	1.00198	-0.396834	0.397892
0.00359994	1.0012	-0.441325	0.442103
0.00319994	0.999848	-0.493735	0.497367
0.00279994	0.996989	-0.568241	0.568421
0.00239994	0.998283	-0.662329	0.66316
0.00199994	1.00187	-0.799264	0.795796
0.00179994	1.0038	-0.88134	0.88422
0.00159994	0.996845	-0.989688	0.994751
0.00139994	0.995143	-1.13797	1.13686
0.00119994	0.999924	-1.32624	1.32635
0.00109994	0.998408	-1.44298	1.44693
0.00099994	0.992615	-1.5858	1.59163

TABLE 2.7. Non-dimensional impedance spectrum obtained with the LT software. Test data according to Eqs. C.32 and C.33 with R = 0.001, N = 968. The results are compared against $Z(Im)^{o}_{theor}$ given by Eq.2.30 and $Z(Re)^{o}_{theor} = 1$.

fR	$Z(Re)^{o}$	$Z(Im)^{o}$	$Z(Im)^{o}_{theor}$
0.2	0.969884	0.0752849	0.00079577
0.18	0.97788	-0.0792639	0.00088419
0.16	1.05228	0.071208	0.00099472
0.14	0.926766	-0.0261453	0.0011382
0.12	1.09001	-0.0136227	0.00132629
0.11	0.963577	-0.0728929	0.00144686
0.0999999	0.934416	0.0430733	0.00159155
0.0899999	1.06546	0.0591958	0.00176838
0.0799999	1.02873	-0.0826	0.00198943
0.0699999	0.922829	-0.0138232	0.00227364
0.0599999	0.998569	0.081948	0.00265258
0.0549999	1.07153	0.0505871	0.00289372
0.0499999	1.0836 8	-0.0347855	0.00318309
0.0449999	1.01937	-0.0860374	0.00353677
0.0399999	0.950126	-0.0665485	0.00397887
0.0359999	0.986986	-0.087024	0.00442097
0.0319999	1.03554	-0.0874956	0.00497359
0.0279999	1.06472	-0.0567821	0.0056841 1
0.0239999	1.09839	-0.0135836	0.00663146
0.0199999	1.0783	0.035032	0.00795776
0.0179999	0.928945	-0.054641	0.00884196
0.0159999	1.04	0.0647493	0.00994721
0.0139999	0.974868	-0.086921	0.0113682
0.0119999	1.01373	0.0715136	0.013263
0.0109999	1.08323	-0.0120112	0.0144687
0.0099999	1.00418	-0.100271	0.0159156
0.0089999	0.935957	-0.0374134	0.017684
0.0079999	0.943844	0.0517629	0.0198945
0.0069999	1.10417	0.0246019	0.0227367
0.0059999	1.02943	-0.100499	0.0265262
0.0054999	1.01307	-0.118724	0.0289377
0.0049999	0.935328	-0.0800734	0.0318315
0.0044999	0.892415	-0.0303942	0.0353684
0.0039999	0.964648	0.015667	0.0397896
0.0035999	1.09454	-0.00530424	0.0442108
0.0031999	1.00317	-0.083252	0.0497373
0.0027999	0.903976	-0.0821789	0.056842 8
0.0023999	1.01665	0.00944831	0.066317
0.0019999	1.16781	-0.174685	0.079581
0.0017999	1.01781	0.100904	0.0884239
0.0015999	0.869424	-0.0861798	0.0994775
0.0013999	1.03925	-0.195862	0.11369
0.0011999	0.981502	-0.0175184	0.132639
0.0010999	0.877023	-0.0737803	0.144698
0.0009999	0.833056	-0.186525	0.15917

and at the lower frequency end 0.08% for the imaginary part and 0.07% for the real part at fR=0.0045 The Table 2.7 shows results of a very flat transient, the 968 points are not enough to cover a suitable length, therefore the results are very inaccurate.

II.6.3. $1/\sqrt{t}$ Transient

The $1/\sqrt{t}$ transient as the response to a potential step has been chosen to produce synthetic data more closely resembling experimental reversible reactions. Naturally the data is truncated at the infinite jump, affecting the accuracy specially at the high frequency. In practice this will not be a problem provided that the apparent high frequency resistance E/i(0) is less than the ohmic resistance between the Luggin probe and the working electrode.

II.6.3.a. Imaginary Axis Laplace Transformation

The theoretical impedance spectrum for the $1/\sqrt{t}$ transient described by Equation C.49 resulting from the potential step perturbation described by C.32, is obtained from the imaginary axis LT in Appendix C, (Equation C.56) as

$$Z(j\omega) = \frac{E}{K\sqrt{\pi\omega}} - \frac{E}{K\sqrt{\pi\omega}} \qquad (2.41)$$

The non-dimensional expressions of the real and imaginary parts of the impedance spectrum, given by

$$Z(Re)^* = Z(Re)\,KE^{-1}R^{-1/2} = \frac{\sqrt{n}}{2\pi} \qquad (2.42)$$

$$Z(Im)^* = Z(Im)KE^{-1}R^{-1/2} = -\frac{\sqrt{n}}{2\pi} \qquad (2.43)$$

as a function of the non-dimensional frequency fR=1/n were compared with the results obtained with the LT software suitably modified to suit the truncated data and the various integration approximations.

In order to simulate the way in which the averagers sample in practice, the first attempt to form the current and time arrays for the LT program, was to consider the first point of current sampled at a time equal to half the sampling rate after the onset of the potential step. No extrapolation of current to t=0 was done, assuming the current to be zero until t=R/2. The result of this attempt is shown in Fig. 2.9. It can be seen that a serious distortion occurs at the high frequency end, this is due to the fact that the contribution of the missing first segment to the area under the transient is significant. This area is used in the calculation of the transform (see Equations A.48, A.52 and A.53 in Appendix A). Fig. 2.10 shows the results of a second attempt where the first point of the current array is assigned and arbitrary value of C(0) = 2.048, when E(0)=E at a time T(0)=0. A dramatic improvement in the accuracy is observed. The real component of the impedance is displaced by a roughly constant amount determined by the value of the first data point. The imaginary values are more accurately reproduced. However it is no good for the experimental data to assign a fixed C(0) value. An extrapolation of the first two data points tentatively set as

$$C(0) = C(1)^2 / C(2) \qquad (2.44)$$

was used to obtain the results of Table 2.8 which are slightly less accurate than those of Fig. 2.10, indicating that a better extrapolation is needed. By trial and error the extrapolation

$$C(0) = C(1)^2 \times 3.33 / C(2) \qquad (2.45)$$

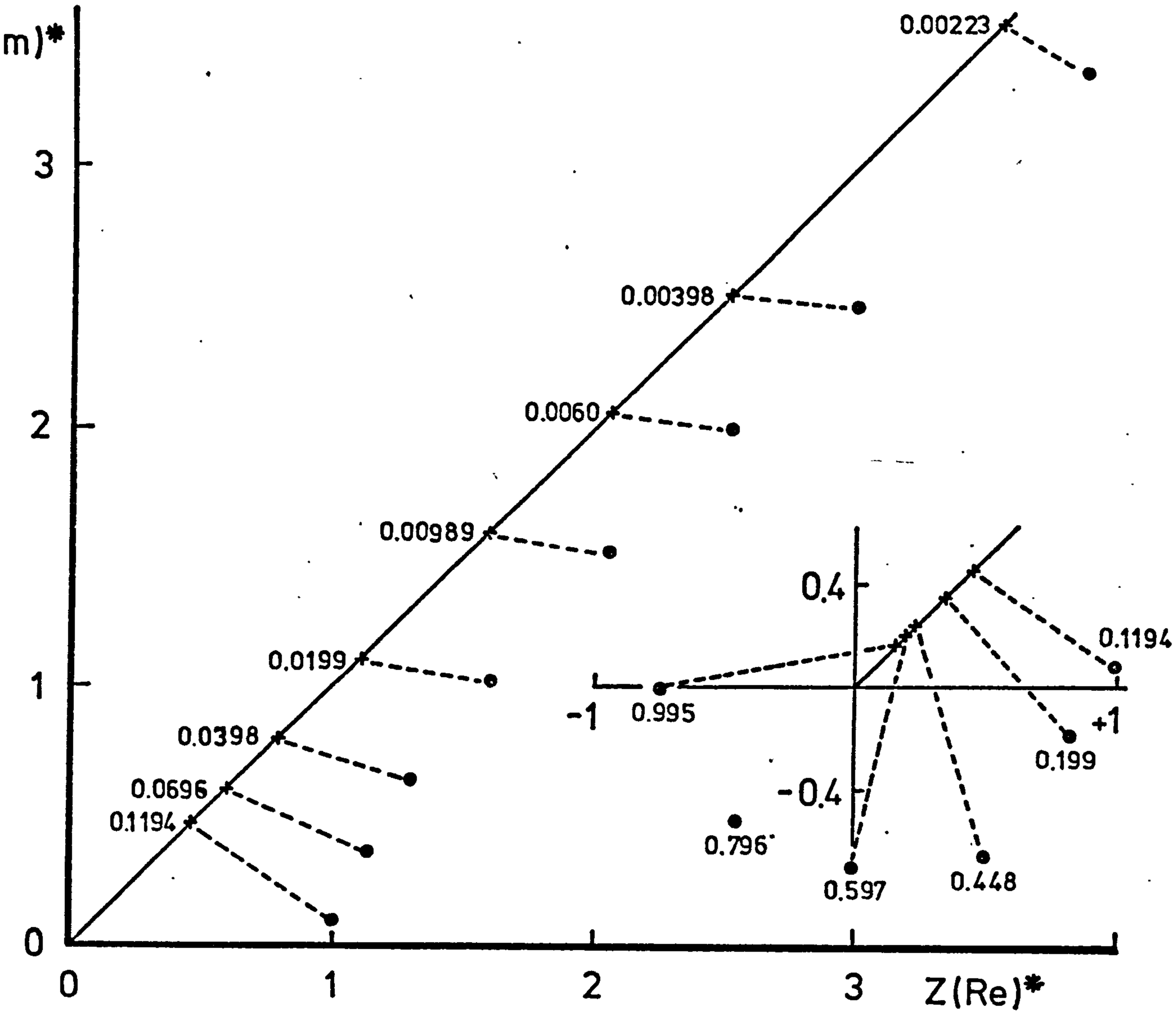

Fig. 2.9. Complex impedance plane plot in non-dimensional form for the test data given by Eqs. C.32 and C.49 ($1/\sqrt{t}$ transient) with C(0) = 0, R = 1, n = 500. (•) Results obtained from LT software. (X) Theoretical values given by Eqs. 2.42 and 2.43. Figures on graph indicate fR values.

Fig. 2.10. Complex impedance plane plot in non-dimensional form for the test data given by Eqs. C.32 and C.49, with C(0) = 2.048, R = 1, n = 500. (●) Results obtained from LT program. (X) Theoretical values given by Eqs. 2.42 and 2.43. Figures on graph indicate corresponding fR values.

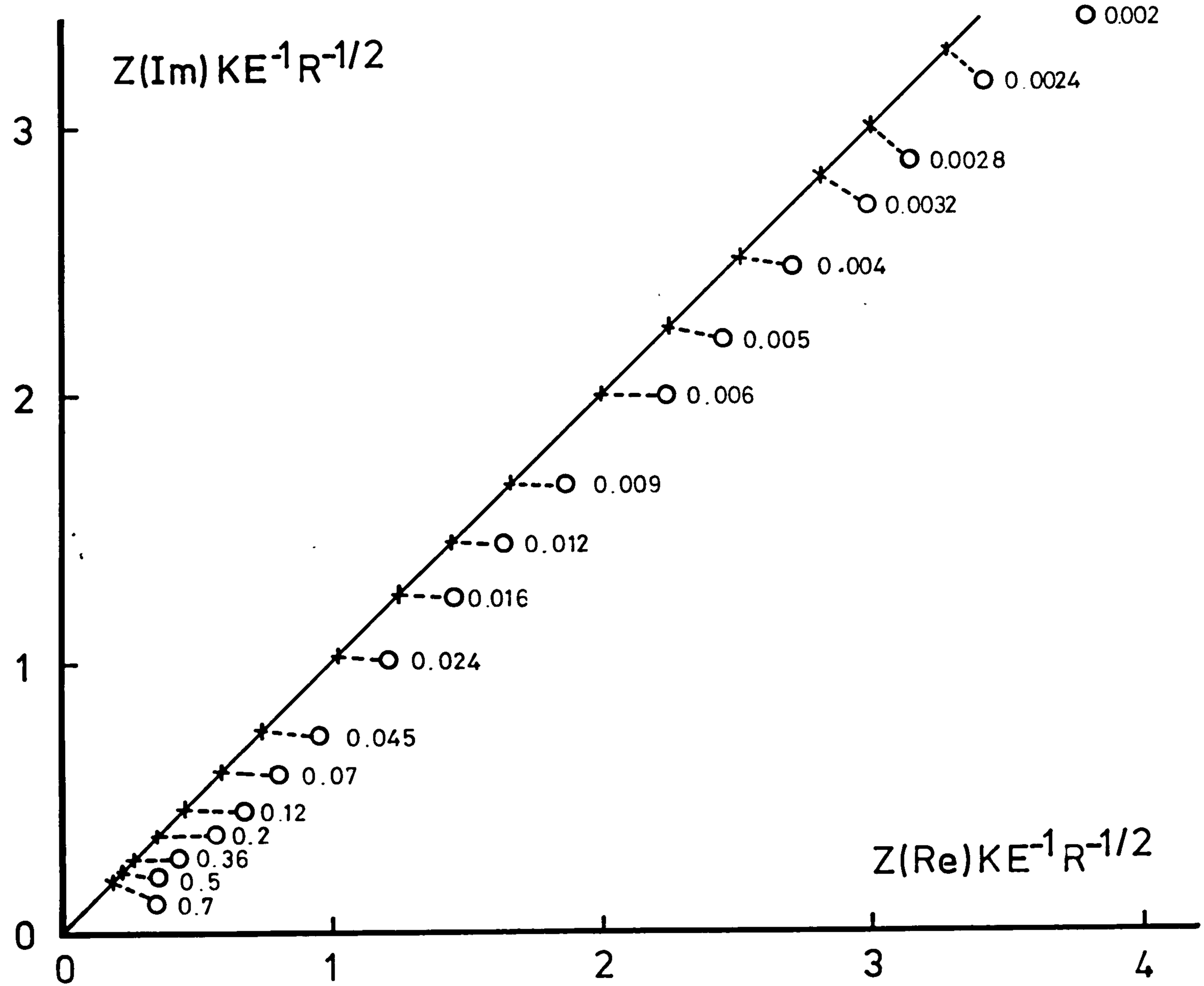
Z(Im) KE-1 R-1/2
3
2
1
0
0
1
2
3
4
Z(Re)KE-1 R-1/2
0.002
0.0024
0.0028
0.0032
0.004
0.005
0.006
0.009
0.012
0.016
0.024
0.045
0.07
0.12
0.2
0.36
0.5
0.7

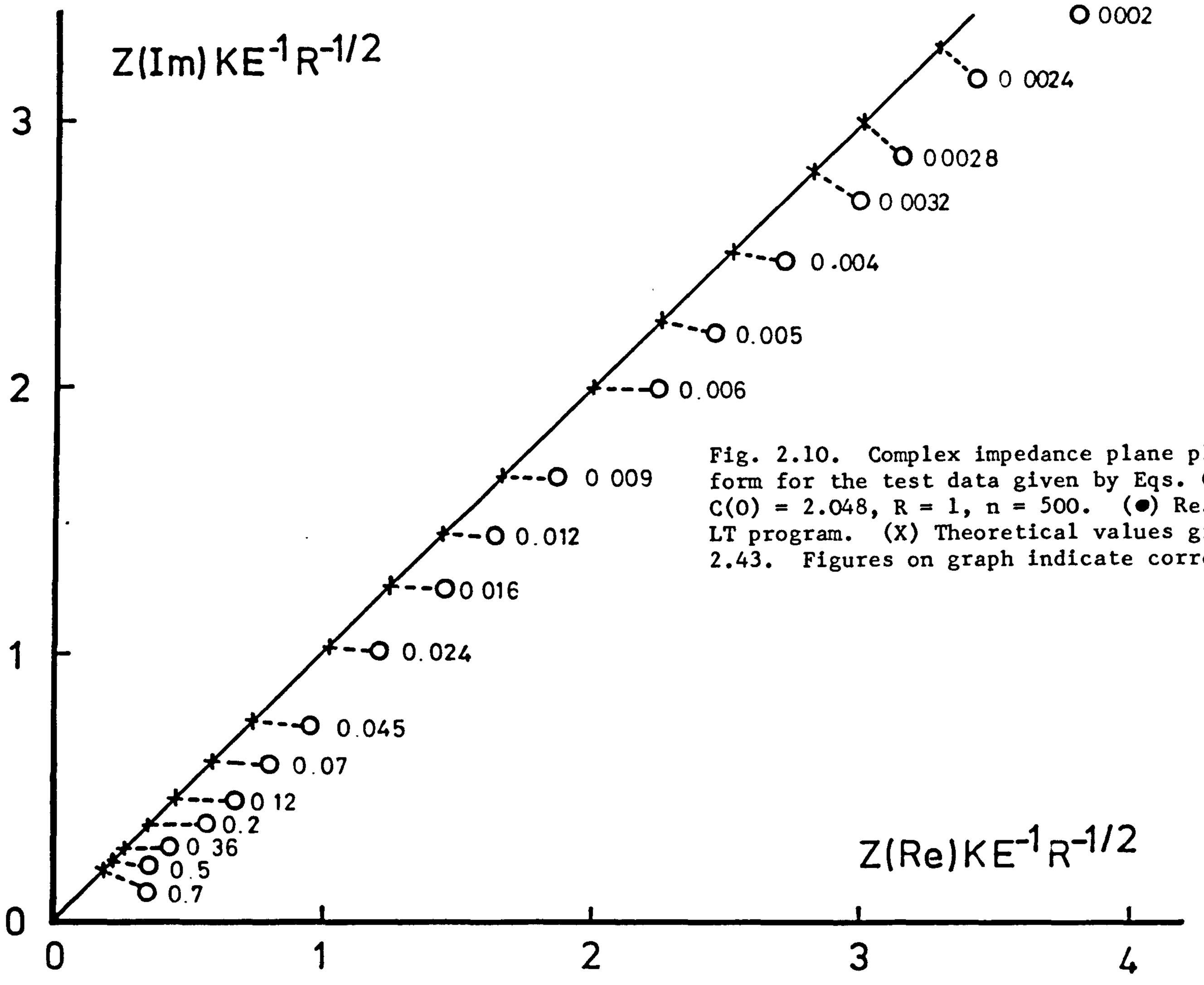

Fig. 2.10. Complex impedance plane plot in non-dimensional form for the test data given by Eqs. C.32 and C.49, with C(0) = 2.048, R = 1, n = 500. (●) Results obtained from LT program. (X) Theoretical values given by Eqs. 2.42 and 2.43. Figures on graph indicate corresponding fR values.

was found to give the best accuracy, the results are shown in Table 2.9 and Fig. 2.11.

The former results were obtained with the linear approximation version of the LT program. At this stage it is convenient to compare the accuracy of the quadratic approximation version which uses the algorithms A. 56 and A. 57 derived in Appendix A. The results are shown in Tables 2.10 to 2.14. In Table 2.10 the extrapolation 2.44 was used, the results only differ slightly from those obtained with the linear approximation in Table 2.8.

In Table 2.11 the extrapolation given by Equation 2.45 was used, there is an improvement in the accuracy comparable with that obtained with the linear approximation counterpart in Table 2.9.

The former results were obtained from a transient $K/\sqrt{Rn}$ with R=1. Keeping the number of points sampled constant we will examine here the effect of varying R, i.e. the effect of varying degrees of apparent flatness or steepness of the current transient. In Table 2.12 a value of R=0.5 and in Table 2.13 a value of R=0.05 gives virtually the same accuracy in the high frequency region, and a slight improvement in the low frequency region as the transient gets flatter. The effect of a steep transient, with R=5, is shown in Table 2.14, as expected, the high frequency region of the impedance spectrum is less accurate due to significant errors of the approximation when trying to fit a very rapidly falling transient, the low frequency region is however accurate.

Other results not shown here were carried on to examine the effect of current test data with only three significant figures of precision. No significant deviation was observed from the normal test data results. Other test data with random noise showed approximately the same degree of noise in the impedance results.

Since the linear approximation takes less computation time than

TABLE 2.8. Non-dimensional impedance results obtained with the LT software. Test data according to Eqs. C.32 and C.49 ($t^{-\frac{1}{2}}$ transient) with R = 1, $C(0) = C(1)^2/C(2)$. Theoretical impedance $Z(T)^*$ given by Eq. 2.43.

fR	Z(Re)*	Z(Im)*	$-Z(T)^*$	1/SQR(fR)
Ø.1	Ø.735301	-Ø.43285	Ø.503291	3.16228
Ø.Ø899999	Ø.765747	-Ø.464298	Ø.530515	3.33333
Ø.Ø799999	Ø.789891	-Ø.50552	Ø.562696	3.53553
Ø.Ø7	Ø.828994	-Ø.543146	Ø.601548	3.77965
Ø.Ø6	Ø.874755	-Ø.60511	Ø.649746	4.Ø8248
Ø.Ø55	Ø.896653	-Ø.634984	Ø.678637	4.26401
Ø.Ø5	Ø.928681	-Ø.664844	Ø.711761	4.47214
Ø.Ø45	Ø.972266	-Ø.705111	Ø.750262	4.71405
Ø.Ø4	1.Ø1933	-Ø.760612	Ø.795773	5
Ø.Ø35	1.Ø6593	-Ø.824164	Ø.850718	5.34523
Ø.Ø3	1.12454	-Ø.889942	Ø.918879	5.7735
Ø.Ø275	1.18Ø18	-Ø.934331	Ø.959738	6.Ø3Ø23
Ø.Ø25	1.2144	-Ø.9708	1.ØØ658	6.32456
Ø.Ø225	1.26872	-1.Ø4544	1.Ø6103	6.66667
Ø.Ø2	1.34467	-1.Ø9483	1.12539	7.Ø7107
Ø.Ø18	1.38524	-1.1701	1.18627	7.45357
Ø.Ø16	1.47443	-1.22627	1.25823	7.9Ø57
Ø.Ø14	1.54335	-1.34195	1.3451	8.45155
Ø.Ø12	1.66776	-1.42189	1.45288	9.12872
Ø.ØØ999997	1.7858	-1.59782	1.59155	1Ø
Ø.ØØ899997	1.86138	-1.65764	1.67764	1Ø.5Ø9
Ø.ØØ799997	1.99256	-1.7284	1.7794	11.18Ø4
Ø.ØØ699997	2.13504	-1.91Ø98	1.9Ø226	11.9523
Ø.ØØ599997	2.24Ø11	-2.Ø7215	2.Ø5468	12.91
Ø.ØØ549997	2.31199	-2.17512	2.14Ø5	13.484
Ø.ØØ499997	2.41Ø59	-2.22893	2.25Ø79	14.1422
Ø.ØØ449997	2.54882	-2.2969Ø9	2.37254	14.9Ø72
Ø.ØØ399997	2.74Ø92	-2.4758	2.51646	15.8114
Ø.ØØ349997	2.95624	-2.67302	2.69Ø21	16.9Ø31
Ø.ØØ299997	3.16698	-2.85422	2.9Ø577	18.2575
Ø.ØØ274997	3.12857	-2.97735	3.Ø3497	19.Ø693
Ø.ØØ249997	3.42104	-3.25679	3.18311	2Ø.ØØØ1
Ø.ØØ224997	3.48415	-3.25763	3.35529	21.Ø82
Ø.ØØ199997	3.73169	-3.79145	3.55883	22.3608
Ø.ØØ179997	4.24437	-3.7Ø878	3.75134	23.5704
Ø.ØØ159997	4.1Ø9Ø9	-3.73241	3.9789	25.ØØØ2
Ø.ØØ139997	4.3375	-4.36213	4.25363	26.7264
Ø.ØØ119997	5.ØØ437	-4.46385	4.59445	28.8679
Ø.ØØØ99997	4.9Ø319	-4.66304	5.Ø3298	31.6232

fR	Z(RE)*	Z(IM)*	-Z(T)*	1/SQR(HZ)
1	Ø.186447	-Ø.Ø814175	Ø.159155	1
Ø.9	Ø.193911	-Ø.Ø972Ø81	Ø.167764	1.Ø54Ø9
Ø.8	Ø.2Ø2781	-Ø.111952	Ø.17794	1.11803
Ø.699999	Ø.212904	-Ø.12703	Ø.19Ø226	1.19523
Ø.599999	Ø.224391	-Ø.143882	Ø.2Ø5468	1.29Ø99
Ø.549999	Ø.23Ø846	-Ø.153671	Ø.214604	1.3484
Ø.499999	Ø.238Ø16	-Ø.164878	Ø.225Ø79	1.41421
Ø.449999	Ø.24622	-Ø.178ØØ8	Ø.237254	1.49Ø71
Ø.399999	Ø.255949	-Ø.193739	Ø.251646	1.58114
Ø.349999	Ø.267971	-Ø.212892	Ø.269Ø21	1.69Ø31
Ø.299999	Ø.283501	-Ø.236929	Ø.29Ø576	1.82574
Ø.274999	Ø.293166	-Ø.251409	Ø.3Ø3496	1.9Ø693
Ø.249999	Ø.3Ø4567	-Ø.268Ø39	Ø.31831	2
Ø.224999	Ø.318217	-Ø.28737	Ø.335528	2.1Ø819
Ø.199999	Ø.334854	-Ø.31Ø18	Ø.355881	2.23607
Ø.179999	Ø.3513Ø	-Ø.331683	Ø.375132	2.35703
Ø.159999	Ø.37Ø625	-Ø.356984	Ø.397888	2.5ØØØ1
Ø.139999	Ø.394853	-Ø.387337	Ø.42536	2.67262
Ø.119999	Ø.425649	-Ø.424687	Ø.459442	2.88676
Ø.Ø99999	Ø.466172	-Ø.472259	Ø.5Ø3293	3.16229
Ø.Ø89999	Ø.491733	-Ø.5Ø1539	Ø.53Ø518	3.33335
Ø.Ø79999	Ø.522264	-Ø.535922	Ø.5627	3.53556
Ø.Ø69999	Ø.559493	-Ø.577136	Ø.6Ø1552	3.77967
Ø.Ø59999	Ø.6Ø6117	-Ø.627876	Ø.649751	4.Ø8252
Ø.Ø54999	Ø.634253	-Ø.658112	Ø.678643	4.26405
Ø.Ø49999	Ø.666651	-Ø.692631	Ø.711768	4.47218
Ø.Ø44999	Ø.7Ø4475	-Ø.732586	Ø.75Ø27	4.7141
Ø.Ø39999	Ø.749367	-Ø.779613	Ø.795783	5.ØØØØ6
Ø.Ø34999	Ø.8Ø38Ø3	-Ø.836138	Ø.85Ø729	5.3453
Ø.Ø29999	Ø.871622	-Ø.9Ø5942	Ø.918894	5.7736
Ø.Ø27499	Ø.9Ø867	-Ø.948Ø29	Ø.959755	6.Ø3Ø33
Ø.Ø24999	Ø.959273	-Ø.995354	1.ØØ66	6.32468
Ø.Ø22499	1.ØØ838	-1.Ø5118	1.Ø6105	6.66681
Ø.Ø19999	1.Ø7866	-1.11592	1.12542	7.Ø7124
Ø.Ø17999	1.13215	-1.17569	1.1863	7.45377
Ø.Ø15999	1.2Ø971	-1.25563	1.25827	7.9Ø594
Ø.Ø13999	1.29575	-1.33147	1.34515	8.45184
Ø.Ø11999	1.39475	-1.45332	1.45294	9.12909
Ø.ØØ999Ø1	1.55416	-1.58481	1.59162	1Ø.ØØØ5
Ø.ØØ8999	1.62949	-1.6565	1.67773	1Ø.5415
Ø.ØØ799Ø1	1.7Ø954	-1.76534	1.77951	11.181
Ø.ØØ6999	1.83152	-1.91801	1.9Ø24	11.9531
Ø.ØØ5999	2.Ø2166	-2.Ø8491	2.Ø5485	12.911
Ø.ØØ549Ø1	2.13626	-2.16181	2.14623	13.4852
Ø.ØØ4999	2.2528	-2.2362	2.25101	14.1435

Z 1 .AS Y= 2 OHMS
EXCELLENT!

TABLE 2.9. Non-dimensional impedance results obtained with the LT software. Test data according to Eqs. C.32 and C.49 ($t^{-\frac{1}{2}}$ transient). R = 1, C(0) = 3.33 $C(1)^2/C(2)$, n = 200. Imaginary result compared with Z(T) given by Eq. 2.43.

TABLE 2.10. Non-dimensional impedance results obtained with the LT software (quadratic approximation). Test data given by Eqs. C.32 and C.49 ($t^{-\frac{1}{2}}$ response). $C(0) = C(1)^2/C(2)$, R = 1, n = 549. Theoretical Z(T) given by Eq. 2.43.

R= 1

FR	Z(RE)*	Z(IM)*	-Z(T)*	1/SQR(F)
Ø.99999	Ø.684817	-Ø.Ø413Ø88	Ø.159155	1
Ø.9	Ø.7392	-Ø.Ø37Ø9Ø2	Ø.167764	1.Ø54Ø9
Ø.8	Ø.775878	Ø.Ø3Ø5378	Ø.17794	1.11Ø3
Ø.699999	Ø.72176	Ø.1Ø7243	Ø.19Ø226	1.19523
Ø.6	Ø.629802	Ø.1Ø3386	Ø.2Ø5468	1.29Ø99
Ø.55	Ø.595895	Ø.Ø784638	Ø.214604	1.3484
Ø.5	Ø.572906	Ø.Ø477291	Ø.225Ø79	1.41421
Ø.45	Ø.556726	Ø.Ø152585	Ø.237254	1.49Ø71
Ø.4	Ø.545417	-Ø.Ø215227	Ø.251646	1.58114
Ø.35	Ø.54Ø338	-Ø.Ø63561	Ø.26902	1.69Ø31
Ø.3	Ø.542758	-Ø.111432	Ø.29Ø575	1.82574
Ø.275	Ø.547292	-Ø.137939	Ø.3Ø3496	1.9Ø693
Ø.25	Ø.554456	-Ø.166542	Ø.318Ø9	2
Ø.225	Ø.564735	-Ø.197Ø5	Ø.335527	2.1Ø819
Ø.2	Ø.578821	-Ø.232114	Ø.35588	2.23607
Ø.18	Ø.593519	-Ø.262665	Ø.375131	2.35702
Ø.16	Ø.612101	-Ø.29675	Ø.397886	2.5
Ø.14	Ø.635751	-Ø.335563	Ø.425359	2.67261
Ø.12	Ø.666313	-Ø.38Ø989	Ø.45944	2.88675
Ø.Ø999999	Ø.7Ø6882	-Ø.436186	Ø.5Ø3291	3.16228
Ø.Ø899999	Ø.732527	-Ø.469Ø89	Ø.53Ø516	3.33333
Ø.Ø799999	Ø.763148	-Ø.5Ø6959	Ø.562697	3.53554
Ø.Ø699999	Ø.8Ø8443	-Ø.551516	Ø.6Ø1548	3.77965
Ø.Ø599999	Ø.847Ø78	-Ø.6Ø5451	Ø.649746	4.Ø8248
Ø.Ø549999	Ø.875177	-Ø.637225	Ø.678638	4.26402
Ø.Ø499999	Ø.9Ø7502	-Ø.673246	Ø.711761	4.47214
Ø.Ø449999	Ø.945207	-Ø.714666	Ø.75Ø263	4.71405
Ø.Ø399999	Ø.989934	-Ø.763129	Ø.795773	5
Ø.Ø349999	1.Ø4412	-Ø.821Ø55	Ø.85Ø718	5.34523
Ø.Ø299999	1.11161	-Ø.892234	Ø.91888	5.77351
Ø.Ø274999	1.14844	-Ø.935271	Ø.959739	6.Ø3Ø24
Ø.Ø249999	1.19885	-Ø.983Ø48	1.Ø0658	6.32457
Ø.Ø224999	1.24737	-1.Ø4Ø08	1.Ø6Ø3	6.66668
Ø.Ø2	1.31467	-1.1Ø548	1.12539	7.Ø7Ø37
Ø.Ø18	1.37451	-1.16726	1.18627	7.45356
Ø.Ø16	1.44Ø8	-1.24Ø32	1.25823	7.9Ø57
Ø.Ø14	1.53Ø27	-1.32866	1.3451	8.45154
Ø.Ø12	1.63632	-1.43918	1.45287	9.12871
Ø.Ø11	1.7Ø6Ø2	-1.5Ø6Ø5	1.51748	9.53463
Ø.ØØ999999	1.77353	-1.58207	1.59155	1Ø
Ø.ØØ899999	1.8559	-1.66695	1.67764	1Ø.54Ø9
Ø.ØØ799999	1.96Ø6	-1.77671	1.7794	11.18Ø3
Ø.ØØ699999	2.Ø8851	-1.89245	1.9Ø226	11.9523
Ø.ØØ599999	2.23871	-2.Ø6389	2.Ø5468	12.9Ø99
Ø.ØØ549999	2.34118	-2.14809	2.14604	13.484
Ø.ØØ499999	2.43Ø25	-2.24133	2.25Ø79	14.1421
Ø.ØØ449999	2.54Ø98	-2.38732	2.37254	14.9Ø71
Ø.ØØ399999	2.71223	-2.54851	2.51646	15.8114
Ø.ØØ359999	2.86Ø77	-2.67371	2.65258	16.6667
Ø.ØØ319999	2.99Ø25	-2.8Ø99	2.81349	17.6777
Ø.ØØ279999	3.15Ø1	-3.Ø5752	3.ØØ774	18.8982
Ø.ØØ239999	3.42363	-3.38719	3.24874	2Ø.4124
Ø.ØØ199999	3.82332	-3.69519	3.55881	22.36Ø7

TABLE 2.11. Non-dimensional impedance results obtained with the LT software (quadratic approximation). Test data given by Eqs. C.32 and C.49 ($t^{-\frac{1}{2}}$ transient). n = 100, $C(0) = 3.33\ C(1)^2/C(2)$. Theoretical impedance Z(T) given by Eq. 2.43.

R= 1

FR	Z(RE)*	Z(IM)*	-Z(T)*	1/SQR(F)
0.99999	0.23264	-0.0420327	0.159155	1
0.9	0.206785	-0.0398655	0.167764	1.05409
0.8	0.183049	-0.057078	0.17794	1.11803
0.699999	0.165668	-0.085852	0.190226	1.19523
0.6	0.153074	-0.12522	0.205468	1.29099
0.55	0.148365	-0.150486	0.214604	1.3484
0.5	0.145266	-0.18141	0.225079	1.41421
0.45	0.145426	-0.219945	0.237254	1.49071
0.4	0.151338	-0.268389	0.251646	1.58114
0.35	0.168262	-0.329729	0.26902	1.69031
0.3	0.206427	-0.405091	0.290575	1.82574
0.275	0.2382	-0.44538	0.303496	1.90693
0.25	0.280984	-0.487287	0.318309	2
0.225	0.335524	-0.524305	0.335527	2.10819
0.2	0.400447	-0.553624	0.35588	2.23607
0.18	0.457394	-0.569934	0.375131	2.35702
0.16	0.51611	-0.580348	0.397886	2.5
0.14	0.57466	-0.587335	0.425359	2.67261
0.12	0.63277	-0.59525	0.45944	2.88675
0.0999999	0.69279	-0.610161	0.503291	3.16228
0.0899999	0.72525	-0.622734	0.530516	3.33333
0.0799999	0.7694	-0.640519	0.562697	3.53554
0.0699999	0.801715	-0.665476	0.601548	3.77965
0.0599999	0.850461	-0.700432	0.649746	4.08248
0.0549999	0.879186	-0.72304	0.678638	4.26402
0.0499999	0.911882	-0.750069	0.711761	4.47214
0.0449999	0.949711	-0.78272	0.750263	4.71405
0.0399999	0.99433	-0.822601	0.795773	5
0.0349999	1.04822	-0.872136	0.850718	5.34523
0.0299999	1.11523	-0.935104	0.91888	5.77351
0.0274999	1.15162	-0.973837	0.959739	6.03024
0.0249999	1.2019	-1.01761	1.00658	6.32457
0.0224999	1.24977	-1.07026	1.06103	6.66668
0.0199999	1.31988	-1.13067	1.1254	7.07108
0.0179999	1.36995	-1.18771	1.18627	7.45358
0.0159999	1.45192	-1.26403	1.25823	7.90571
0.0139999	1.53037	-1.33466	1.3451	8.45157
0.0119999	1.63306	-1.45183	1.45288	9.12874
0.00999992	1.79008	-1.57009	1.59155	10

TABLE 2.12. Non-dimensional impedance obtained with the LT software (quadratic approximation). Test data given by Eqs. C.32 and C.49 ($t^{-\frac{1}{2}}$ response). n = 549, R = 0.5, C(0) = 3.33 $C(1)^2/C(2)$. Theoretical impedance Z(T) given by Eq. 2.43.

R= Ø.5

FR	Z(RE)*	Z(IM)*	-Z(T)*	1/SQR(F)
Ø.2	Ø.393405	-Ø.557724	Ø.35588	1.58114
Ø.18	Ø.451617	-Ø.574935	Ø.375131	1.66667
Ø.16	Ø.511816	-Ø.585762	Ø.397886	1.76777
Ø.14	Ø.571822	-Ø.592626	Ø.425359	1.88982
Ø.12	Ø.631142	-Ø.599982	Ø.45944	2.Ø4124
Ø.11	Ø.661288	-Ø.605716	Ø.479869	2.13201
Ø.Ø999999	Ø.692011	-Ø.614061	Ø.5Ø3291	2.23607
Ø.Ø899999	Ø.724958	-Ø.626143	Ø.53Ø516	2.35702
Ø.Ø799999	Ø.76Ø612	-Ø.643479	Ø.562697	2.5
Ø.Ø699999	Ø.8Ø1658	-Ø.667945	Ø.6Ø1548	2.67261
Ø.Ø599999	Ø.85Ø238	-Ø.7Ø25	Ø.649746	2.88675
Ø.Ø549999	Ø.879144	-Ø.725Ø02	Ø.678638	3.Ø1512
Ø.Ø499999	Ø.911551	-Ø.751756	Ø.711761	3.16228
Ø.Ø449999	Ø.948964	-Ø.784Ø81	Ø.75Ø263	3.33334
Ø.Ø399999	Ø.993692	-Ø.823Ø9	Ø.795773	3.53554
Ø.Ø359999	1.Ø3528	-Ø.862206	Ø.838819	3.72678
Ø.Ø319999	1.Ø8479	-Ø.9Ø8957	Ø.889703	3.95285
Ø.Ø279999	1.14526	-Ø.966592	Ø.951132	4.22578
Ø.Ø239999	1.2205	-1.Ø3889	1.Ø2734	4.56436
Ø.Ø199999	1.3168	-1.13169	1.1254	5.Ø0Ø1
Ø.Ø179999	1.37628	-1.18981	1.18627	5.27Ø48
Ø.Ø159999	1.44607	-1.25742	1.25823	5.59Ø19
Ø.Ø139999	1.53071	-1.34Ø65	1.3451	5.97616
Ø.Ø119999	1.63604	-1.44417	1.45288	6.455
Ø.Ø1Ø9999	1.7Ø496	-1.5Ø6Ø9	1.51749	6.74203
Ø.ØØ99999	1.77149	-1.5746	1.59155	7.Ø711
Ø.ØØ89999	1.86269	-1.65Ø4	1.67765	7.4536
Ø.ØØ79999	1.95621	-1.74847	1.77941	7.9Ø574
Ø.ØØ69999	2.Ø8329	-1.85221	1.9Ø227	8.4516
Ø.ØØ59999	2.23Ø83	-1.98842	2.Ø5469	9.12878
Ø.ØØ54999	2.33Ø28	-2.Ø6212	2.14606	9.53471
Ø.ØØ49999	2.41845	-2.13981	2.25Ø81	1Ø.ØØØ1
Ø.ØØ44999	2.52641	-2.23622	2.37256	1Ø.541
Ø.ØØ39999	2.68921	-2.36182	2.51649	11.185
Ø.ØØ35999	2.834	-2.44415	2.65261	11.7853
Ø.ØØ31999	2.95232	-2.5Ø367	2.81352	12.5ØØ2
Ø.ØØ27999	3.11538	-2.67377	3.ØØ779	13.3633
Ø.ØØ23999	3.37473	-2.85505	3.2488	14.434
Ø.ØØ19999	3.66377	-2.74251	3.55889	15.8118
Ø.ØØ17999	3.86571	-2.88153	3.75141	16.6671

TABLE 2.13. Non-dimensional impedance obtained with the LT software (quadratic approximation). Test data given by Eqs. C.32 and C.49. n = 549, $C(0) = 3.33\ C(1)^2/C(2)$. Theoretical $Z(T)^*$ given by Eq. 2.43.

R= Ø.ØS

FR	Z(RE)*	Z(IM)*	-Z(T)*	1/SQR(F)
Ø.2ØØØ1	Ø.393Ø6	-Ø.557722	Ø.3558	Ø.499999
Ø.18ØØ1	Ø.451616	-Ø.574936	Ø.3751 3	Ø.527Ø45
Ø.16	Ø.511819	-Ø.585767	Ø.397886	Ø.559Ø16
Ø.14	Ø.571827	-Ø.592626	Ø.425358	Ø.597613
Ø.12	Ø.631144	-Ø.599977	Ø.459439	Ø.645496
Ø.11	Ø.661289	-Ø.6Ø5713	Ø.479868	Ø.674199
Ø.1	Ø.692Ø14	-Ø.614Ø55	Ø.5Ø329	Ø.7Ø7106
Ø.Ø9ØØØ3	Ø.724957	-Ø.62614	Ø.53Ø514	Ø.745355
Ø.Ø8ØØØ2	Ø.76Ø617	-Ø.643475	Ø.562696	Ø.79Ø568
Ø.Ø7ØØØ2	Ø.8Ø1657	-Ø.667951	Ø.6Ø1547	Ø.845153
Ø.Ø6ØØØ2	Ø.85Ø24	-Ø.7Ø25Ø5	Ø.649745	Ø.91287
Ø.Ø55ØØ1	Ø.879126	-Ø.724996	Ø.678636	Ø.953461
Ø.Ø5ØØØ1	Ø.911531	-Ø.751739	Ø.71176	Ø.999999
Ø.Ø45ØØ1	Ø.948939	-Ø.784Ø52	Ø.75Ø261	1.Ø54Ø9
Ø.Ø4ØØØ1	Ø.993679	-Ø.823881	Ø.795772	1.11803
Ø.Ø36ØØ1	1.Ø353	-Ø.862354	Ø.838818	1.17851
Ø.Ø32ØØ1	1.Ø8482	-Ø.9Ø8995	Ø.8897	1.25
Ø.Ø28ØØ1	1.14527	-Ø.966651	Ø.951129	1.3363
Ø.Ø24	1.22Ø56	-1.Ø3895	1.Ø2734	1.44337
Ø.Ø2	1.31677	-1.13151	1.12539	1.58114
Ø.Ø18	1.37623	-1.18966	1.18627	1.66666
Ø.Ø16	1.44636	-1.25807	1.25823	1.76777
Ø.Ø14	1.53Ø67	-1.34Ø96	1.3451	1.88982
Ø.Ø12	1.63563	-1.44313	1.45287	2.Ø4124
Ø.Ø11	1.7Ø5Ø9	-1.5Ø57	1.51748	2.13201
Ø.Ø1	1.77187	-1.57566	1.59155	2.23607
Ø.ØØ899999	1.86286	-1.65229	1.67764	2.35702
Ø.ØØ799999	1.95682	-1.75Ø84	1.7794	2.5
Ø.ØØ699998	2.Ø816	-1.84307	1.9Ø226	2.67261
Ø.ØØ599998	2.23228	-2.ØØ4Ø8	2.Ø5468	2.88675
Ø.ØØ549998	2.3285	-2.Ø5763	2.14604	3.Ø1512
Ø.ØØ499998	2.42Ø54	-2.14931	2.25Ø79	3.16228
Ø.ØØ449998	2.52781	-2.25229	2.37254	3.33334
Ø.ØØ399997	2.69Ø2Ø9	-2.35214	2.51646	3.53554
Ø.ØØ359997	2.82673	-2.39344	2.65259	3.72679
Ø.ØØ319997	2.96Ø92	-2.56Ø2	2.81349	3.95286
Ø.ØØ279997	3.1ØØ95	-2.59155	3.ØØ775	4.22579
Ø.ØØ239997	3.37668	-2.87405	3.24875	4.56438
Ø.ØØ199997	3.7364	-3.Ø1941	3.55883	5.ØØØ4
Ø.ØØ179997	3.94644	-3.15656	3.75134	5.27Ø51

TABLE 2.14. Non-dimensional impedance obtained with the LT software (quadratic approximation). Test data given by Eqs. C.32 and C.49. n = 549, $C(0) = 3.33\ C(1)^2/C(2)$. Theoretical impedance Z(T)* given by Eq. 2.43.

R= 5

FR	Z(RE)*	Z(IM)*	-Z(T)*	1/SQR(F)
0.200001	0.393401	-0.557718	0.35588	4.99999
0.180001	0.451611	-0.574934	0.37513	5.27045
0.16	0.511812	-0.585765	0.397886	5.59016
0.14	0.571817	-0.592628	0.425358	5.97613
0.12	0.631137	-0.599981	0.459439	6.45496
0.11	0.661286	-0.605705	0.479868	6.74199
0.1	0.692015	-0.614049	0.50329	7.07106
0.0900002	0.724957	-0.626137	0.530515	7.45355
0.0800002	0.760624	-0.643485	0.562696	7.90568
0.0700002	0.801659	-0.667944	0.601547	8.45153
0.0600001	0.850231	-0.702509	0.649745	9.1287
0.0550001	0.879123	-0.72499	0.678637	9.53462
0.0500001	0.911532	-0.751754	0.71176	9.99999
0.0450001	0.948927	-0.784044	0.750261	10.5409
0.0400001	0.993663	-0.823935	0.795772	11.1803
0.036	1.03529	-0.862237	0.838818	11.7851
0.032	1.08483	-0.909009	0.889701	12.5
0.028	1.14523	-0.966633	0.95113	13.363
0.024	1.22054	-1.03886	1.02734	14.4338
0.02	1.31672	-1.13164	1.12539	15.8114
0.018	1.3763	-1.19022	1.18627	16.6667
0.016	1.44597	-1.25789	1.25823	17.6777
0.014	1.53056	-1.34051	1.3451	18.8982
0.012	1.63575	-1.44218	1.45288	20.4124
0.011	1.70432	-1.50298	1.51748	21.3201
0.00999996	1.7712	-1.57389	1.59155	22.3607
0.00899995	1.86305	-1.65538	1.67764	23.5703
0.00799995	1.95743	-1.75195	1.77941	25.0001
0.00699995	2.08177	-1.85138	1.90227	26.7262
0.00599994	2.22975	-1.99384	2.05469	28.8676
0.00549994	2.32981	-2.0574	2.14605	30.1513
0.00499994	2.41615	-2.12742	2.2508	31.623
0.00449994	2.52863	-2.26608	2.37255	33.3335
0.00399994	2.69364	-2.37439	2.51647	35.3556
0.00359993	2.83023	-2.41934	2.6526	37.2681
0.00319993	2.95241	-2.51832	2.81351	39.5289
0.00279993	3.1191	-2.74024	3.00777	42.2582
0.00239993	3.37007	-2.85878	3.24877	45.6442
0.00199993	3.72894	-3.05485	3.55887	50.0009
0.00179993	3.91306	-3.03486	3.75138	52.7056
0.00159993	4.1069	-3.20484	3.97895	55.9029

the quadratic, and is of similar accuracy we decided to use the linear approximation in the subroutine to take the LT of the experimental data in the automated version of the program, named JAM, after the persons in our laboratory that contributed to its development.

II.6.4. Pb^{++} Reduction

II.6.4.1. Experimental

A fast electrochemical system was initially chosen, as this represents the most difficult case in that the i(t) response to a square E(t) pulse is changing rapidly. The system investigated was the reduction of a $5X10^{-3}$M $Pb(NO_3)_2$ + 1.0 M $HClO_4$ solution at Hg. The Hg electrode was a hanging Hg drop (HMDE) attached to a Hg plated Pt spike sealed into glass. The electrode was contained in the cell shown in Fig. 2.16a

Each Hg drop was produced in the capillary attached to the syringe by turning the micrometer five divisions. From this capillary the drop was collected by the HMDE and translated to a position near the tip of the Luggin probe connected to the reference electrode.

From measurements with a travelling microscope the area of the Hg drop was calculated as 0.05 cm^2, using the formula of a truncated sphere $A = R^2 + D^2$. Two types of reference electrodes were used, S.C.E., and a Pb(0.4M)/Hg amalgam in contact with the aqueous solution. This reference electrodes were not ideal but were found to be suitable as they did not change during the time scale of the experiment. The amalgam reference electrode had a measured potential of -0.185 V against a standard hydrogen electrode. AnalaR $Pb(NO_3)_2$, AnalaR $HClO_4$ and triply distilled water were used to make up the solution which was deareated with N_2 prior to use. The counter electrode was a Pt spiral.

Fig. 2.16 HDE cell, convertible into Hg drop mounted on a capillary.

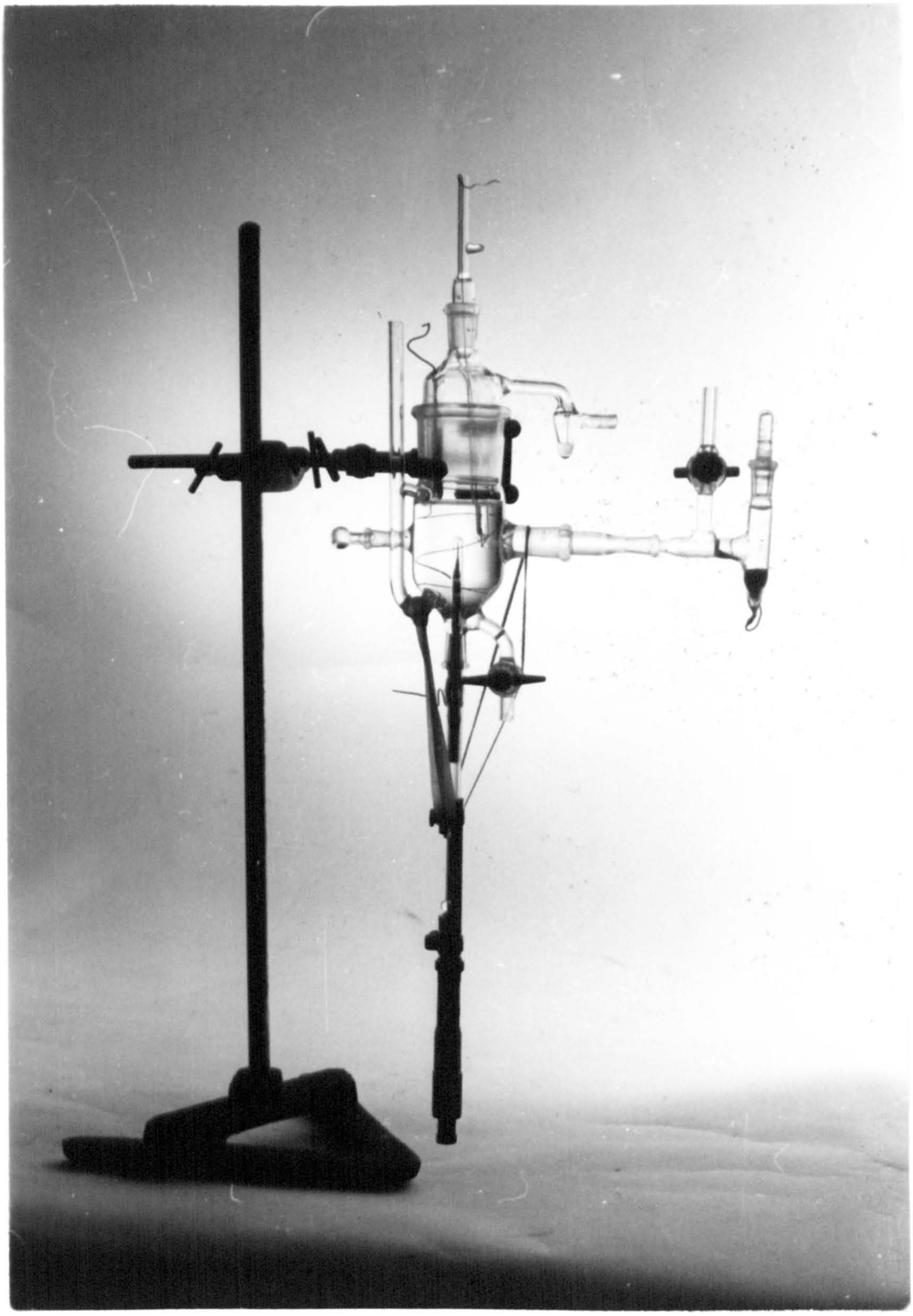

Fig. 2.16a HDE cell, convertible into Hg drop mounted on a capillary.

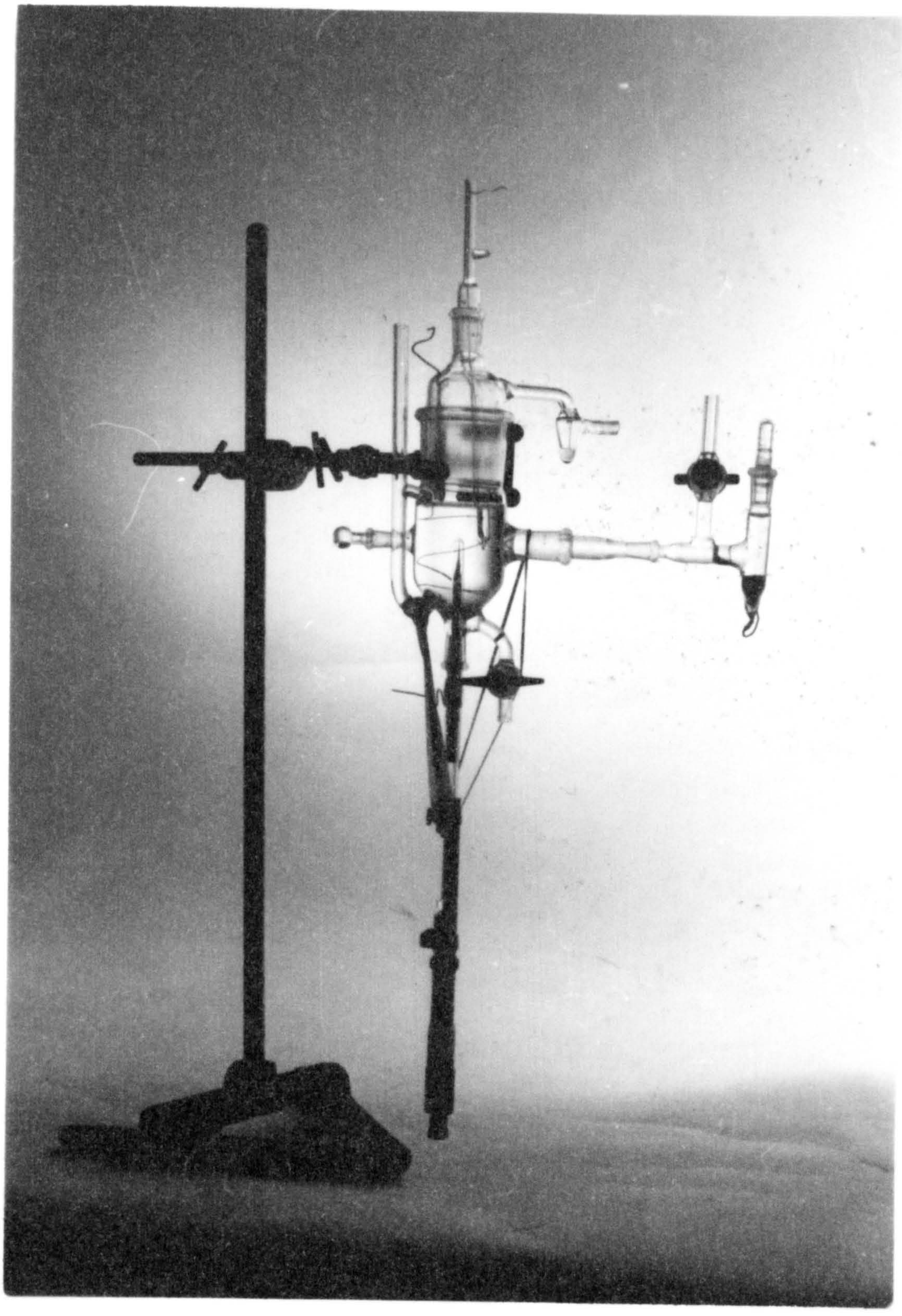

II.6.4.2. Fourier Transform Impedance

A double potential pulse, as shown in Fig. 2.16A,was applied to the HMDE. The first pulse determines the d.c. potential and was 30 mS in length. The second, small amplitude (10 mV) pulse was used to sample the impedance characteristics. The potential step applied was close enough to a perfect signal to make it unnecessary to sample it. The i(t) response labelled B in Fig. 2.16 was sampled with the DAQUAD program. With the potentiostat used the time of double layer charging in the second pulse was negligible compared to the sampling rate of 150μs per point. This data was averaged from 40 successive perturbations (at a 0.33 s repetition rate) on the same drop, in order to reduce noise. No significative build up of amalgam took place because between pulses the lead was dissolved at the base potential of -270 mV vs SCE. The anodic transient was complete before the next pulse. Fig. 2.17 shows the stationary i-E curve obtained from the current at the end of the first pulse. This curve has the characteristics of a 2e reversible reaction. The value of i_d suggests that the diffusion layer is 2.66×10^{-1} cm.

After sampling, using the DLOAD program, the current just prior to the second pulse was subtracted from the second pulse, and the first pulse replaced by a zero level line. The data was then processed by DAQUAD to obtain A_r and B_r. The program, CDFILE was used to obtain C_r and D_r. Since the data was only 512 points long, an interpolation of the time domain data was carried on in order to improve the accuracy of the DAQUAD program. The results expressed as Z(Im) vs Z(Re) are shown in Fig. 2.18, for both the L and FFT software, also shown in the figure are values obtained by manual Transfer Function Analyser (TFA) (from S.E. Laboratories model SM 272) analysis of the sine wave response. The results of the TFA are somewhat lower due to slight differences in area and some poisoning as the imaginary part of the response became less with time. Also in a continuous

Fig. 2.16. A) Profile of the potential step applied to the HMDE, area = 0.05 cm^2 and B) resulting Pb^{++} reduction current. Solution 5 x 10^{-3}M $Pb(NO_3)_2$ + 1.0M $HClO_4$, sampling rate = 150 μs/point; average of 40 pulses recorded at 330 ms intervals.

Fig. 2.17. i-E plot for Pb^{++} reduction at a HMDE obtained from potentiostatic pulses, as in Fig. 2.16. Current sampled at 35.75 ms after the start of the first pulse. Solution 5 x 10^{-3}M $Pb(NO_3)_2$ + 1.0M $HClO_4$; A = 0.05 cm^2.

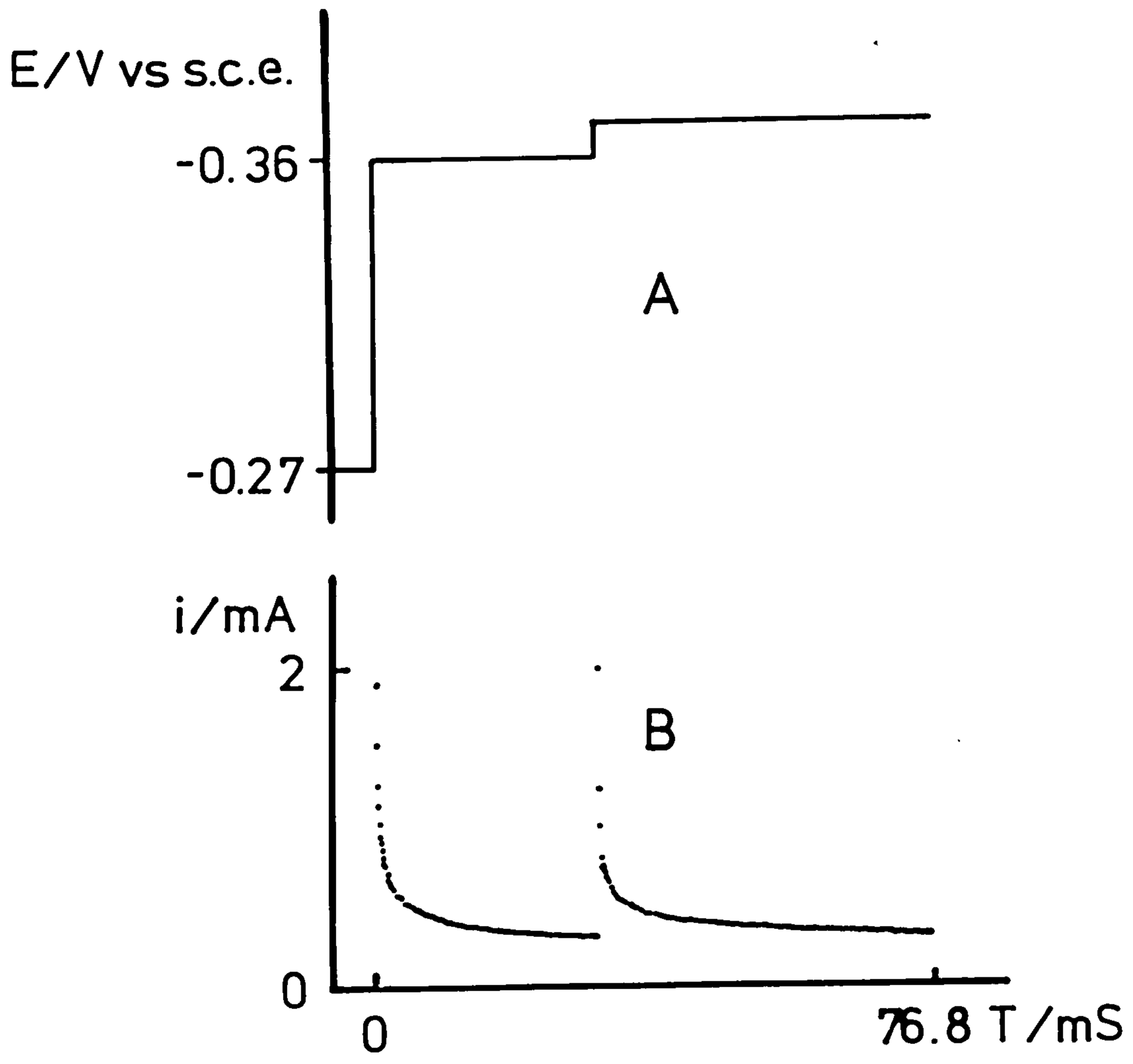
E/V vs s.c.e.
-0.36
-0.27
A
i/mA
2
0
B
0
76.8 T/mS

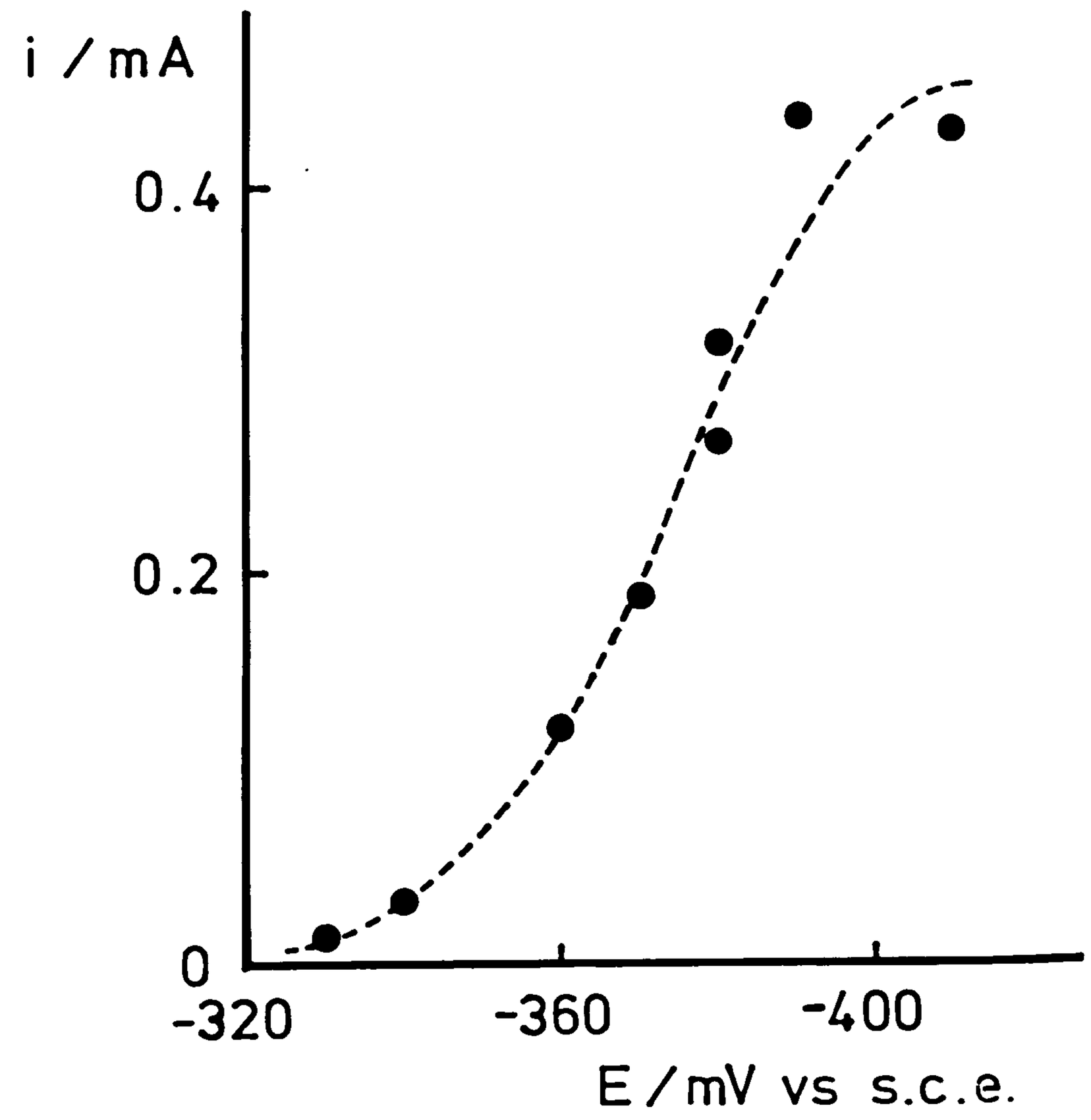
i / mA
0.4
0.2
0
-320
-360
-400
E / mV vs s.c.e.

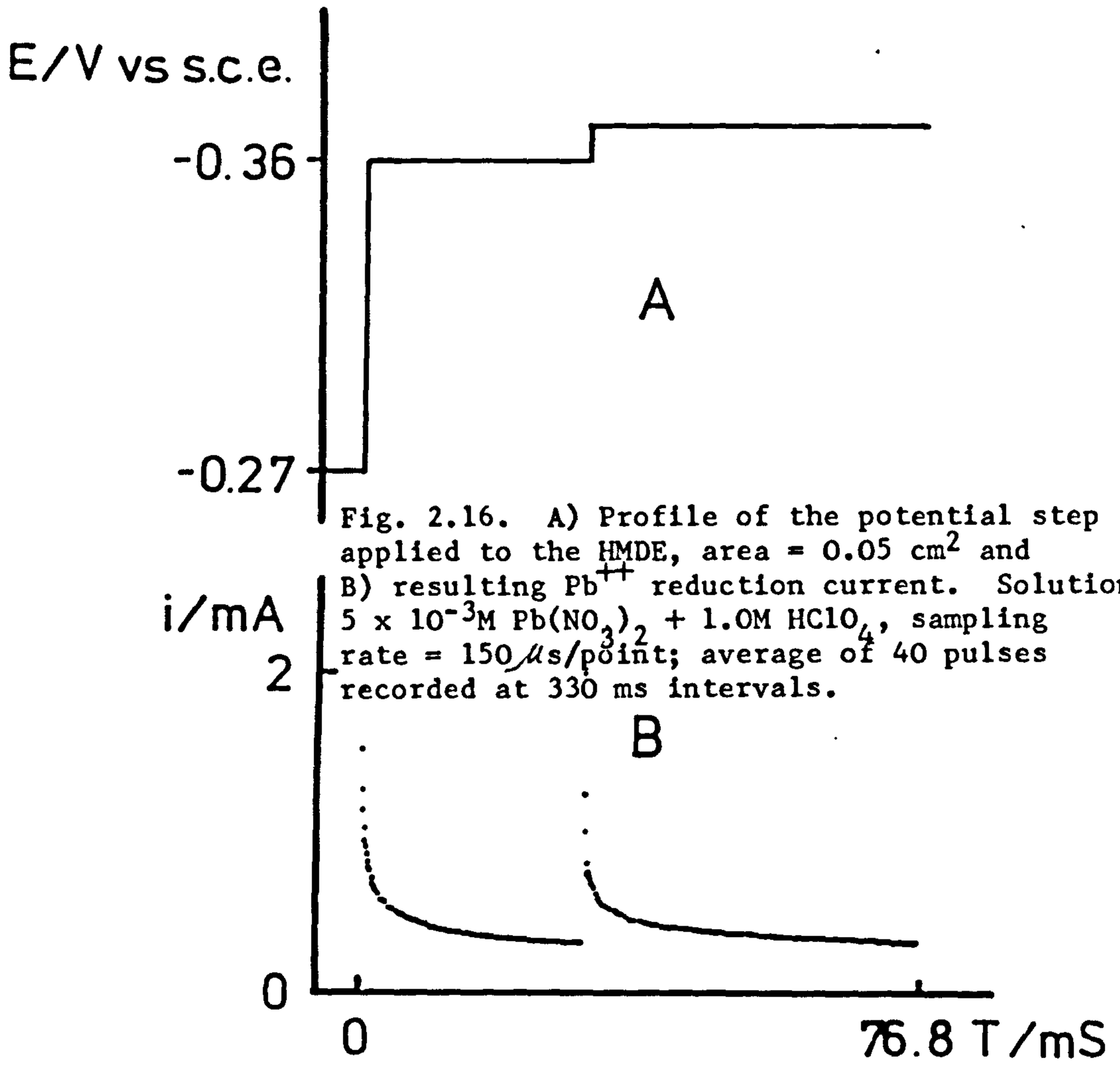

Fig. 2.16. A) Profile of the potential step applied to the HMDE, area = 0.05 cm^2 and B) resulting Pb^{++} reduction current. Solution 5×10^{-3}M $Pb(NO_3)_2$ + 1.0M $HClO_4$, sampling rate = 150 μs/point; average of 40 pulses recorded at 330 ms intervals.

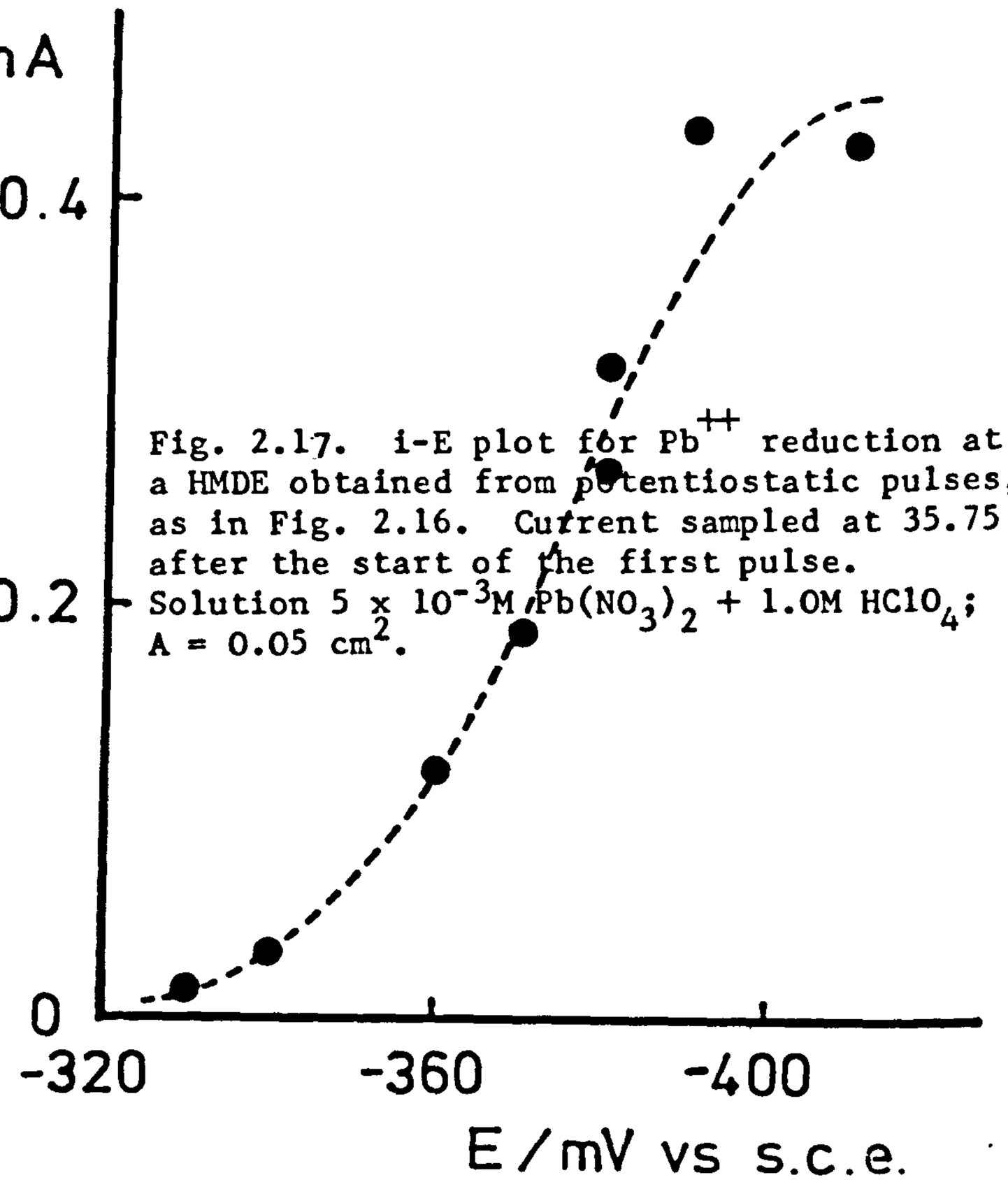

Fig. 2.17. i-E plot for Pb^{++} reduction at a HMDE obtained from potentiostatic pulses, as in Fig. 2.16. Current sampled at 35.75 ms after the start of the first pulse. Solution 5×10^{-3}M $Pb(NO_3)_2$ + 1.0M $HClO_4$; A = 0.05 cm^2.

Fig. 2.18. Complex impedance plane plot for Pb^{++} reduction at the HMDE, area = 0.05 cm^2, at -360 mV vs S.C.E. from data shown in Fig. 2.16, computed with (o) FFT software, (X) LT software. TFA measurements (●) under the same experimental conditions. Figures on graph refer to the frequency in Hz.

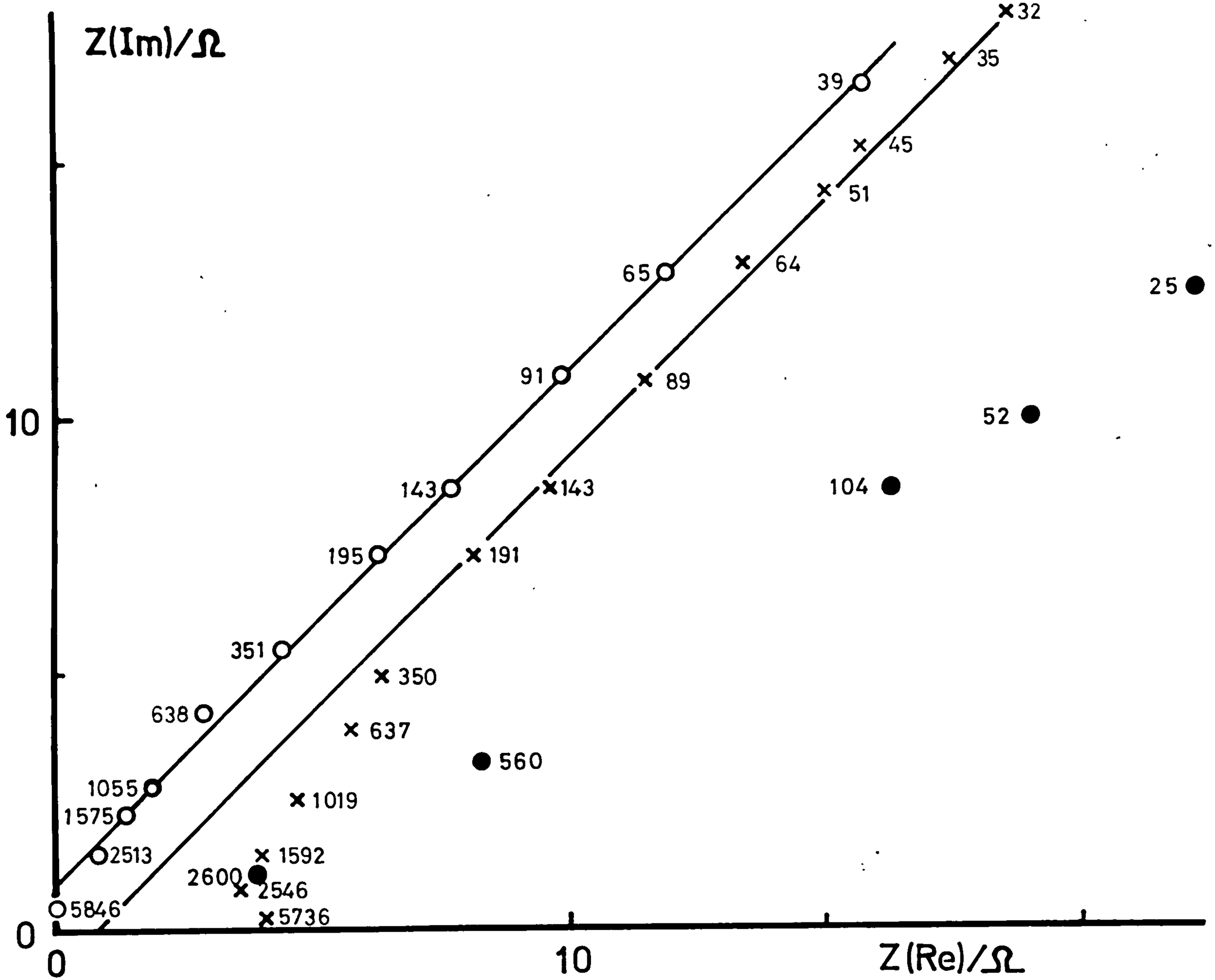
Z(Im)/Ω
10
0
0
10
Z(Re)/Ω
32
35
39
45
51
65
64
25
91
89
52
143
143
104
195
191
351
350
638
637
560
1055
1019
1575
2513
1592
2600
2546
5846
5736

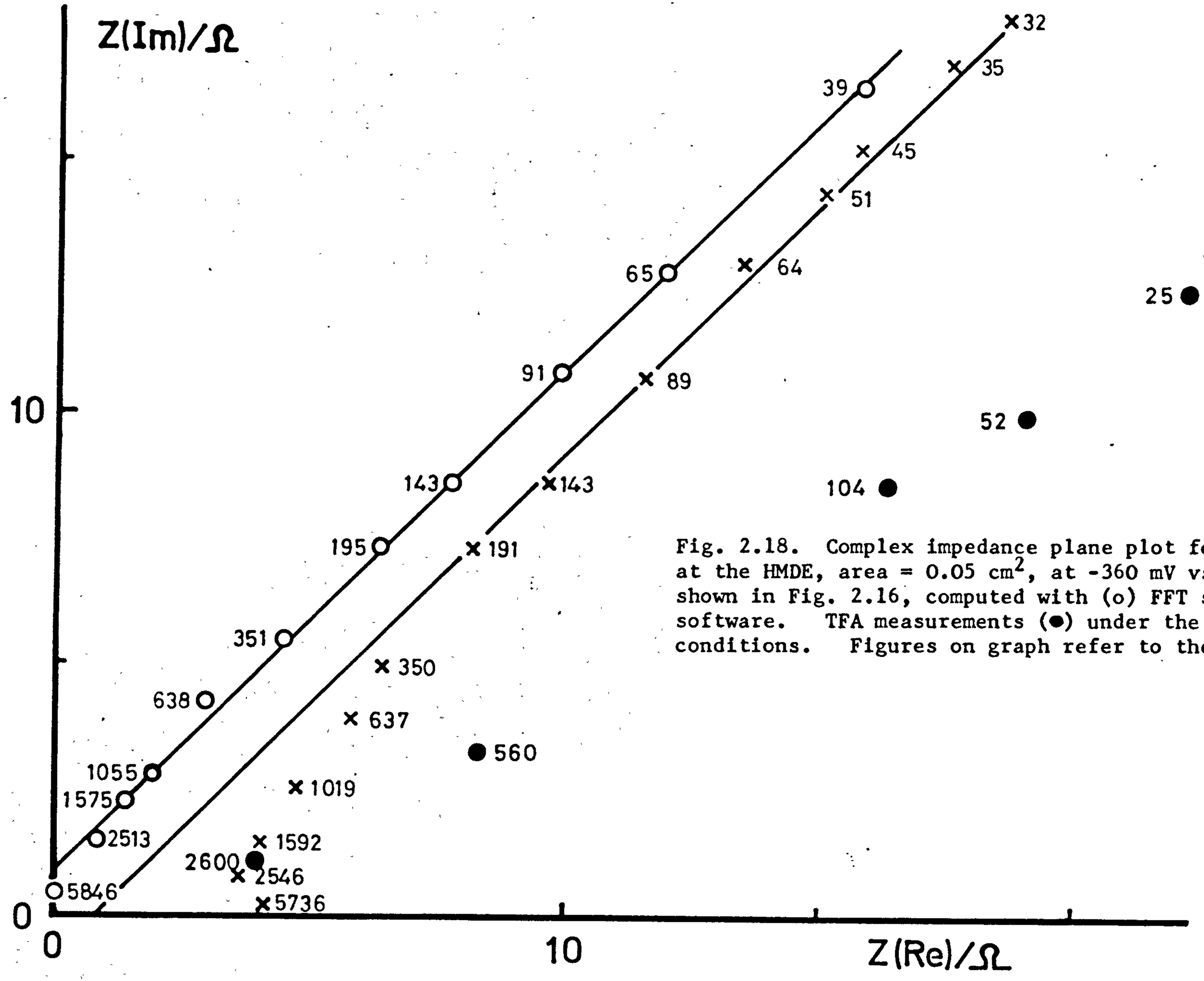

Fig. 2.18. Complex impedance plane plot for Pb^{++} reduction at the HMDE, area = 0.05 cm^2, at -360 mV vs S.C.E. from data shown in Fig. 2.16, computed with (o) FFT software, (X) LT software. TFA measurements (●) under the same experimental conditions. Figures on graph refer to the frequency in Hz.

experiment some build up of Pb as an amalgam is unavoidable, and may be a contributing factor.

Fig. 2.19 shows a Randles type analysis of the imaginary part of the data. The results are similar to those of Timmer et al[26] for a Pb^{2+}/KNO_3 solution. For example for a reversible redox reaction for the case of a.c. superimposed on a reversible d.c. wave[27]

$$\sigma = \sigma_m \cosh^2\left[\frac{nF}{2RT}(E - E_{1/2})\right] \qquad (2.48)$$

Where σ_m is defined by

$$\sigma_m = \frac{4RT}{n^2F^2\sqrt{2}\,(C_o^* D_o^{1/2} + C_R^* D_R^{1/2})} \qquad (2.49)$$

where σ is defined by $Z'' = \sigma\omega^{-\frac{1}{2}}$

Timmer et al give a measured value of 125 Ω cm^2 s$^{-\frac{1}{2}}$ in 1M KNO_3 solution at $E_{\frac{1}{2}}$ = -402 mV (S.C.E.). This value corrected for electrode area concentration and potential of Fig. 2.19 gives 99.7 Ω cm^2 s$^{-\frac{1}{2}}$ for the slope of the graph Z'' vs $f^{-\frac{1}{2}}$.

Although the i(t) data was averaged, it is possible to generate similar results from a single pass. It would have been better to use the BASAV sampler instead of DAQUAD to have a faster sampling rate (as low as 25μs per point). However, by comparison with the impedance spectrum obtained with the non interpolated data processed with the LT software, no alteration resulted from the interpolation performed.

II.6.4.3. Laplace Transform Impedance

Exactly the same data shown in Fig. 2.16 was processed by the Laplace Transform programs. The results are shown in Fig. 2.18. The equivalent Randles plot of the imaginary part plotted as a function of

Fig. 2.19. Randles plot for Pb^{++} reduction at -360 mV vs S.C.E., from data of Fig. 2.18; (o) FFT software. (X) LT software.

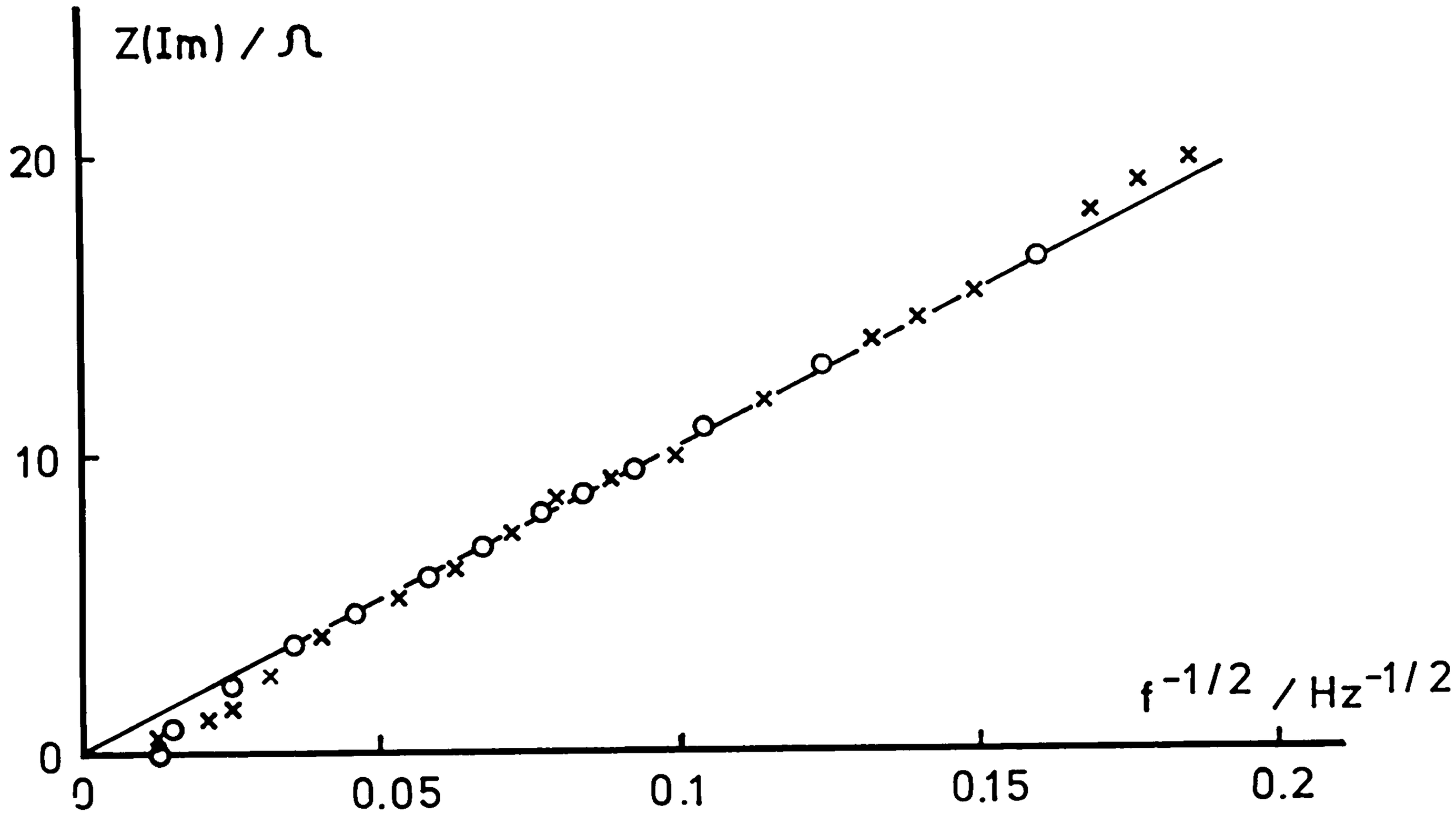
Z(Im) / Ω
20
10
0
0
0.05
0.1
0.15
0.2
f^-1/2 / Hz^-1/2

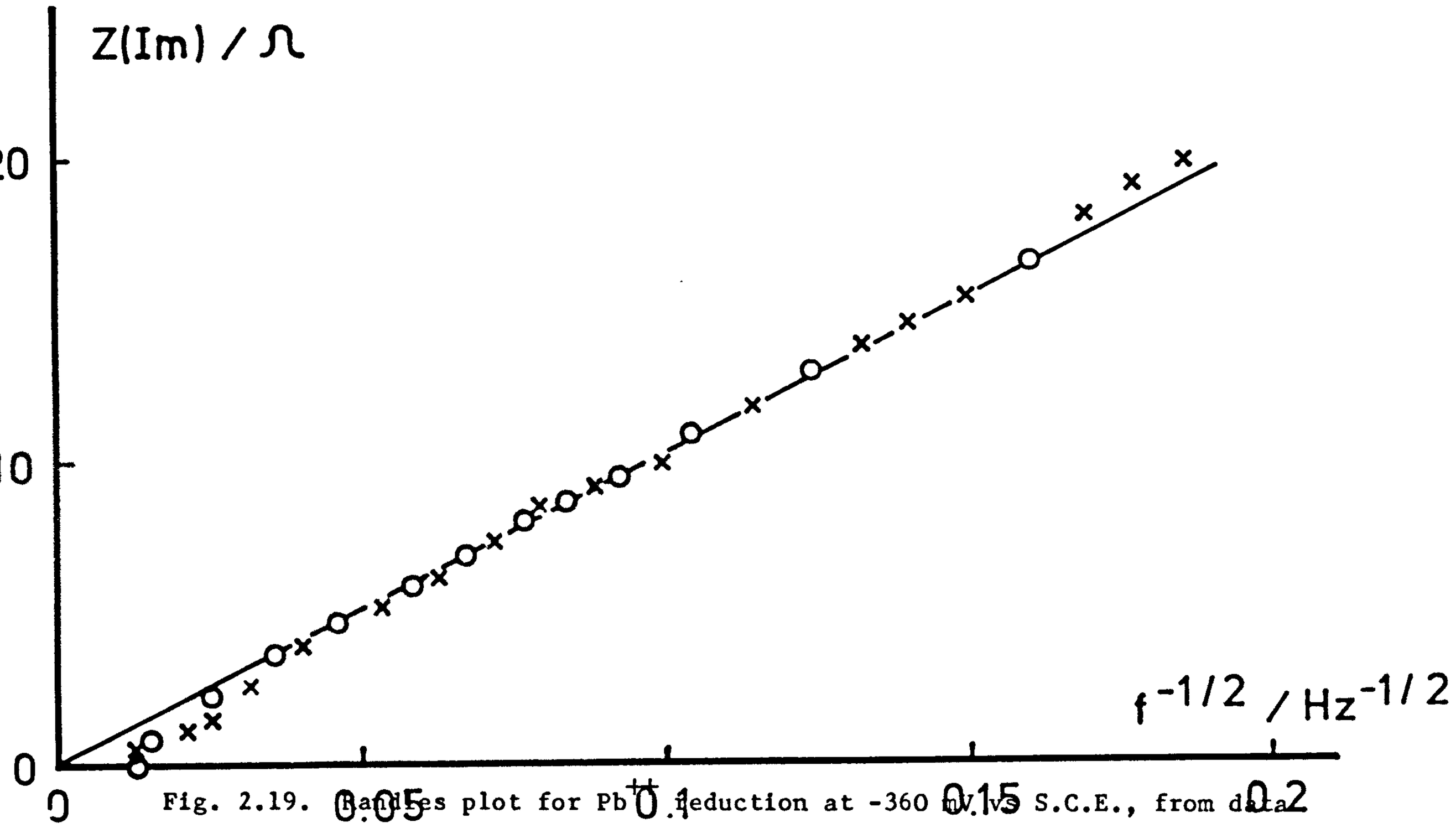

Fig. 2.19. Randles plot for Pb^{++} reduction at -360 mV vs S.C.E., from data of Fig. 2.18; (o) FFT software. (X) LT software.

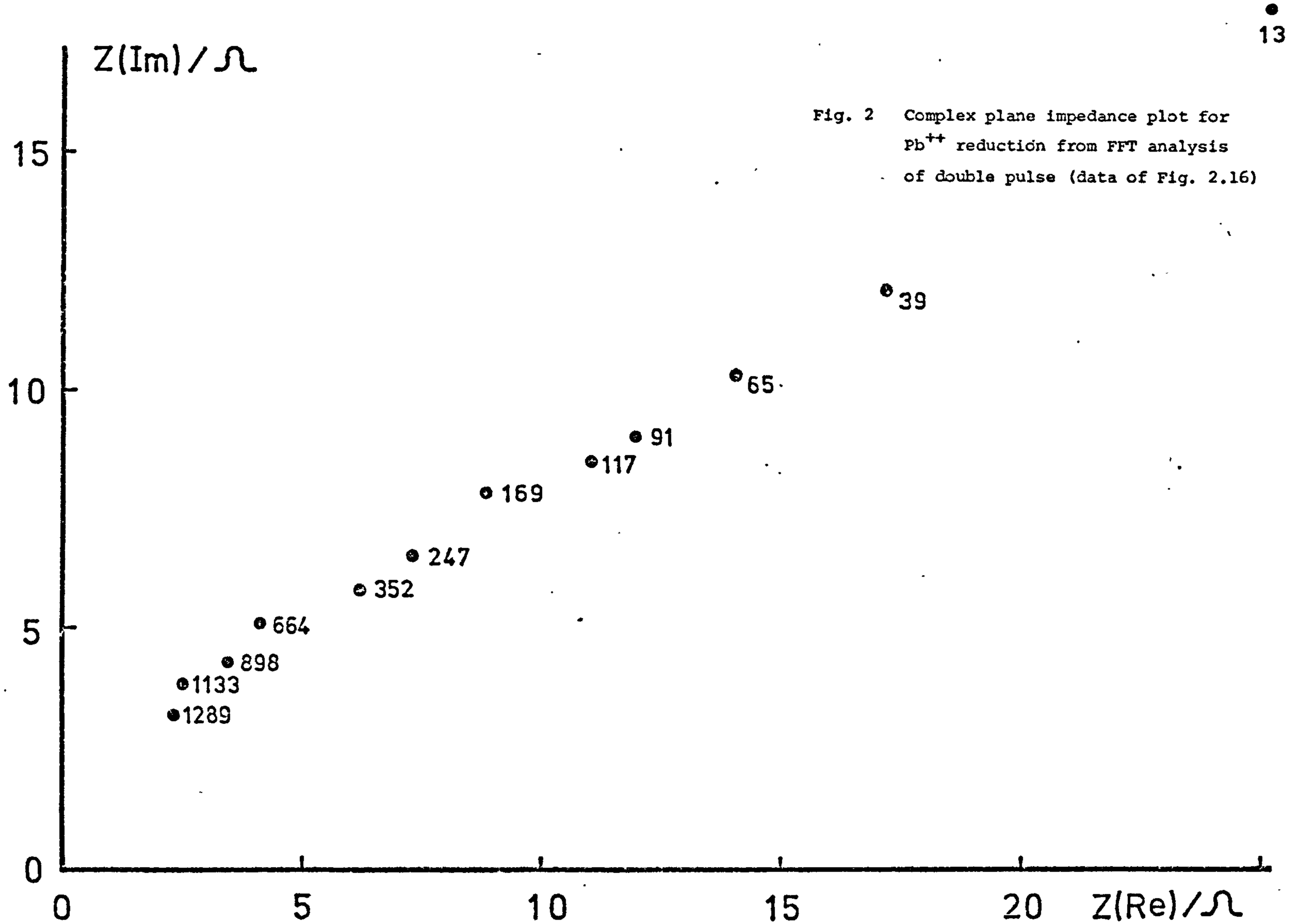

Fig. 2 Complex plane impedance plot for Pb^{++} reduction from FFT analysis of double pulse (data of Fig. 2.16)

$f^{-\frac{1}{2}}$ is shown in Fig. 2.19. The slope of the graph is $104 \Omega s^{\frac{1}{2}}$ at E = -360 mV SCE ($E_{\frac{1}{2}}$ is $\sim$ -372 mV for this case). As the previous work on test programs shows, the imaginary part Z(Im) is expected to be accurate. As shown in Fig. 2.18 there is some uncertainty in the real part Z(RE). This could be substantially improved by sampling at a faster rate than 150μs per point.

Measurements have also been made of the potential dependence of the impedance to test how far the method can be used. An example of an actual run is shown in Fig. 2.20 and 2.21. Fig. 2.22 shows for completeness an analysis of the imaginary part of the impedance Z(Im) at a fixed frequency of 31.8 Hz as a function of potential, based on the Equation (2.48). In the Figure a good fit is shown to the expected value of n = 2. The minimum value of σ_m gives according to Equation (2.49) a value of $D_0 = 1.17 \times 10^{-5}$ cm s^{-1}. These calculations were undertaken as a check on the values given by the impedance method.

The value of σ used in this graph is independent of frequency up to $\sim$ 1 KHz. Table 2.15 shows the value of σ deduced from the experimental graphs 2.20 and 2.21. This shows the variation in the data which is $\sim$ $520 \pm 50 \Omega s^{-\frac{1}{2}}$. It is clear that the results are satisfactory and are comparable with data obtained by phase sensitive detection. The advantage of using the computer is that now the processing and curve fitting to models, which is a vital part of any electrochemical experiment could now be carried out by computer.

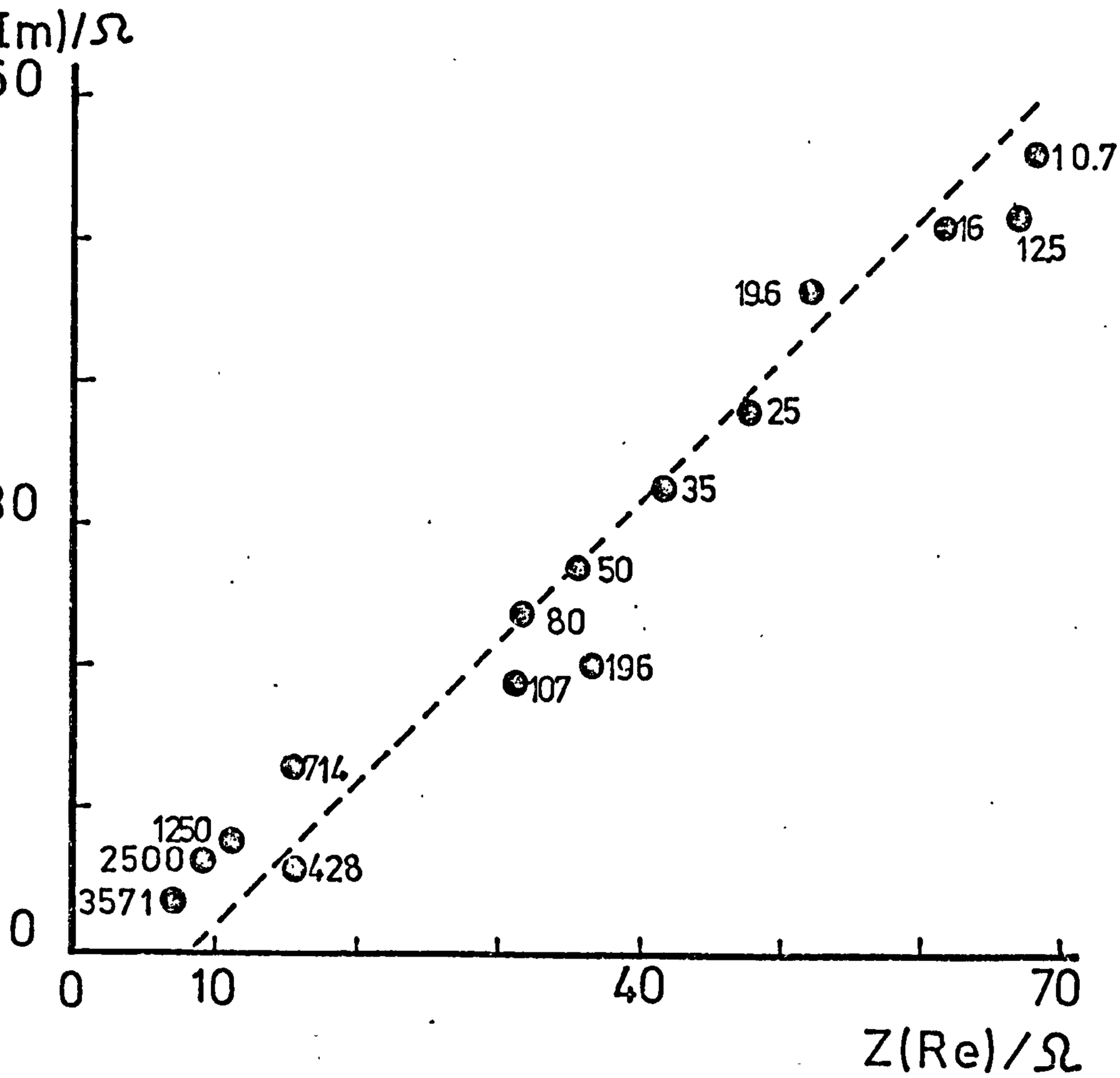

Fig. 2.21. Complex impedance plane plot for the reduction of Pb^{++} at the HMDE, obtained with the LT software from data of Fig. 2.20. Figures on graph indicate frequency in Hz.

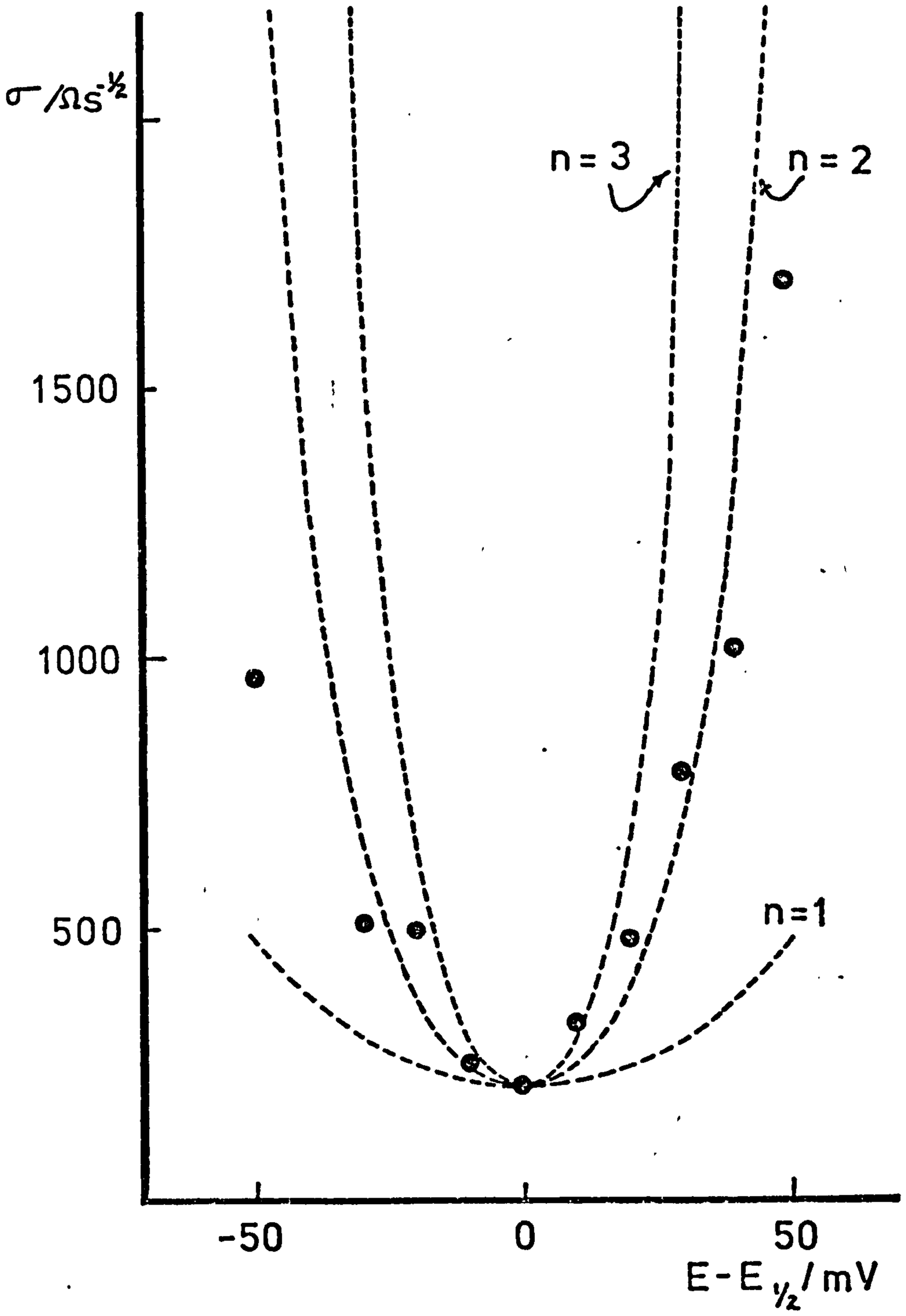

Fig. 2.22. Analysis of the Warburg impedance $\sigma\sim$, as a function of potential based on Eq. (2.48). (•) Results obtained from Z(Im) values determined with the LT software at a fixed frequency of 31.8 Hz, for Pb^{++} reduction at the HMDE in a solution 5×10^{-3}M $Pb(NO_3)_2$ + 1M $HClO_4$. Broken lines calculated according to Eq. 2.48 with indicated values of n and $\sigma_m = 212\ \Omega\ s^{-\frac{1}{2}}$.

REFERENCES

1. D.E. Smith, Anal. Chem., 48 (1976) 221A, 517A.
2. C. Gabrielli, M. Keddam and J.C. Lestrade, 21st Meeting I.S.E. Prague, 1970, p.221.
3. D.E. Smith in "Computers in Chemistry and Instrumentation", Vol. 2 (ed. J.S. Mattson, H.B. Mark, Jr. and H.D. Macdonald, Jr.), Dekker, 1972, Chp. 12.
4. A.A. Pilla in "Computers in Chemistry and Instrumentation", Vol. 2 (ed. J.S. Mattson, H.B. Mark, Jr. and H.D. Macdonald, Jr.), Dekker, 1972, Chp.6.
5. W. Lorenz and K. Schulze, J. Electroanal. Chem., 65 (1975) 141.
6. J.W. Cooley and J.W. Tukey, Math. Comp., 19 (1965) 297.
7. S.C. Creason, J.W. Hayes and D.E. Smith, J. Electroanal. Chem., 47 (1973) 9.
8. R. de Levie, J.W. Thomas and K.M. Abbey, J. Electroanal. Chem., 62 (1975) 111.
9. M. Sluyters-Rehbach and J.H. Sluyters, "Electroanalytical Chemistry", (ed. A.J. Bard), Dekker, 1970, Chp. 1.
10. J.E. Rothman, Decuscope, 7, No. 3, p. 3.
11. H.B. Sierra Alcazar, A.N. Fleming and J.A. Harrison, Surface Technology (in press).
12. B. Timmer, M. Sluyters-Rehbach and J.H. Sluyters, J. Electroanal. Chem., 18 (1968) 93.
13. M.D. Wijnen, Rec. Trav. Chim., 79 (1960) 1203.
14. E. Levart, E.P. d'Ange d'Orsay, J. Electroanal. Chem., 19 (1968) 335.
15. H.P. Van Leeuwen, D.J. Kooijman, M. Sluyters-Rehbach and J.H. Sluyters, J. Electroanal. Chem., 23 (1969) 475.
16. H.B. Sierra Alcazar, A.N. Fleming and J.A. Harrison, J. Electroanal. Chem. (in press).

17. M. Sluyters-Rehbach and J.H. Sluyters in Electroanalytical Chemistry (ed. A.J. Bard) Vol. 4, pg.1, Dekker 1970.

18. K. Doblhofer and A.A. Pilla, J. Electroanal. Chem., 39, 91 (1972).

19.

20. J.W. Cooley and J.W. Tukey, Math. Comp., 19 (1965) 297.

21. Operational Mathematics by R.U. Churchill, Second Ed. McGraw-Hill Kogakusha, p.2.

22. The Fast Fourier Transformation and its Implementation, James E. Rothman, Digital Equipment Corporation.

23. J.W. Cooley and J.W. Tukey, "An algorithm for the machine calculations of complex Fourier Series", Math of computers, Vol. 19, p.p. 297-301 April, 1965.

24. Getting on the air DEC-S8-OSGAB-A-D, Digital Equipment Corporation.

25. PLT Handler by Alan Cleary, Psychology Department, University of Newcastle upon Tyne.

26. B. Timmer, M. Sluyters-Rehbach and J.H. Sluyters, J. Electroanal. Chem. 18 (1968) 93.

27. M. Sluyters-Rehbach and Jan H. Sluyters, Electroanalytical Chem. 4, 1 Ed. A.J. Bard.

CHAPTER III

THE ELECTRODE KINETICS OF ZINC DEPOSITION

III.1. Introduction

The Zn deposition reaction in acid solution has been the subject of many investigations. The interest in this system revolves around the fact that Zn^{2+} discharge reaction is one of the few slow electrochemical reactions in which 2e are transferred. Much debate centres on whether these are transferred in a single 2e or two separate le steps. The reason for the electron transfer being slow is also of interest. A slow electron reaction is also a useful tool with which the effect of the structure of the double layer on the kinetics of the reaction can be investigated. However the work in this thesis is directed mainly towards a comparison of the rate of reduction of Zn^{2+} ions on Hg and on solid Zn and this review of previous work will be divided in this way.

A body of work also exists on the reduction of alkaline solutions of Zn^{2+}. This mainly deals with the problem of what complexes are present in solution and which one is discharged at the electrode and will not be exhaustively reviewed here.

III.2. Reduction of Zn^{2+} on Hg

The original and very fine early measurements of Randles and Sommerton[1] showed that a rate constant at E_e (equivalent to $i_c/nFC_{Zn^{++}}$) had the following values

Zn^{2+} 10^{-3}M	1M KNO_3	3.5×10^{-3} cm s^{-1}
	1M KCl	4.0×10^{-3}
	1M KBr	8.0×10^{-3}
	1M KCNS	1.7×10^{-2}
	1M KI	7.0×10^{-2}

Gerischer[2] measured the exchange current i_o as a function of Zn and Zn^{2+} concentration in $NaClO_4$ solution. At the low concentrations he used, the data fits the equation

$$i_o = nF k_{SH} [Zn^{2+}]^{(1-\alpha_1/(\alpha_1+\beta_1))} [Zn]^{\alpha_1/(\alpha_1+\beta_1)}$$

The actual values of the parameters were found to be

$$i_o = 1.02 [Zn]^{0.28} [Zn^{2+}]^{0.72} \text{ A cm}^{-2} \qquad (3.1)$$

where the concentrations are in mol l^{-1}. However this information is not so useful without potential dependence data. As shown earlier α_1 and β_1 are related to the Tafel slopes a, b(in mV) by

$$\frac{1}{a} = \frac{\alpha_1}{2.303} \qquad (3.2)$$

$$\frac{1}{b} = \frac{-\beta_1}{2.303} \qquad (3.3)$$

Koryta[3] made kinetic measurements at the dropping Hg electrode and found a = 90 - 120 mV by an analysis of $\log \frac{i}{i_d - i}$ vs E curves. However the Tafel slope depended on ionic strength in $NaNO_3$ solution.

Hush and Blackledge[4] analysed the charge transfer resistance R_D obtained from impedance measurements, using bridge measurements, as a function of potential and Zn^{2+} concentration. They used a theory which assumed that the a.c. was superimposed on a d.c. wave away from equilibrium.

A simplified theory due to Gerischer[2] gives if

$$i = nF\, k_{SH}\, [Zn^{++}]^{s} \exp \alpha_1 (E - E_o) \qquad (3.4)$$

then

$$\ln R_D = \ln \left(\frac{dE}{di}\right) = -\ln \left[nF\, k_{SH}\, \alpha_1 \left[Zn^{2+}\right]^{s}\right] - \alpha_1 (E - E_o) \qquad (3.5)$$

and if by the Nernst equation at constant $[Zn]$

$$\left[Zn^{2+}\right]^{s} = \exp - \frac{nF(E - E_o)}{RT} \qquad (3.6)$$

$$\frac{RT}{nF} \frac{d \ln Rd}{dE} = 1 - \frac{RT}{nF} \alpha_1 = \frac{RT}{nF} \beta_1 \qquad (3.7)$$

This procedure may not be accurate as the stationary i - E curve was not analysed to check that it was reversible. Since then more detailed theoretical analysis of a.c. on reversible, pseudo reversible d.c. waves has been made. On the basis of Equation (3.7) Hush and Blackledge determined $\frac{RT}{nF} \alpha 1$ from the straight line graph of ln R_D vs E. At high ionic strength they find a limiting value of 0.31. This corresponds to a Tafel slope of 97 mV. They also find, (their Fig.4) that the Tafel slope becomes smaller as the ionic strength decreases. For example it is 60 mV at $\sim$ 0.1 M. They also but less accurately measured polarographic i - E curves for the dissolution of amalgam electrodes. They found in 2M $NaClO_4$ a Tafel slope of 47 mV for the anodic reaction. A two step reduction of Zn^{2+} was tentatively suggested on this basis.

In a further paper these authors confirmed the rate constants measured by Randles and Sommerton at E_e for the Zn^{2+} reduction in the presence of Cl^-, Br^-, I^- and CNS^-. They also found in 1M solutions, from impedance measurements, that the Tafel slope varied from 97 mV in Cl^- to

75 mV in CNS^- and 30 mV in I^- containing solution.

In a series of papers Sluyters and his co-workers have investigated the Zn^{2+} reduction by a number of techniques. They were also able to investigate the reaction of a wide potential range by applying imposed d.c. over a wide range of potential.

The first attempt[6] shows that the Zn^{2+} reduction at the streaming Hg electrode showed two peaks in the cathodic a.c. polarogram under some conditions. These diagrams were constructed by calculation from the real Z' and imaginary Z'' part of the measured impedance, so as to eliminate the double layer capacity contribution. These peaks were interpreted as Zn^{2+} and Zn^+ reduction waves. A subsequent paper[7] showed, however, that similar diagrams could be generated from a better theory for the a.c. impedance of a.c. on an irreversible d.c. wave. A similar theory for a.c. polarography on reversible and irreversible d.c. waves has been given by other authors[12,13].

An analysis[8] of the plots of θ - E and σ - E for 3×10^{-3}M Zn^{2+} + 3×10^{-3}M Zn/Hg in 1M KCl (pH 3) showed that the data could be fitted experimentally with a single electron transfer. The Tafel slope was suggested to be $\sim$ 90 mV.

Teppema et al[9] and Sluyters-Rehbach[10] et al reinvestigated the effect of the anion on the rate of the Zn^{2+} reduction and the Tafel slope. They[9] found 87.5 mV in 1M KI and 104 mV in 0.5M KCl + 0.5M KI by a galvanostatic method of measuring the standard rate constant as a function of concentration of Zn^{2+}, Zn and the KCl/KI ratio (= x). They state that as I^- and NO_3^- have little tendency[14] to complex formation and Cl^- is known to complex appreciably with Zn^{2+} then chloro complexes should be accounted for. They do this by assuming that Zn^{2+} is reduced and calculate its concentration from equilibrium data[14]. In addition they separately apply the Frumkin double layer potential correction to the k_{SH} - x curve. They

suggest that k_{SH} correlates with the adsorbed charge q', obtained by the Grahame and Parsons method[15,16]. Unfortunately considerable doubt has been put on the Frumkin method and the calculation of adsorbed charge by a series of six papers by Cooper and Harrison in these laboratories. In a further paper[10] they reinvestigated the problem in more detail by a.c. impedance. They say that this method is preferable as the d.c. potential can be varied greatly, compared to the measurement of i_o or k_{SH} as a function of E_c or the analysis of d.c. i - E curves which concentrates on data near to $E_{\frac{1}{2}}$. These authors confirm the Tafel slopes of Hush and Blackledge in the anodic region and also their previous finding[9] that the calculated value of k_{SH}(assuming a fixed value of Tafel slope) is not constant when estimated for various potentials. They are of the opinion k_{SH} correlates with q'. A weakness of this paper is that they do not seem to appreciate that a difference in the anodic and cathodic Tafel slopes is commonly observed for two step reactions (for example the well known Cu^{2+} reduction). A review and some further experiments based on the Faradaic rectification method have also been given[11].

Tamamushi et al approached the problem from polarograph i - E. They analysed the cathodic wave only. The observed pseudo reversible waves depended on the anion. Only in ClO_4^- and NO_3^- could the entire wave shape be predicted. In I^- this was not the case. However their implicit assumption that $\alpha + \beta = 1$ is not correct for a 2e reaction. However the slopes of the $\log \frac{i}{i_d - i}$ /E plots at the most negative potentials, given in their Table 1 should be meaningful. They indicate that in Br^- a cathodic Tafel slope of 74 mV and in ClO_4^- a 62 mV Tafel slope. I^- has a reversible wave. The kinetic parameters α and k_{SH} were recalculated[19]. The latest paper[20] in which the Zn^{2+} reduction in 1M KCl, KBr, KCNS was investigated by square wave polarography. The results show that the standard rate increases with the anions in the order $CNS^- > Br^- > Cl^-$ and also that the Tafel slope is steepest in CNS^-. A number of authors

have achieved similar experimental results[21,22]. Larionov and Dudrin have suggested that adsorbed complexes should be considered.

Salie[24] made extensive conventional a.c. measurements in the Zn^{2+} reduction system[24]. He measured the concentration dependence of the exchange current to obtain the value of α. By changing the Zn^{2+}/Zn ratio in order to change E_e he could change the potential over a large range. He found that α was a function of E_e. He states that this is characteristic of a 2e reaction in which the i_o's for the separate electron exchange steps affect the overall reaction. On this basis by curve fitting he obtained values of the separate reaction exchange currents.

A similar argument has been used by Ericksrud[25] who has analysed i - E curves derived from galvanostatic measured for two separate reactions according to the equations of Hurd[26]. Unfortunately in the galvanostatic method the double layer charging cannot be eliminated.

III.3. The Reduction of Zn^{2+} on Solid Zn

A reasonably complete investigation has been carried out by Gaiser and Heusler[27]. They measured the anodic and cathodic Tafel slopes of the stationary i-E curves (measured after 1 sec). They found an anodic Tafel slope of 40 mV in Zn^{2+} free solution which was independent of pH from 3.7 to 2.5. A 120 mV slope was also observed at high potentials. It is possible that the i-E curves have not been corrected accurately for the ohmic drop. The cathodic Tafel slope of 120 mV was measured at pH 4.6 to avoid the influence of the H_2 evolution reaction. It was first order in Zn^{2+} concentration. The measurements were extended to malonate solutions by Heusler and Knodler[28].

Hurlen and Fischer[29] report anodic and cathodic galvanostatic measurements in 5×10^{-3}M $ZnCl_2$ + KCl at pH 3.0. The results are similar to those in ClO_4^- solution and a 40 mV anodic and 120 mV cathodic Tafel

slope are reported. The curves depend on Cl^- concentration. Hurlen and Eriksrud[30] report that in 5×10^{-3}M $ZnCl_2$ + 0.99M KCl i_o was 0.8 mA cm^{-2}, and suggest that the cathodic reaction and not the anodic reaction depends on the nature of the salt.

Clarke and Hampson[31] investigated the reaction in ClO_4^- solution. They report on i_o of 0.35 mA cm^{-2} independent of Zn^{2+} concentrations, which nullifies their results.

Epelboin et al[32] have investigated the deposition of Zn at high concentrations of Zn^{2+}, in the region of 1M, in Na_2SO_4 and NH_4Cl, at the rotating disc. For currents lower than 10 mA and pH 4.3 they observe a stationary i-E curve which is S shaped. At pH 2.0 the curve is a single curve which is shifted to more negative potentials. Impedance diagrams measured at pH 4.3 show some very characteristic features; a high frequency semicircle coupled to two inductive semicircle-like features. The authors interpret these measurements by a theory of multiple stationary states in which they set up the equations for a series of competing electrochemical reactions. These are the H_2 evolution reaction, the Zn deposition reaction (assumed to go in two le steps) and coupling between the two reactions. These ideas have been developed in a series of papers[32,33,34,35]. The authors also show that an adsorbed intermediate in a single electrochemical reaction[33] can also lead to an inductive impedance.[33] Davison, Harrison and Thompson, however,[36] have pointed out that surface relaxations due to electrocrystallisation can probably cause similar effects. The quoted experiments on Pd deposition where an inductive impedance is observed in the potential region where rising i-t transients are observed when a pulse is applied. Many other systems show similar behaviour. A good example is shown in the review of measurements of the Paris school by Wiart, Lejay and Lenoir[37], namely for the deposition of Ag. A distorted high frequency semicircle is observed in the impedance coupled to a low

frequency inductance. For such a simple le reaction this result is very difficult to explain, as the authors do, by invoking adatoms. The most likely explanation is a surface structure relaxation.

There is a suggestion in the literature[38] that simultaneous H_2 evolution suppressed the Zn reaction. However this disagrees with the Epelboin et al results and interpretation that it has a catalytic effect.

REFERENCES

1. J.E.B. Randles, K.W. Sommerton (part 4) Trans. Far. Soc. 48 (1952) 951

2. H. Gerischer Z. Physik. Chem. 202 (1953) 302

3. J. Koryta Electrochim. Acta 6 (1962 67

4. N.S. Hush, J. Blackledge J. Electroanal. Chem. 5 (1963) 420

5. N.S. Hush, J. Blackledge J. Electroanal. Chem. 5 (1963) 435

6. M. Sluyters-Rehbach, A.B. Ijzermans, B. Timmer, J.B. Griffioen, J.H. Sluyters Electrochim. Acta 11 (1966) 483

7. B. Timmer, M. Sluyters-Rehbach, J.H. Sluyters J. Electroanal. Chem. 14 (1967) 169

8. B. Timmer, M. Sluyters-Rehbach, J.H. Sluyters, J. Electroanal. Chem. 14 (1967) 181

9. P. Teppema, M. Sluyters-Rehbach, J.H. Sluyters, J. Electroanal. Chem. 16 (1968) 165

10. M. Sluyters-Rehbach, J.S. M.C. Brenkel, J.H. Sluyters, J. Electroanal. Chem. 19 (1968) 85

11. F. van der Pol, M. Sluyters-Rehbach, J.H. Sluyters, J. Electroanal. Chem. 58 (1975) 177

12. H. Matsuda, Z. Elektrochem. 62 (1958) 977

13. G.H. Aylward, J.W. Hayes, R. Tamamushi, Proc. 1st Australian Conf. Electrochem. 1963, Pergamon Press, 1964 p.323

14. L.G. Sillen, A.E. Martell, Stability Constants, The Chemical Society, London

15. D.C. Grahame, R. Parsons, J. Amer. Chem. Soc. 83 (1961) 1548

16. D.C. Grahame, J. Amer. Chem. Soc. 80 (1958) 4201

17. I.L. Cooper, J.A. Harrison, a series of papers on the structure of the double layer (in press in J. Electroanal. Chem. and Electrochim. Acta)

18. R. Tamamushi, K. Ishibashi, N. Tanaka, Z. Phys. Chem. (NF) 35 (1962) 209

19. R. Tamamushi, N. Tanaka, Z. Phys. Chem. (NF) 39 (1963) 117

20. R. Tamamushi, K. Matsuda, J. Electroanal. Chem. 80 (1977) 201

21. R.J. Brodd, J. Electrochem. Soc. (Japan) 37 (1969) 181

22. A. Hamelin, Electrochim. Acta 9 (1964) 289

23. O.V. Larionov, Ya.V. Dudrin, Sov. Electrochem. 8 (1972) 1760

24. G. Salie, Z. Phys. Chem. 244 (1970) 1

25. E. Eriksrud, J. Electroanal. Chem. 76 (1977) 27

26. R.M. Hurd, J. Electrochem. Soc. 109 (1962) 327.

27. L. Gaiser, K.E. Heusler, Electrochim. Acta 15 (1970) 161

28. K.E. Heusler, R. Knodler, Electrochim. Acta 18 (1973) 855

29. T. Hurlen, K.P. Fischer, J. Electroanal. Chem. 61 (1975) 165

30. T. Hurlen, E. Eriksrud, J. Electroanal. Chem. 63 (1975) 157

31. J.T. Clarke, N.A. Hampson, J. Electroanal. Chem. 26 (1970) 307

32. I. Epelboin, M.K. Souri, R. Wiart, Electrochem. Soc. 122 (1975) 1206

33. I. Epelboin, M. Ksouri, R. Wiart, J. Electroanal. Chem. 65 (1975) 373

34. I. Epelboin, M. Ksouri, R. Wiart, J. Electroanal. Chem. 58 (1975) 433

35. E. Lejay, R. Wiart, C.R. Acad. Sc. Paris 277C (1973) 833

36. W. Davison, J.A. Harrison, J. Thompson, Far. Disc. Chem. Soc. No.56 (1974) 171

37. R. Wiart, E. Lejay, F. Lenoir, Interfinish 1972 (ed. Ibl et al) Forster Verlag, Zurich, 1973

38. V.N. Vitova, A.T. Vagramyan Sov. Electrochemistry 2 (1966) 1052

CHAPTER IV

EXPERIMENTAL

IV.1. Introduction

This chapter details the experimental aspects which are common to all the work in this thesis, excluding specific equipment used in connection with on line measurements, as well as experimental work used to test the LT and FFT impedance determination method. They are described in Chapter II.

This chapter contains four sections, the first describes the electronic hardware used to generate potentiostatic signals and measure and record the current response, the second describes the cells used and the preparation of electrodes, the third describes the materials and reactives used and finally the fourth section describes a stressometer developed in this laboratory from a model in Cannings Ltd. No experiments were performed to measure stress due to lack of time, nevertheless the apparatus constructed is described since it is thought that relevant information on zinc electrocrystallization could be derived because with this design the stress can be monitored while potentiostatically sweeping the potential.

IV.2. Instrumentation

IV.2.1. Potentiostats

Two potentiostats were used in most of the experimental work to be discussed. A Chemical Electronics Ltd. potentiostat (model TR7012A) was used for most of the RDE work, and sweep and pulse measurements in the HMDE. This potentiostat is a solid state instrument having a zener-stabilised reference potential circuit and allows a maximum cell voltage

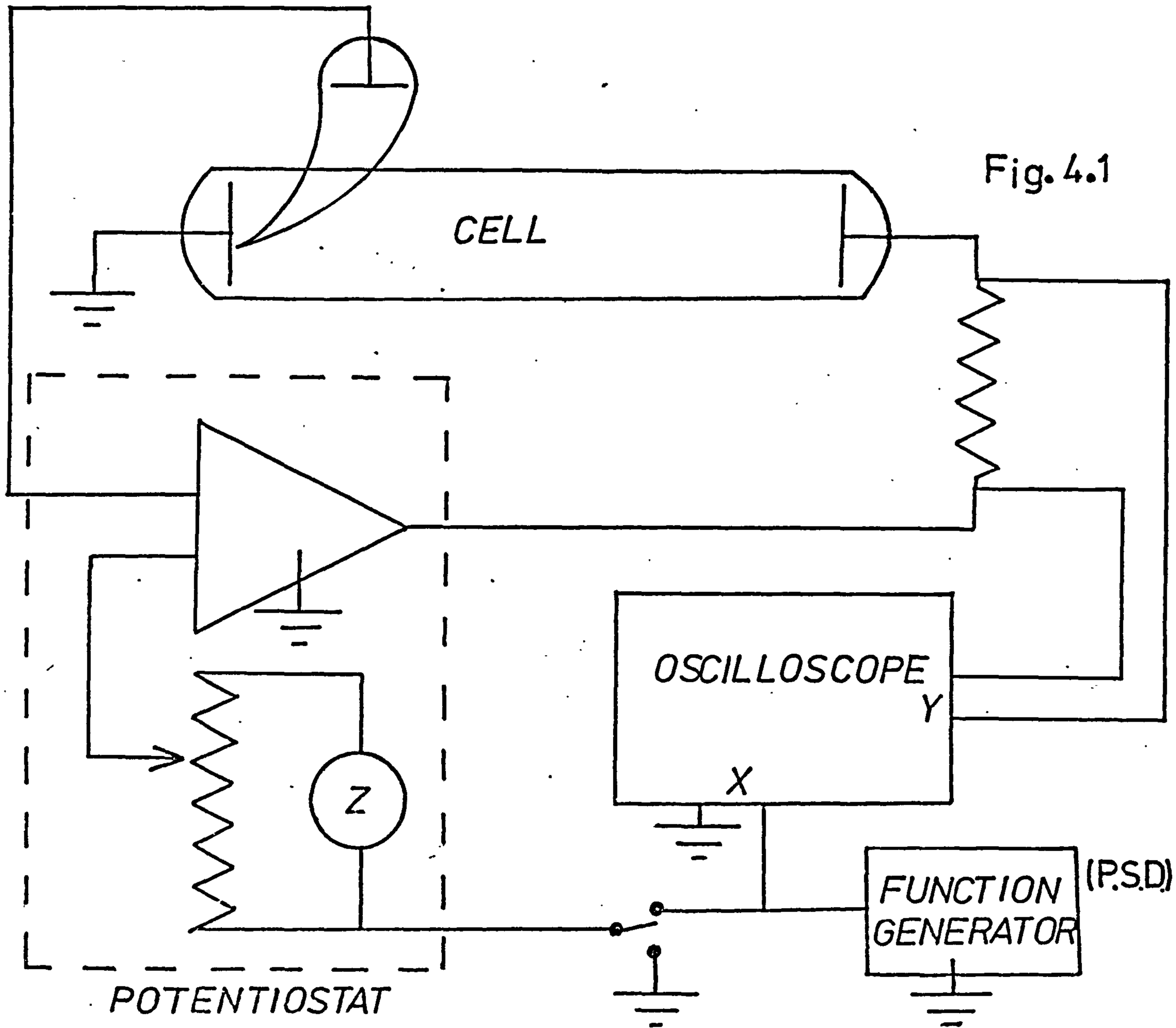
CELL
OSCILLOSCOPE
Y
X
Z
FUNCTION
GENERATOR
(P.S.D)
POTENTIOSTAT

Fig. 4.1

(working to auxiliary electrode) of 70V or a maximum cell current of 2A. The design criteria of these potentials have been discussed by Bewick[1,2,3,4] and Brown[5]. Typically the instrument was capable of stabilising a fixed potential at $\pm$ 0.5 mV over long periods and had a rise time of approximately 30μs for a square wave input. A block diagram of the circuit used for sweeps and pulse measurements at the HMDE and RDE is shown schematically in Fig.41.

IV.2.2. Function Generators

The voltage functions could be superimposed on the potential maintained by the potentiostat. The potential sweep and pulse generator used was made in this department from a design created by O.R. Brown[5]. This instrument could supply square wave pulses of an amplitude $\pm$ 3V for durations ranging from 32μs to several seconds. The sweep range was $\pm$ 3V at sweep rates ranging from 0.1 mV s^{-1} to 1000V s^{-1}. Multi-sweep and pulse profiles could be obtained with a repetition rate between 100μs to 33 s. Triggering could be done at different positions in the profile (see also Section II.6.4.a).

For PSD measurements a Brookdeal signal source (Type 471) was used to superimpose a small (approximately 10 mV peak to peak) sinusoidal signal on the d.c. potential. The two frequency scales (either logarithmic or linear) allowed a range from 1 MHz to 10^{-3} Hz to be covered. The TFA used has a built-in waveform generator with a sinusoidal or square wave of frequency range 10 KHz to 0.001 Hz.

IV.2.3. Current measurement and recording

The current flowing through the cell could be measured directly from the analogue ammeter incorporated in the TR 70/2A Potentiostat or from the digital ammeter in the DT 2101 Potentiostat. For more accurate

current measurements the analogue ammeter was substituted by measuring the potential drop across a calibrated resistor (100 or 1000 Ω) placed in series with the subsidiary electrode, by means of a digital voltmeter (Solartron LM 1620). With the DT 2101 potentiostat, the digital ammeter gave good accuracy; instead of measuring resistor, it uses an operational amplifier to measure the current.

Current-potential curves from linear sweep or pulse measurements were recorded automatically on a Bryans X-Y chart recorder (Type 2600 A4), the output of the function generator being fed simultaneously into the potentiostat and the X-axis of the recorder. For short time pulse experiments and for sweep rates $> 1V\ s^{-1}$, the i - t curves were displayed on an oscilloscope (Tektronix 502A Dual Beam). The curves were recorded photographically using a polaroid camera.

IV.2.4. A.c. Impedance Measurements

Initially the measurements were made with a phase sensitive detector (PSD) which covers only the high frequency range (10K to 5 Hz), however most work was done with the manual transfer function analyser (TFA) and only for some measurements on the RDE, the automated frequency response analyser AFRA was used. Description of these equipment follows.

IV.2.4.1. Phase Sensitive Detector (PSD)

Measurements were made using the circuit shown in Fig. 4.2. The PSD used was a Brookdeal Type 411 and the reference unit (RU) was a Brookdeal Type 422 in conjunction with a signal source (SS), Brookdeal Type 471. The principle of operation is illustrated in the block schematic of Fig. 4.3 which represents a PSD as a voltage controlled gate with output resistance R. The reference voltage switches the signal V_s on and off every half cycle. When the reference and signal are of the same frequency and phase, the PSD acts as a half wave rectifier and gives a mean direct voltage

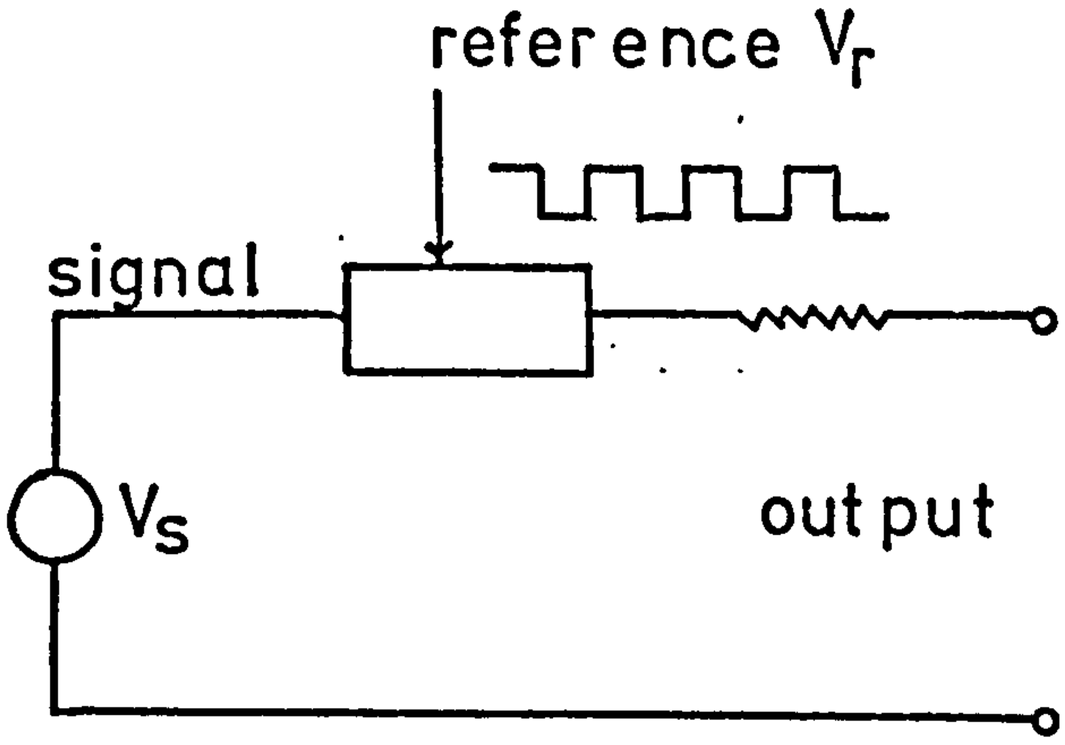

Block schematic of P S D
Fig. 4.3

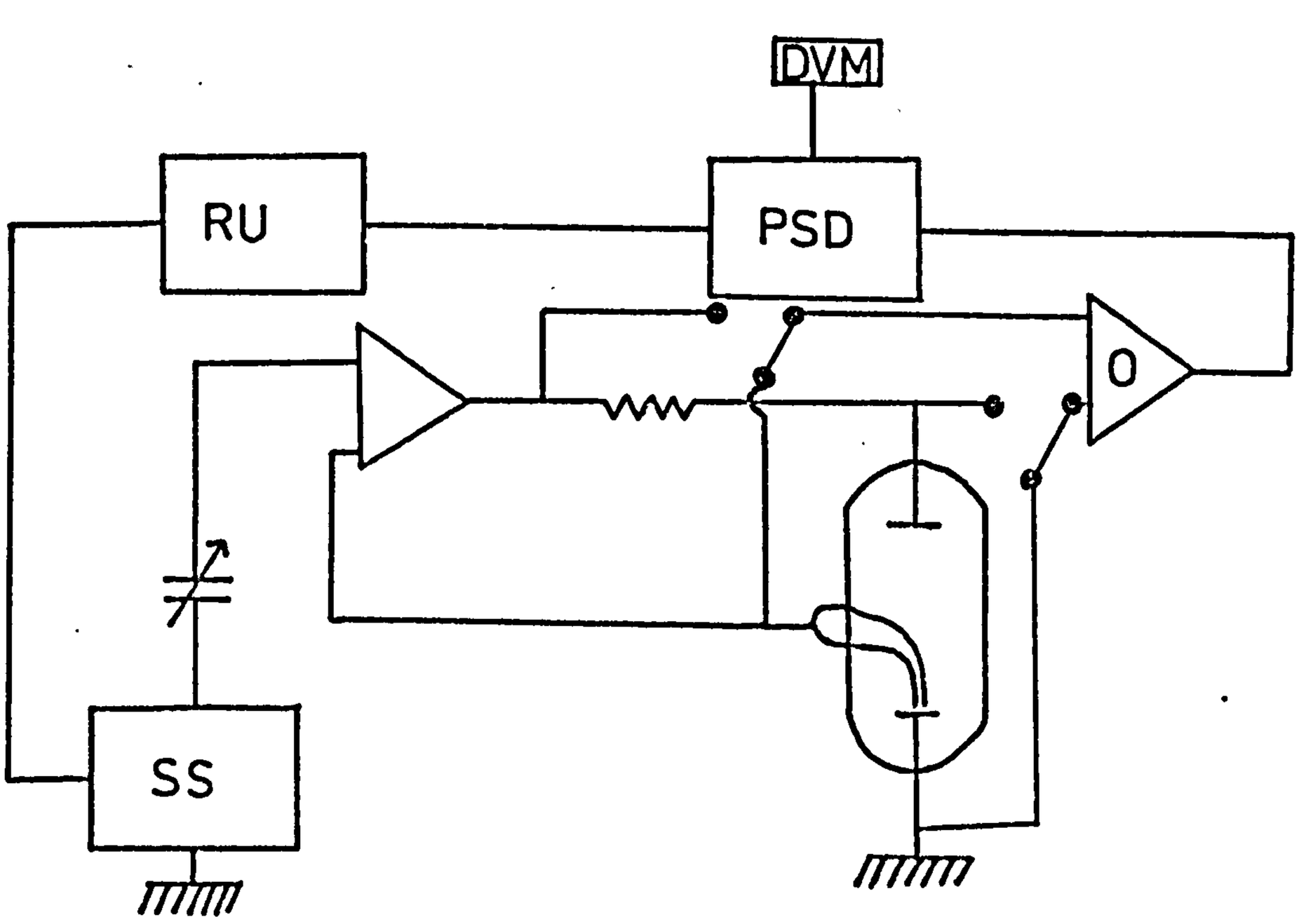

Fig. 4.2 PSD CIRCUIT

proportional to the amplitude of the signal voltage. When they are in antiphase the d.c. output is reversed. When the signal and reference are in quadrature the mean output is zero. These results may be summarised by $V_{out} \propto V_s . \cos \phi$ where V_{out} is the average output voltage, V_s is the signal voltage and ϕ is the phase angle between the signal and reference, the output of the P.S.D. is a direct voltage (which can be accurately monitored on a DVM. The total impedance at each frequency was estimated from the signals across the cell (reference to working electrode) and the current measuring resistor by the method described in Appendix D.

IV.2.4.2. Transfer Function Analyser (TFA)

The TFA used was a S.E. Electronics Model SM 272. This instrument is essentially the same as the PSD, SS and RU in Fig. 4.2 put together in one unit, with the difference that the in-phase and out of phase components are evaluated simultaneously with twin PSD circuits, allowing faster measurements. If this manual unit were interfaced with a LAB-MINICOMPUTER, as it is feasible, the resulting system would be equivalent to the AFRA described below. The TFA method of operation is based on a technique known as homodyne rectifier detection, which is a highly selective phase sensitive detector circuit. The result is the same as that of the PSD, i.e. $V_{out} = V_s \cos \phi$. This voltage is the value displayed in the "R" display. A second complete homodyne detector circuit provides the 'Q' display and will display $V_s \sin \phi$ because the 'Q' homodyne detector is driven by the reference shifted 90^o. Only the synchronous component of the return signal will produce d.c at the rectifier output, all a.c. components having frequencies other than that of the reference signal will produce no d.c. This provides high noise rejection capability. Clearly a d.c. component is also completely rejected. Both homodyne rectifier circuits have active filters to reduce odd and higher order harmonic contribution to the d.c. The third harmonic contri-

bution is greatly reduced by having the PSD open during ⅔ of the reference half period (which is equal to the period of the third harmonic). The S.S. circuit can generate sine, triangular or square waveforms in a frequency range from 9.99 Hz to 0.01 Hz. The frequency range could be extended to 0.001 Hz with an external 10μF capacitor.

A small sine waveform of $\sim$ 8 mV peak to peak was used for all experiments. The settling (integration) time for high frequencies (9.9 KHz to 100 Hz) was approximately 2 s (selectivity 0.8 Hz) and approximately 2000 s for low frequencies (0.5 to 0.01 Hz), with the correlator circuit set at a selectivity of 0.8 mHz. When the measurement readings off the cartesian displays 'R' and 'Q' were made according to the following diagram

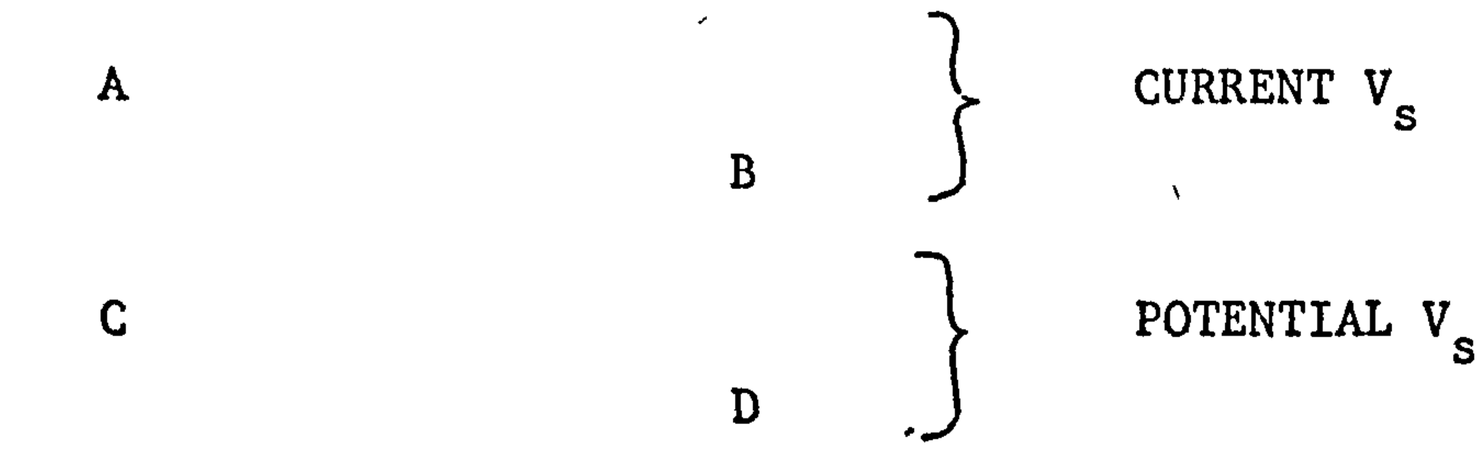

the impedance was calculated in a programmable TEXAS SR-52 calculator according to Equations 2.24 and 2.25.

IV.2.4.3. Automatic Frequency Response Analyser (AFRA)

This instrument measures the system's frequency response in a way essentially the same as described above for the TFA system, with the advantage that the operation is automatic and therefore, results at high frequence are obtained faster than with the manual TFA system. At low frequencies it has no significant advantages over the manual system since integration times are big in comparison with the time taken to change input signal and calculate the results manually.

The AFRA consists[6] basically of a programmable generator that

provides a stimulating signal; a correlator to analyse the system's response and a display to present the results. The interfacing with the experimental system is shown in Fig. 4.4. The generator provides a potential a.c. signal ΔE of known amplitude and frequency which is in the form $A \sin wt$. The fundamental system response to this signal will be in the form $R \sin (wt + \theta)$, and besides this fundamental term, harmonics due to system non-linearities together with random noise will also be present in the output. The Analyser section of the AFRA takes this current response as well as the ΔE signal and by a correlation process determines R and θ. This technique has the advantage of rejecting all harmonics present in the systems output and also minimising the effect of random noise. The maximum frequency is limited to 10 KHz, the minimum frequency down to 0.1 mHz. The response is given once a measurement has been completed and can be displayed as Z(Im) and Z(Re) or amplitude and phase angle ϕ. The results together with the measurement frequency are then transferred to either a teletype printer or a tapepunch. Simultaneously the results can be plotted on an X-Y recorder.

In an ideal situation, the frequency range from 10 KHz to 10 Hz can be covered[7] in 30 s (at 10 points per decade). However[7], it must be emphasised that below 10 Hz the time for a single measurement is equal to the period of the signal (10^3s at 10^{-3} Hz) and this becomes the major contribution to the total experimental time. In most practical applications a certain amount of random noise is invariably superimposed on the signal to be analysed. Since this is essentially an averaging instrument, when noise is troublesome, greater accuracy can be obtained by increasing the integration (averaging) time. Typically[7] to cover the frequency range from 10 KHz to 0.4 Hz integrating over 10 times the minimum theoretical period, it takes 16 minutes to complete the measurements.

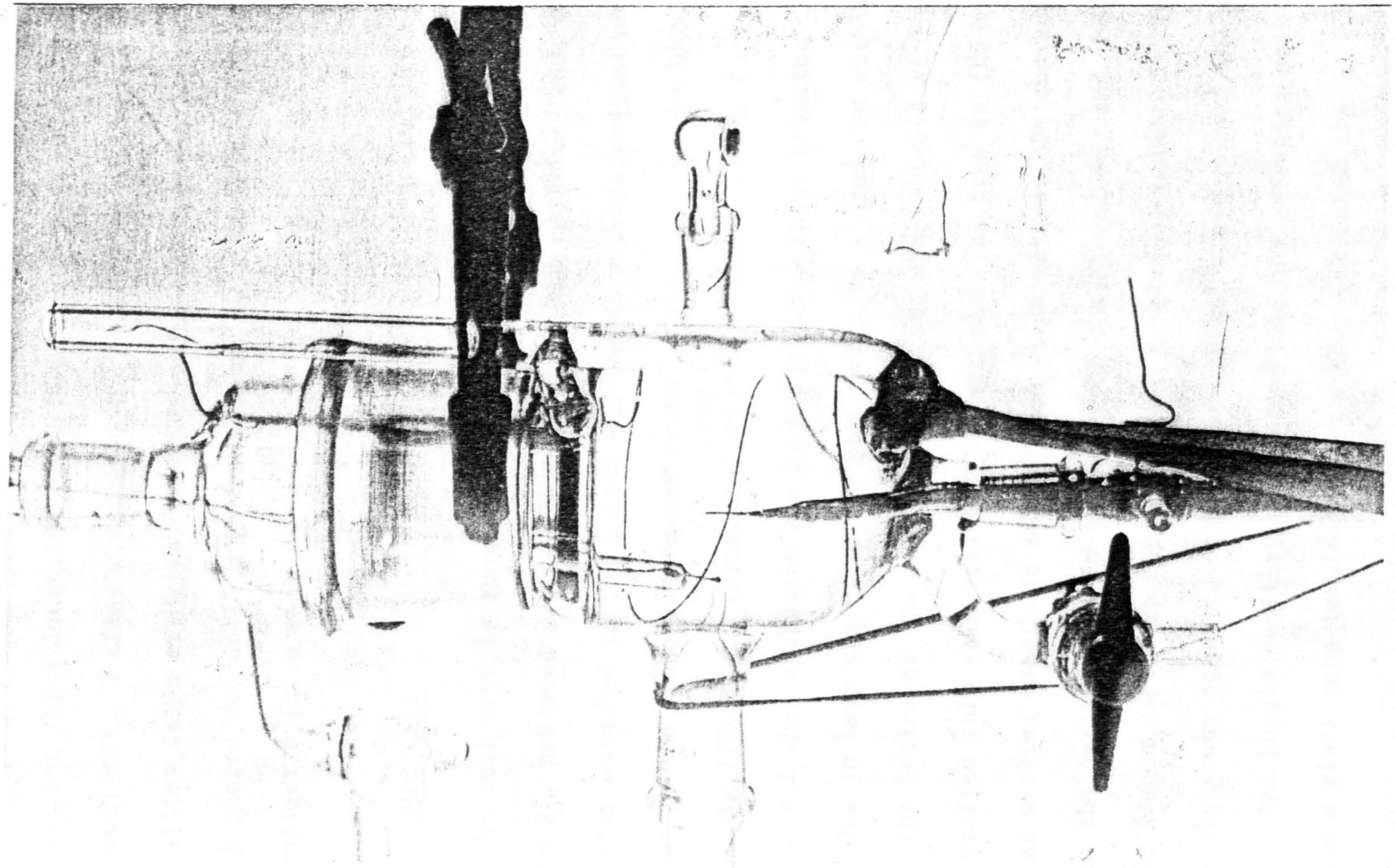

IV.3. Cells and Electrodes

IV.3.1. Hanging Mercury Drop Electrode (HMDE)

The HMDE was prepared with a platinum spike embedded into a glass rod and rube. The end was ground conic and the Pt spike flat before Hg plating for a long time ($\sim$ 1 hour) in a solution of $Hg_2(NO_3)_2$ acidified with HNO_3. After rinsing with triple distilled water it was ready to collect drops of Hg in the cell, which will adhere to the permanently plated Hg, until a good shake was applied to get rid of one drop and collect a fresh one.

IV.3.2. HMDE Cell

The cell used is shown in Fig. 4.5. The upturned syringe, filled with Hg, produced reproducible drops in the capillary end, when the micrometer attached to the bottom was turned a predetermined number of divisions. The drop thus formed could be picked up by the HMDE and, by rotating the HMDE stem, translated to the proximity of the Luggin capillary. All this operation can be performed without breaking the gas seal, in order to keep the N_2 atmosphere, which is introduced with a bubbler in the bottom of the cell and output through a liquid seal in the top. If desired this same cell can be used with the drop in the syringe capillary as working electrode since there is an external Pt contact sealed into the syringe body in contact with the Hg column, and the syringe and Luggin capillary can be rotated to close proximity. The auxilliary electrode consists of a Pt wire spiral wound around the.working electrode. The Luggin capillary which provided the reference point in the cell was a glass tube terminating in a fine chamfered tip 1 mm away from the Hg drop. The reference electrode connected to the Luggin capillary was separated by a glass frit as described below. A provision was made to connect a second reference electrode to the cell in order to

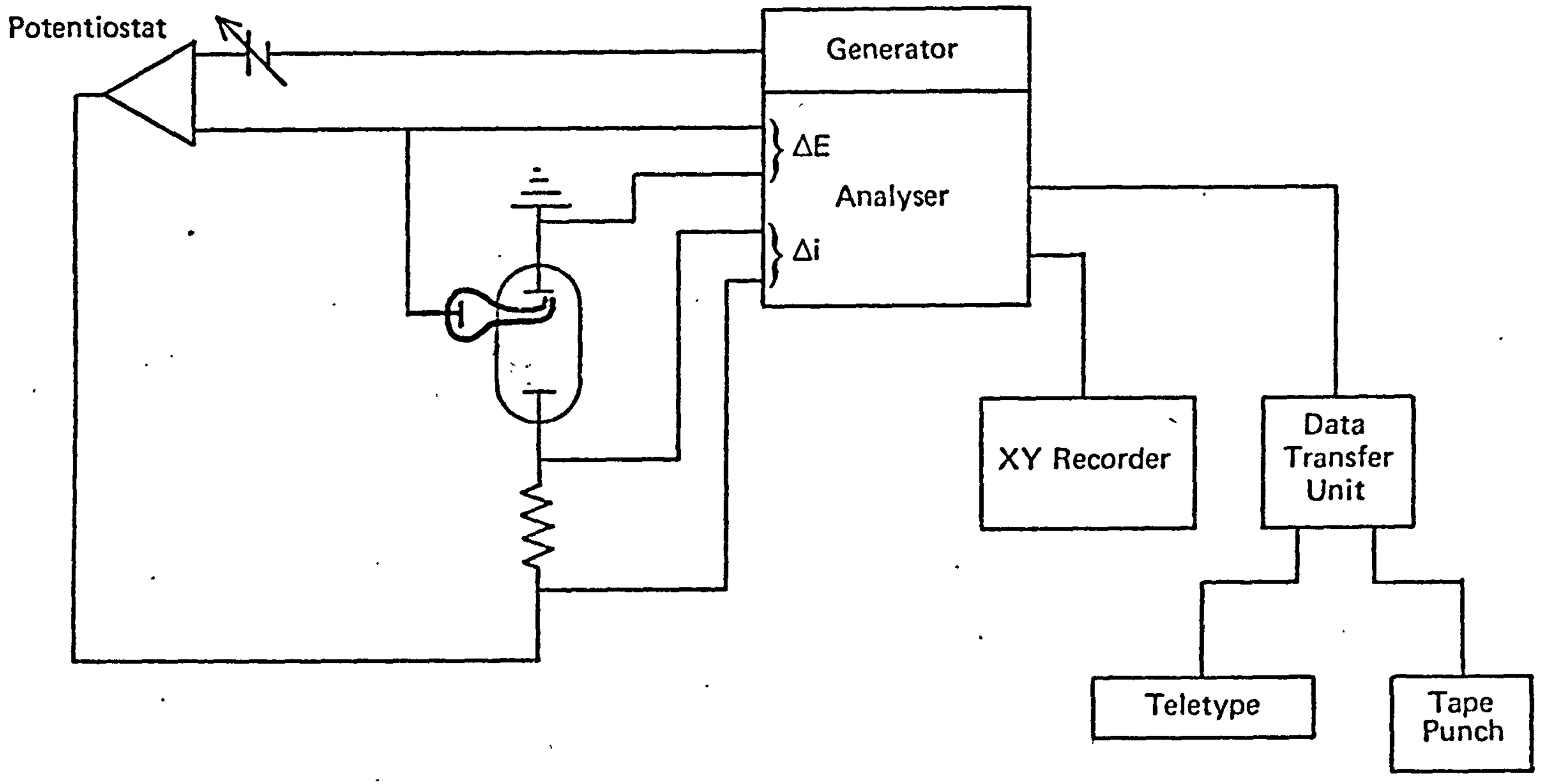

Fig. 4.6 Circuit Diagram used with Frequency Response Analyser

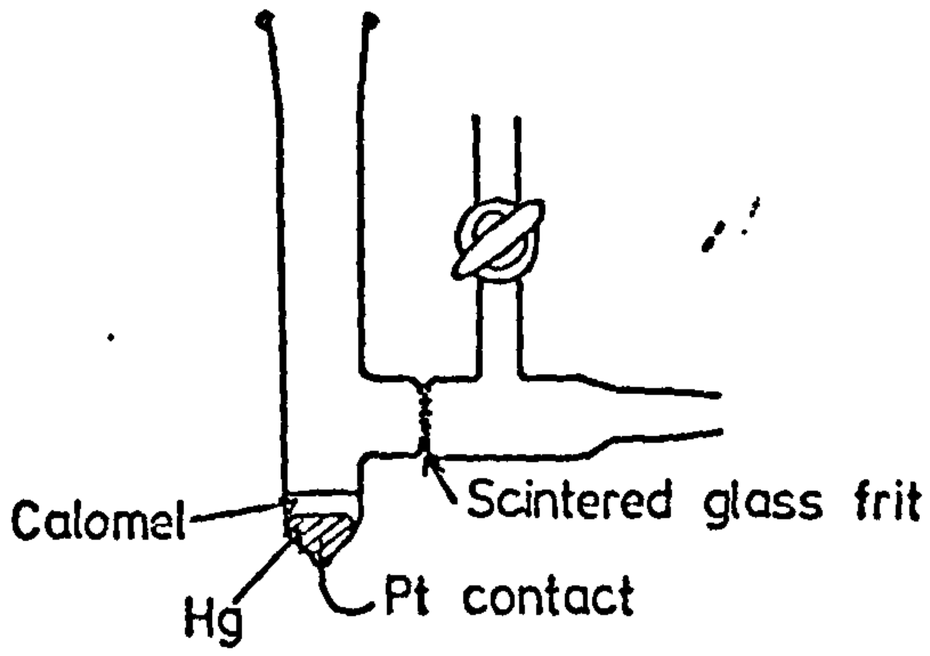

Fig. 4.6 REFERENCE ELECTRODE

FIG. 4.7 DIAGRAMATIC REPRESENTATION OF ROTATING DISC ELECTRODE

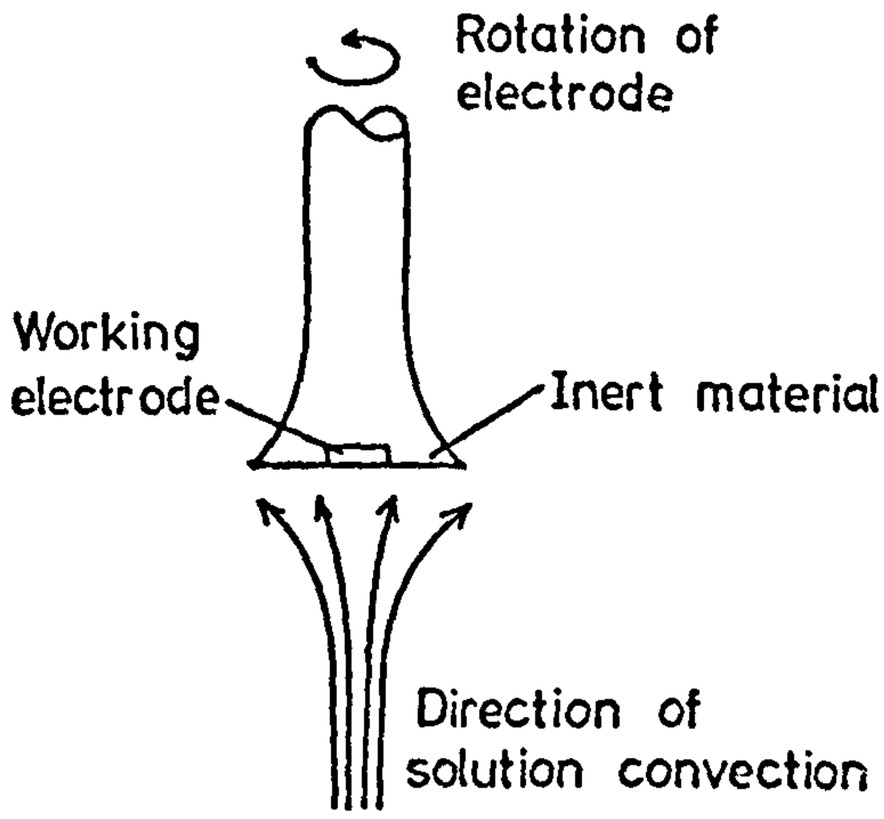

control the potential of both the HMDE and the Hg in the syringe capillary by means of a second potentiostat, but the experimental conditions found did not require this refinement.

For the amalgam HMDE measurements, the amalgam was formed 'in situ', from the working solution. For concentrated amalgam drop, the solution was refreshed before measurement. The amalgam concentration was determined coulometrically. The size of the drop was measured with a travelling microscope outside the cell and the surface calculated with the formula of the truncated sphere $A = D^2 + R^2$ where D is the height of the drop and R the radius of the Pt spike.

IV.3.3. Reference Electrode

All Zn^{++} system measurements were made using a saturated calomel electrode (KCl) the design is shown in Fig. 4.6. A sintered glass frit served to separate the calomel/saturated KCl from the solution in the main part of the cell. Four reference electrodes were prepared and the potential of each, relative to the other reference electrodes in the same solution of saturated KCl, was checked to ensure that the maximum difference between any pair of electrodes was $\pm$ 0.2 mV, also periodically fresh reference electrodes were prepared.

IV.3.4. Rotating Disc Electrode (RDE)

A scheme of the Zn RDE used is shown in Fig. 4.7. The Zn used was from a rod supplied by Koch-Light Laboratories, purity 6N and cut to give discs 5.00 mm in diameter. The Teflon holder was manufactured to make a tight fit with the disc, but it was also secured with a trace of Araldite resin to prevent the solution leaking up the side of the electrode. Electrical contact was made to the back of the ring via a spring attached to the metal shaft. The Zn RDE was mechanically polished to a mirror

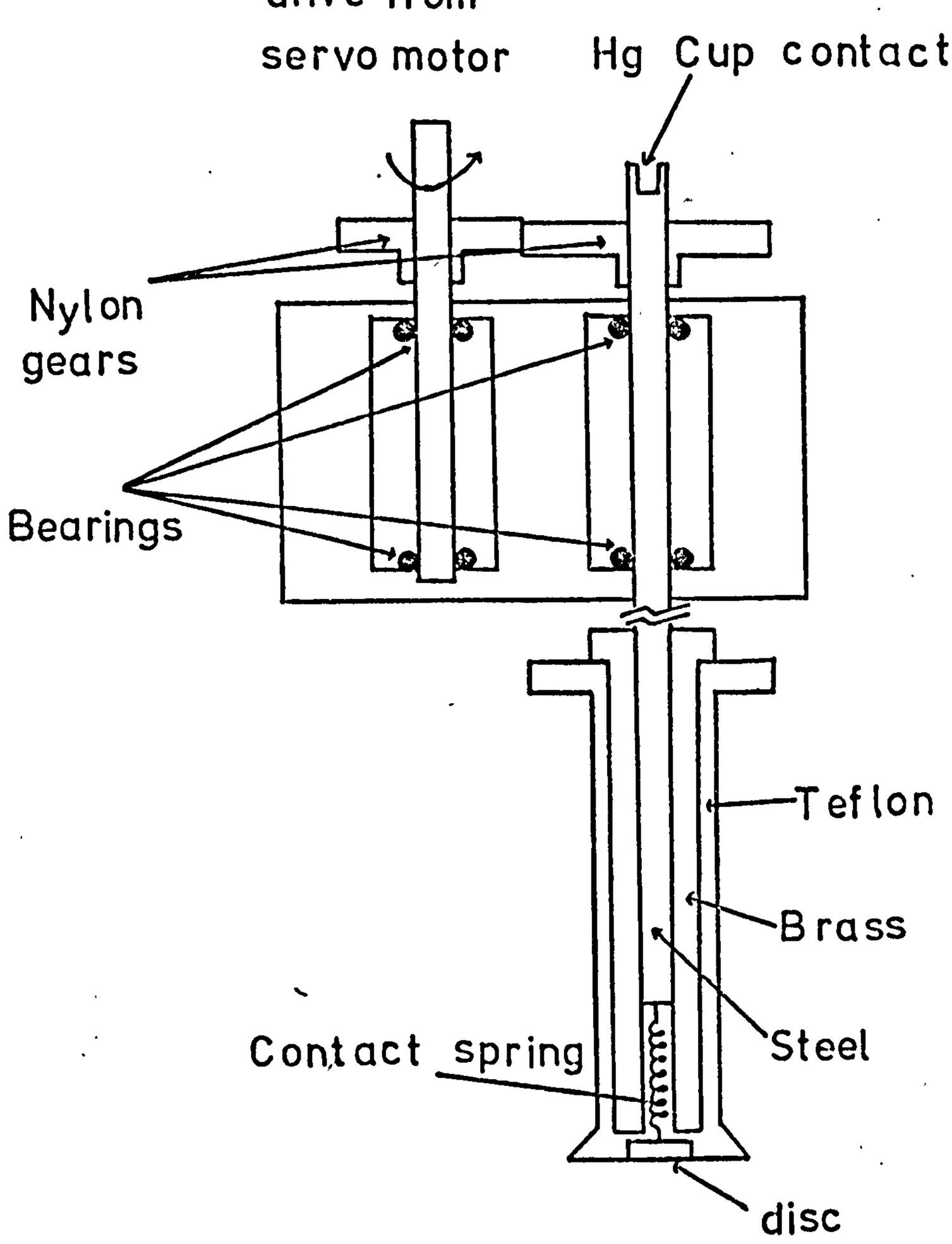

Fig. 4.8 Rotating disc electrode assembly

FIG. 4.9 CELL FOR ROTATING DISC ELECTRODE

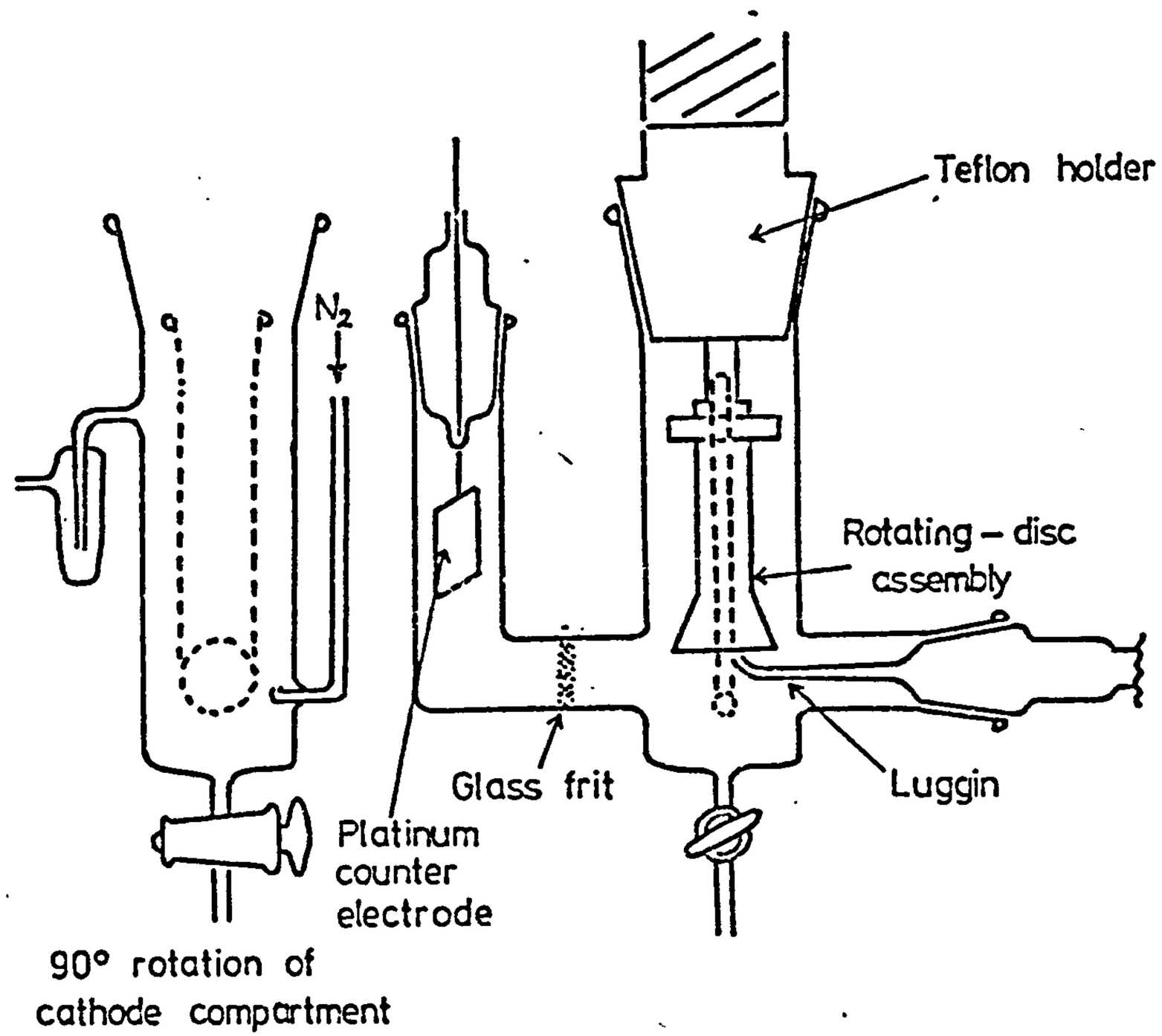

finish using alumina powder (1-5 m particle size) slurry in triply distilled water, supported on a "selvyt" cloth. The rotating disc assembly used had the design shown in Fig. 4.8. Contact to the external circuit was made through a small mercury pool in a cup at the top of the shaft. The electrode was rotated via the shaft, nylon gears and a flexible rubber coupling to a controlled drive unit. This drive unit comprised a motor generator, driven and controlled by means of a specially designed Velodyne servoamplifier. This was a solid state instrument which allowed for the variation of the rotation speed from zero to approximately 100 Hz. The rotation speed was measured by a perforated disc attached to the motor shaft and a specially made photo-cell circuit in conjunction with a Timer Counter model TC 11 from Advanced Instruments.

IV.3.5. RDE Cell

The cell used is shown in Fig. 4.9. The cathode and anode compartments are separated by a glass frit to prevent mixing of any possible reaction products. A nitrogen bubbler was used to deareate the solution.

IV.4. Solutions and Materials

The electrolyte solutions used were made up with triple distilled water and AnalaR reagents $ZnSO_4.7H_2O$ and KCl. AristaR HCl was added to some solutions to attain the pH value specified. The following table gives the concentrations.

SOLUTION	Zn^{++} /M l^{-1}	KCl /M l^{-1}	HCl	pH
1	0.1	0.9	Yes	3
2	0.01	1	Yes	3
2a	0.01	1	No	4.7
2b	0.01	1	Yes	4.3
2c	0.01	1	Yes	various < 3
2d	0	1	Yes	3
3	0.003	1	Yes	3
3a	0.003	1	Yes	various < 3

All glassware was cleaned in chromic acid, rinsed in triple distilled water and dried prior to use. AnalaR Hg_2Cl_2 and double distilled mercury ground together in a mortar were used in the preparation of the reference electrode. BOC "white spot" nitrogen was used to deareate the solutions in the cells.

IV.5. Stressometer

A stressometer was built based on a model by Norris[9] kindly demonstrated by W. Canning and Co. Ltd. where it was developed on the principle of Hoar and Arrowsmith[10]. Some modifications were made in order to be able to monitor stress continuously while controlling the electrodeposition of metals in the potentiostatic or galvanostatic mode. In the first place, instead of measuring the deformation or force of a one sided plated strip at the end of a fixed plating time, the strip was fixed and the force required to prevent the strip from bending measured continuously. Both force and deformation methods are equivalent, as demonstrated by Brezhnev[11], but with the force method is easier to monitor the stress when the force is applied by means of solenoid coils and servocontrolled current acting on a Fe rod attached to the strip. In

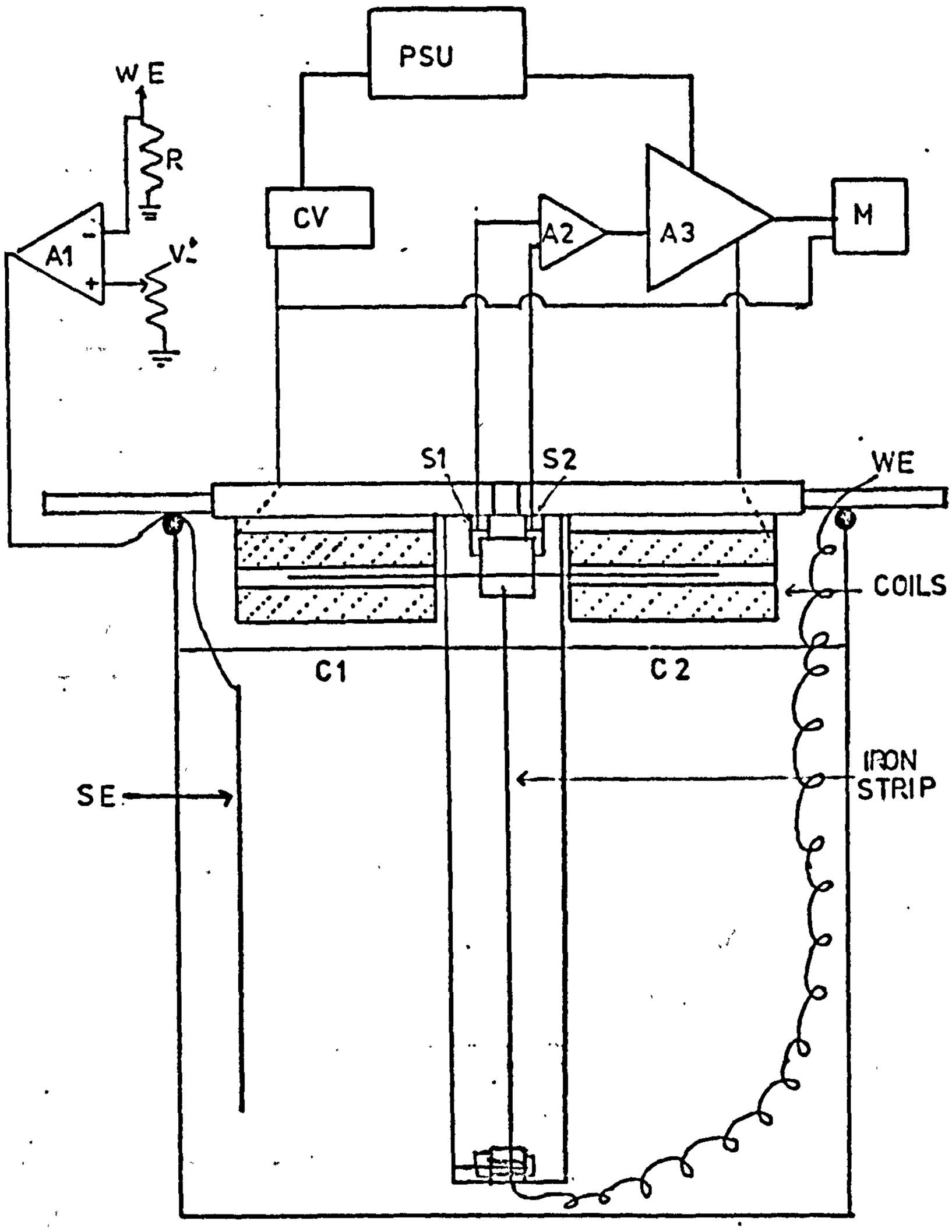

Fig. 4.10. Stressometer cell, allowing galvanostatic or potentiostatic control while monitoring stress continuously. WE working electrode; SE secondary electrode; RE reference electrode; C1, C2, coils, S1, S2 sensors.

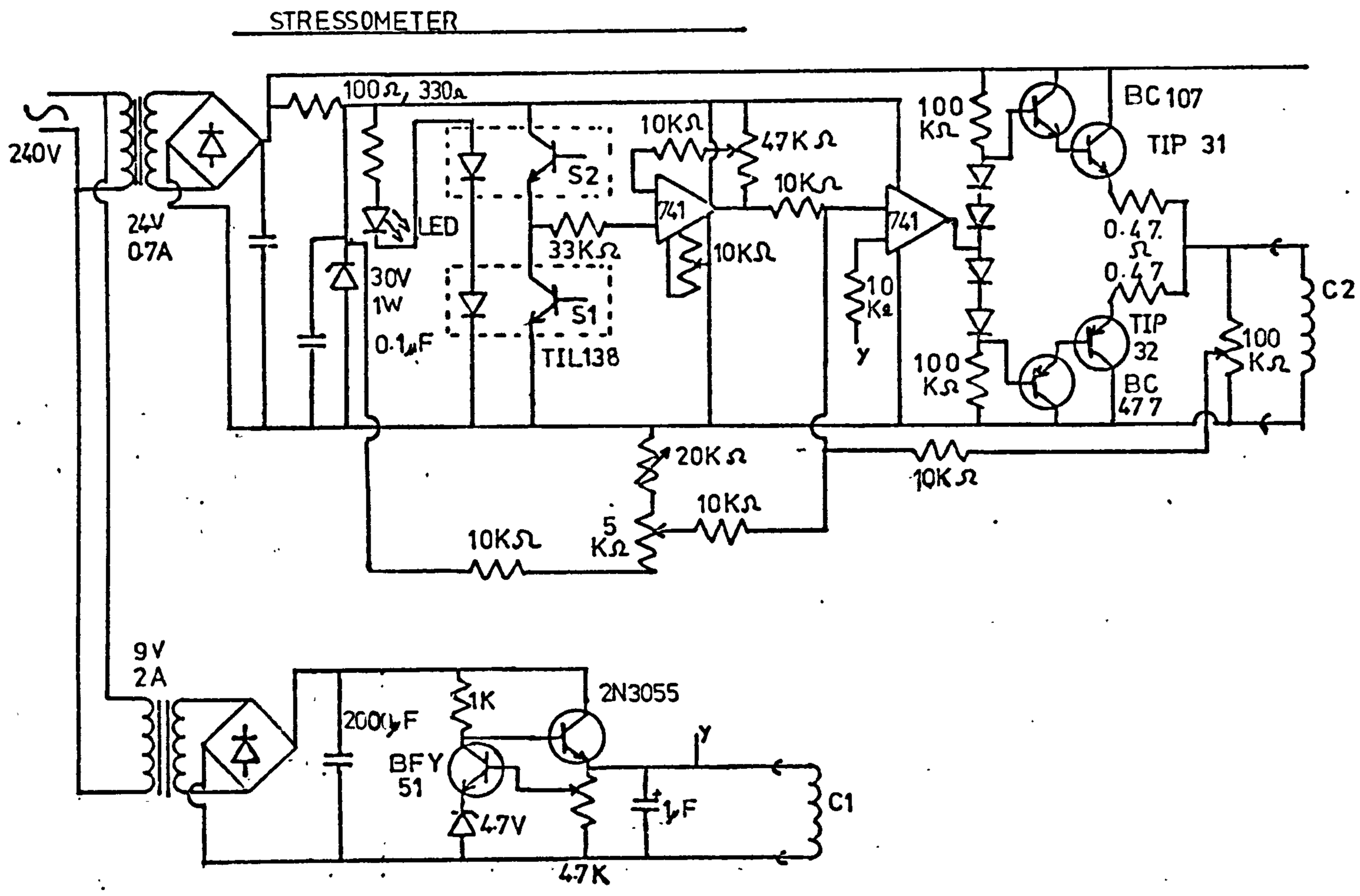

Fig. 4.11. Continuous stress monitoring circuit.

the second place, plating is carried on a three electrode cell as shown in Fig. 4.10, where a Luggin capillary connected to a reference electrode is positioned close to the strip, allowing potentiostatic control.

The use of two coils enables reversal of stress, if this occurs during plating, to be observed. It is also necessary to use two coils in conjunction with two proportional control photocells in order to keep the strip fixed by servocontrol. The circuit is shown in Fig. 4.11. This circuit applies a constant force to one coil and a variable servo controlled force to the other side.

The cell was made of perspex, as well as the frame that holds the strip by means of a clamp. Electrical contact is made at the bottom of strip by means of a wire insulated with "Lacomite". The strips are made of thin metal sheet 1 x 15 cm with an iron wire soldered perpendicularly on the top, meant to be inserted in both coils. A "flag" of this metal sheet is soldered also on the top to allow the photo cell servo-control. After insulating one side of the test strip with "Lacomite" and left to dry, degreasing with CCl_4 is necessary before plating. For more stringent preconditioning, moping and chemical and electrochemical polishing could be prescribed.

Preliminary runs demonstrated that the stressometer designed is operational. Due to lack of time no measurements on Zn system were done. The characteristic stresses found in this system by previous workers[12,13] indicate that valuable correlations could be obtained measuring stress potentiostatically. At the time of writing the stressometer is being used by a colleague in this laboratory to measure stress during Cu deposition.[14]

REFERENCES

1. A. Bewick and O.R. Brown, J. Electroanal. Chem. 15 (1967) 129.

2. A. Bewick and M. Fleischmann,Electrochim. Acta 8 (1965) 89.

3. A. Bewick, M. Fleischmann and M. Liller ibid 1 (1959) 83.

4. A. Bewick ibid 13 (1968) 825.

5. O.R. Brown ibid 13 (1968) 317.

6. Frequency Response Analyser 1174 Operating Manual. The Solartron Electronic Group Ltd.

7. R.D. Armstrong, M.F. Bell, Adrienne A. Metcalfe, J. Electroanal.Chem. Vol. 77 (1977) 287.

8. P.C.G. Danby, Electronic Engineering, January 1970.

9. P.J. Norris, Electroplating and Metal Finishing.

10. T.P. Hoar and D.J. Arrowsmith, Trans. Inst. Met. Finishing, 1966, 44, 105.

11. A.V. Brezhnev and A.A. Martynenko, Elecktrokhimiya Vol. 4, No. 12 (1968) 1470.

12. M.J. Popereka, "Internal Stresses in Electrolytically Deposited Metals". Z. knizhnoye izdatelstvo, Novosibirsk, 1966.

13. M. Ya. Popereka, Zhur. Prikl. Khim. 36, 1748 (1963).

14. J.A.H. Harrison, P. Stronach Work to be published.

CHAPTER V.

EXPERIMENTAL RESULTS

V.1. Zn^{++} Reduction on HMDE

V.1.1. LT Analysis of Double Pulses

The current response to double potential pulses was recorded and analysed with the on-line minicomputer. The double pulse was superimposed on a base potential of -900 mV vs SCE where virtually no Zn deposition takes place. The first pulse raised the potential to the measuring level for a time long enough ($\sim$ 100 ms) to relax the transient and then a second pulse of small amplitude ($\sim \pm$ 10 mV) provided the current transient on which the impedance was determined via LT. An analysis of the underlying d.c. wave is shown in Figs. 5.1 and 5.2. The current level was measured at the end of the first pulse. It is clear that the wave is practically reversible as demonstrated by the 30 mV decade Tafel slope of the log i vs E plot and the log (i_L - i/i) vs E according to

$$E = E_o + \frac{RT}{nF} \ln\left(\frac{i_L - i}{i} \frac{D_R}{D_o}\right) \qquad (5.1)$$

From Fig. 5.1 the half-wave potential $E_{\frac{1}{2}}$ is estimated to be -1.012V vs S.C.E.

The second pulse in the potential profile was a small step (10 to 20 mV) in the cathodic or anodic direction, superimposed on the first potential pulse. The second pulse lasted 320 mS and the potential was then returned to the base, -0.9V vs S.C.E., where any Zn deposited during the double pulse was dissolved off the HDE. The resulting anodic transient was observed with the oscilloscope. A repetition period of 1 to 10 s was chosen in each case to ensure complete relaxation of this Zn dissolution transient before consecutive double pulses, (necessary for averaging purposes) so that measurements were made on pure mercury.

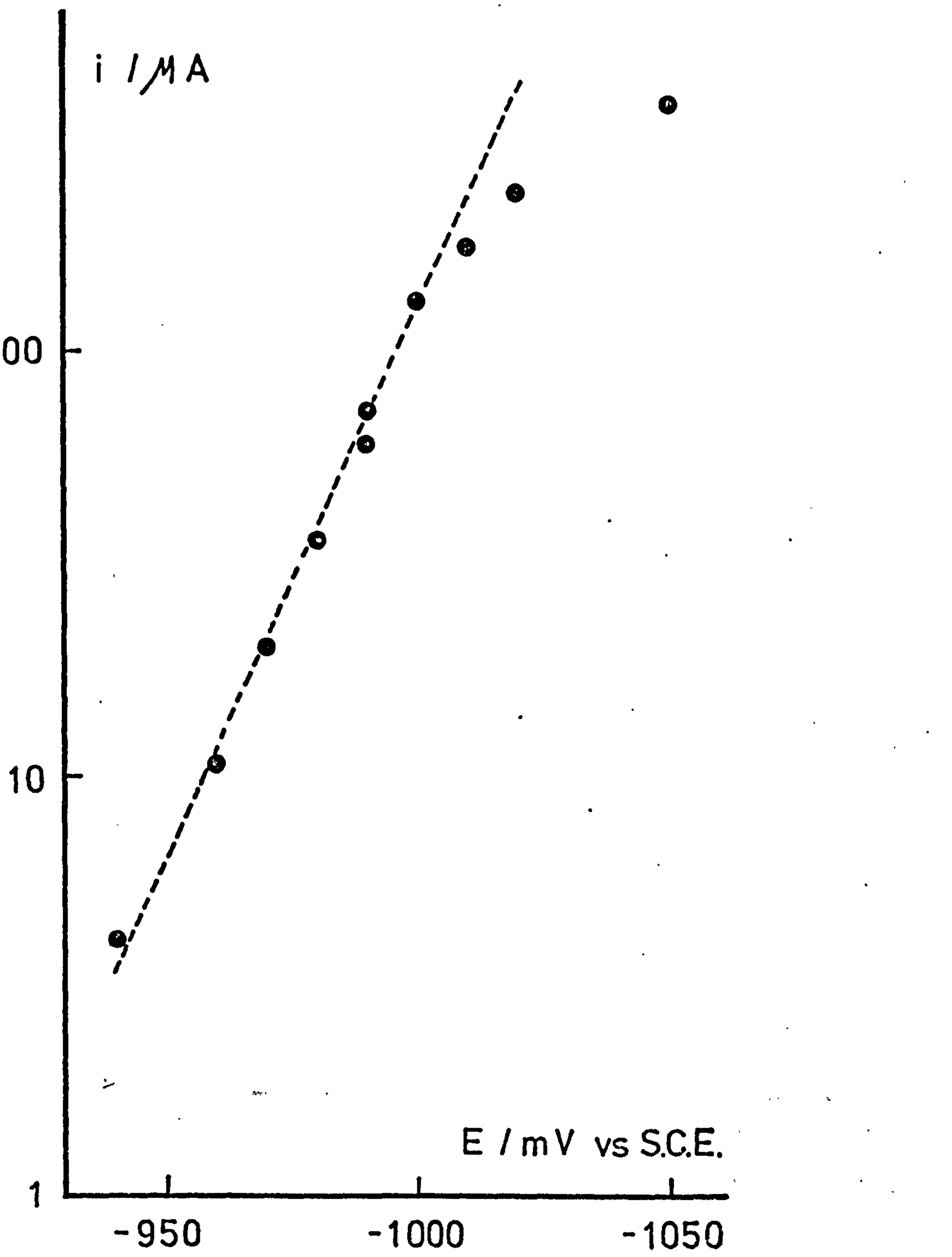

Fig. 5.1. log i-E plot for Zn^{++} reduction at a HMDE, obtained from potentiostatic pulses, as in Figs. 2.6 and 5.3. Current sampled at $\sim$ 100 ms after the start of the first pulse. Electrode area = 0.05 cm^2, solution 2 (10^{-2}M Zn^{++}, pH = 3). Base potential = -0.9V vs S.C.E. Tafel slope (broken line) a = 30 mV/decade.

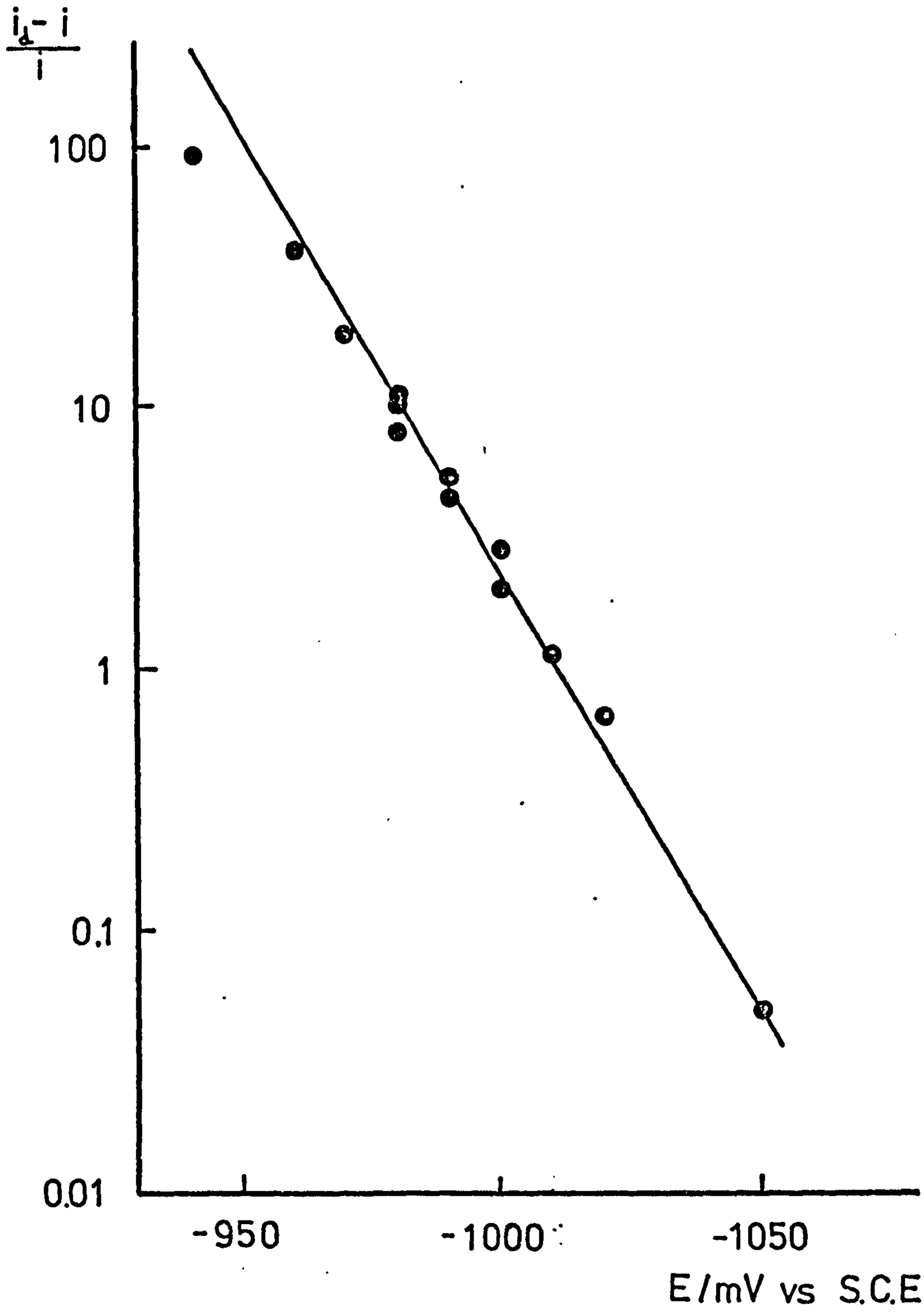

Fig. 5.2. Analysis of the experimental data of Fig. 5.1 according to Eq. 5.1. Tafel slope (broken line) a = 30 mV/decade.

Typical current responses to the second potential pulse are shown in Figs. 5.3 and 5.4, plotted directly with the LAB/8E minicomputer system. The current transients were averaged ($\sim$ 20 times) in order to reduce random noise, nevertheless the calculated impedance spectra were somewhat scattered due to the remaining random noise in the current signal. The program JAH was used to obtain the results, with the extrapolation given by Equation 2.44 to fit the flatish current transients observed. Other extrapolations did not alter the results significantly. The high frequency region of the calculated impedance spectra were generally in error, due to the unaccounted potential oscillations in the so-called 'potentiostat rise time'.

Three types of impedance spectra could be observed: a semicircle (Fig. 5.5a), a cluster of points centred around a value on the real axis at low frequencies (Table 5.1) and a small Warburg line at low frequencies (Fig. 5.5b). The semicircle is probably due to the sampling of a portion of the double layer charging current. According to orthodox analysis, the high frequency intersection of the semicircle with the real axis gives R_{sol}, and the low frequency extrapolation of the semicircle gives $\Theta + R_{sol}$. The cluster of points is obtained when the double layer charging current is not sampled. With no capacity, the position of the cluster in the real axis determines $\Theta + R_{sol}$. When diffusion polarisation takes place, instead of cluster of points in the real axis, a Warburg line is obtained, from which $\Theta + R_{sol}$ can be determined at the intersection with the Z(Re) axis. The R_{sol} values determined from the semicircle or from high frequency TFA measurements were about 10 Ω . The charge transfer resistance was estimated as the value of Z(Re) at $\sim$ 40 Hz, since at about this frequency the semicircle and Warburg intersected the real axis.

The response is expected to have an irreversible a.c. characteristic on a pseudo-reversible or reversible d.c. wave. The appropriate

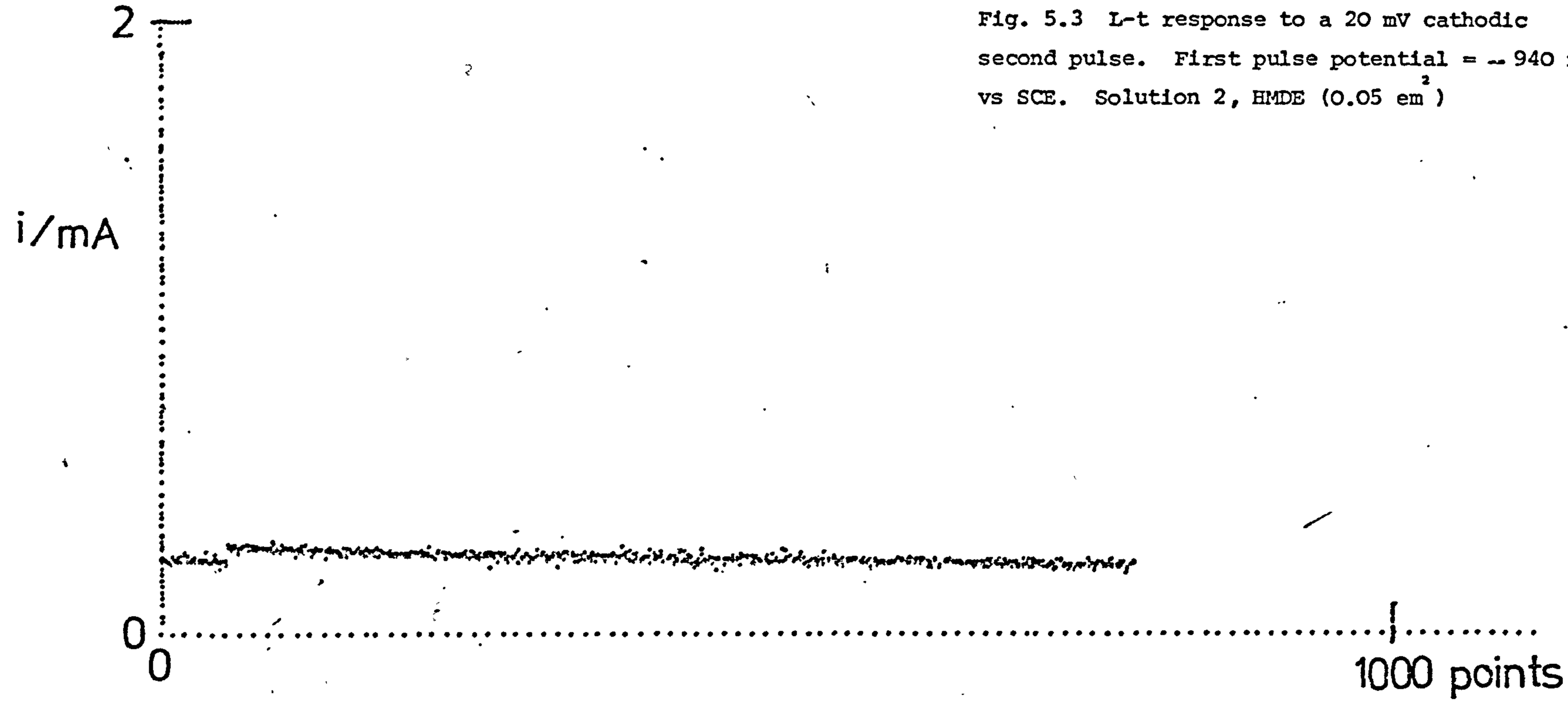

Fig. 5.3 L-t response to a 20 mV cathodic second pulse. First pulse potential = -- 940 mV vs SCE. Solution 2, HMDE (0.05 em^2)

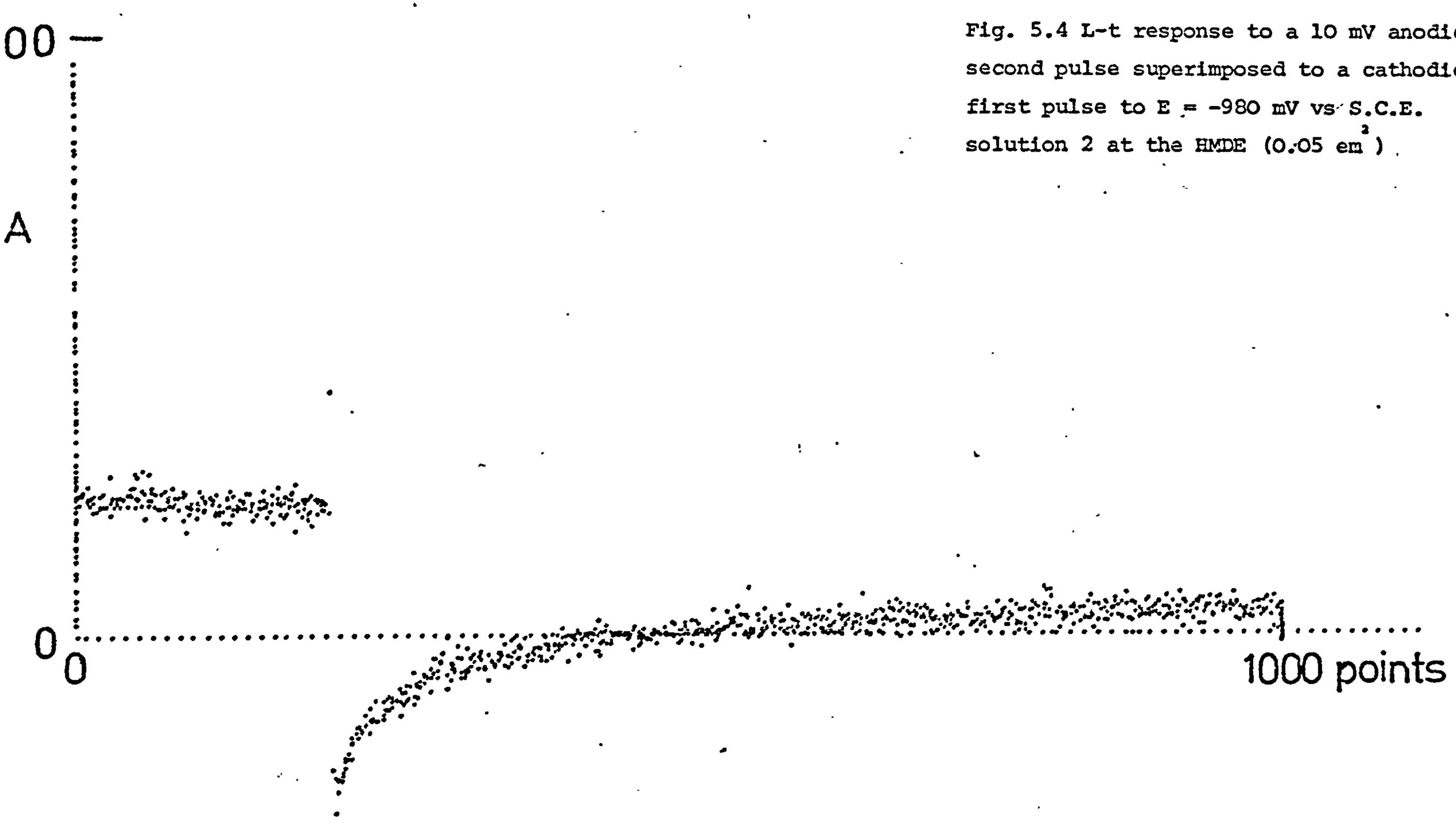

Fig. 5.4 L-t response to a 10 mV anodic second pulse superimposed to a cathodic first pulse to E = -980 mV vs S.C.E. solution 2 at the HMDE (0.05 cm^2).

TABLE 5.1. Complex impedance results obtained with the LT software for double pulses on HMDE in solution 2 (10^{-2}M Zn^{++}, pH = 3) from -0.9 to -1.01V vs S.C.E. Second pulse = 10 mV anodic. A = 0.05 cm^2, current transient averaged 20 times, repetition period = 10 s.

F/HZ	Z(RE)	Z(IM)
6250	-83.6804	-0.0940962
5625	44.6485	-28.7901
5000	34.3175	-71.6945
4375	-59.4087	166.982
3750	16.3958	24.9906
3437.5	33.7245	50.6156
3125	-40.2862	-30.6309
2812.5	32.3897	-167.564
2500	-14.5963	27.4555
2187.5	15.6694	66.5062
1875	28.1068	39.4904
1718.75	25.1837	20.0459
1562.5	51.7341	-29.2339
1406.25	147.549	57.5055
1250	59.8487	148.919
1125	62.3849	38.1027
1000	81.5512	42.2638
875	56.6384	-6.38261
750	46.0189	-2.42445
625	69.4031	12.2526
562.5	72.6012	-17.2891
500	61.0335	-8.85384
437.5	83.0545	2.69532
375	59.1019	-10.9184
343.75	64.6083	-11.9579
312.5	56.8762	-4.67415
281.25	57.8919	6.47964
250	56.7368	-9.70928
218.75	65.7523	-5.55267
187.5	62.8697	-10.3072
171.875	67.3166	-4.65469
156.25	74.2525	5.16291
140.625	72.0412	-3.06925
125	59.9457	-6.02777
112.5	69.7634	-0.433781
100	66.6739	-14.4754
87.5005	69.3653	-0.574099
75.0005	77.4544	-11.0623
62.5005	66.4665	-3.92482
56.2504	71.3175	-11.8146
50.0004	78.4742	-5.62016
43.7504	71.7721	-2.94273
37.5004	72.2514	-9.27329
34.3754	76.1111	-9.80252
31.2504	78.6802	-6.7315
28.1254	77.0448	-3.27801
25.0004	73.277	-3.37843
21.8754	71.0078	-6.94088
18.7504	72.0467	-12.0276

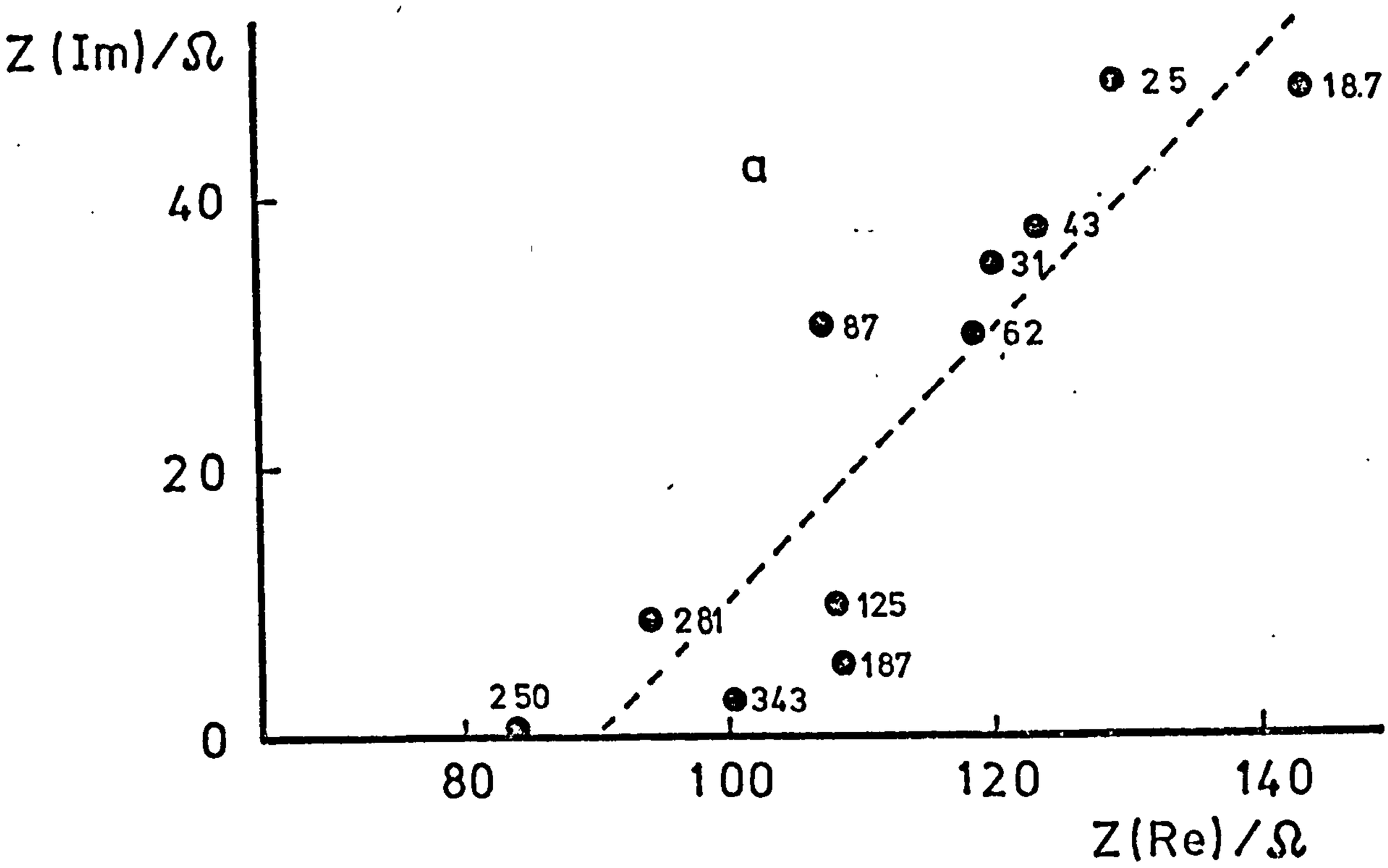

Fig. 5.5. Complex impedance plane plots for cathodic double pulses at the HMDE in solution 1 (10^{-2}M Zn^{++}, pH = 3). Results obtained with the LT software for a) first pulse = -0.94V second= -0.960V vs S.C.E. b) first pulse E = -0.98V, second pulse = E = -0.99V vs S.C.E. Base potential for a) and b) = -0.9V vs S.C.E. Electrode area = 0.05 cm^2. Figures on graph indicate frequency in Hz.

general equation (see Chapter I) is

$$Z(j\omega) = \frac{1}{\left(\frac{\partial i}{\partial E}\right)_{C_O^s, C_R^s}} + \frac{1}{nF\sqrt{D_R j\omega}} \frac{\left(\partial i/\partial C_R^s\right)_{E, C_O^s}}{\left(\partial i/\partial E\right)_{C_O^s, C_R^s}}$$

$$+ \frac{1}{nF\sqrt{D_O j\omega}} \frac{\left(\partial i/\partial C_O^s\right)_{E, C_R^s}}{\left(\partial i/\partial E\right)_{C_O^s, C_R^s}} \qquad (5.2)$$

which becomes on substituting the appropriate values (see Chapter I) for a.c. irreversible, reversible d.c.

$$\theta_{rev} = \frac{RT}{n^2F^2k_{SH}} \frac{\exp -\alpha_1\phi + \left(a_R/a_O\right)\exp \beta_1\phi}{C_O^* + \left(a_R/a_O\right)C_R^*} \qquad (5.3)$$

$$\sigma_{O,rev} = \frac{RT\left[1 + \left(a_R/a_O\right)\exp\left(-nF\phi/RT\right)\right]}{n^2F^2\sqrt{2}\left(C_O^* + \frac{a_R}{a_O}C_R^*\right)D_O^{1/2}} \qquad (5.4)$$

$$\sigma_{R,rev} = \frac{RT}{n^2F^2\sqrt{2}} \frac{\exp\left(nF\phi/RT\right) + a_R/a_O}{\left(C_O^* + \frac{a_R}{a_O}C_R^*\right)D_R^{1/2}} \qquad (5.5)$$

$$\sigma_{rev} = \sigma_{O,rev} + \sigma_{R,rev} \qquad (5.6)$$

In this case $C_R^* = 0$. It is expected that for $\phi = -(E - E_O)$ positive (going cathodic)

$$\theta_{rev} = \frac{RT}{n^2F^2k_{SH}} \frac{\exp \alpha_1\phi}{C_O^*} \qquad (5.7)$$

the θ - E curve goes through a minimum and for ϕ negative (going anodic)

$$\theta_{rev} = \frac{RT\ a_R\ \exp\beta_1\phi}{n^2F^2a_O\ k_{SH}\ C_O^*} \qquad (5.8)$$

It is also expected that a quasi-irreversible reaction would approach Equations 5.7 and 5.8 at potentials not far from E_O.

Fig. 5.6 shows a log Θ vs E plot from L.T double pulse analysis. The curve has a minimum near E_o = -1.025V vs S.C.E. According to Equation 5.7, the slope of the anodic branch is $\alpha_1/2.303 = 1/a$, and according to Equation 5.8, the slope of the cathodic branch is $\beta_1/2.303 = 1/b$. Values of a = 120 mV/decade and b = 40 mV/decade are compatible with the results in Fig. 5.6.

at $E = E_o$

$$\theta_{rev} = \left(1 + \frac{a_R}{a_o}\right) \frac{RT}{n^2 F^2 k_{SH} C_o^*} \qquad (5.9)$$

For $\Theta = 3.5\ \Omega\ cm^2$ estimated from Fig. 5.6, and $a_R/a_o = 1.5$, a value of $k_{SH} = 4.8 \times 10^{-3}$ cm s^{-1} is obtained.

Fig. 5.7 shows a log σ vs E plot for average σ values taken around 50 Hz from impedance spectra at different potentials, according to

$$\sigma = Z(Im)\, 2\pi f \qquad (5.10)$$

From Equations 5.4, 5.5 and 5.6 it is expected that σ is infinite at potentials far from E_o and have a minimum near E_o. If $\frac{a_R}{a_o} = (D_R/D_O)^{\frac{1}{2}}$, σ_{rev} is a symmetrical function with a minimum at the reversible half wave potential $E_{\frac{1}{2}}$.

$$\sigma_{rev} = \sigma_m \cosh^2 \left[-\frac{nF}{2RT}\left(E - E_{\frac{1}{2}}\right)\right] \qquad (5.11)$$

$$\sigma_m = \frac{4RT}{n^2 F^2 \sqrt{2}\left(C_o^* D_o^{\frac{1}{2}} + C_R^* D_R^{\frac{1}{2}}\right)} \qquad (5.12)$$

The broken line in Fig. 5.7 represents Equation 5.11 with n = 2, $\sigma_m = 7.5\ \Omega\ s^{-\frac{1}{2}}\ cm^2$, a good agreement with the experimental results is observed, although in the cathodic branch a contribution of the H^+ reduction reaction might be present.

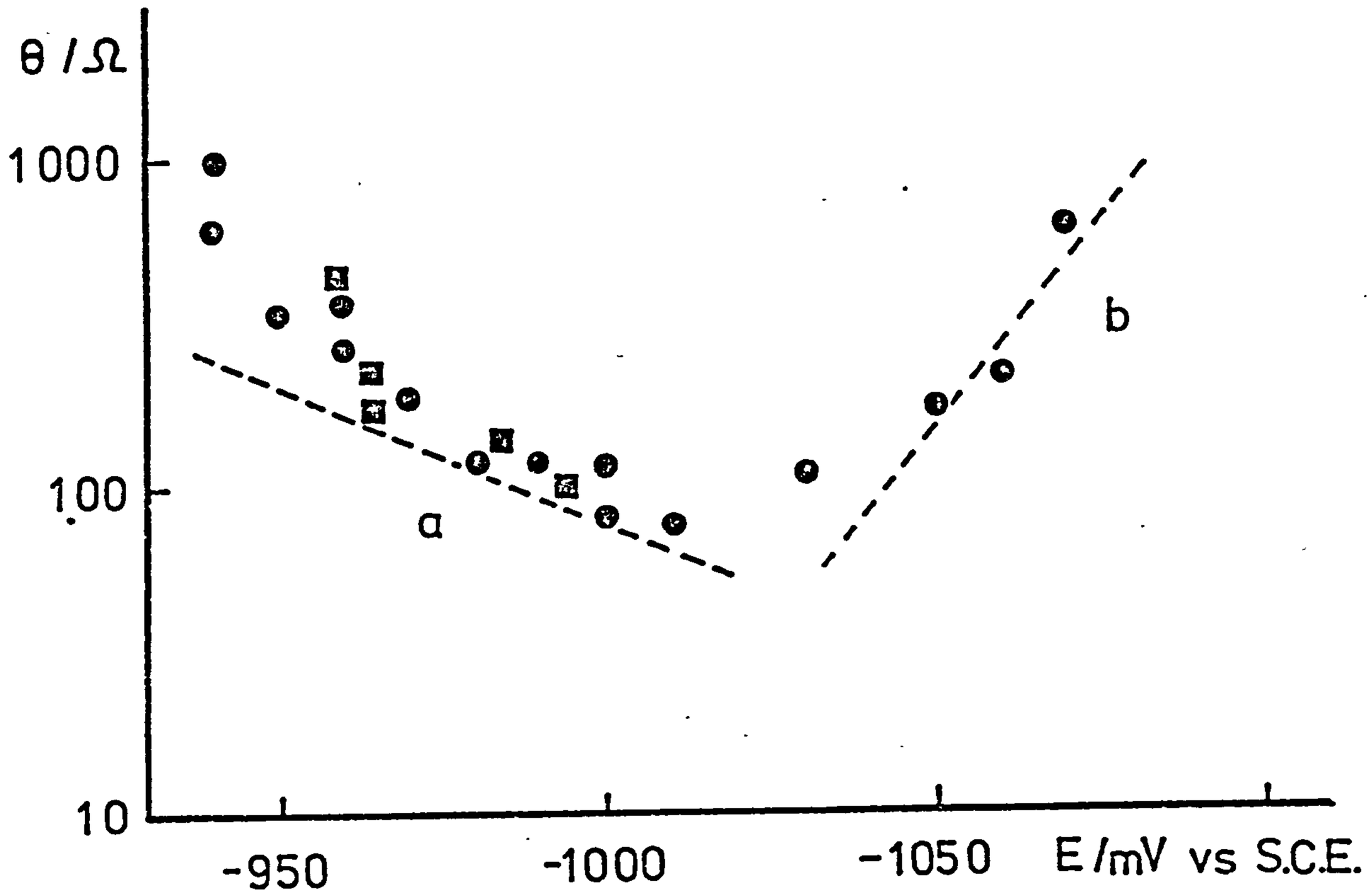

Fig. 5.6. Log θ vs E plot from impedance spectra obtained with the LT software. Solution 2, HMDE area = 0.05 cm^2. (●) from double pulses, (■) from linear sweep measurements. Tafel slopes a = 120 mV/dec., b = 40 mV/dec.

Fig. 5.7. Log σ vs E plot for Zn^{++} reduction at the HMDE. Solution 1 (10^{-2}M Zn^{++}, pH = 3), A = 0.05 cm^2. (•) average σ values taken around 50 Hz from impedance spectra according to Eq. 5.10. Broken line represents Eq. 5.11 with n = 2, σ_m = 7.5 $\mu s^{-\frac{1}{2}}$ cm^2.

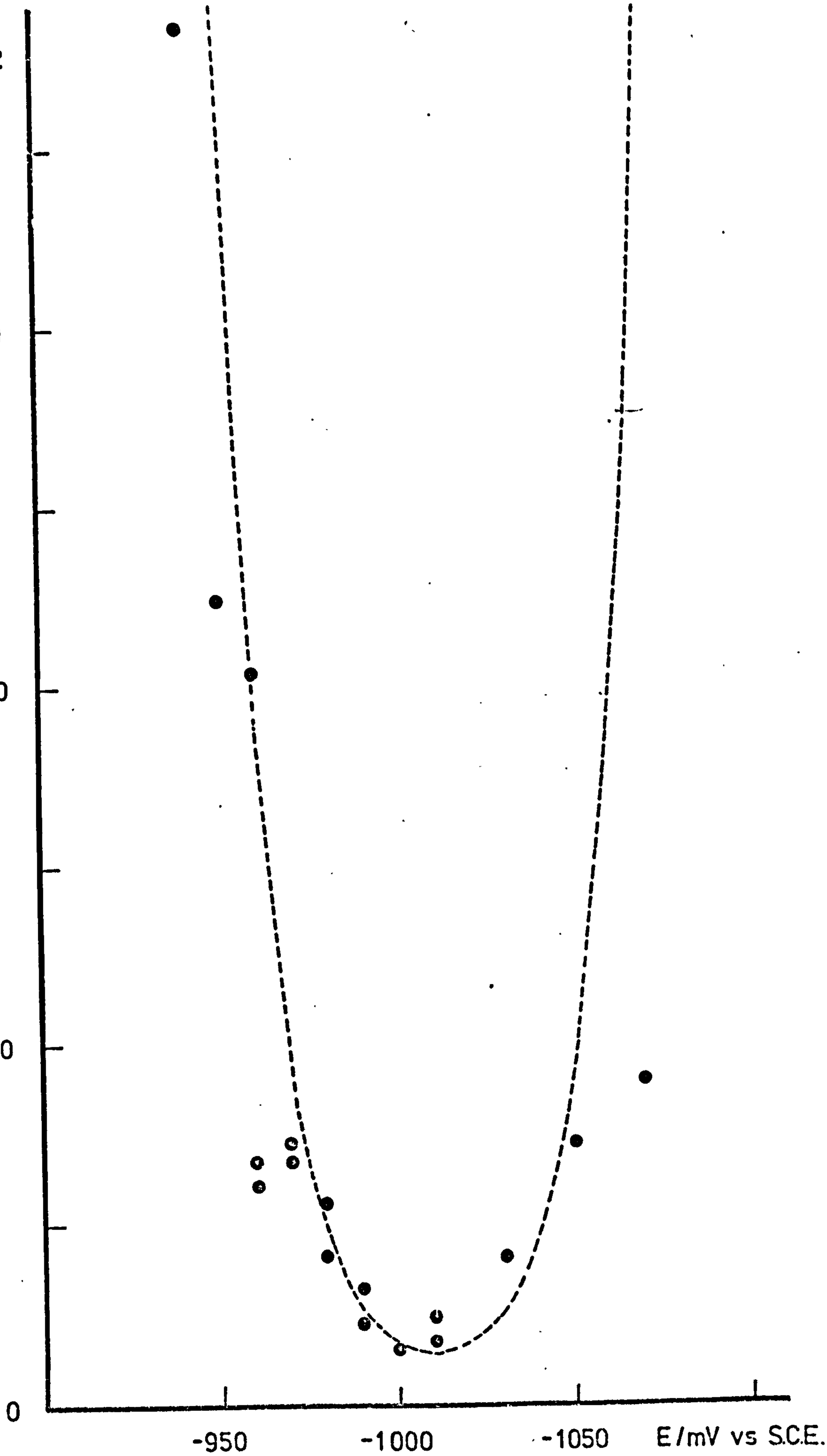
σ-1 Ω s$^{-1/2}$
3000
2000
1000
0
-950
-1000
-1050
E/mV vs S.C.E.

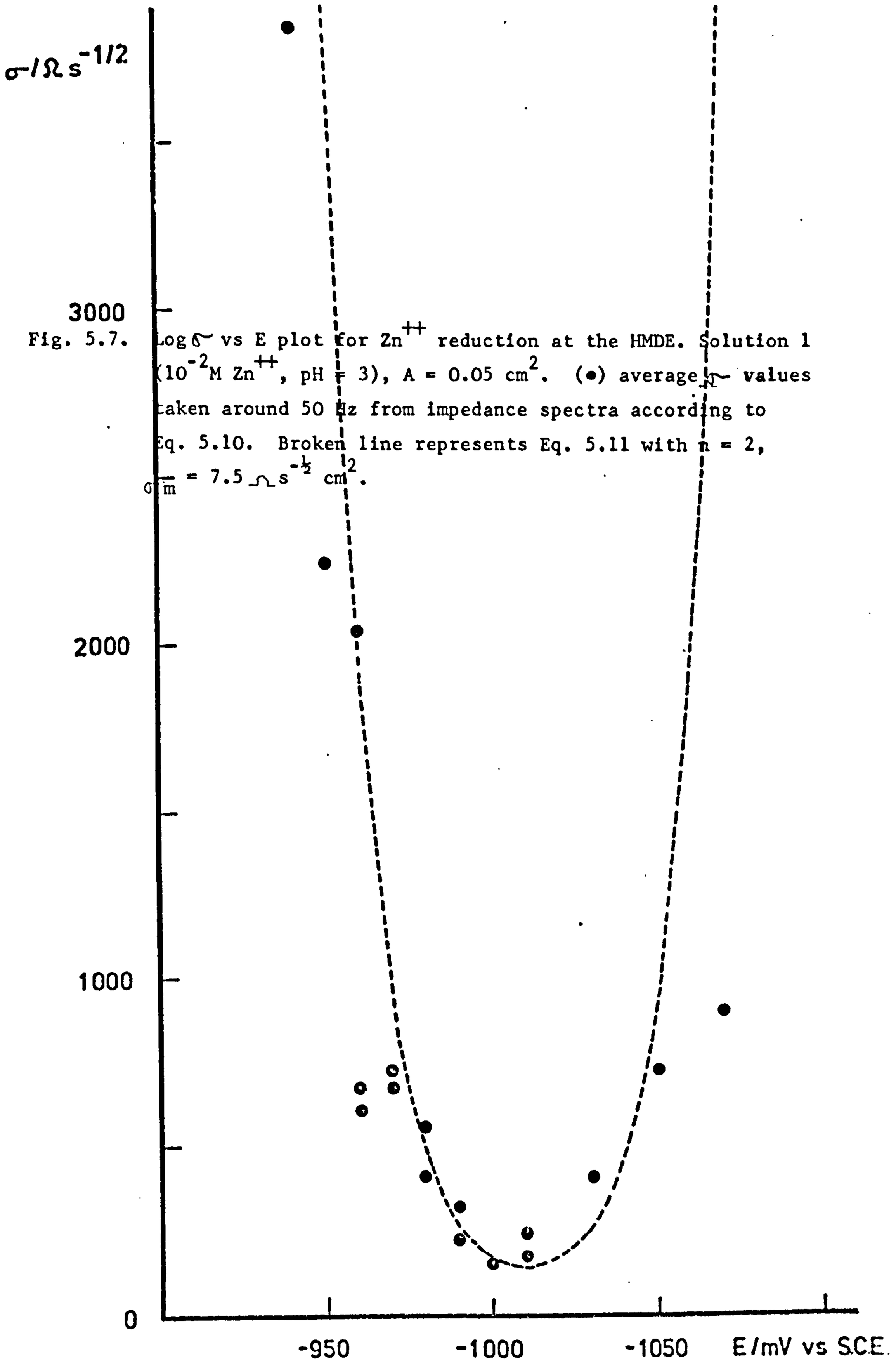

Fig. 5.7. Log σ vs E plot for Zn^{++} reduction at the HMDE. Solution 1 (10^{-2}M Zn^{++}, pH = 3), A = 0.05 cm^2. (●) average σ values taken around 50 Hz from impedance spectra according to Eq. 5.10. Broken line represents Eq. 5.11 with n = 2, $\sigma\sqrt{m}$ = 7.5 Ω^{-1} s$^{-\frac{1}{2}}$ cm^2.

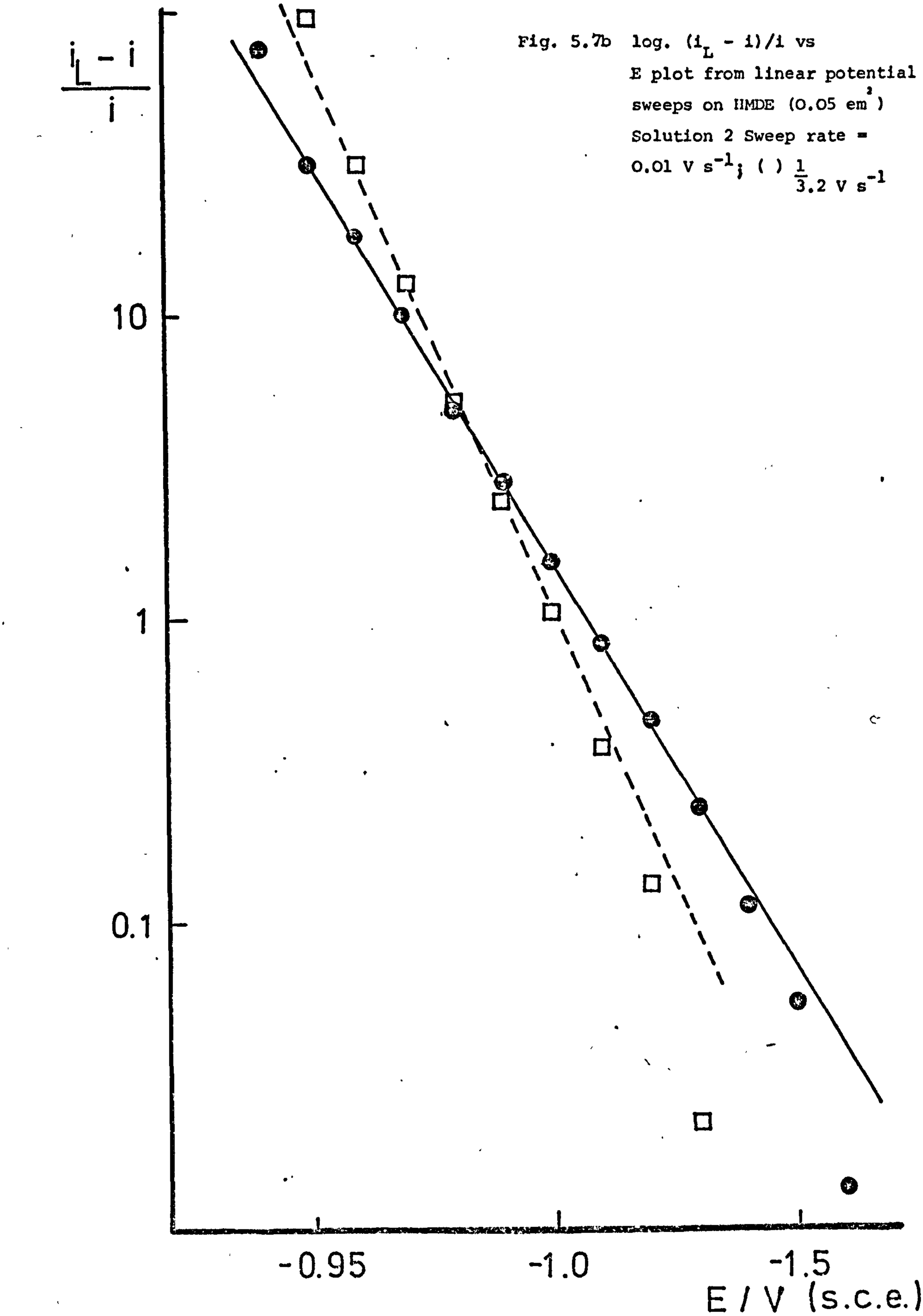

Fig. 5.7b log. $(i_L - i)/i$ vs E plot from linear potential sweeps on HMDE (0.05 cm^2) Solution 2 Sweep rate = 0.01 V s^{-1}; ( ) $\frac{1}{3.2}$ V s^{-1}

The double pulse impedance measurements were extended to the cathodic region where the H^+ reduction reaction occurs in parallel with the Zn^{++} reduction.

The equivalent circuit for this scheme is

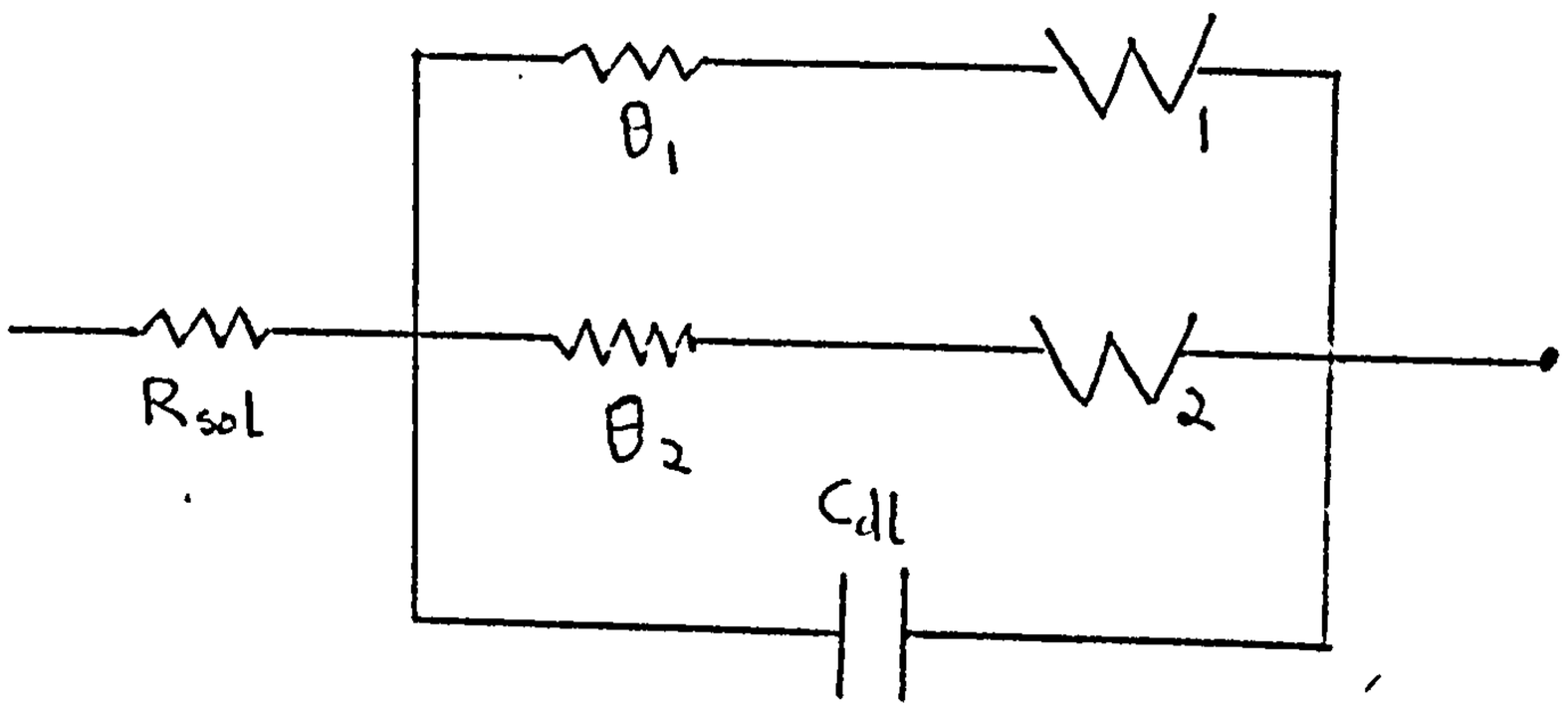

where the subscripts 1 and 2 refer to the Zn^{++} reduction and H^+ reduction reactions respectively. The observed θ is given by

$$\frac{1}{\theta} = \frac{1}{\theta_1} + \frac{1}{\theta_2} \qquad (5.13)$$

and the observed σ by

$$\frac{1}{\sigma} = \frac{1}{\sigma_1} + \frac{1}{\sigma_2} \qquad (5.14)$$

The corresponding equivalent circuits, with C_{dl} eliminated and R_{sol} negligible are

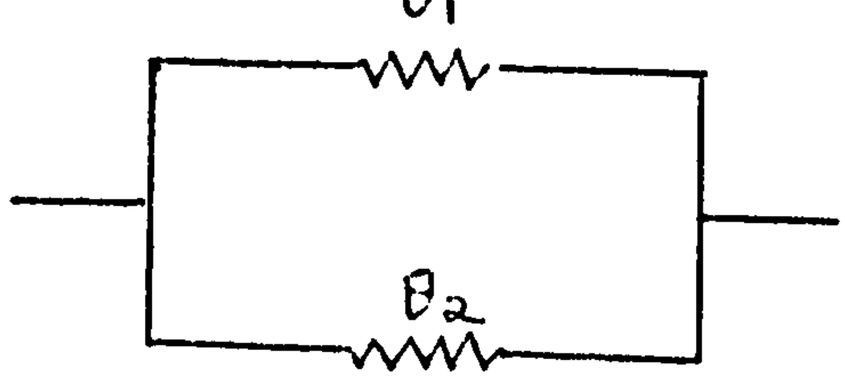

DIAGRAM 2

and

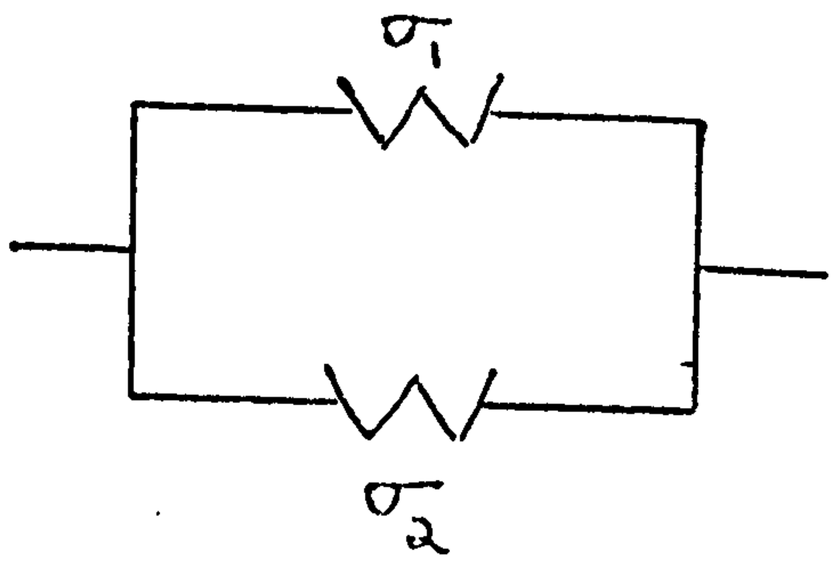

DIAGRAM 3

The observed cathodic limiting current i_L is given by

$$i_L = (i_L)_1 + (i_L)_2 \tag{5.15}$$

According to the "diffusion layer theory"

$$i_L = \frac{2F D_{o,1} C^*_{o,1}}{\delta} + \frac{F D_{o,2} C^*_{o,2}}{\delta} \tag{5.16}$$

therefore

$$\frac{(i_L)_2}{(i_L)_1} = X = \frac{D_{o,2} C^*_{o,2}}{2 D_{o,1} C^*_{o,1}} \tag{5.17}$$

and

$$(i_L)_2 = i_L/(1 + \tfrac{1}{X}) \tag{5.18}$$

$$(i_L)_1 = i_L/(1 + X) \tag{5.19}$$

Experimental measurements at extended cathodic potentials were made from -0.9 and -1.0V vs S.C.E. base potential, at this latter potential a light amalgam (~ 0.04M) is formed. Typical current responses to the second pulse are shown in Figs. 5.8 and 5.9. The corresponding impedance results are shown in Table 5.2 and Fig. 5.10. A log θ vs E plot is shown in Fig. 5.11. Although the results are somewhat scattered, the θ values obtained from the light amalgam (solid circles) and from pure mercury (open circles) agree with each other within experimental error. The curve shows a maximum at around E = -1.05V vs S.C.E. and at more cathodic potentials θ becomes independent of E. To explain this behaviour two hypotheses could be made: 1) Zn^{++} reduction is d.c. reversible with a d.c. irreversible H^+ reduction occurring in parallel. 2) Zn^{++} reduction is quasi-irreversible with H^+ reduction occurring in parallel (at cathodic potentials).

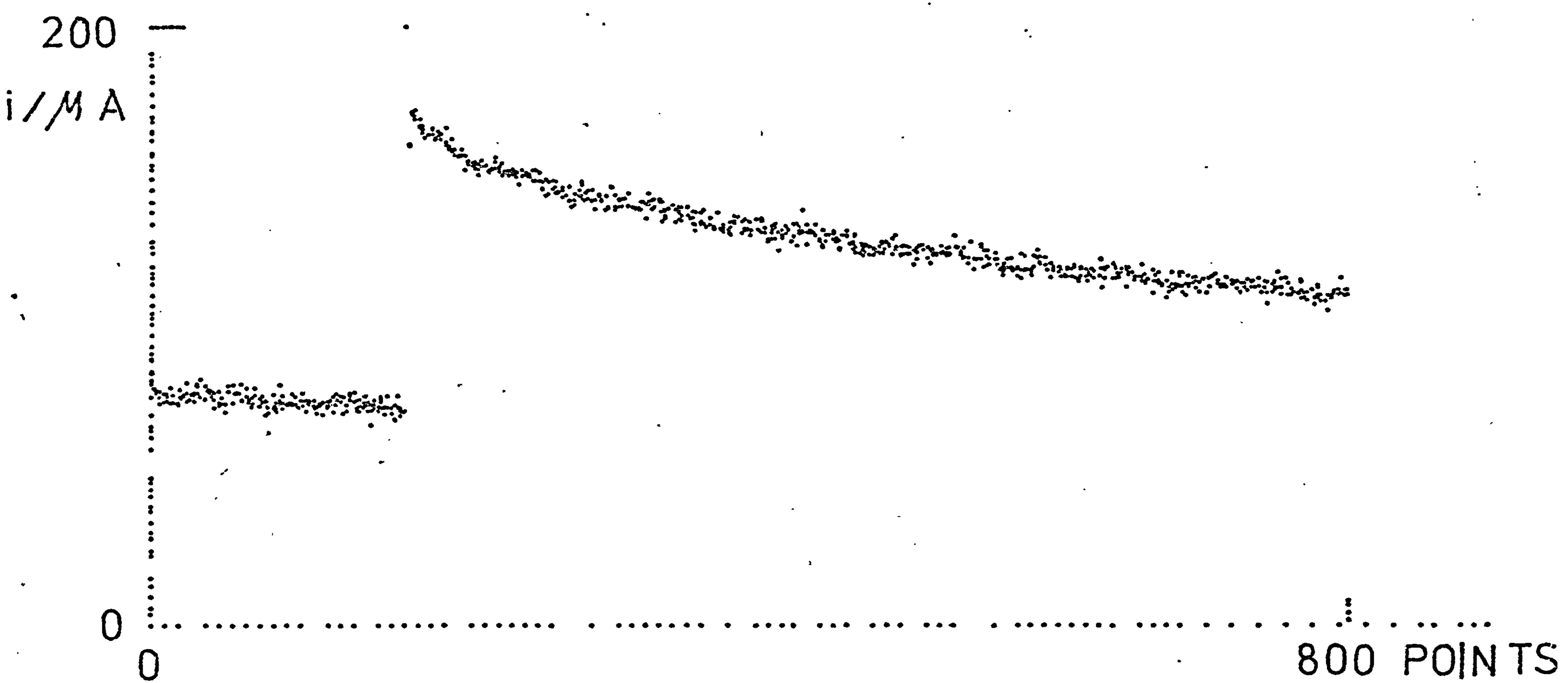

Fig. 5.8

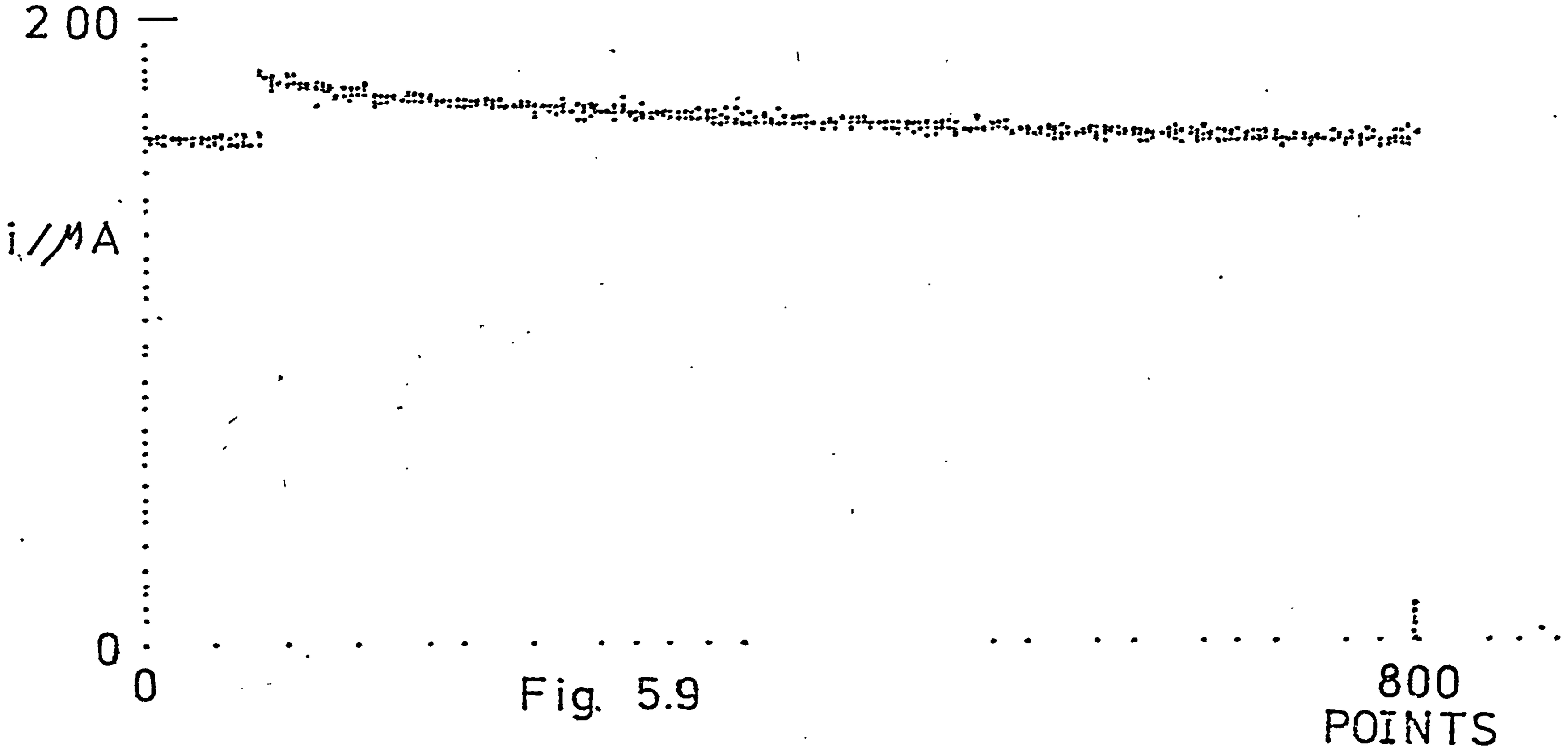

Fig. 5.9

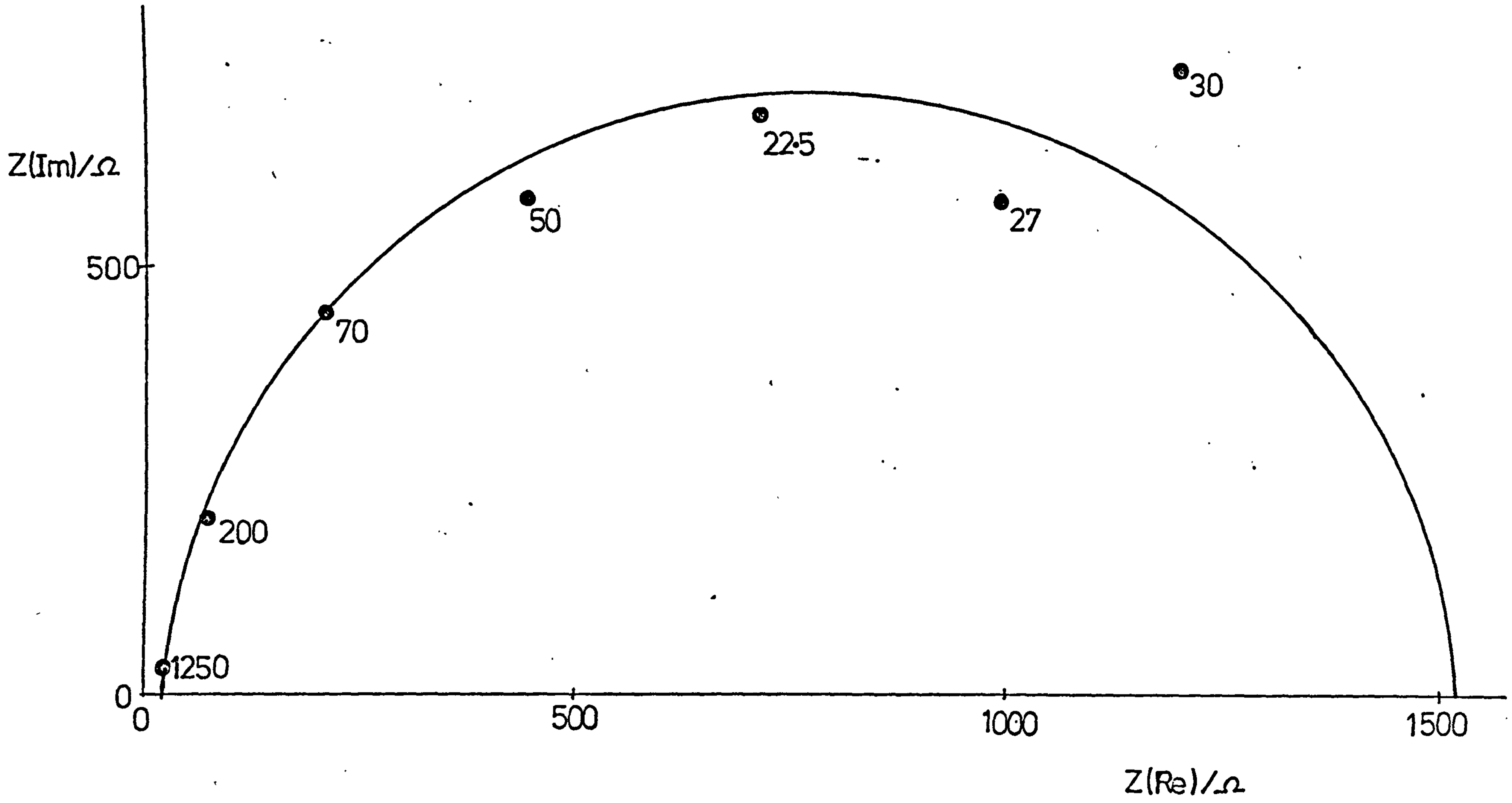

Fig. 5.10 Complex impedance plane plot from LT analysis of double pulse shown in Fig. 5.9.

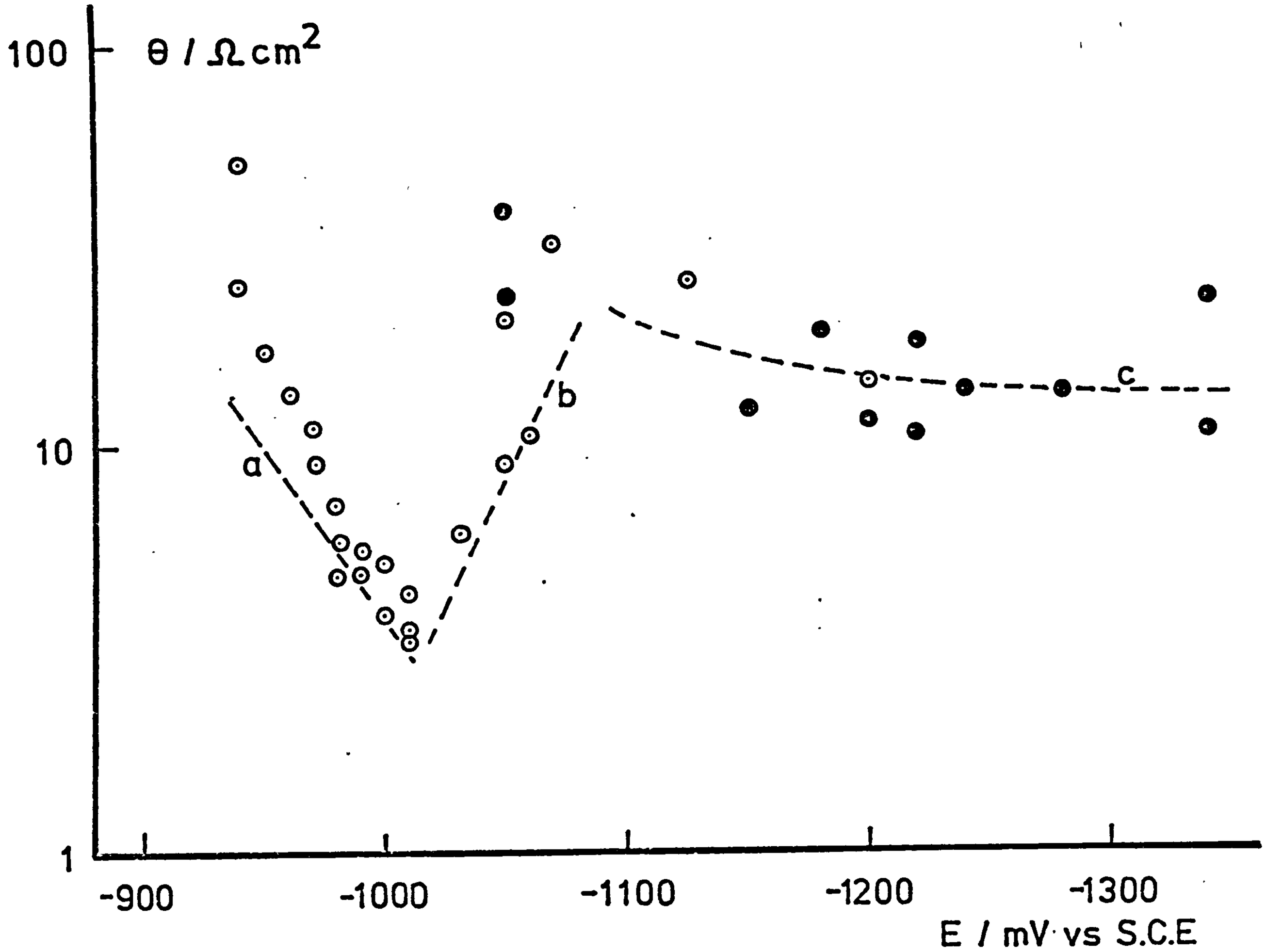

Fig. 5.11. Extended log θ vs E plot from data of runs exemplified in Figs. 5.8 to 5.10. Solution 2. (●) θ from pulses with -0.9V vs S.C.E. base potential. (○) θ from pulses with -1.0V vs S.C.E. Tafel slopes a = 120 mV/dec., b = 40 mV/dec. Section C of broken line corresponds to pseudo irreversible Zn^{++} reduction.

With hypothesis 1, as ϕ_1 goes positive θ_1 would increase according to Equation 5.8 tending to ∞ , but with H^+ reduction in parallel, there would be a transition region (at E = -1.05V vs S.C.E.) where both θ_1 and θ_2 contribute to θ, and at more cathodic potentials, according to Equation 5.13 and diagram 2, as θ_1 tends to ∞ the observed θ would be determined only by θ_2, which itself would be given by (see Chapter I)

$$\theta = \theta_2 = \frac{a_2}{2.303\,(i_L)_2} \qquad (5.20)$$

With the experimental values $i_L = 5.4 \times 10^{-3}$ A cm^2 and $\theta \simeq 12\,0$ cm^2, and using Equations 5.17 and 5.18 with $D_{o,2}/2D_{o,1} \simeq 1$, $(i_L)_2$ is obtained and used in Equation 5.20 to give a value for a_2 of 13.6 mV/decade. This ludicrous value discards hypothesis 1. Even accepting that the H^+ reduction occurs in parallel with the Zn^{++} reduction, the flat section of curve log θ - E in Fig. 5.11, observed approximately from E = -1.1 to -1.34V vs S.C.E., is completely determined by θ_1. This result, confirmed by the TFA measurements reported in Section V.1.3, leads to hypothesis 2, that Zn^{++} reduction on HMDE is quasi-reversible. The complete appropriate equation is

$$\vartheta = \frac{RT}{n^2 F^2 k_{SH}} \times \frac{1 + a_0 \exp(-\alpha_1 \phi) + (a_0/a_R) \exp(nF\phi/RT)}{\left[\frac{-\alpha_1 RT}{nF} a_0 + \left(\frac{a_0}{a_R}\right) \exp -\beta_1 \phi\right] C_0^* + \frac{\beta_1 RT}{nF} a_0 \exp\left(\frac{nF\phi}{RT}\right) + \exp(-\beta_1 \phi)\, C_R^*} \qquad (5.21)$$

The overall shape of the experimental log θ - E curve is analogous to the numerical simulation of Equation 5.21 reported by Sluyters et al[1] for $k_{SH} = 5 \times 10^{-3}$ cm s^{-1}, $C_o^* = 10^{-6}$ mol cm^{-3}, $C_R^* = 0$ (curve 1 of their Fig. 6a, reproduced in Fig. 1. of this work). At very cathodic (far from E_o) potentials

$$\theta = \theta_1 = \frac{a_1}{2.303\,(i_L)_1} \qquad (5.22)$$

With $\frac{D_{o,2}}{2D_{o,1}} \simeq 1$, Equation 5.19 gives $(i_L)_1 = 4.9 \times 10^{-3}$ A cm^2. With θ = 12 Ω cm^2 Equation 5.22 gives a_1 = 136 mV/decade.

For quasi-irreversible and irreversible processes

$$\sigma = \sigma_O + \sigma_R \qquad (5.23a)$$

where

$$\sigma_o = \frac{RT \exp(\alpha_1 \phi)}{n^2 F^2 (2D_o)^{1/2}} \cdot \frac{1 + a_o \exp(-\alpha_1 \phi) + \frac{a_o}{a_R} \exp\left(\frac{nF}{RT}\phi\right)}{\left[a_o(-\alpha_1)\frac{RT}{nF} + \frac{a_o}{a_R}\exp -\beta_1\phi\right]C_o^* + \left[a_o(-\beta_1)\frac{RT}{nF}\exp\frac{nF}{RT} + \exp(-\beta_1\phi)\right]C_R^*} \qquad (5.23b)$$

$$\sigma_R = \frac{RT \exp(-\beta_1 \phi)}{n^2 F^2 (2D_R)^{1/2}} \cdot \frac{1 + a_o \exp(-\alpha_1 \phi) + \frac{a_o}{a_R} \exp\left(\frac{nF}{RT}\phi\right)}{\left[a_o \alpha_1 \frac{RT}{nF} + \frac{a_o}{a_R}\exp(-\beta_1\phi)\right]C_o^* + \left[a_o(-\beta_1)\frac{RT}{nF}\exp\left(\frac{nF}{RT}\right) + \exp(-\beta_1\phi)\right]C_R^*} \qquad (5.23c)$$

Fig. 5.12 shows the extended log σ - E plot. The first curve on the left corresponds to Zn^{++} reduction and has already been discussed with the d.c. reversible approach (justified at potentials near E_o). The behaviour of Equations 5.23 for a quasi-irreversible process is similar to that obtained for the d.c. reversible approach, as demonstrated by the simulated curves 1 and 2 of Sluyters[1] Fig. 6b (reproduced in Chapter I as Fig. 1.). This means that σ_1 tends to ∞ as ϕ_1 goes cathodic. A maximum is observed at E = -1.05V vs S.C.E. This is the transition region where the two parallel reactions 1 and 2 contribute to σ according to Equation 5.14 and Diagram 3, at more cathodic potentials σ observed is

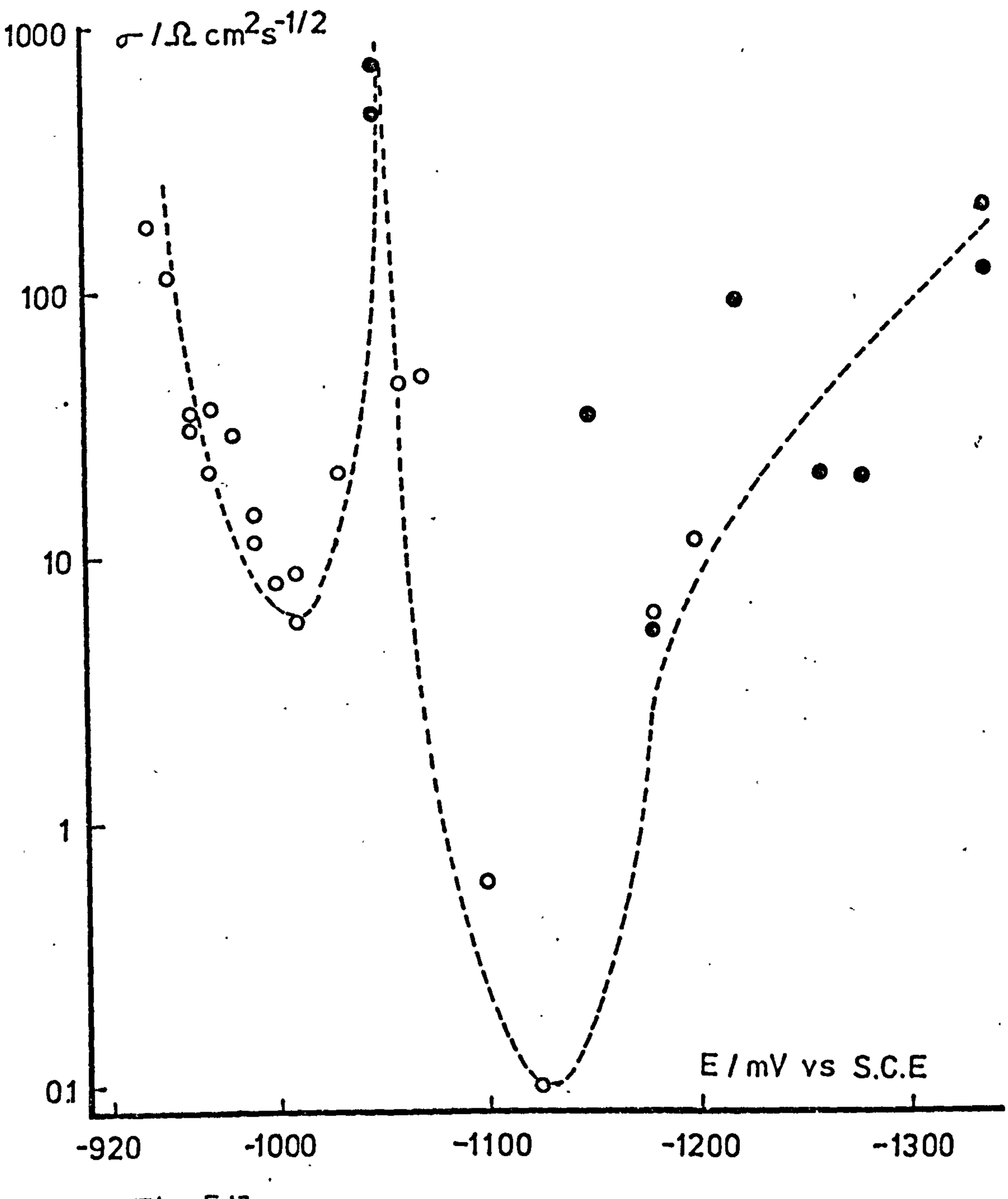

Fig. 5.12

log σ -E plot from extended impedance determinations with the LT software. (O) From pulses with -0.9V vs S.C.E. base potential. (●) From pulses with -1.0V vs S.C.E. base potential. Solution 2.

determined only by σ_2. At E = -1.120V vs S.C.E. the logσ - E curve shows a minimum. This is qualitatively compatible with the simulated curve 4 of Sluyters[1] Fig. 5b (Fig. 1 in this work) for $k_{SH} = 10^{-5}$, $C_R^* = 0$, $C_o^* = [H^+] = 10^{-6}$ mole cm^{-3}. The rise following the minimum in Fig. 5.12 is also compatible with the aforementioned curve 4. At extreme cathodic potentials it is expected that log σ becomes a linear function of ϕ according to

$$\sigma \simeq \sigma_2 = \frac{k_{SH,2} \quad exp[(\alpha_1)_2 \phi_2]}{(2D_{o,2})^{1/2} (i_L)_2 (\alpha_1)_2} \qquad (5.24)$$

therefore the slope of the cathodic extreme of the log σ - E curve in Fig. 5.12 is $(\alpha_1)_2/2.303 = 1/a_2$. A Tafel slope of $a_2 = \sim 120$ mV/decade, indicating a single step irreversible H^+ reduction, is consistent with the experimental results.

V.1.2. L.T. Analysis of linear potential sweeps

Some preliminary runs were carried out using the sweep analysis outlined in Appendix B. A typical potential profile is shown in Fig. 5.13, from a base potential of -0.9V vs S.C.E. The corresponding current response, as plotted out by the minicomputer is shown in Fig. 5.14. The resulting impedance spectra calculated with the Z10 program are shown in Fig. 5.15. The θ values obtained from LT analysis of sweeps at various potentials are plotted as squares in Fig. 5.6 and agree with the θ values obtained from double pulse analysis. The initial idea of using a linear potential sweep perturbation instead of the second potential step, was to diminish or eliminate the potentiostat rise time and be able to detect double layer capacity. Unfortunately the wave-form generator used produced a small gap between the first pulse and the linear potential sweep, where the potential oscillated strongly, therefore impairing the achievement

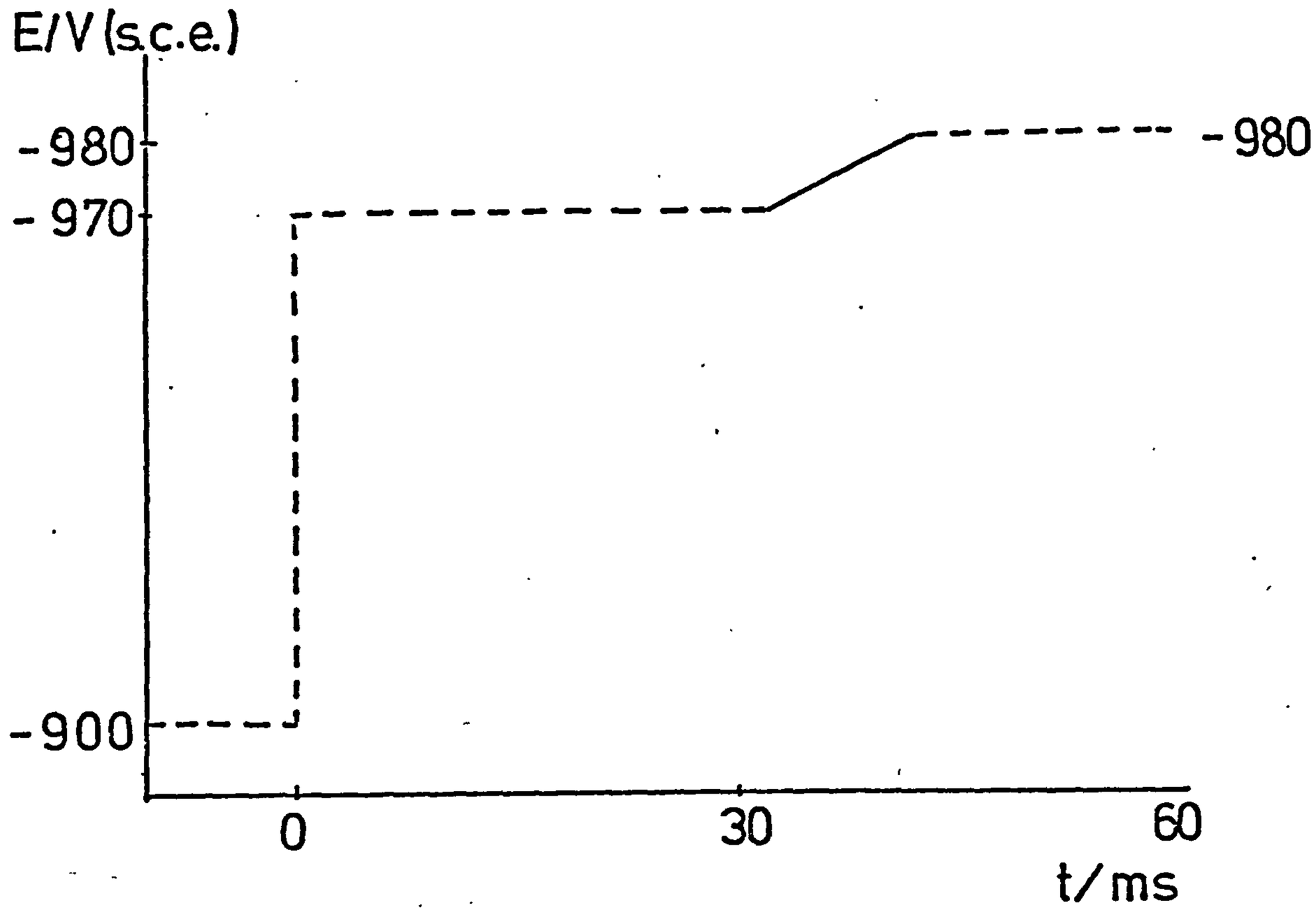

Fig. 5.13. Potential profile used to determine impedance from LT analysis of linear potential sweeps. Solid line indicates what is actually used by the Z10 program. Sweep rate = 1 V/s.

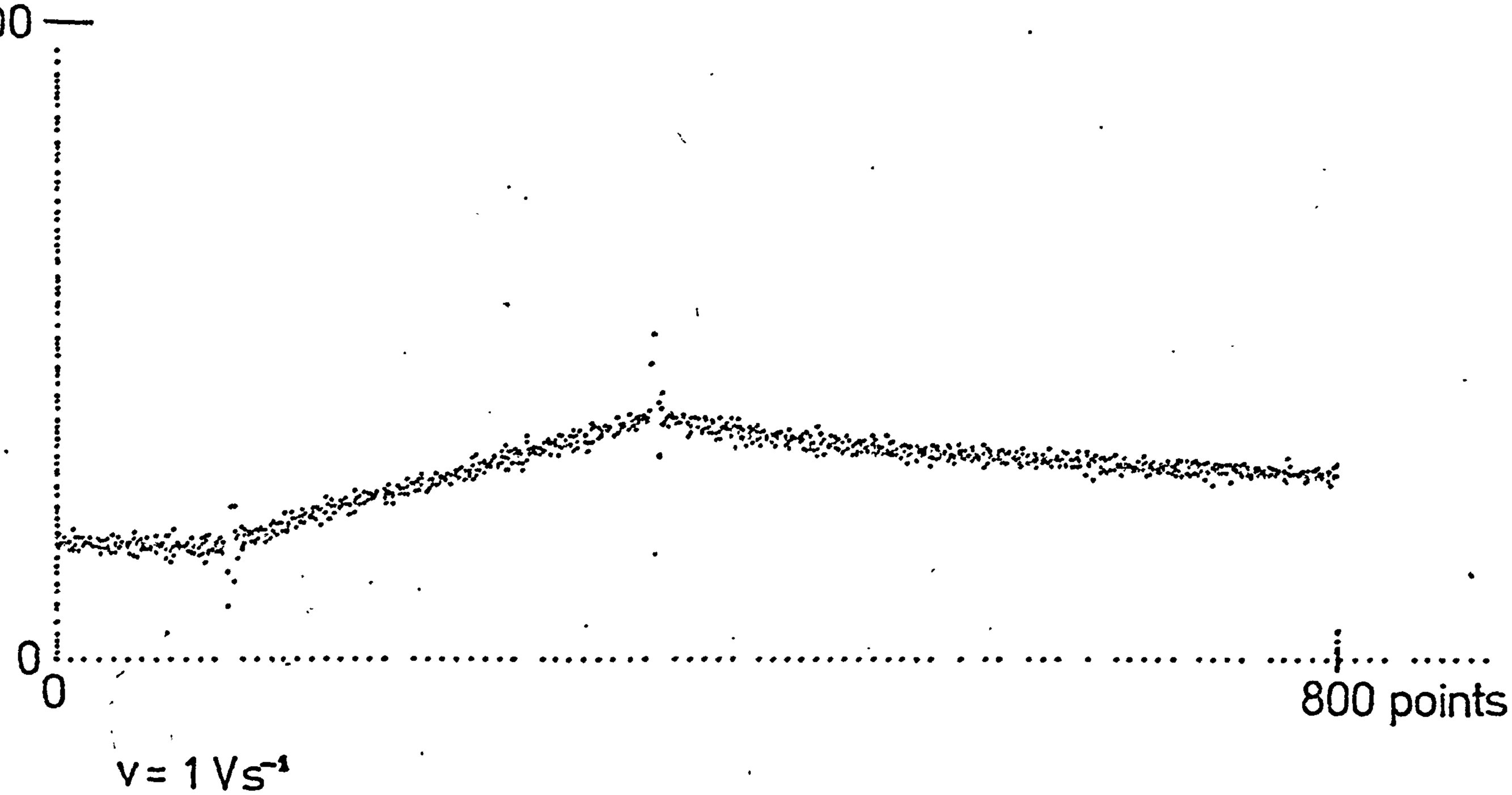

Fig. 5.14. Current response to the linear potential sweep described in Fig. 5.13. (Only part of the first pulse shown). Sampling rate = 30 s/point. Solution 2. A = 0.05 cm^2 HMDE. E = -0.97V vs S.C.E.

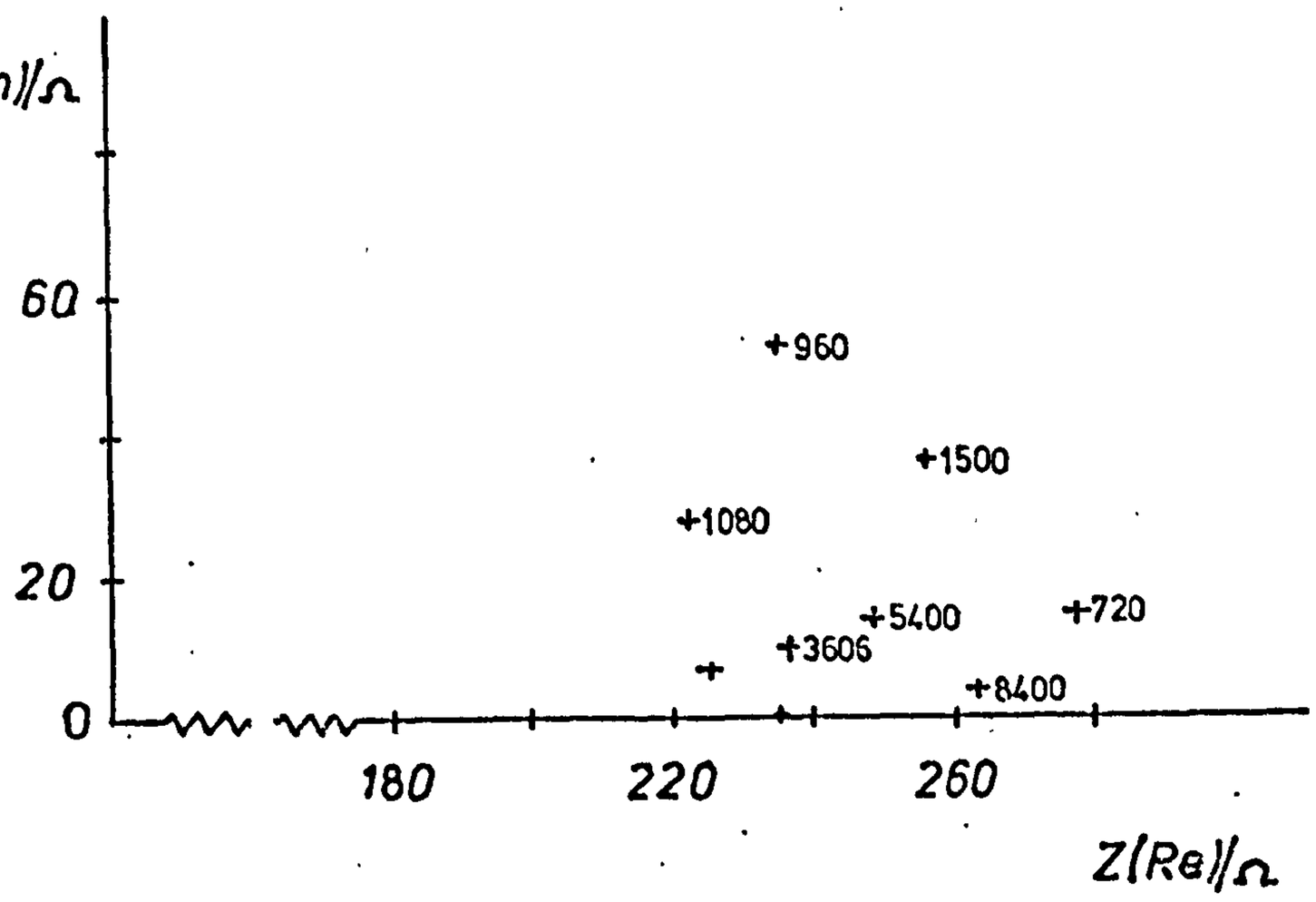

Fig. 5.15. Impedance results from LT sweep analysis corresponding to data of Figs. 5.13 and 5.14. θ is determined by the position of the cluster of points on the Z(Re) axis.

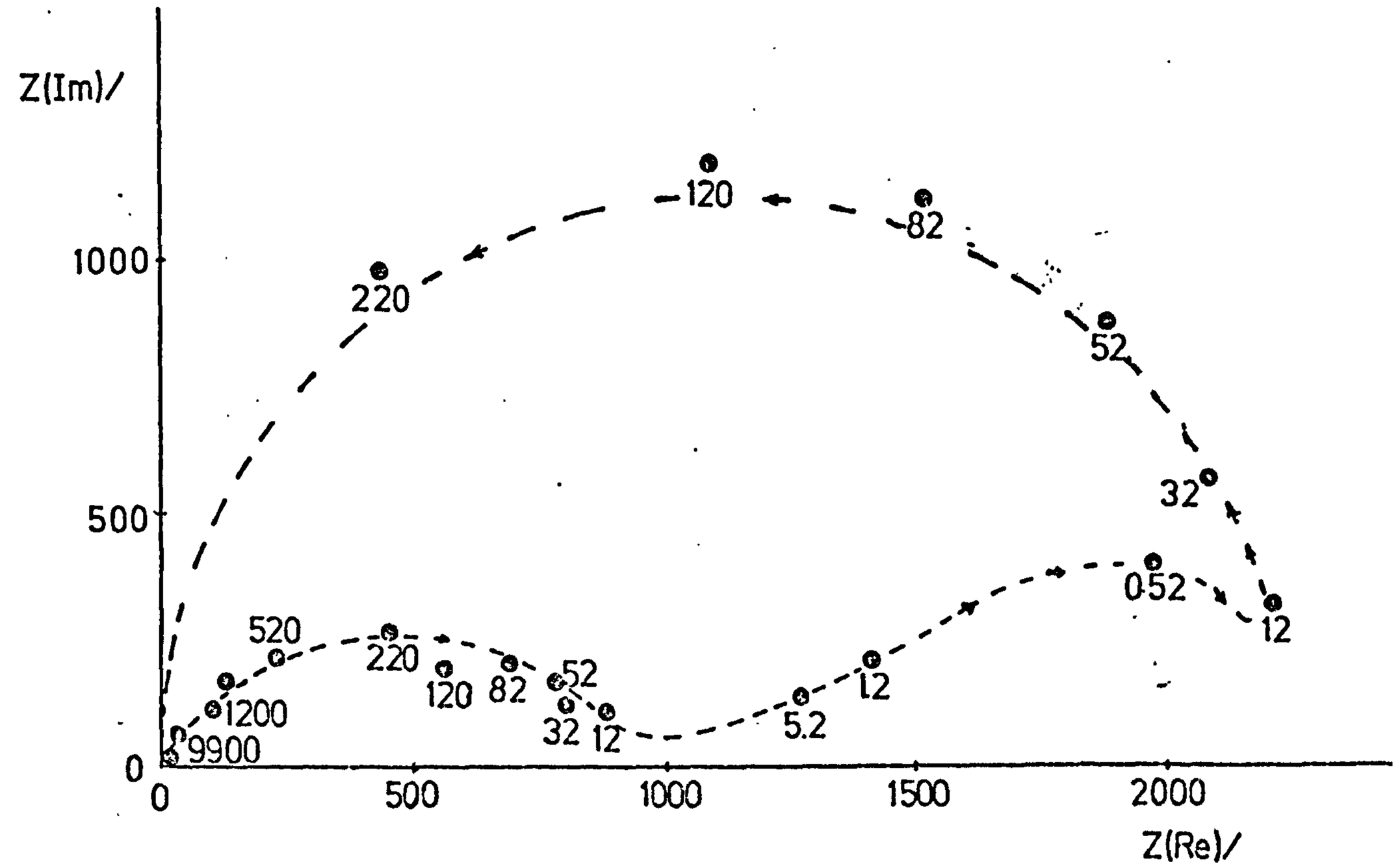

Fig. 5.16. Complex impedance plane plot from TFA measurements on HDE, solution 2, E = -1.0V vs S.C.E. amalgam Zn concentration 0.038M. Figures on graph indicate the frequency in Hz_2 The arrows indicate order of measurements. A = 0.05 cm^2.

of the original aim. With improved equipment the method might prove useful to detect double layer capacity.

V.1.3. A.c. Impedance

The impedance of a Zn amalgam HDE (hanging drop electrode), resulting from a small a.c. potential perturbation superimposed on various base potentials, was determined at various Zn^{++} concentrations and pH, using a TFA or a PSD in order to study concentrated amalgams. The amalgam was formed 'in situ', allowing a mercury drop to stand at the base potential until equilibrium was achieved, i.e. zero current.

Fig. 5.16 shows the impedance measurements, performed in the order indicated by the arrows, at a potential E = -1.0V vs S.C.E., in solution 2 (10^{-2}M Zn^{++}, pH = 3) and 0.038M Zn amalgam HDE. In Fig. 5.17 a similar result is observed at E = -1.1V vs S.C.E. (1.35M Zn/Hg). This behaviour could be characteristic of electrode poisoning or of amalgam formation. During the time taken to make a measurement at low frequency, the electrode active surfaces diminishes and therefore the complex plane semicircle increases in diameter. When taking measurements at high frequencies (in a shorter time) a second, bigger semicircle forms. This fact permits one to distinguish between the start of a Warburg impedance and a poisoning or amalgam forming effect. In Fig. 5.18 the θ values obtained without these effects are plotted as log θ vs E. Open circles correspond to measurements in solution 2 (10^{-2}M Zn^{++}, pH = 3), the numbers are the measured molarity of the amalgam.

Fig. 5.19 shows the Warburg-like impedance spectrum taken at E = -0.9, virtually on a pure mercury HDE. A similar result is shown in Fig. 5.20 for solution 1 (10^{-1}M Zn^{++}, pH = 3). An attempt was made to estimate θ, by extrapolating a semicircle, but this result is not very

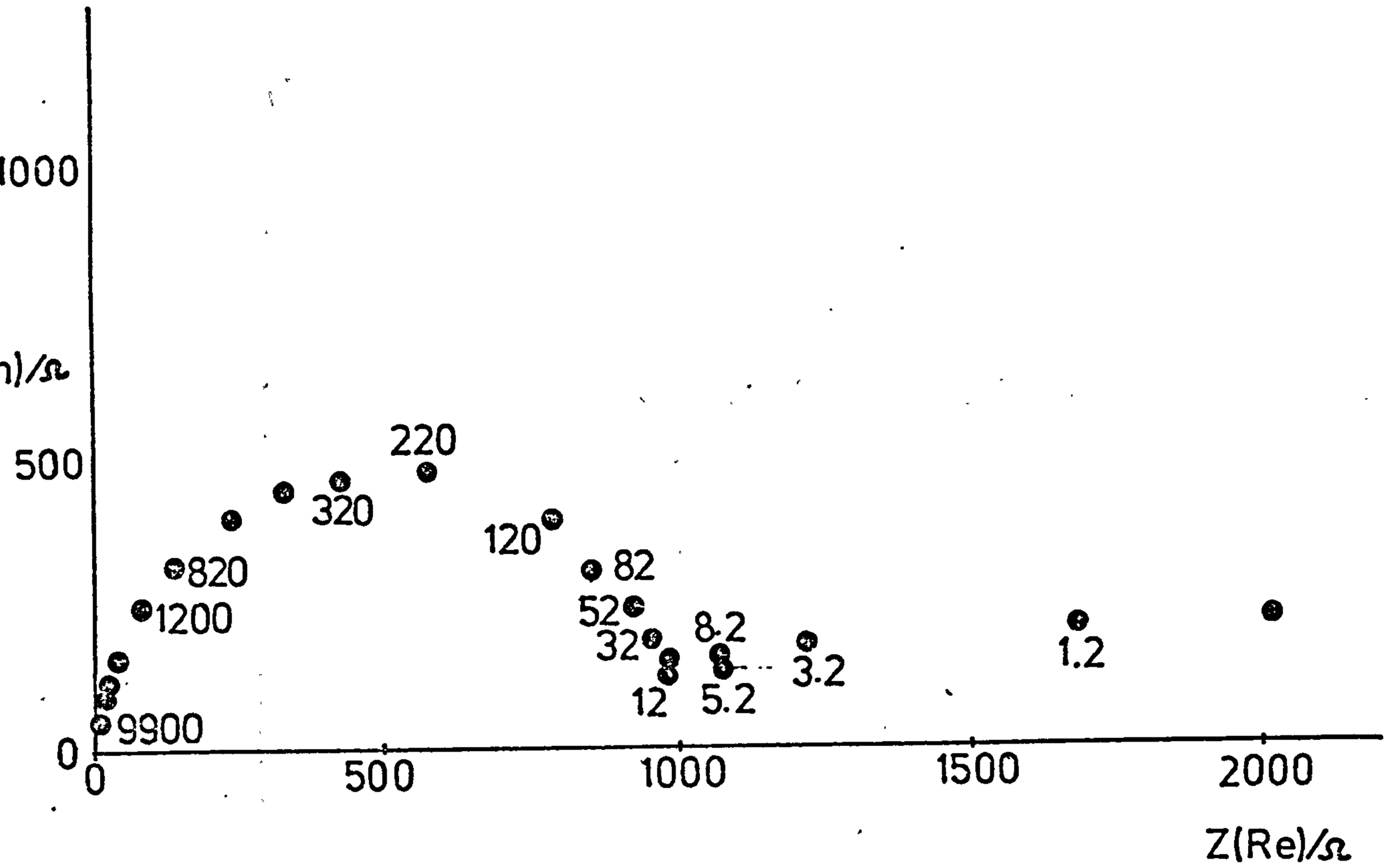

Fig. 5.17. Complex impedance plot from TFA measurements at HDE. Amalgam concentration 1.35M Zn/Hg. E = -1.1V vs S.C.E. Solution 2 (10^{-2}M Zn^{++}, pH = 3). A = 0.05 cm^2.

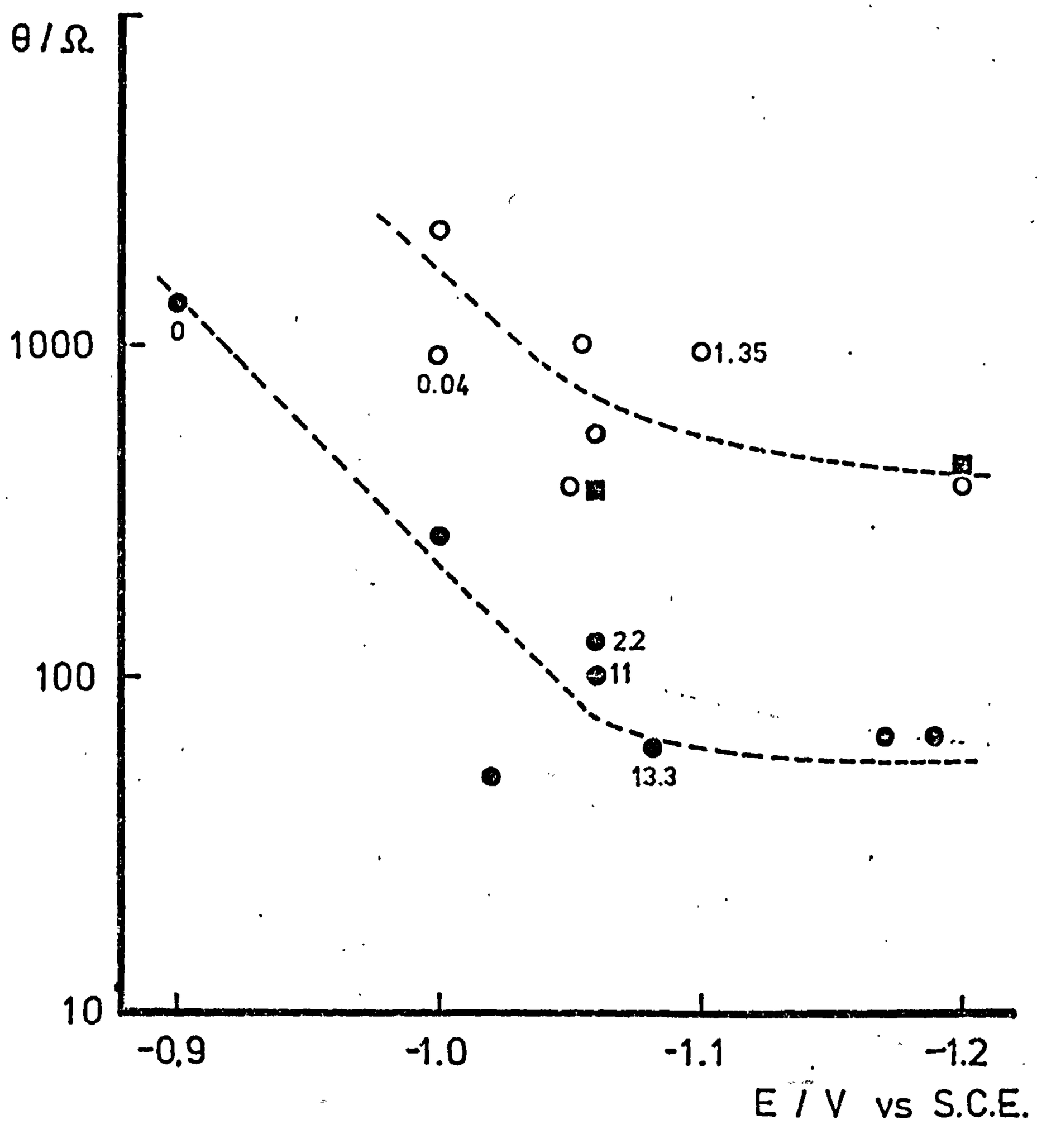

Fig. 5.18. Log θ vs E plot from TFA measurements at HDE (amalgam and pure mercury). (●) Results from solution 1(10^{-1}M Zn^{++}, pH = 3). (O) Results from solution 2 (10^{-2}M Zn^{++}, pH = 3). (■) Results from solution 2a (10^{-2}M Zn^{++}, pH = 4.6). Electrode area 0.05 cm^2.

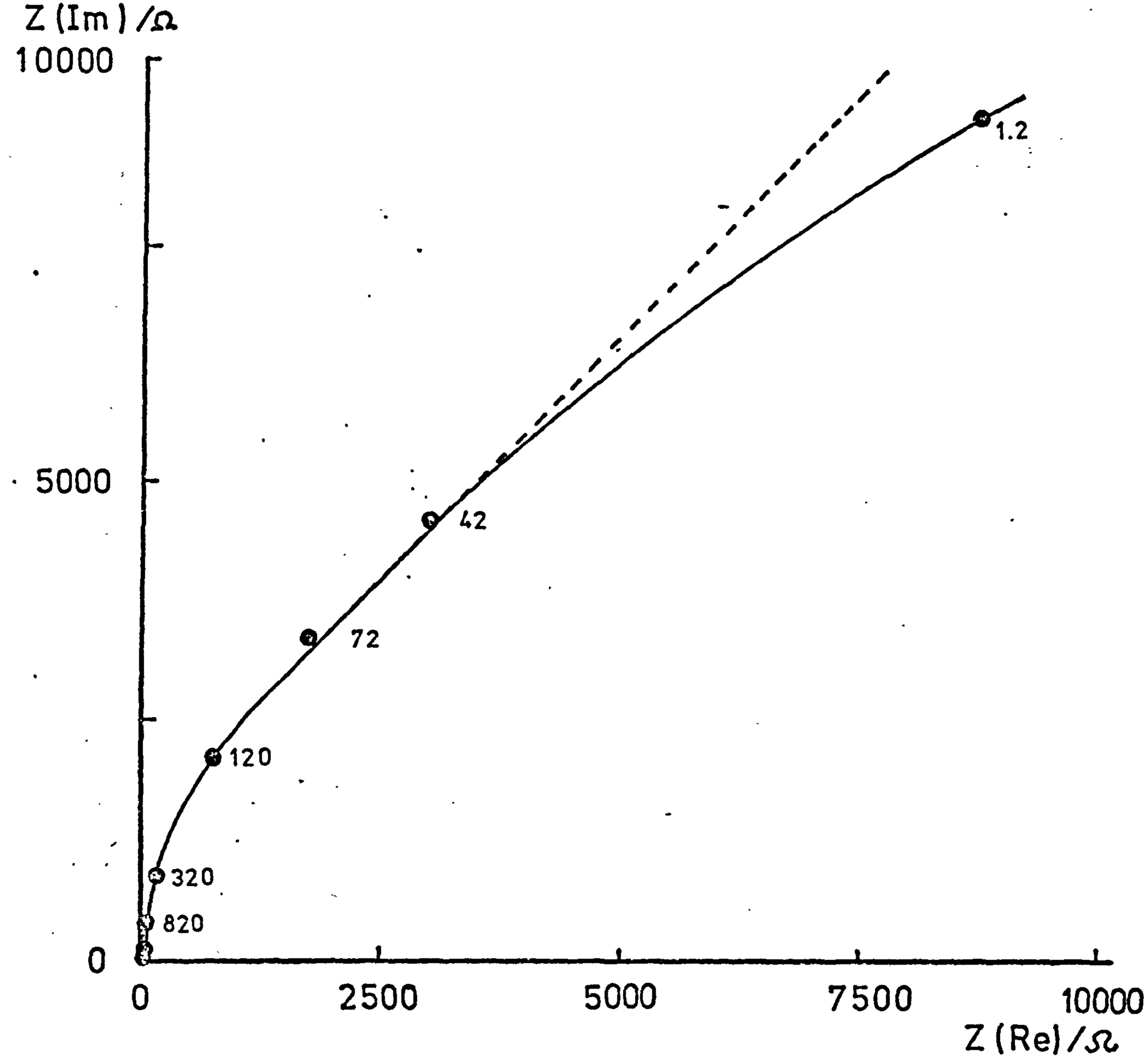

Fig. 5.19. Complex impedance plane plot from TFA measurements taken at E = -0.9V vs S.C.E. on HMDE. area 0.05 cm^2 solution 2. Broken line slope = 45^o

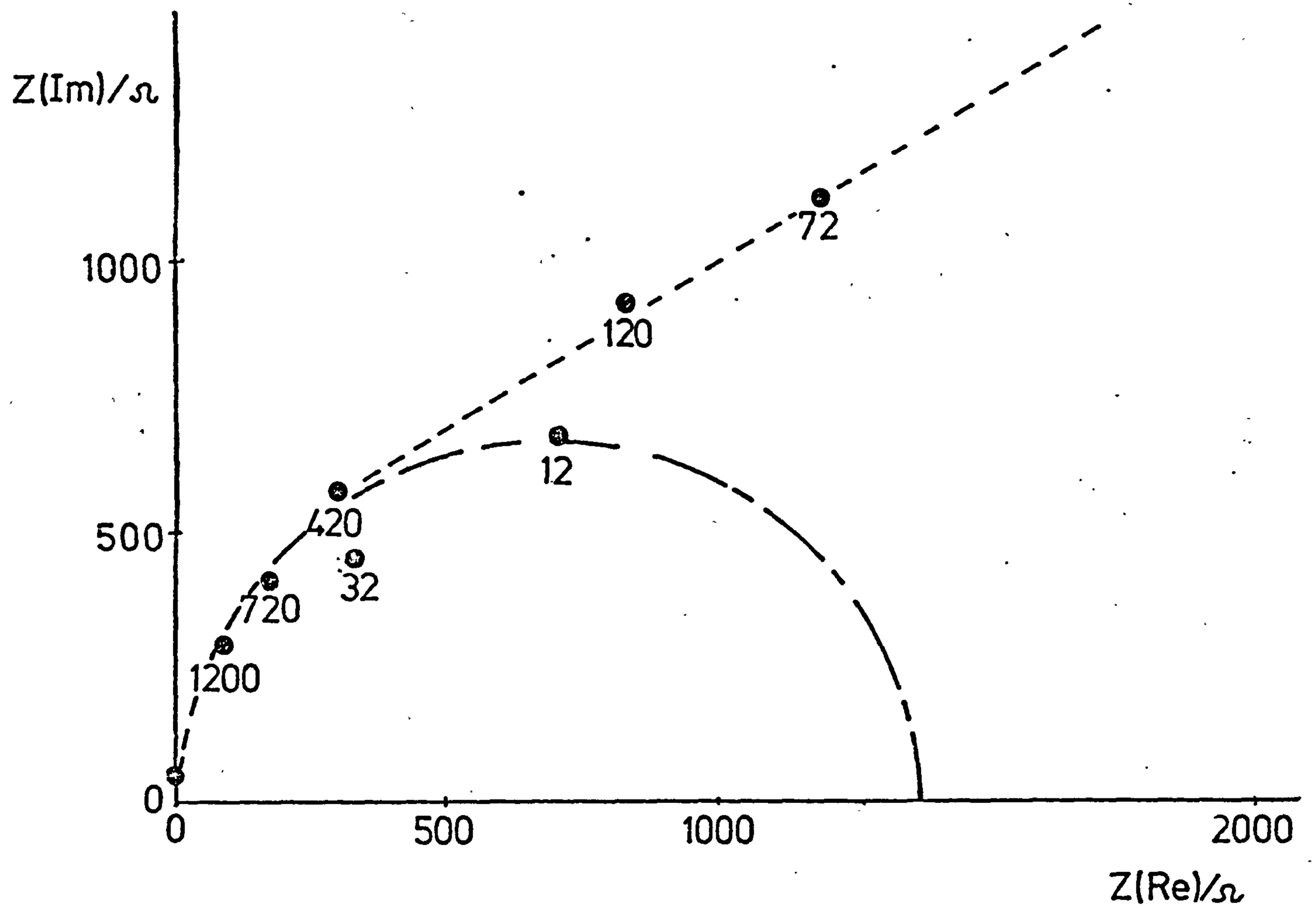

Fig. 5.20. Complex impedance plane plot from TFA measurements on HMDE, solution 1 (0.1M Zn^{++}, pH = 3), E = -0.9V vs S.C.E. A = 0.05 cm^2. Figures on graph indicate frequency in Hz.

reliable. At more cathodic potentials, increasingly concentrated amalgams were formed, and semicircles were obtained as impedance spectra. Typical examples for solution 1 are shown in Figs. 5.21 and 5.22, at E = -1.062 and -1.083V vs S.C.E. respectively. At this last potential the amalgam HDE was oversaturated (13M) and the surface most probably had metallic zinc. At more cathodic potentials (E < -1.083V vs S.C.E.), non equilibrium measurements were made in the steady state. An example is shown in Fig. 5.23, a semicircle was obtained and the i_{ss} current was measured.

Two θ values obtained from measurements on solution 2a (10^{-2}M Zn^{++}, pH = 4.7) are plotted in Fig. 5.18 as squares. They are of similar value than those obtained at pH = 3 (solution 2). This result is in agreement with the conclusion reached from the L.T. double pulse analysis, that θ does not depend on H^{+}.

The results in Fig. 5.18 show that cathodic values of θ not at equilibrium depend on $[Zn^{++}]$, a ten fold increase in concentration causes an almost ten fold decrease in θ values. Compared with pure mercury (Figs. 5.6 and 5.11), the θ values of Fig. 5.18 agree within experimental error. The i - E curve from slow sweeps (see Figs. 5.27 and 5.29) suggest depending on sweep rate a quasi-irreversible or even a reversible reaction. The appropriate theoretical expression (Equation 5.21) for θ for a.c. on a pseudo reversible wave is rather complicated. Qualitatively, the shape of both curves in Fig. 5.18 could fit the simulated curves 2 or 3 in Sluyters[1] Fig. 7a (reproduced in this work in Fig. 1) representing Equation 5.21 with $C_o = C_R = 10^{-6}$ mole cm^{-3} and $k_{SH} = 10^{-3}$ or 10^{-4} cm s^{-1}.

At about E = -1.2V vs S.C.E. the simplifcation

$$a_1 = 2.303\ (i_L)_1\ \theta_1 \qquad (5.25)$$

can be applied. From Equation 5. and the measured $(i_L) = 1.5 \times 10^{-4}$A,

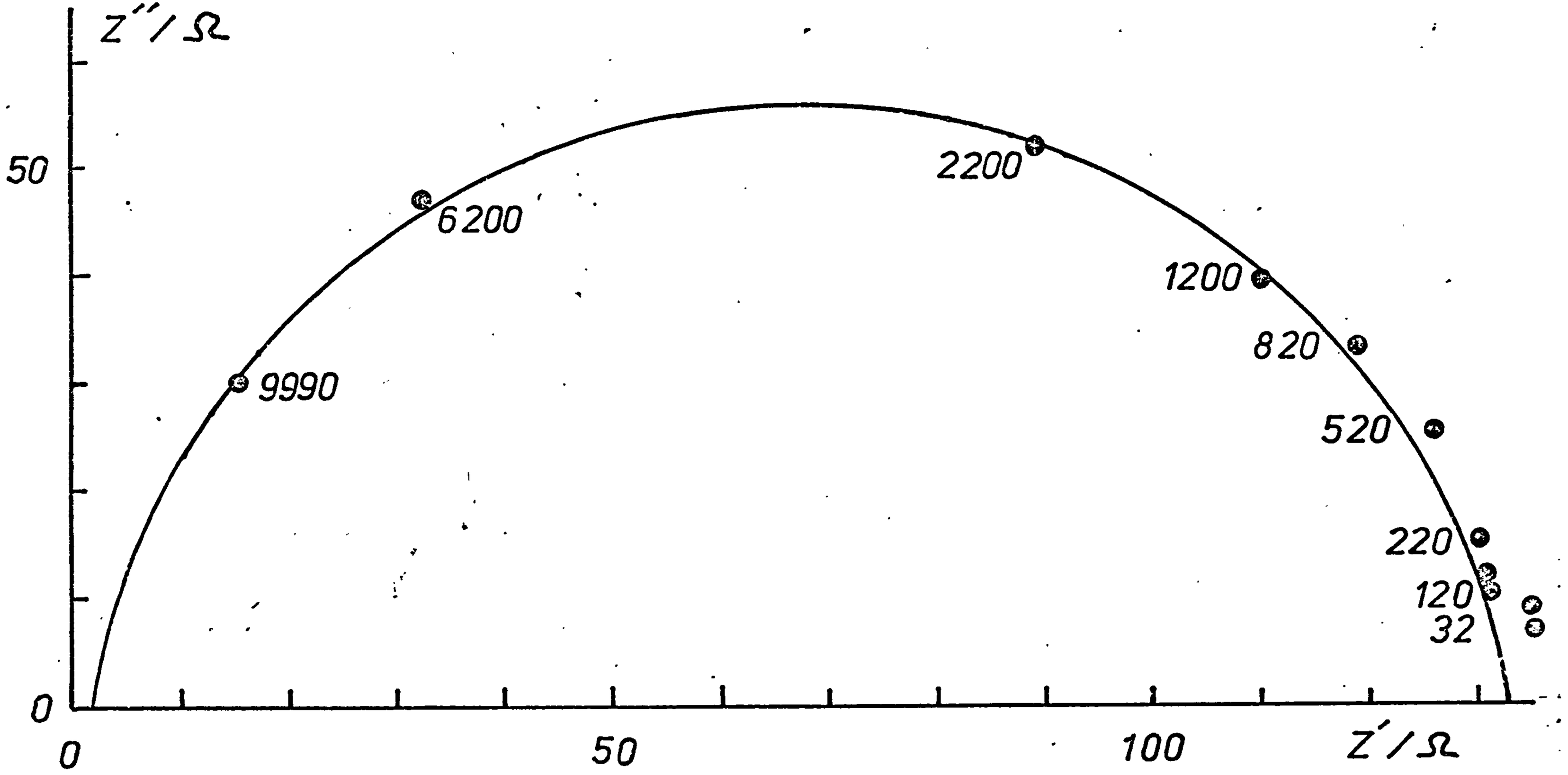

Fig. 5.21. Complex impedance plot for 0.1M Zn^{2+} + 1M KCl (pH = 3), on a Hg(Zn) HDE (0.051 cm^2) at E_e = -1.062V vs S.C.E.

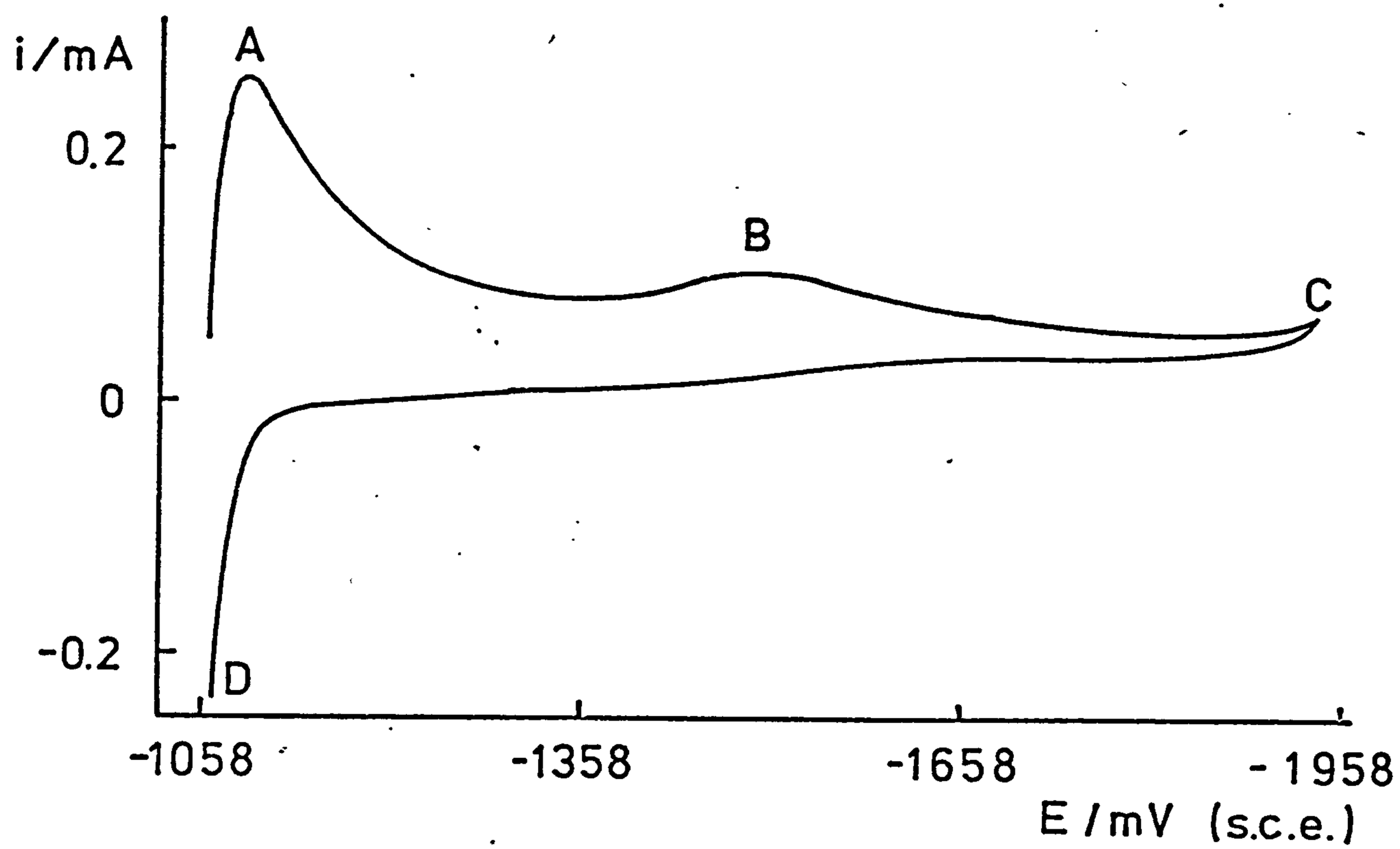

Linear potential sweep on Hg (Zn) HDE solution 2, from E_e = -1.058 V vs SCE. Sweep rate z 0.1 V s^{-1}.

a value of 1.36×10^{-4}A was obtained for $(i_L)_1$ in solution 2. With this value and the measured $\theta = \theta_1 = 394\Omega$ a Tafel slope of $a_1 = 123$ mV/decade is obtained. Similarly, from the data of Fig. 5.23 a Tafel slope of $a_1 = 138$ mV/decade was obtained for solution 1.

The corresponding $C_{d.L}$-E curve is shown in Fig. 5.23.a This confirms that poisoning is not a major factor and that the TFA results are genuine. For the values of θ which are numbered in Fig. 5.18 the appropriate equation for equilibrium namely

$$\theta = \frac{RT}{n^2 F^2 k_{SH}} \frac{1}{(C_o^*)^{\beta_1 RT/nF} (C_R^*)^{\alpha_1 RT/nF}} \qquad (5.26)$$

is to be used to interpret the measurements. As C_o^* is constant then

$$\log \frac{\theta_1 (C_R^*)_1}{\theta_2 (C_R^*)_2} = \frac{29}{a} \qquad (5.27)$$

Thus the cathodic Tafel slope can also be predicted. The 2.2M and 11M amalgams suggest a $\sim$ 50 mV and the 11M and 13M amalgams suggest a $\sim$ 203 mV. Using equation 5.26 with a = 120 mV and b = 40 mV, values which seem likely, gives for the 2.2M amalgam $k_{SH} = 4.6 \times 10^{-5}$ cm s^{-1} and for the 11M amalgam $k_{SH} = 4 \times 10^{-5}$ cm s^{-1}. The value of 4.6×10^{-5} cm s^{-1} is equivalent to a value of i_o, given by

$$i_o = \frac{RT}{nF\theta}$$

of 2×10^{-3}A cm^{-2} and a value of $\log \frac{i_o}{C} = 2 \times 10^2$A cm mol^{-1}. This is approximately 10 times lower than given by Salie[6].

V.1.4. Linear Potential Sweep Measurements on HDE

The measurements were made at various solution Zn^{++} concentrations, pH, and on pure mercury and amalgams of various concentrations using sweep

Fig. 5.23. Complex impedance plane plot for solution 1, on a Hg(Zn) HDE (0.05 cm^2) at E = -1.190V vs S.C.E.
i_{ss} = 0.685 mA.
The frequencies are 9900, 6200, 4200, 1200, 920, 720, 120, 72, 2.2, 0.5 Hz.

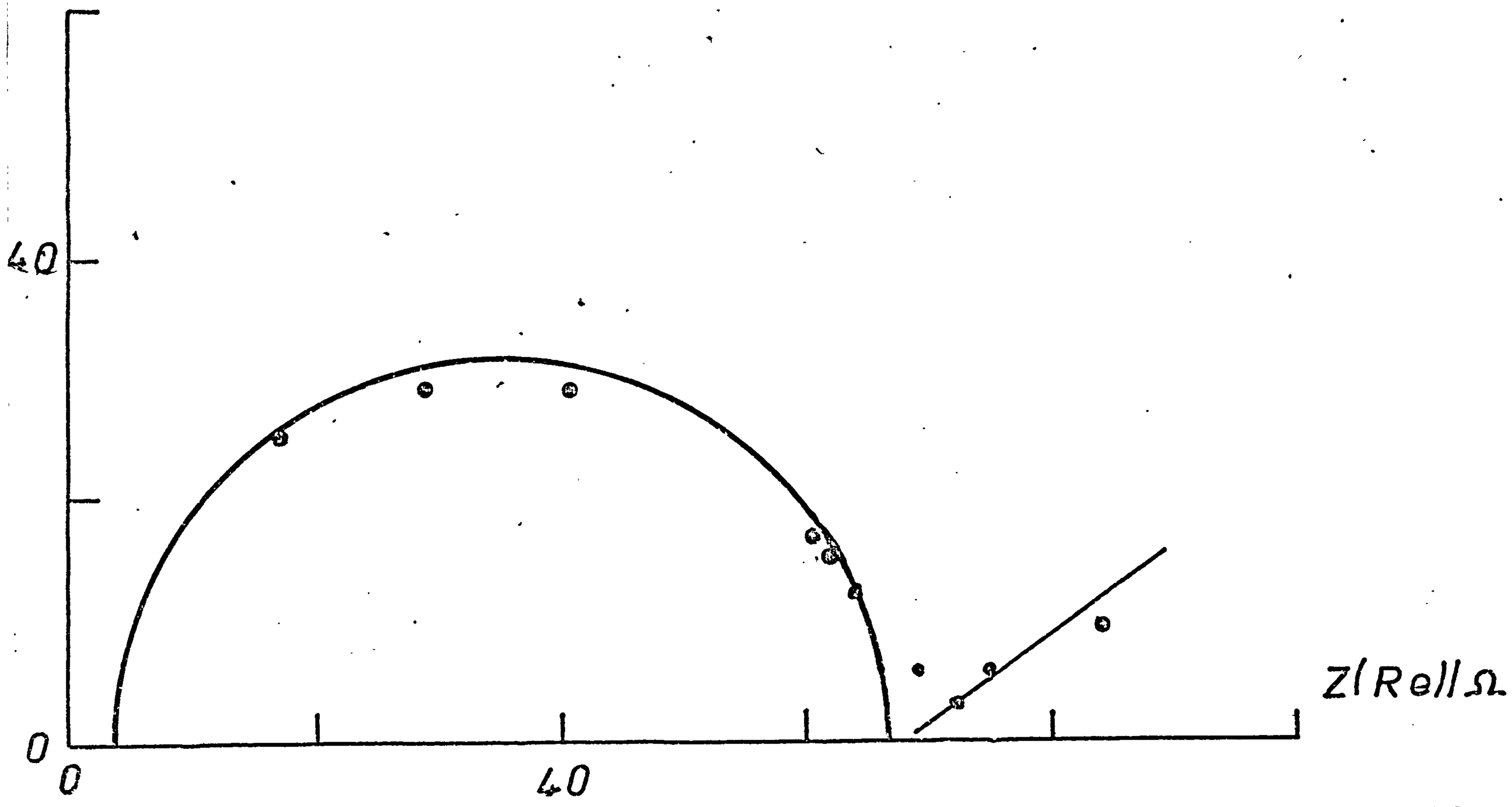

rates from 0.001V s^{-1} to 100V s^{-1} and covering a wide range of potential.

Figs. 5.24 to 5.26 show linear potential sweeps on solution 2 (10^{-2}M Zn^{++}, pH = 3). Cathodic peaks A, B and C correspond to Zn^{++} reduction, H^{+} reduction, and solvent reduction respectively. The anodic peak D is caused by Zn dissolution. It can be seen that as sweep rate decreases, peaks A and B move to the left (anodic direction) and D moves to the right. At lower sweep rates the potential between the anodic and cathodic Zn peaks tends to 40 mV. An analysis of the cathodic wave at two sweep rates is shown in Figs. 5.27 and 5.27b. The Tafel slope at the foot of the wave is 30-40 mV and under these conditions the wave is practically reversible.

Fig. 5.28 shows linear potential sweeps in solution 2c (10^{-2}M Zn^{++}, pH 4.3). The peaks A and D corresponding to zinc reduction and dissolution, respectively, are increasingly separated from one another by increasing the sweeping rate, peak C corresponds to solvent reduction. Although H^{+} reduction does not give a peak, this contribution is distinct in region B. At low sweep rates peak A coalesces into region B as seen in Fig. 5.29.

Fig. 5.30 shows the reduction of solution 3 (3×10^{-3}M Zn^{++} + 1M KCl, pH = 3). The Zn^{++} and H^{+} waves labelled X and Y, are separated from one another and from the solvent reduction, labelled Z, at high sweep rate (v) and coalesce at low sweep rate. This shows that the Tafel slope for H^{+} reduction is different from that for Zn^{++} reduction. H^{+} reduction is certainly irreversible although much slower than the Zn^{++} reduction. As the reaction is clearly pseudo reversible there is some difficulty in analysing the sweep data. For example Fig. 5.31 shows that at low sweep rate E_p is independent of v, and that E_p depends on amalgam concentration as expected for a reversible electrode reaction. The curve for pure Hg (◪) suggests that above 100 mV s^{-1} it may be possible to analyse as an

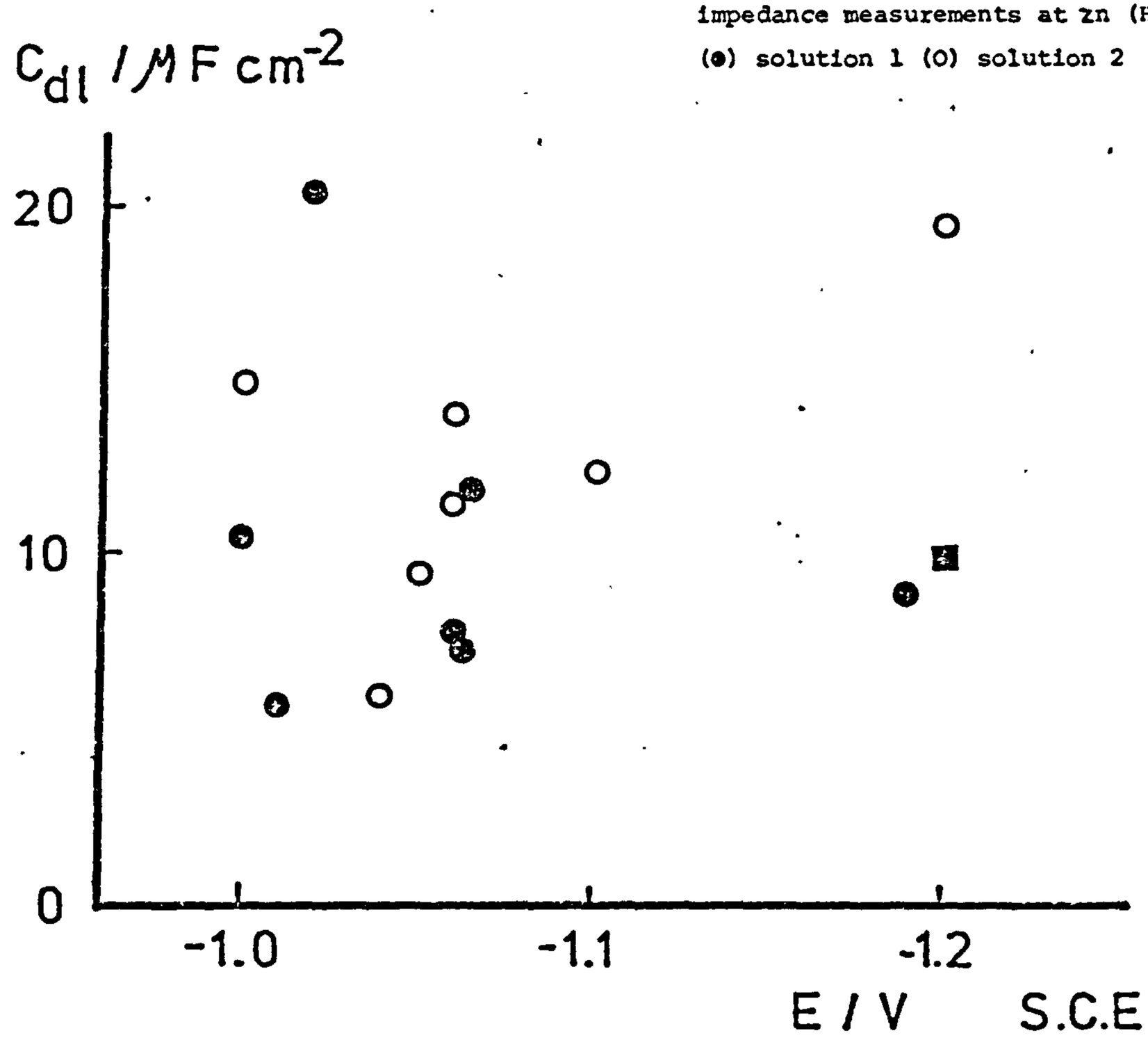

Fig. 5.23a C_{dl} vs E plot from T F A impedance measurements at Zn (Hg) HDE. (●) solution 1 (○) solution 2 (■) solution 2a.

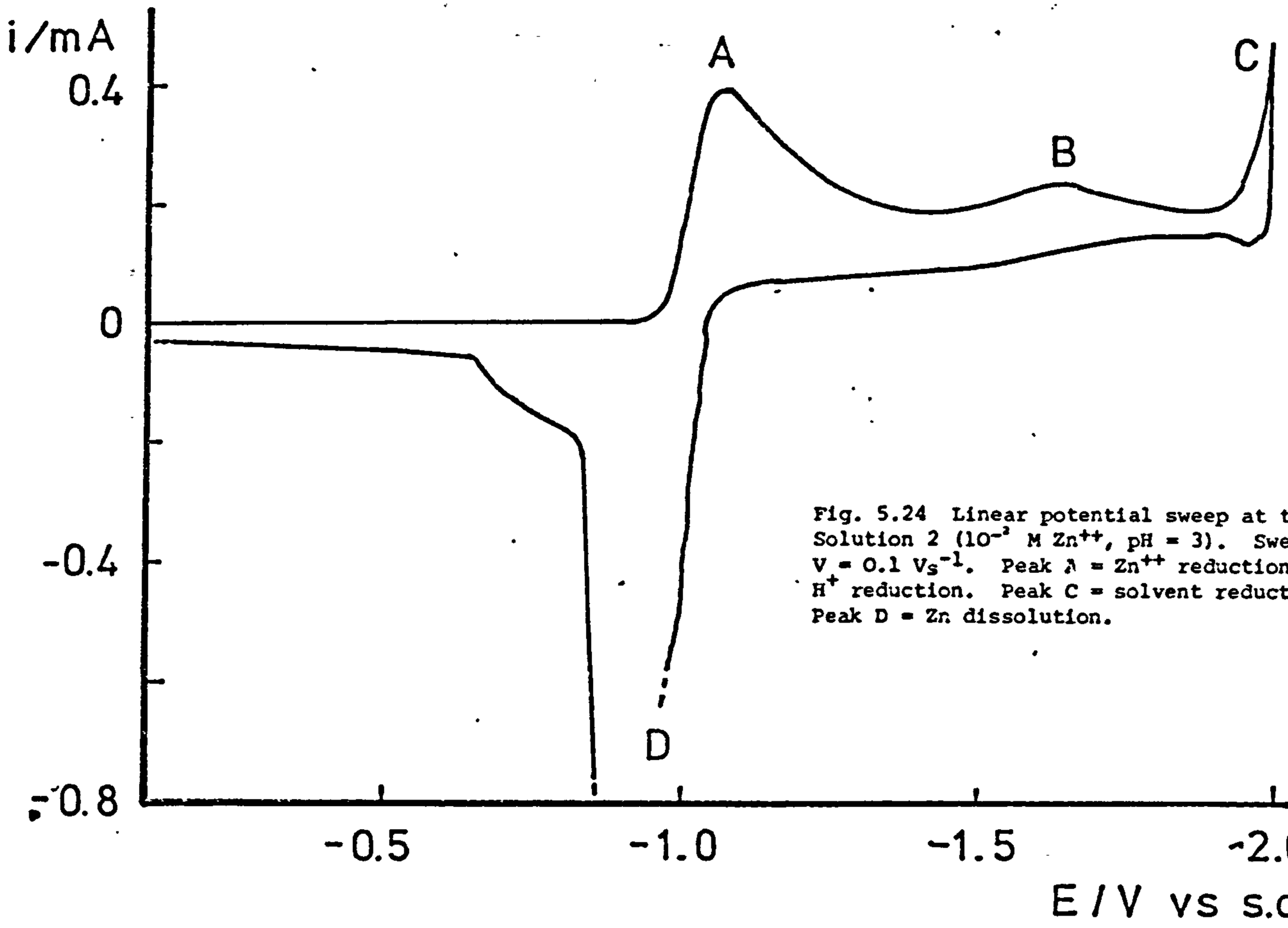

Fig. 5.24 Linear potential sweep at the HMDE. Solution 2 (10^{-2} M Zn^{++}, pH = 3). Sweeping rate $V = 0.1\ V_S^{-1}$. Peak A = Zn^{++} reduction. Peak B = H^+ reduction. Peak C = solvent reduction. Peak D = Zn dissolution.

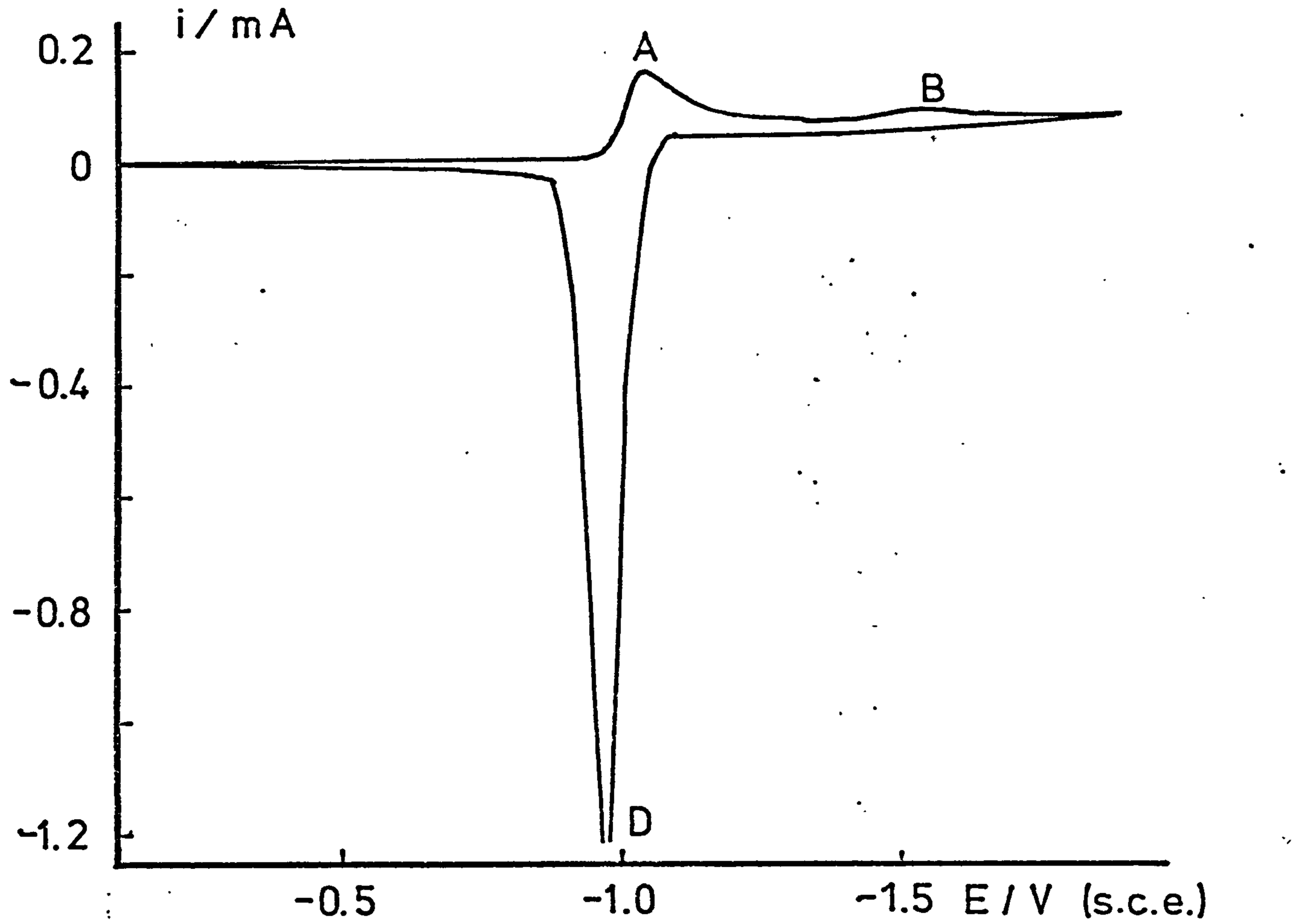

Fig. 5.24.a Linear potential sweep at the HMDE from solution 2 (10^{-2}M Zn^{++}, pH = 3). Electrode area = 0.05 cm^2. V = 0.01 V s^{-1}

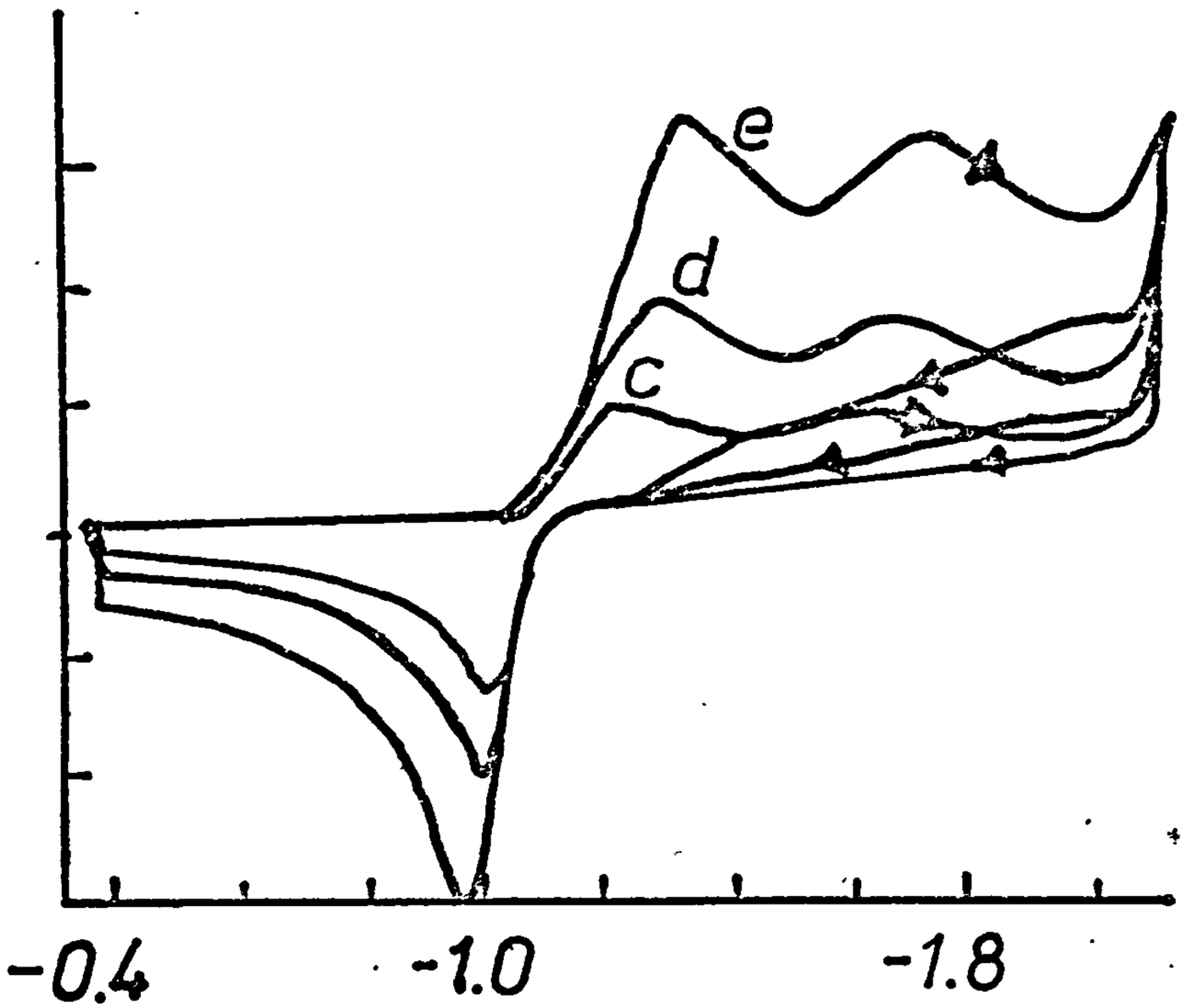

Fig. 5.25. Linear potential sweeps on solution 2. Sweep rates c) 0.1 V s^{-1}, d) 1 V s^{-1}, e) 3.2 V s^{-1}. From oscilloscopic measurements at Hg/Zn, HDE.

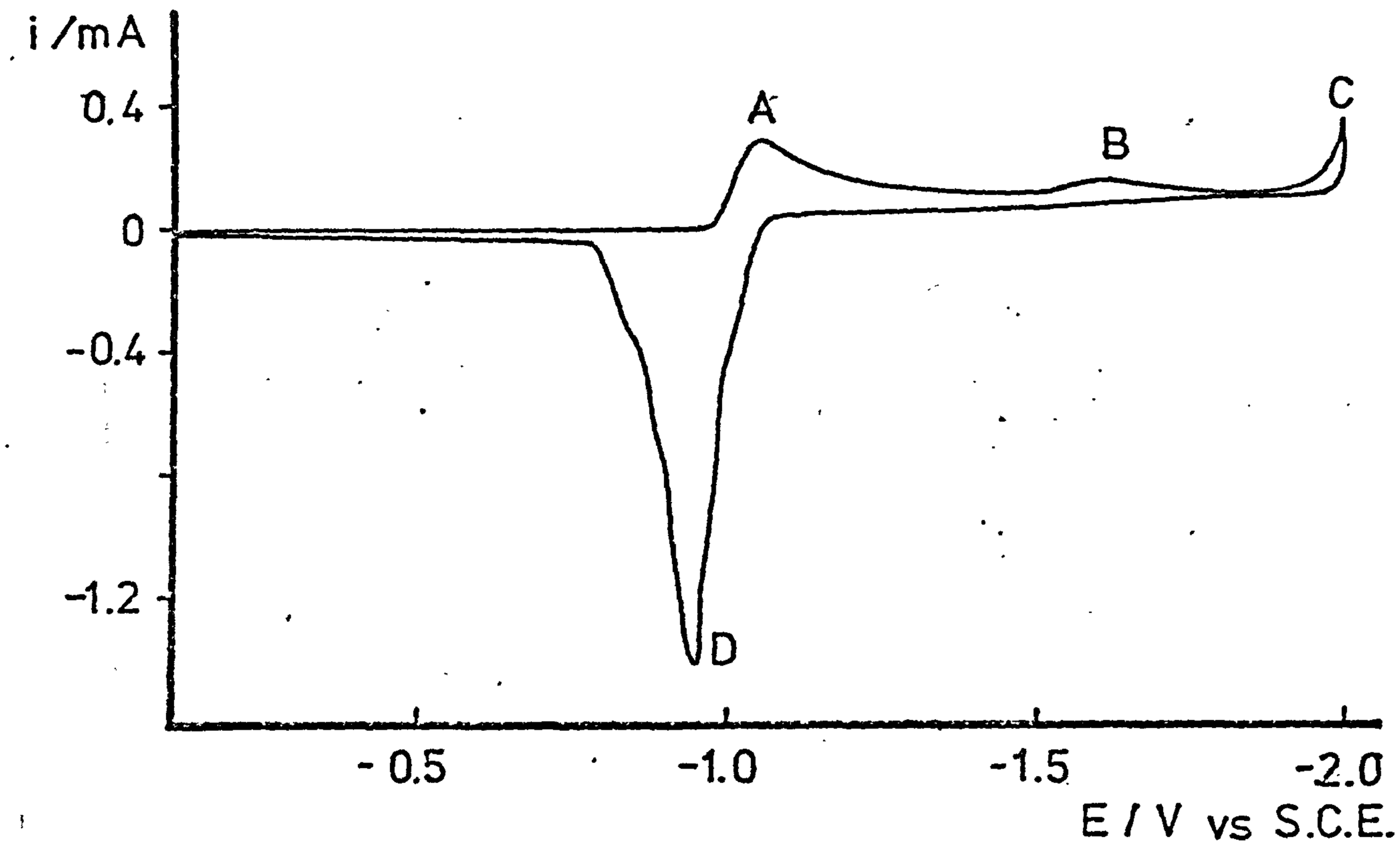

Fig. F.25. Linear potential sweep from solution 2 at the HDE (A = 0.05 cm^2)
Sweep rate V = 3/32 V s^{-1}

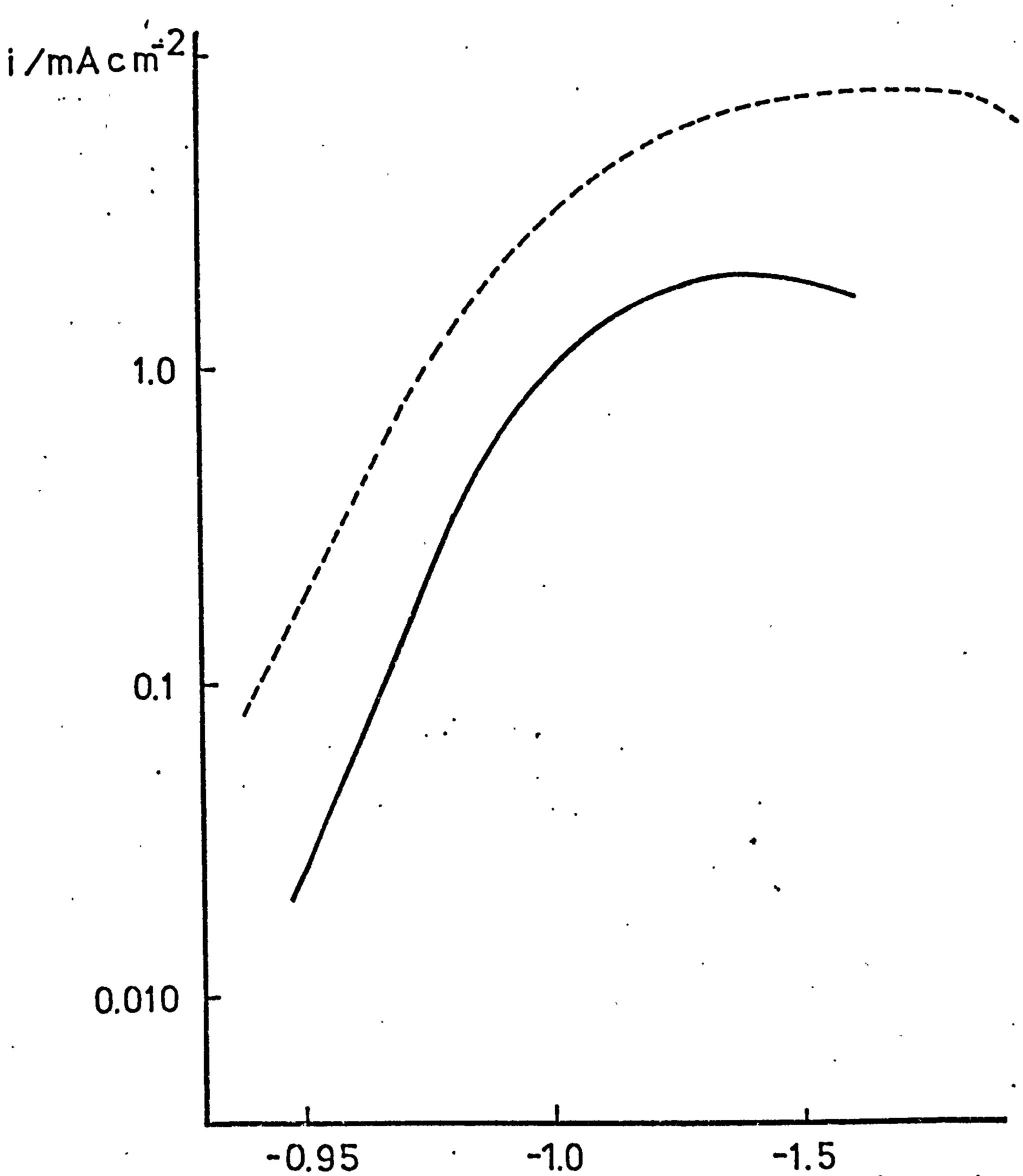

Fig. 5.27. log i vs E plot for the data of Figs. 5.24 and 5.25.
Broken line V = $1/3.2 V s^{-1}$, Tafel slope a = 40 mV/dec.
Solid line V = $0.01 V s^{-1}$, Tafel slope = 30 mV/dec.

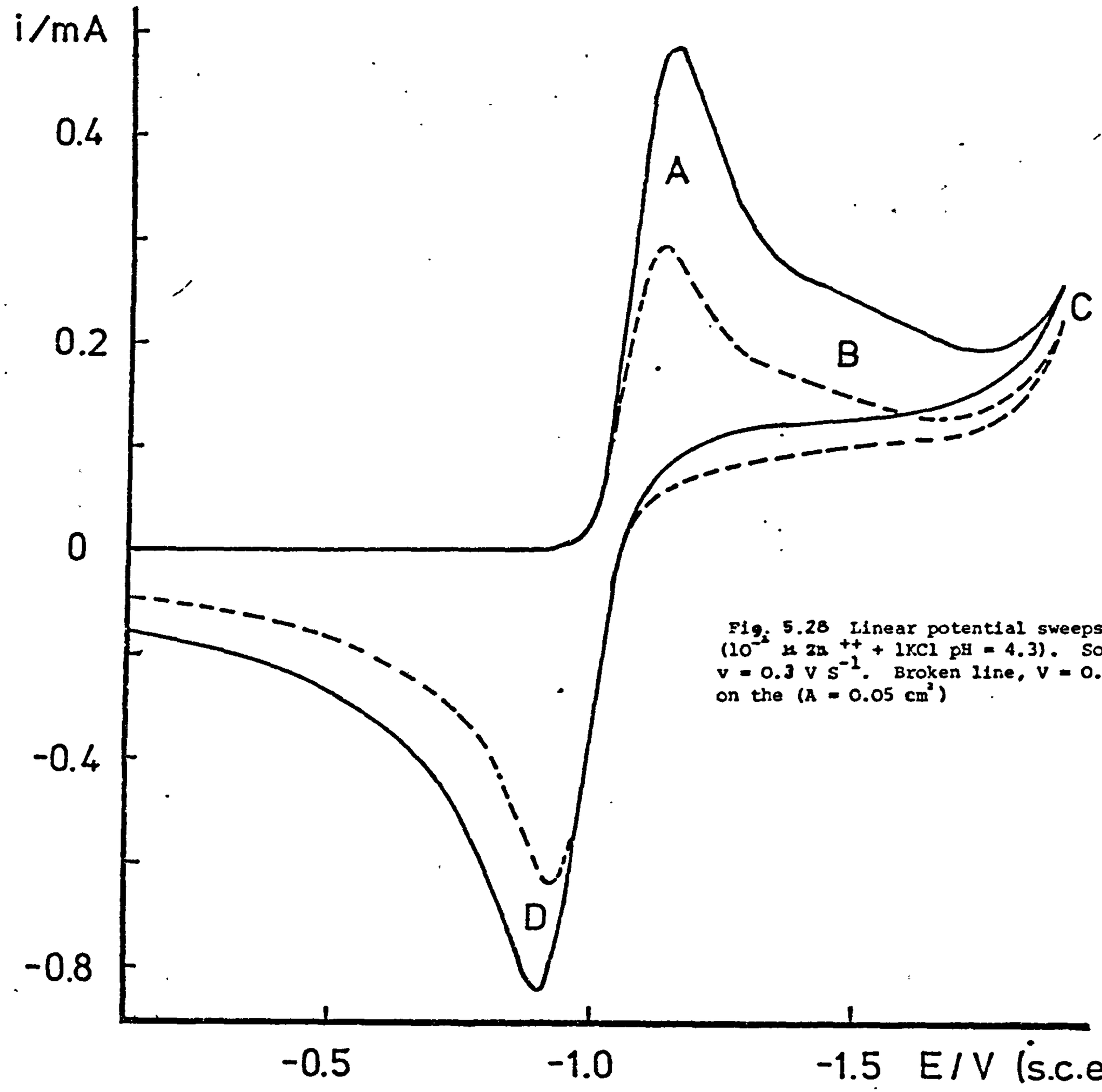

Fig. 5.28 Linear potential sweeps in solution 2C (10^{-2} M Zn^{++} + 1KCl pH = 4.3). Solid line, v = 0.3 V S^{-1}. Broken line, V = 0.1 Vs^{-1}. Measured on the (A = 0.05 cm^2)

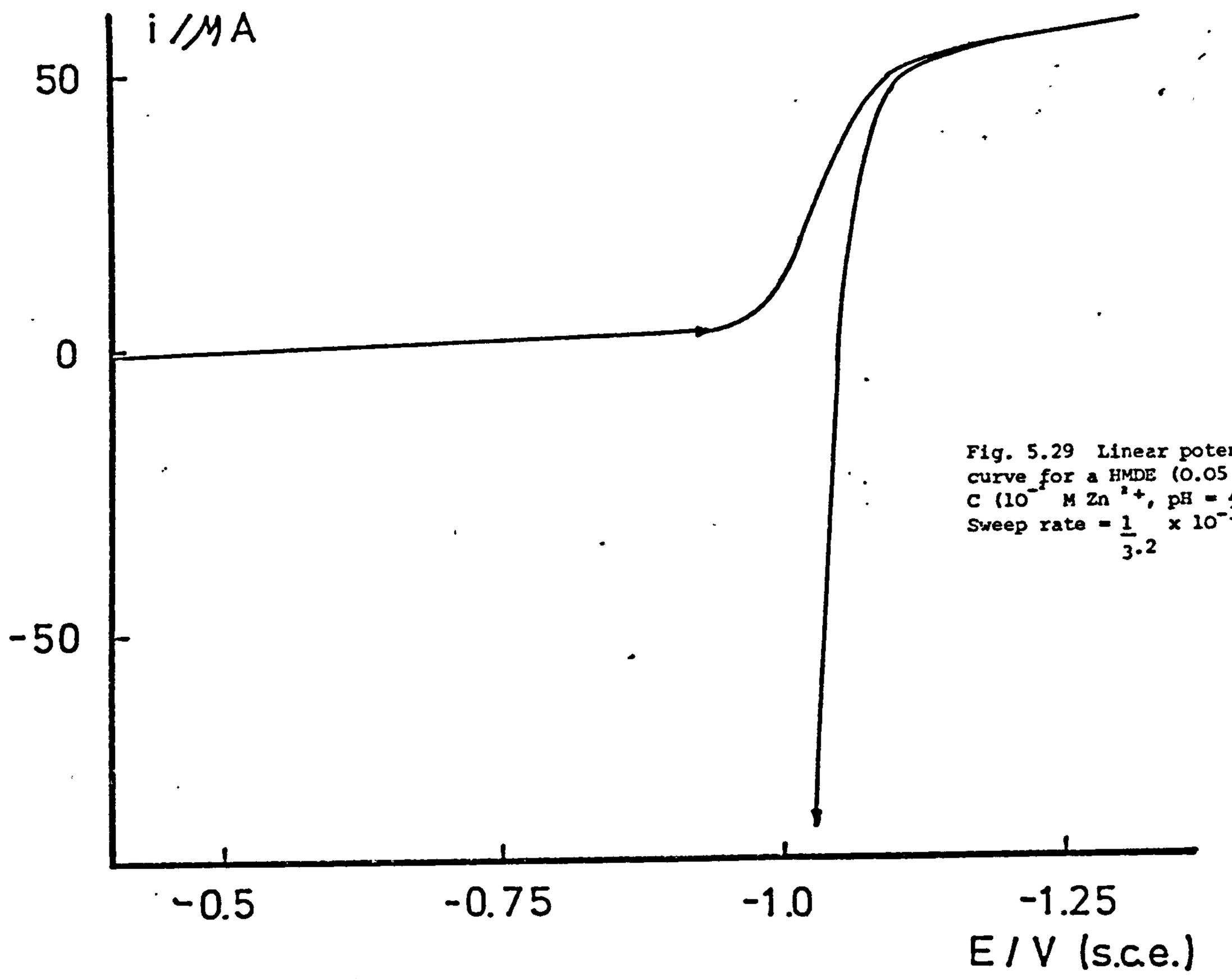

Fig. 5.29 Linear potential sweep curve for a HMDE (0.05 cm^2) solution 2 C (10^{-2} M Zn^{2+}, pH = 4.3).
Sweep rate = $\frac{1}{3.2} \times 10^{-3}$ V/s^{-1}

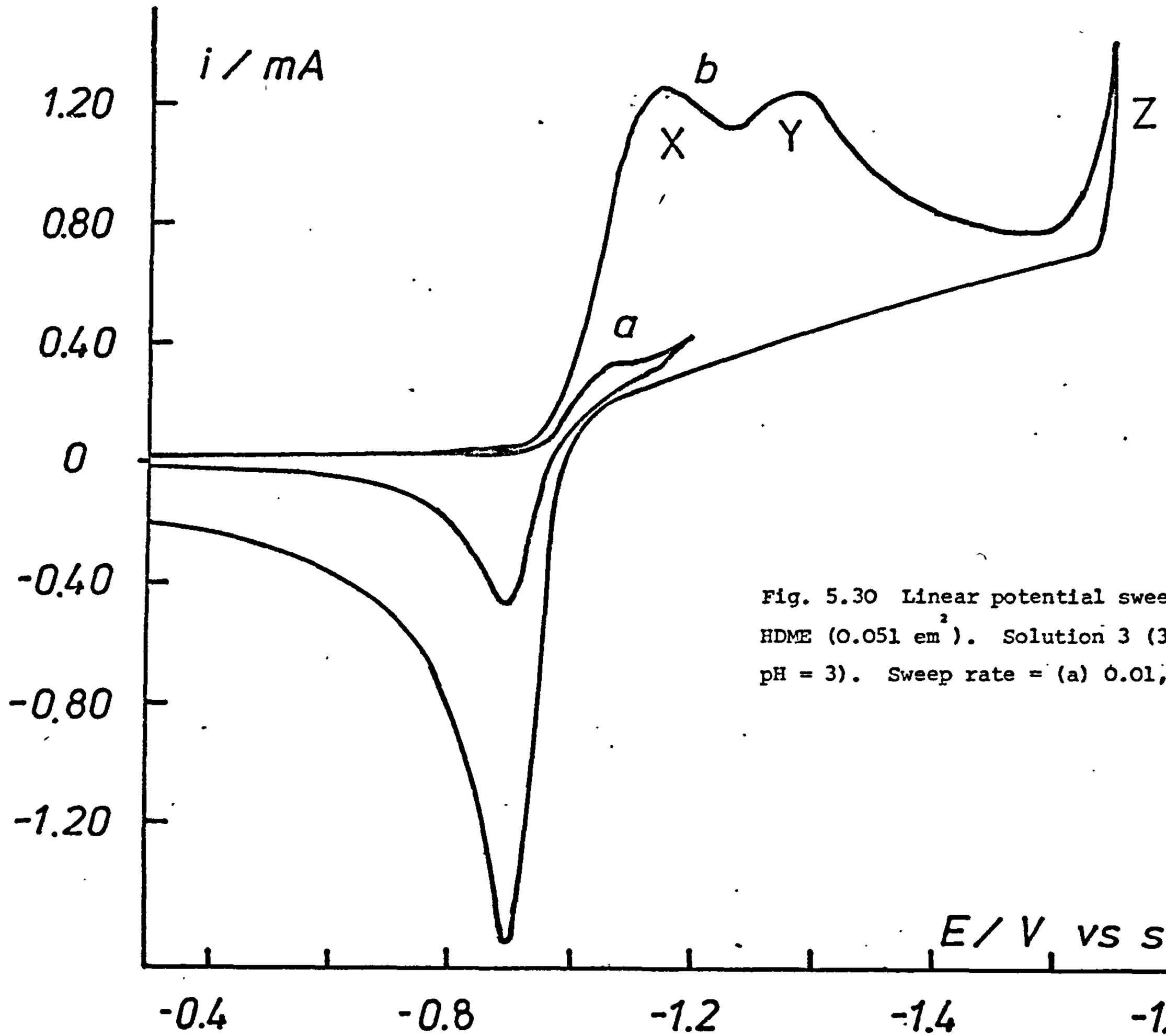

Fig. 5.30 Linear potential sweep curve for a HDME (0.051 em^2). Solution 3 (3×10^{-3} M Zn^{++}, pH = 3). Sweep rate = (a) 0.01, (b) 0.3 Vs^{-1}.

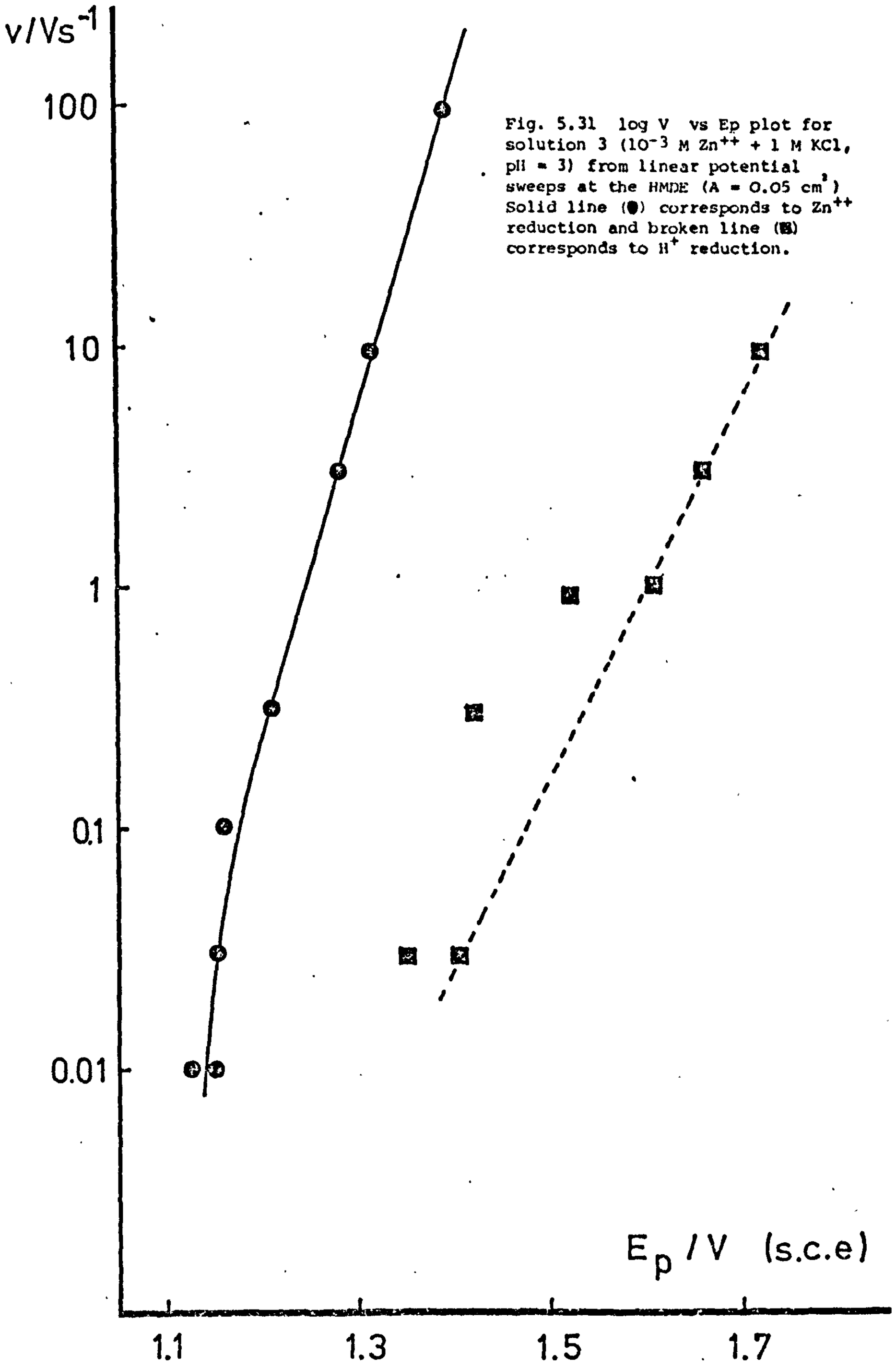

Fig. 5.31 log V vs Ep plot for solution 3 (10^{-3} M Zn^{++} + 1 M KCl, pH = 3) from linear potential sweeps at the HMDE (A = 0.05 cm^2) Solid line (●) corresponds to Zn^{++} reduction and broken line (■) corresponds to H^+ reduction.

irreversible reaction where the analysis is simplest. The equations for the analysis, if a sufficiently high sweep rate is used, are

$$i_p = 0.496\, n F A C D^{1/2} \left(\frac{2.303\, v}{a}\right)^{1/2} \qquad (5.28)$$

$$\frac{dE_p}{d \log v} = a \qquad (5.29)$$

These can be compared with the expected reversible behaviour at low sweep rate given by

$$i_p = 0.447\, n F A C D^{1/2} \left(\frac{nFv}{RT}\right)^{1/2} \qquad (5.30)$$

$$E_p = \text{constant} \qquad (5.31)$$

There is a transition between the low v and high v behaviour. Fig. 5.32 shows the variation of E_p with v for 3×10^{-3}M Zn^{2+} solution. The curve suggests that above 0.5V s^{-1} sweep rate the equation 5.29 can be applied and a $\simeq$ 150 mV. The corresponding $i_p/v^{1/2}$ graph is shown in Fig. 5.33. Greater than v = 0.5V s^{-1} the curve seems to approach $\sim$ 120 mV. However there is some uncertainty due to double layer charging and ohmic resistance, especially at such high sweep rates. Probably one can only say that a is 50-120 mV. A similar behaviour is observed in 10^{-2}M Zn^{2+} which is also shown in Fig. 5.33. The curve is independent of pH. Here also the Tafel slope fits $\sim$60 mV at medium sweep rates and may be $\sim$ 120 mV at higher sweep rates.

V.1.5. Double Pulse Measurements

Measurements were made over a wide range of conditions in order to determine in what state the Zn metal existed in the mercury. The

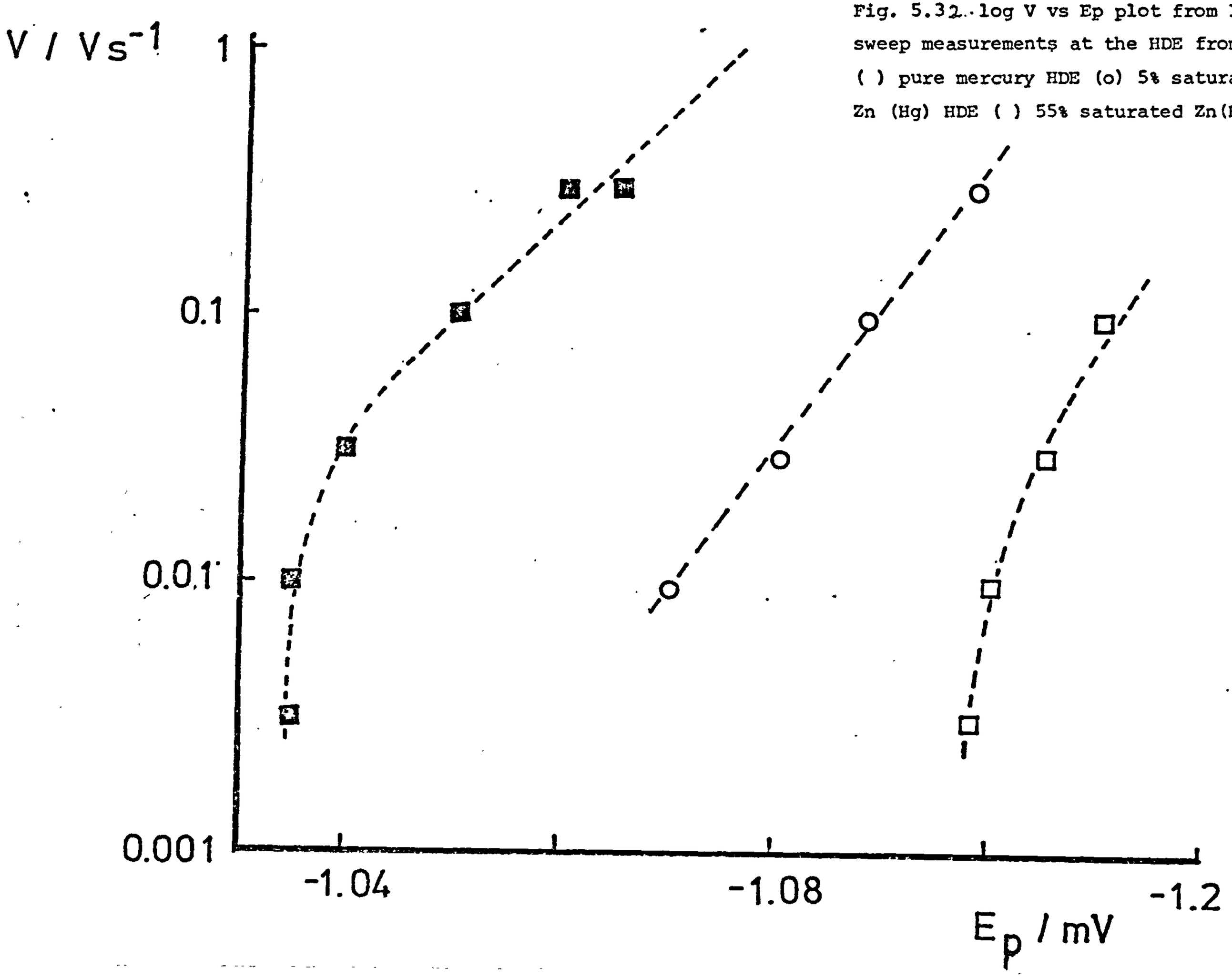

Fig. 5.32. log V vs Ep plot from linear sweep measurements at the HDE from solution 2 ( ) pure mercury HDE (o) 5% saturated Zn (Hg) HDE ( ) 55% saturated Zn(Hg) HDE.

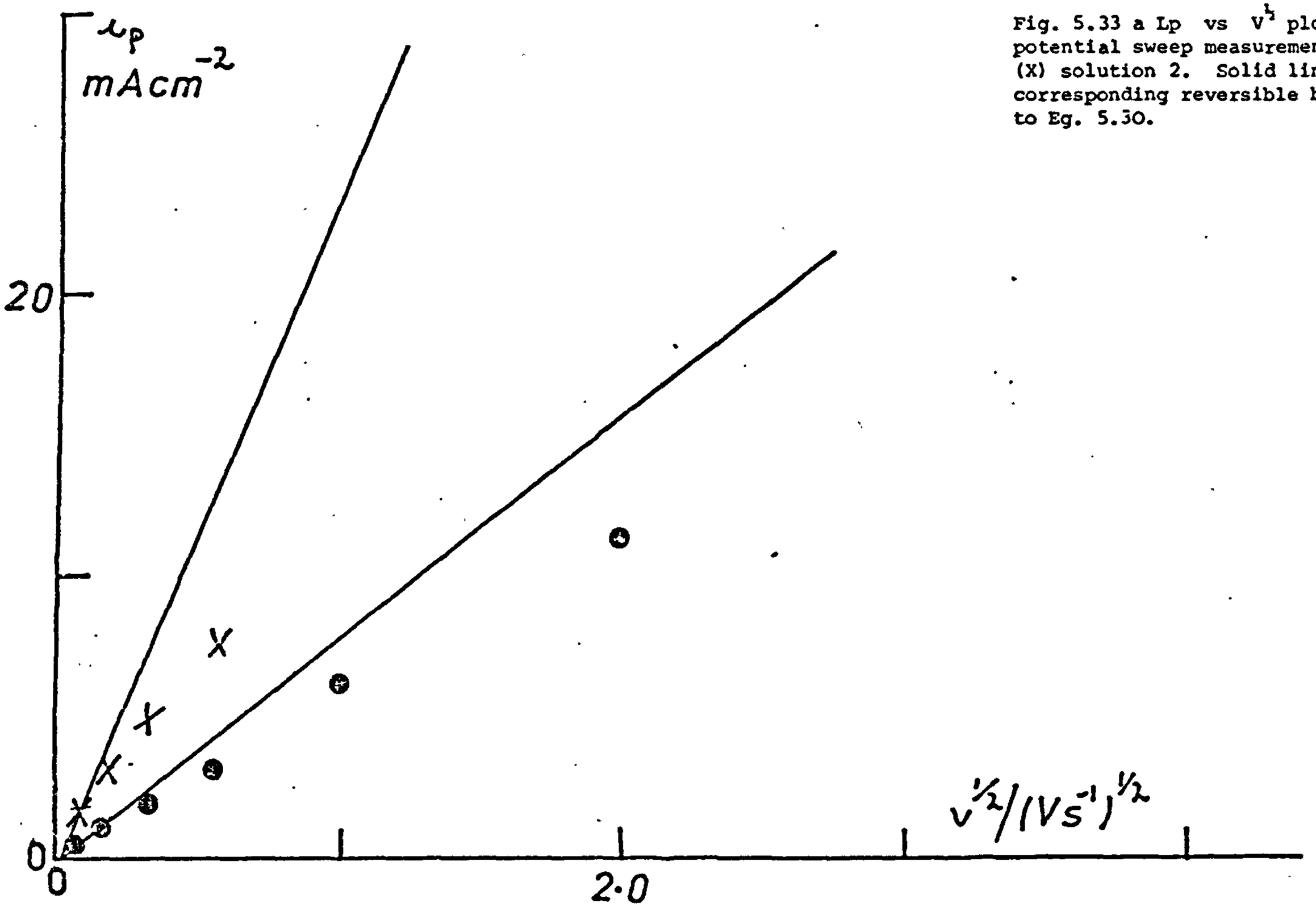

Fig. 5.33 a Lp vs $V^{\frac{1}{2}}$ plot from linear potential sweep measurements for (●) solution 3 (X) solution 2. Solid linear represent corresponding reversible behaviour according, to Eg. 5.30.

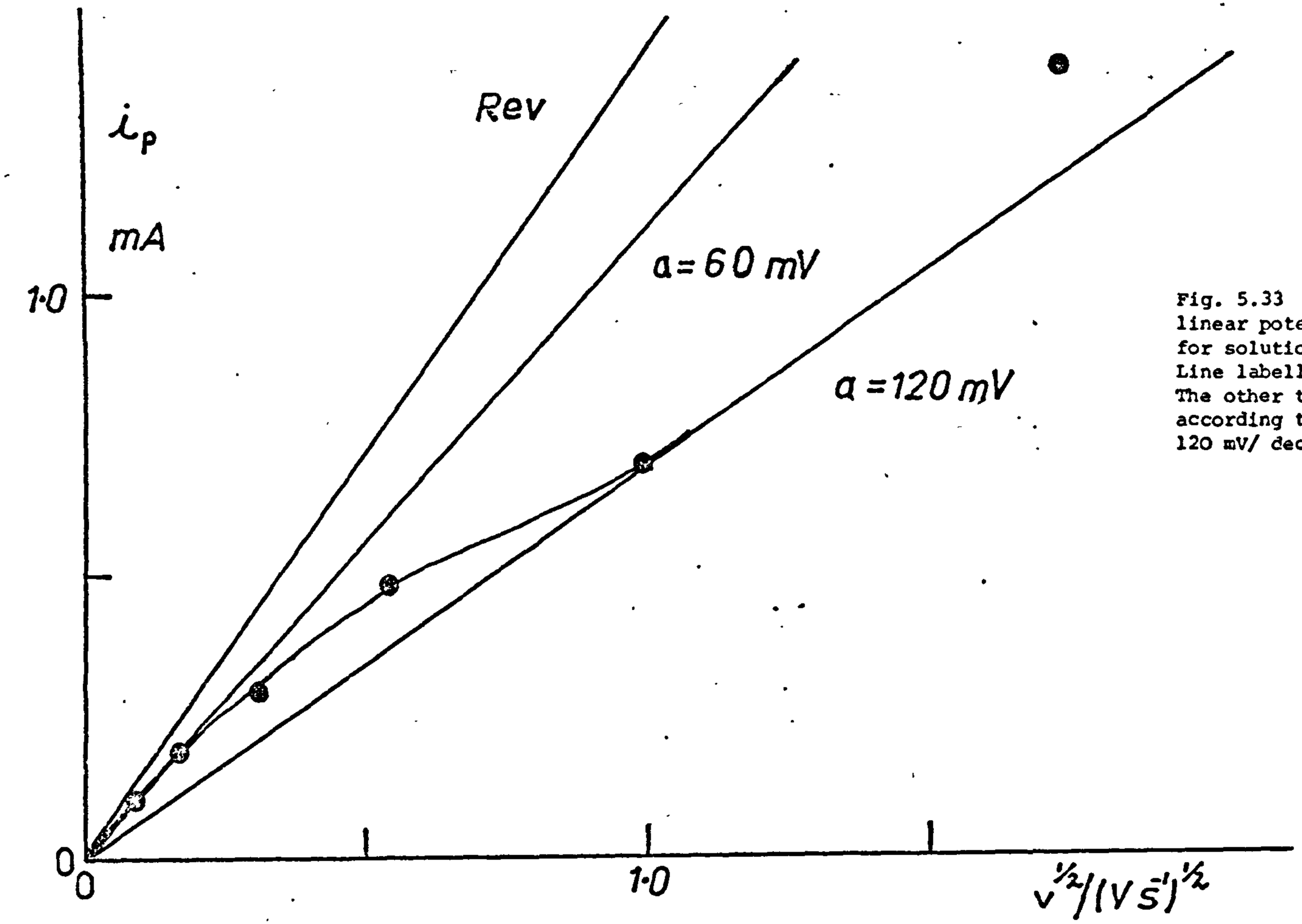

Fig. 5.33 b Lp vs $V^{\frac{1}{2}}$ plot from linear potential sweep measurements for solution 2C (10^{-3} M Zn^{++}, pH = 4.3). Line labelled Rev represents Eg. 5.30. The other two lines are calculated according to Eg. 5.28 with a = 60 and 120 mV/ dec respectively.

Fig. 5.33 i_p vs $V^{\frac{1}{2}}$ plot from linear potential sweep curves at the HMDE, solution 3, recorded with the oscilloscope. Solid line represents reversible behaviour according to Eq. 5.30.

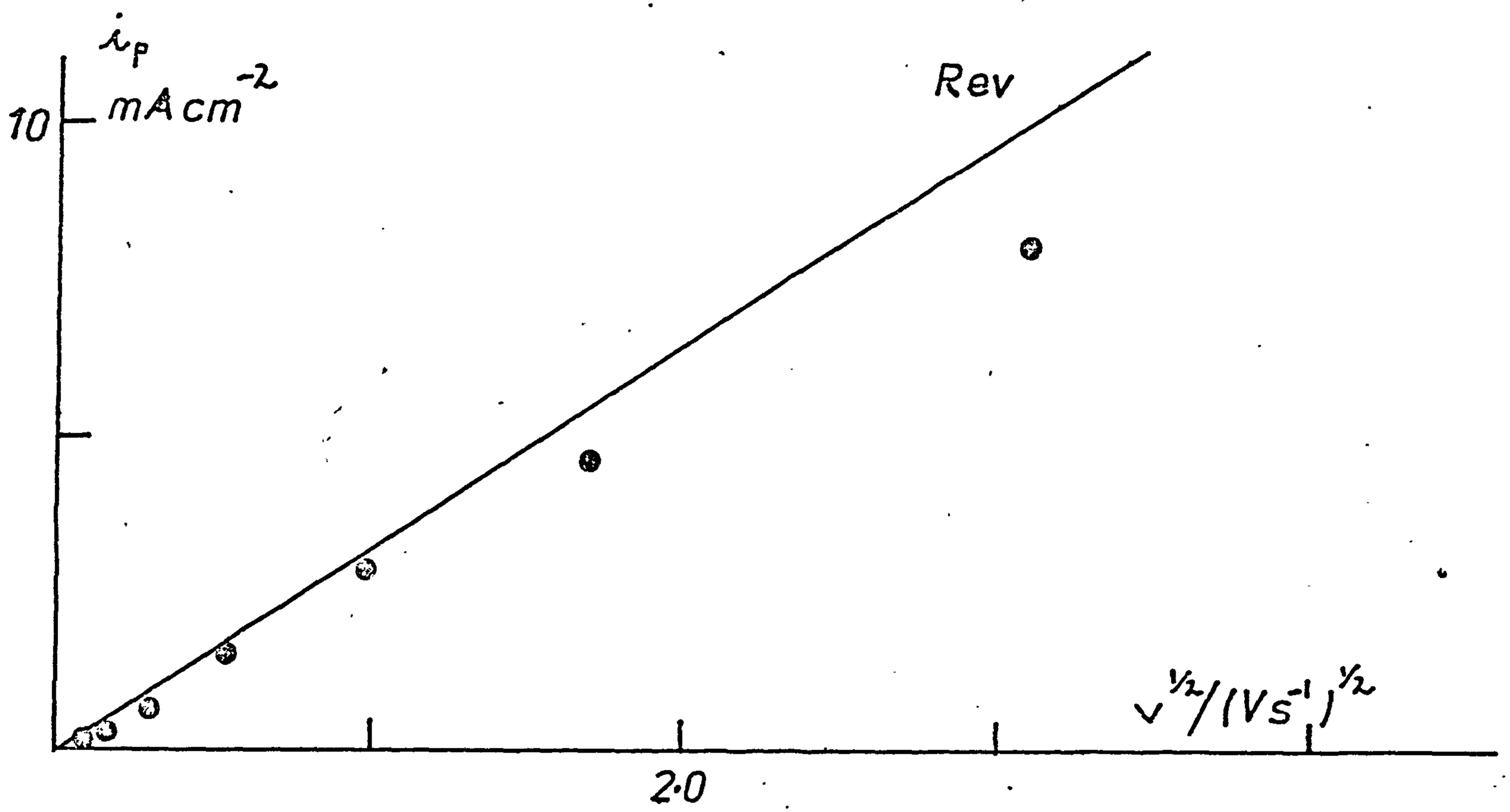

experiment was modelled on the paper of Schwarz and Shain[4] who considered the reaction scheme

$$Zn^{++} + 2e \rightleftharpoons Zn \xrightarrow{K} \text{product}$$

A typical result is shown in Fig. 5.34 a and b. Analysis is effected by taking the cathodic current, i_c, at a time $t - \tau$ where τ is the cathodic pulse length. The corresponding anodic current, i_a, at time t from the start of the cathodic pulse is also measured. Values of $\frac{i_a}{i_c}$ as a function of $(t - \tau)/\tau$ can be fitted to a theoretical curve. i_a/i_c should be independent of τ for a particular value of $(t - \tau)/\tau$. Fig. 5.35 shows that the results are scattered however i_a/i_c for $(t - \tau)/\tau = 0.5$ is 0.41. This corresponds to $K = 0$. This shows that Zn is present in a freely available form, as suggested by previous measurements[5]. This investigation was important as some metals show very strong compound formation with Hg.

V.2. Measurements at solid Zn

V.2.1. A.c. Impedance

TFA measurements and automatic F.R.A. measurements were made on this system. Large time effects were observed so the most consistent measurements were obtained with the automatic bridge. Fig. 5.36 shows a typical result. The complex impedance diagram consists of an almost perfect semicircle coupled to a Warburg impedance denoting diffusion. At one potential -1240 mV S.C.E. surface area changes may be reflected in the measured impedance. With manual TFA measurements some results are similar to the A.F.R.A. measurements however some measurements are different depending on the history of the measurement. Fig. 5.37 shows a θ - E curve, in 10^{-2}M Zn^{2+} solution, taken from A.F.R.A. measurements. Up to 1130 mV the curve has the shape expected theoretically, given by

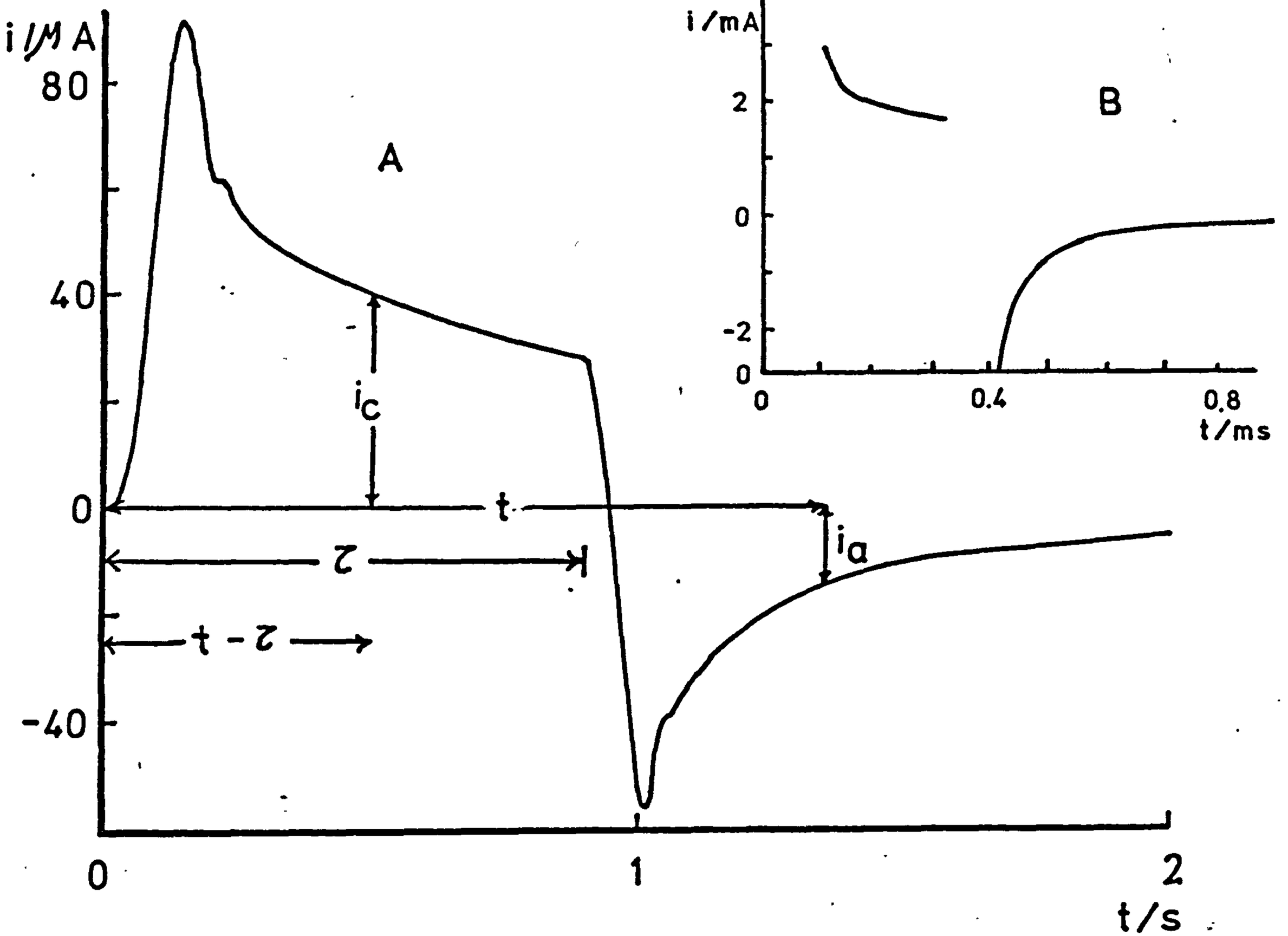

Fig. 5.34 Potentiostatic double pulses at the HMDE from solution 3. Obtained with A) X Y recorder; B) oscilloscope. (E = -0.1 to -1,3 V vs SCE)

Fig. 5.35 $\log\tau$ vs i_a/i_{lc} plot from double pulses at the HMDE, as in Fig. 5.34. (●) Results measured at $(t-\tau)/\tau = 0.5$. Broken line represents expected theoretical values for K = 0 (based on Ref.4)

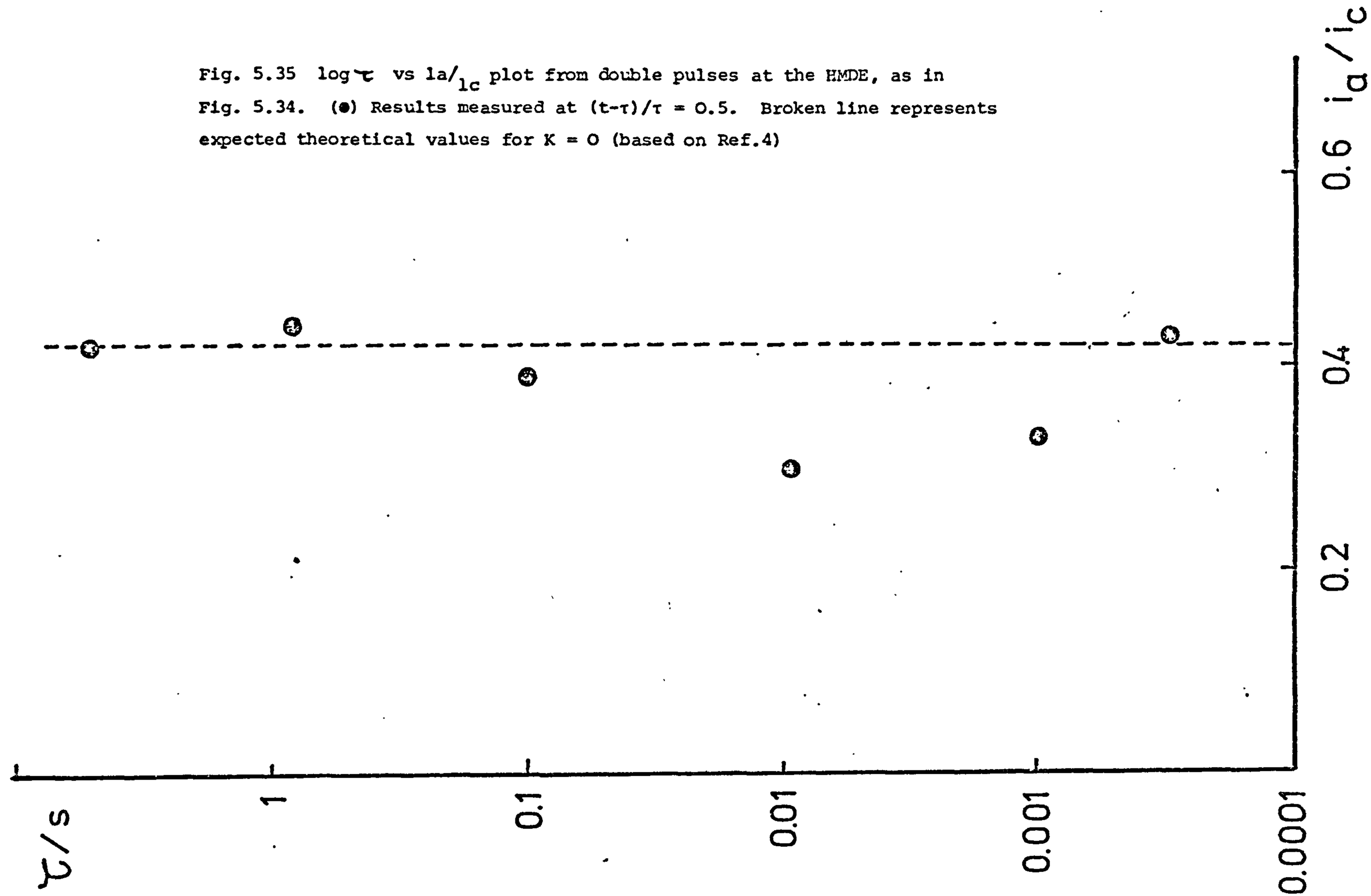

Fig. 5.36 Complex impedance plane plate for solution 2 reduction on a Zn RDE (0.02 cm^2). Rotating speed = 15 Hz. Measured with the AFRA at E = a) - 1.26 V vs S.C.E. Figure on graph indicate the frequency in Hz.

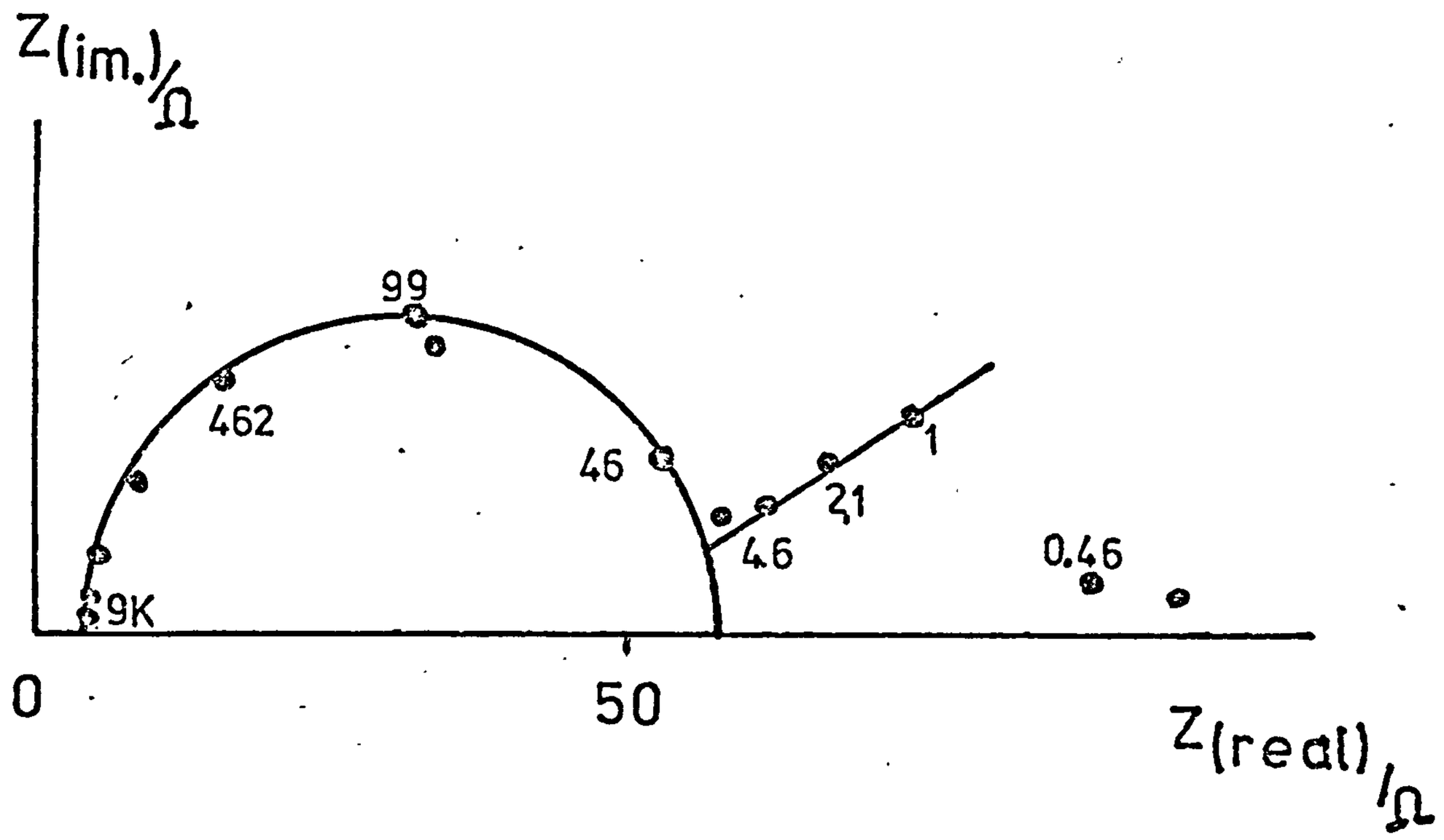

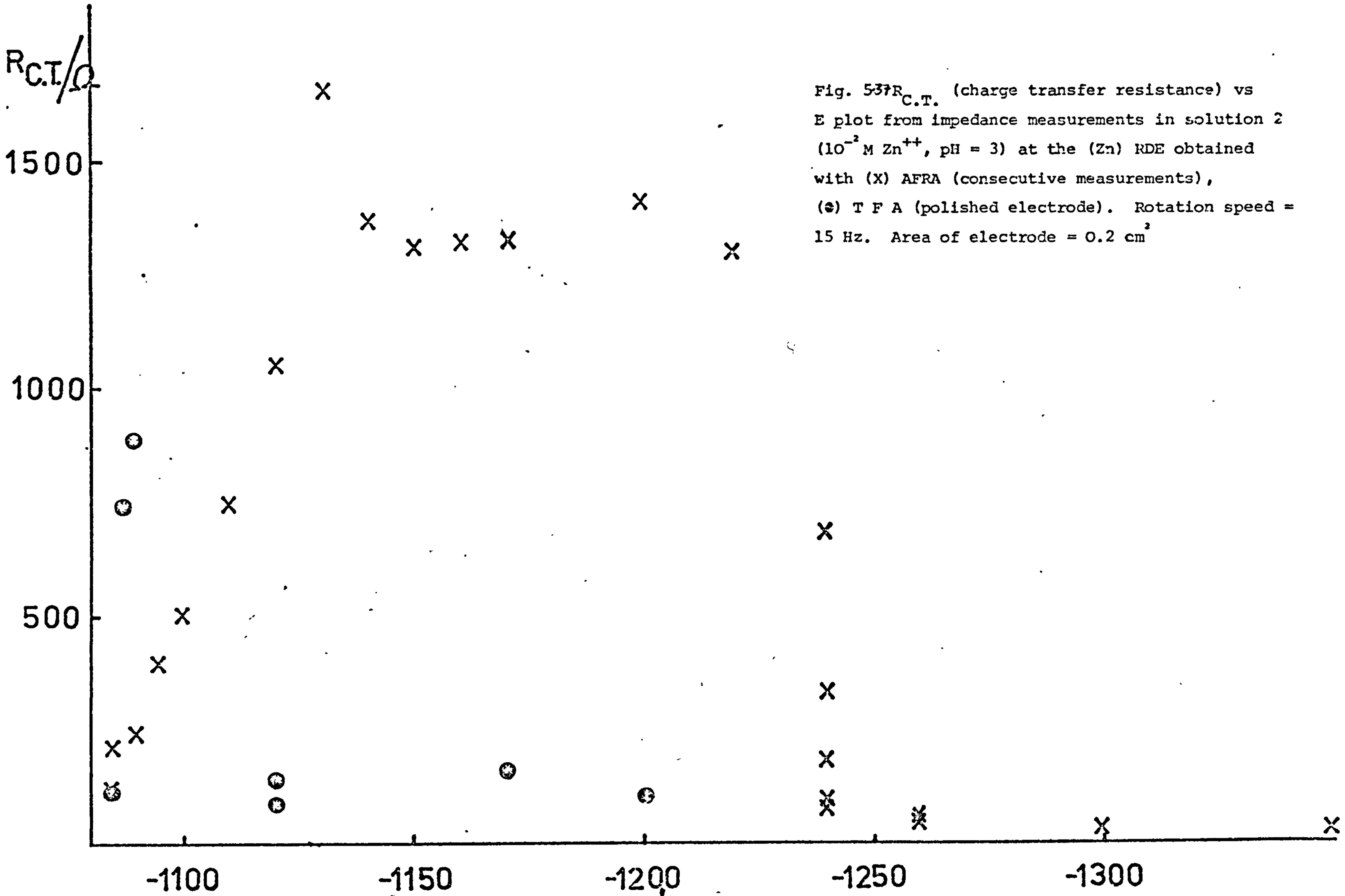

Fig. 537 $R_{C.T.}$ (charge transfer resistance) vs E plot from impedance measurements in solution 2 (10^{-2} M Zn^{++}, pH = 3) at the (Zn) RDE obtained with (X) AFRA (consecutive measurements), (⊛) T F A (polished electrode). Rotation speed = 15 Hz. Area of electrode = 0.2 cm^2

$$\theta_{rev} = \frac{RT}{n^2 F^2 k_{SH}} \exp \beta_1 \phi \qquad (5.32)$$

The reversible d.c. wave is used as the rotation speed of the electrode was low, 15 Hz, see the next section for the discussion of i - E behaviour. Fig. 5.37 suggests that $b \sim 40$ mV. On this basis using Equation 5.32 then $k_{SH} = 2.4 \times 10^{-7}$ cm s^{-1}. Similar results are obtained in 3×10^{-3} Zn^{2+} solution taken by manual TFA measurements. Up to about-1160 mV the curve has the features given by Equation 5.32. k_{SH} has a value of 2×10^{-8} cm s^{-1} according to Equation 5.32. It is striking that Fig. 5.38 is displaced from Fig. 5.37. It is predicted by Equation 5.32 that the curve should be independent of concentration. Clearly the electrode can have differences in reactivity.

In both Figs. 5.37 and 5.38 after about -1140 mV the curve remains steady this is probably due to the same phenomen as observed in Fig. 5.11 for the reduction of Zn^{2+} on pure Hg. A similar calculation according to

$$a = 2.303\, i_L \theta \qquad (5.33)$$

gives a = 160 mV (the H_2 evolution limiting current has been ignored as this is $\sim$ 10% of i_L). In the region of -1200 mV the sudden drop in θ must be attributed to dendrite formation. This method is a sensitive detection of where exactly large surface area changes occur. This may have some practical ramifications in for example the investigation of battery and plating systems. Within the experimental error pH change 2 to 3 does not seem to have a significant effect. It was also observed that the electrode sometimes could be very active or inactive. This is illustrated in Fig. 5.37 and also in 5.39 where some TFA results are shown. The exact reason for this needs to be investigated in more detail.

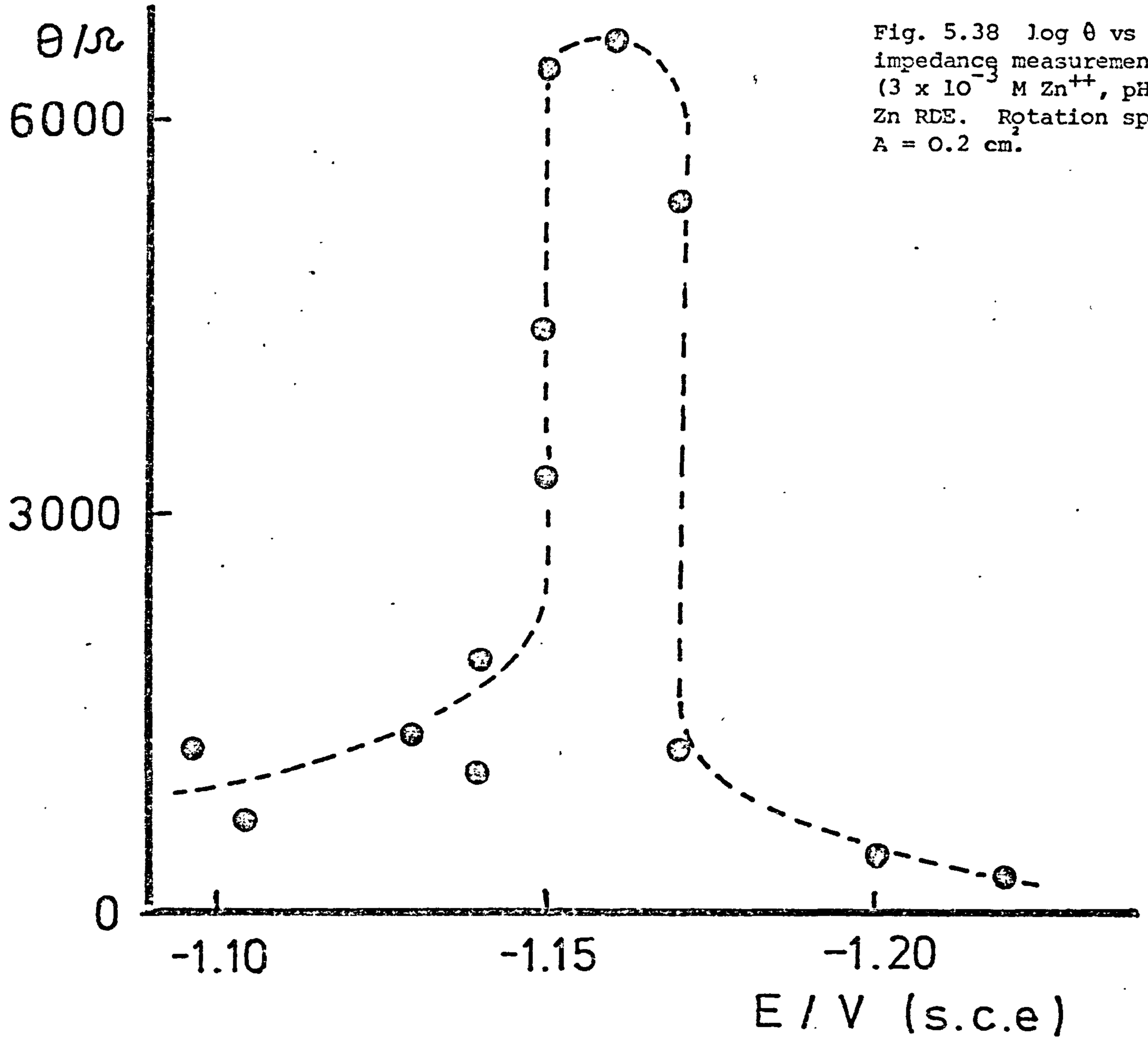

Fig. 5.38 log θ vs E plot from TFA impedance measurements in solution 3 (3×10^{-3} M Zn^{++}, pH = 3) at polished Zn RDE. Rotation speed = 15 Hz, A = 0.2 cm^2.

Fig. 5.39. Complex impedance plots for a 10^{-2}M + 1M KCl solution (pH = 3) on a Zn rotating disc (0.2 cm^2) rotation speed = 15 Hz. Active and inactive O electrodes at a) E_e = -1085 and b) E = -1170 mV vs S.C.E.

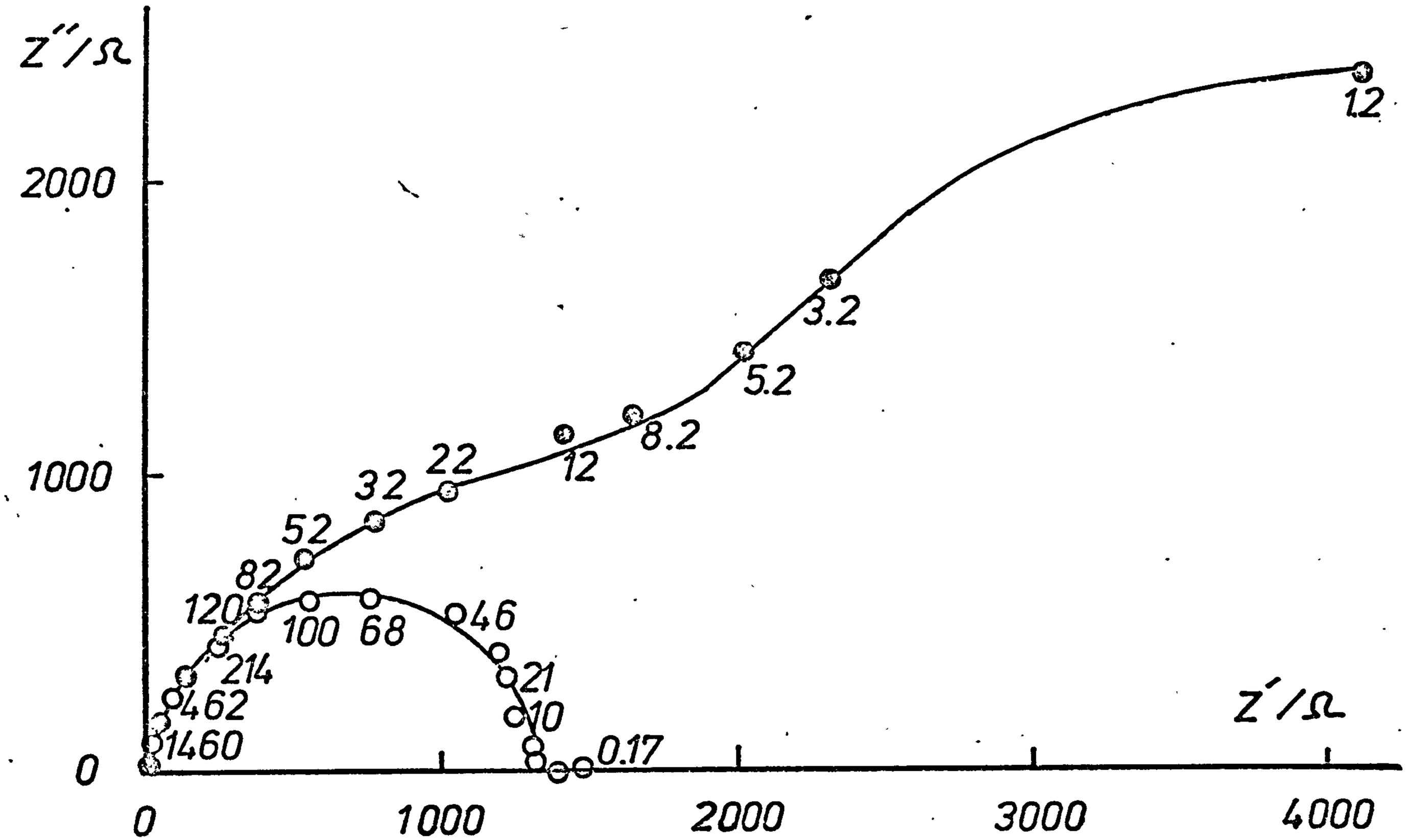
Z''/Ω
2000
1000
0
0
1000
2000
3000
4000
Z'/Ω
1460
462
214
120
82
52
32
22
12
8.2
5.2
3.2
1.2
100
68
46
21
10
0.17

Fig. 5.39. Complex impedance plots for a 10^{-2}M + 1M KCl solution (pH = 3) on a Zn rotating disc (0.2 cm^2) rotation speed = 15 Hz. Active and inactive O electrodes at a) E_e = -1085 and b) E = -1170 mV vs S.C.E.

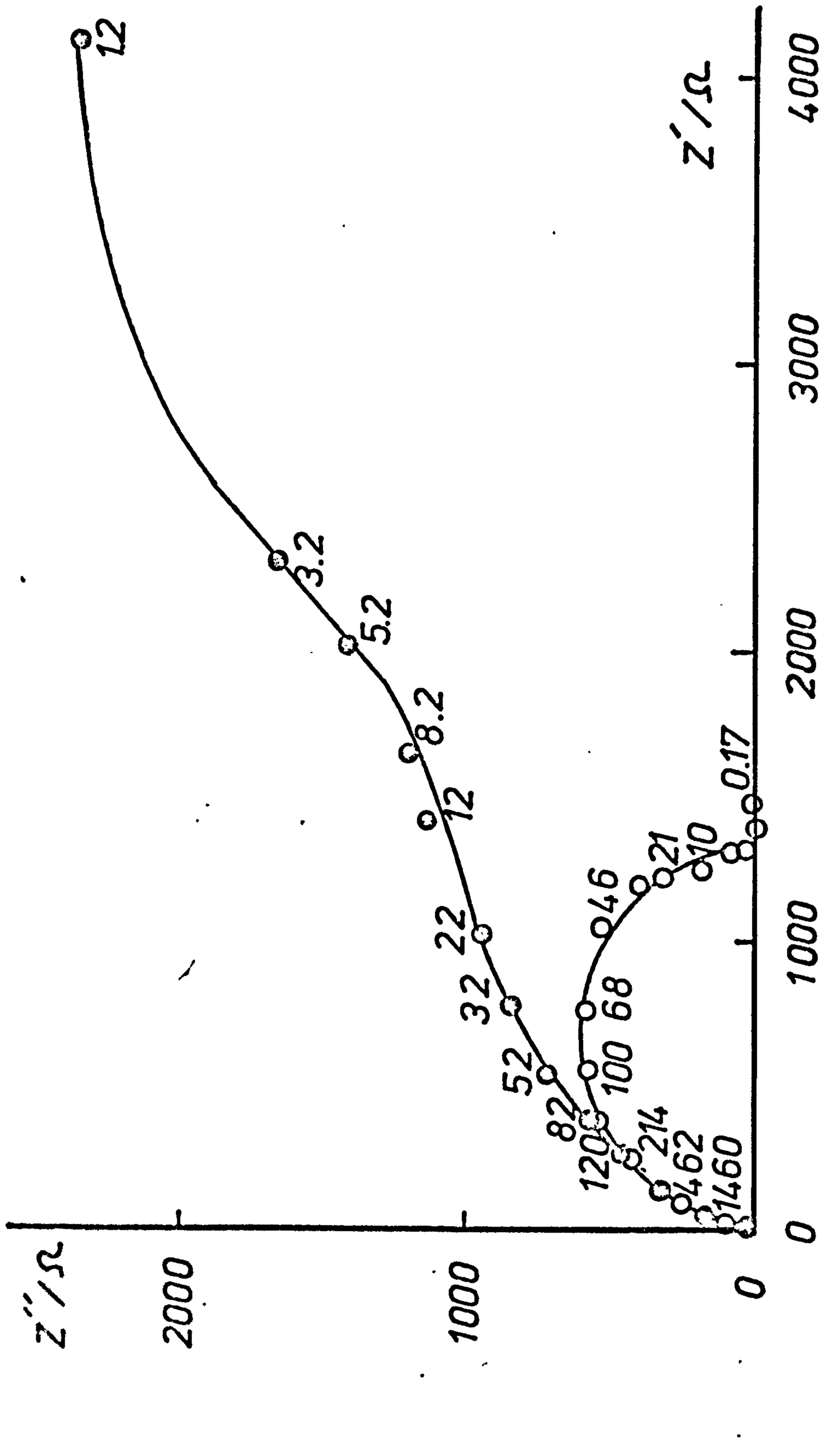

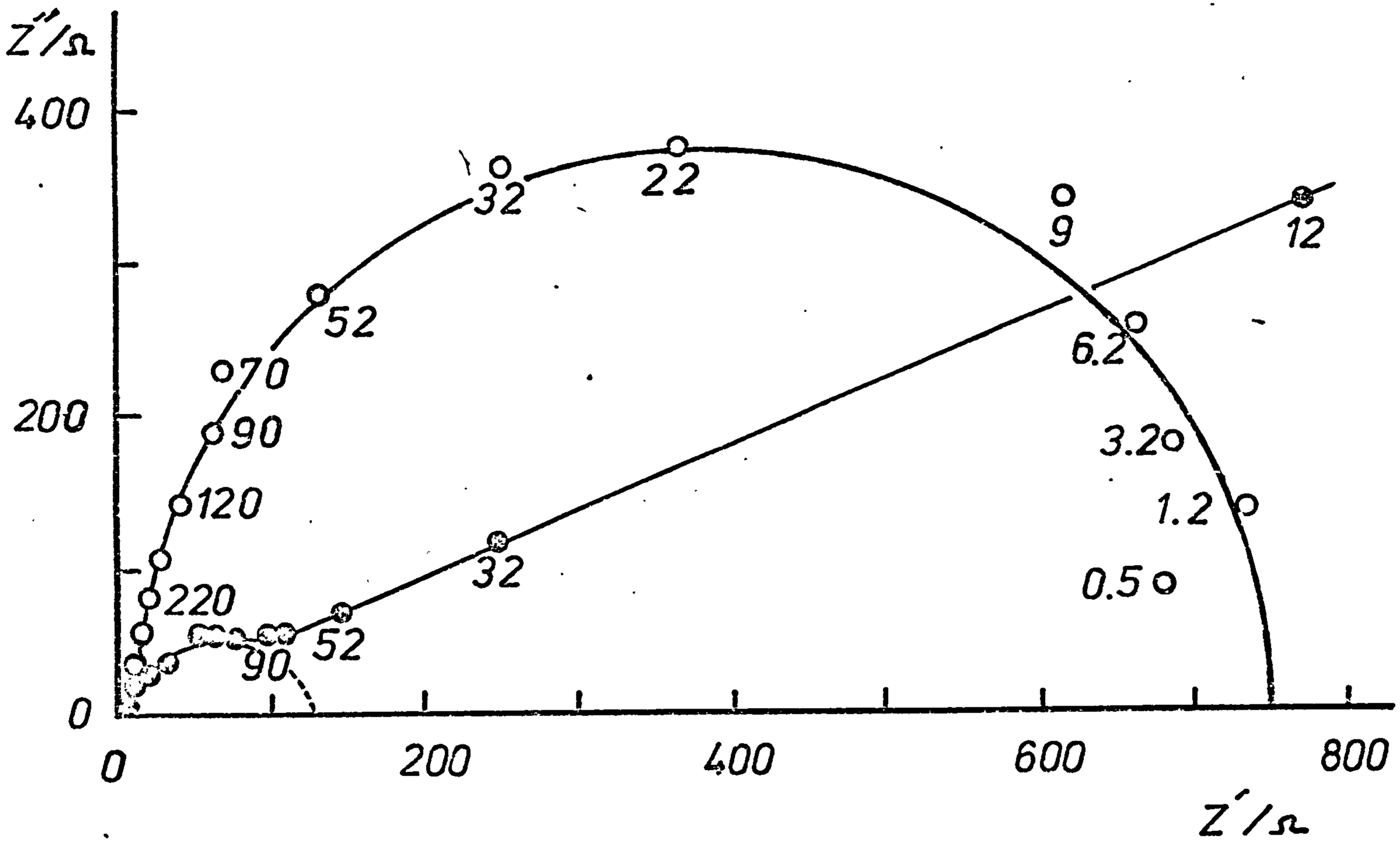
Z''/Ω
400
200
0
0
200
400
600
800
Z'/Ω
70
52
32
22
9
12
6.2
3.2
1.2
0.5
90
120
220
32
52
90

A very inactive electrode could be associated with pH changes as the solution is unbuffered. There is some evidence for this in the section where i - t curves are discussed. The double layer capacities calculated from the top of the semicircle from the measurements used to draw Fig. 5.37 are shown in Fig. 5.40. The figures suggest that the metal is uniformly active until -1240 mV when the area, as measured by C_{dl}, increases rapidly with potential. The T.F.A. results are more scattered but follow the same trend. -1240 mV is not a significant potential as it varies with the particular history of the electrode, for example in a T.F.A. run the potential was -1170 see Fig. 5.40 (at a lower concentration of Zn^{2+}).

V.2.2. Linear potential sweep measurements

Fig. 5.41 gives a review of a number of linear potential sweep results. The graph shows the relation of the measurements on solid Zn to those on Hg.

The curve for solid Zn is some 100 mV negative to pure Hg and is slightly positive to a saturated amalgam, showing that the Zn surface is fairly uniformly active. Due to the low rotation speed at the rotating Zn disc the i-E curve is nearly reversible. However the upper part of the curve leading into the diffusion current has a much slower dependence of i on E. This is probably a particular feature of metal deposition reactions and is probably due to the electrode behaving more like a porous electrode. A further point about the diagram is that the H_2 evolution reaction does not seem to be very significant on Hg or on Zn. More detail of the behaviour of solid Zn is shown in Fig. 5.42. The curves were recorded from left to right. The first curve is fairly inactive and becomes active in subsequent sweeps. Although the measure-

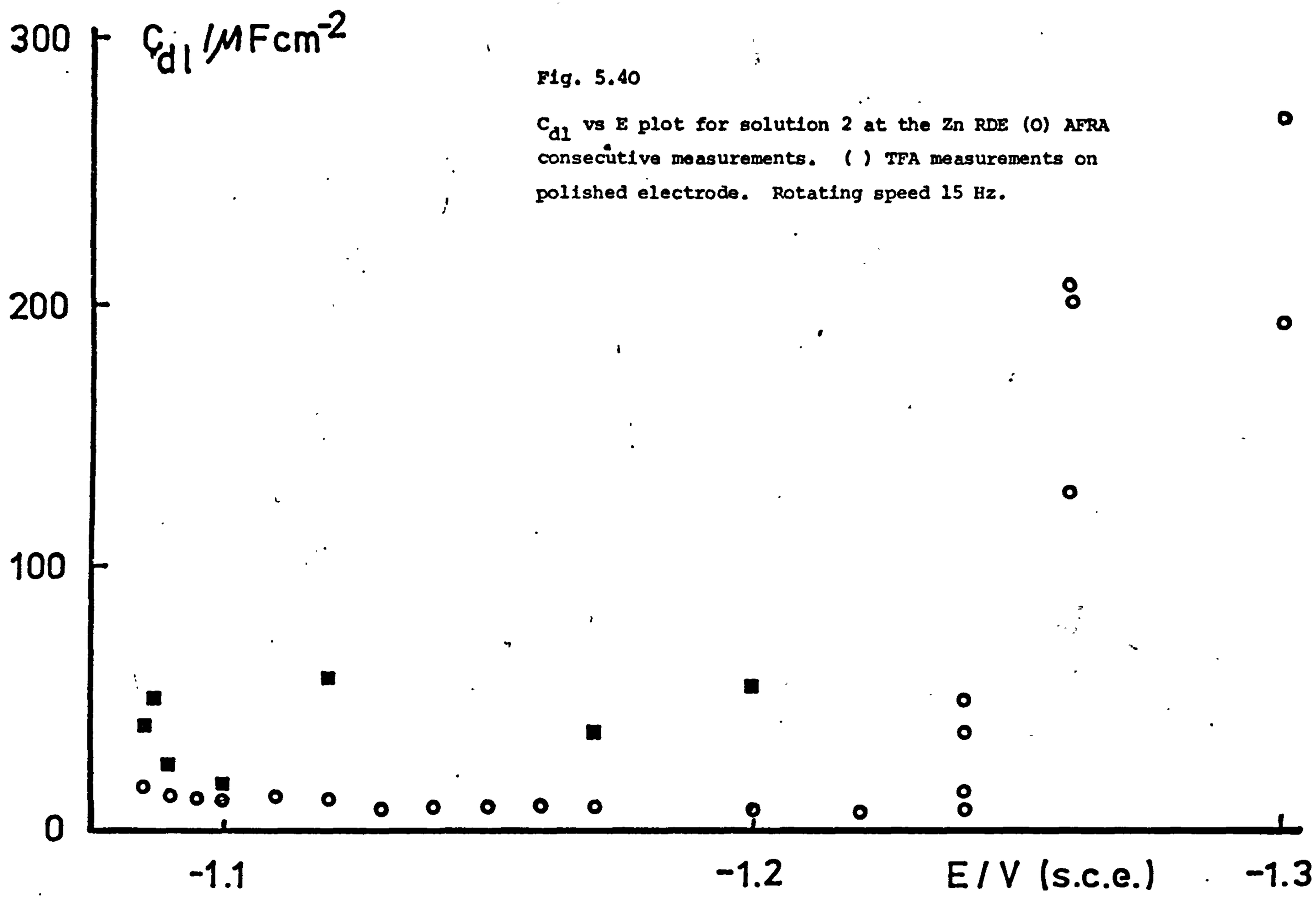

Fig. 5.40

C_{dl} vs E plot for solution 2 at the Zn RDE (O) AFRA consecutive measurements. ( ) TFA measurements on polished electrode. Rotating speed 15 Hz.

Fig. 5.41 $\log i$ vs E, plot from linear potential sweep measurements at $V \sim 0.1\ V\ s^{-1}$. a) HMDE, solutions 2, b) Zn RDE, solution 2, rotation speed = 11.25 Hz c) Zn(Hg) oversaturated amalgam HDE, solution 2. d) Zn RDE, solution 4 (base electrolyte 1 M KCl, pH = 3) rotating speed 11.25 Hz e) Zn RDE, solution 3, rotation speed 11.25 Hz.

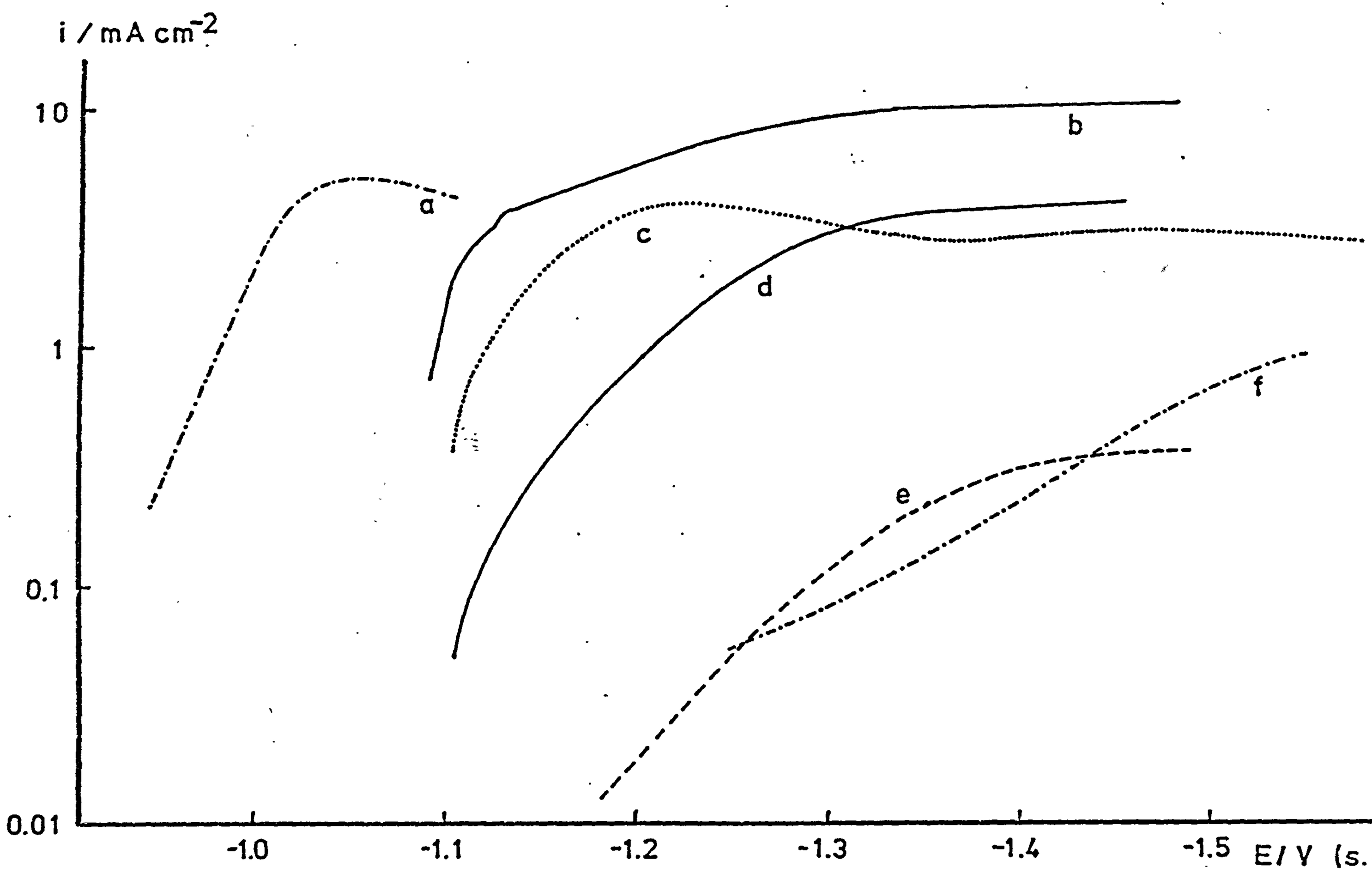

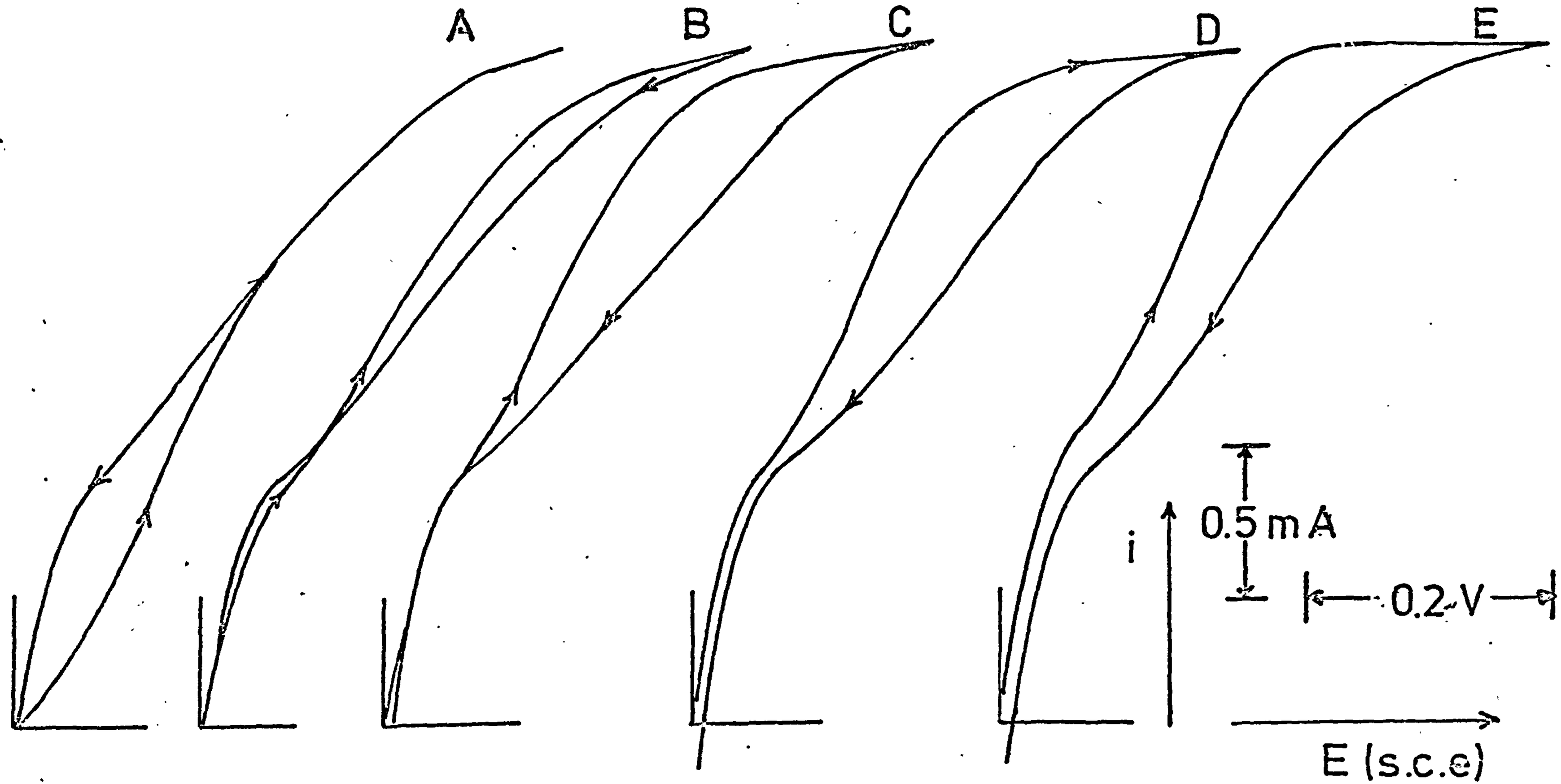

Fig. 5.42 Linear potential sweep for solution 2 reduction at the Zn RDE from E = -1.087V vs SCE. Rotating speed 15 Hz, A = 0.2 cm^2. Sweep rates a) $\frac{1}{320}$, b) 0.1, c) $\frac{1}{32}$, d) 0.1 V e) $\frac{1}{3.2}$ $V\ S^{-1}$. Order of measurements from L to R, starting with a polished electrode.

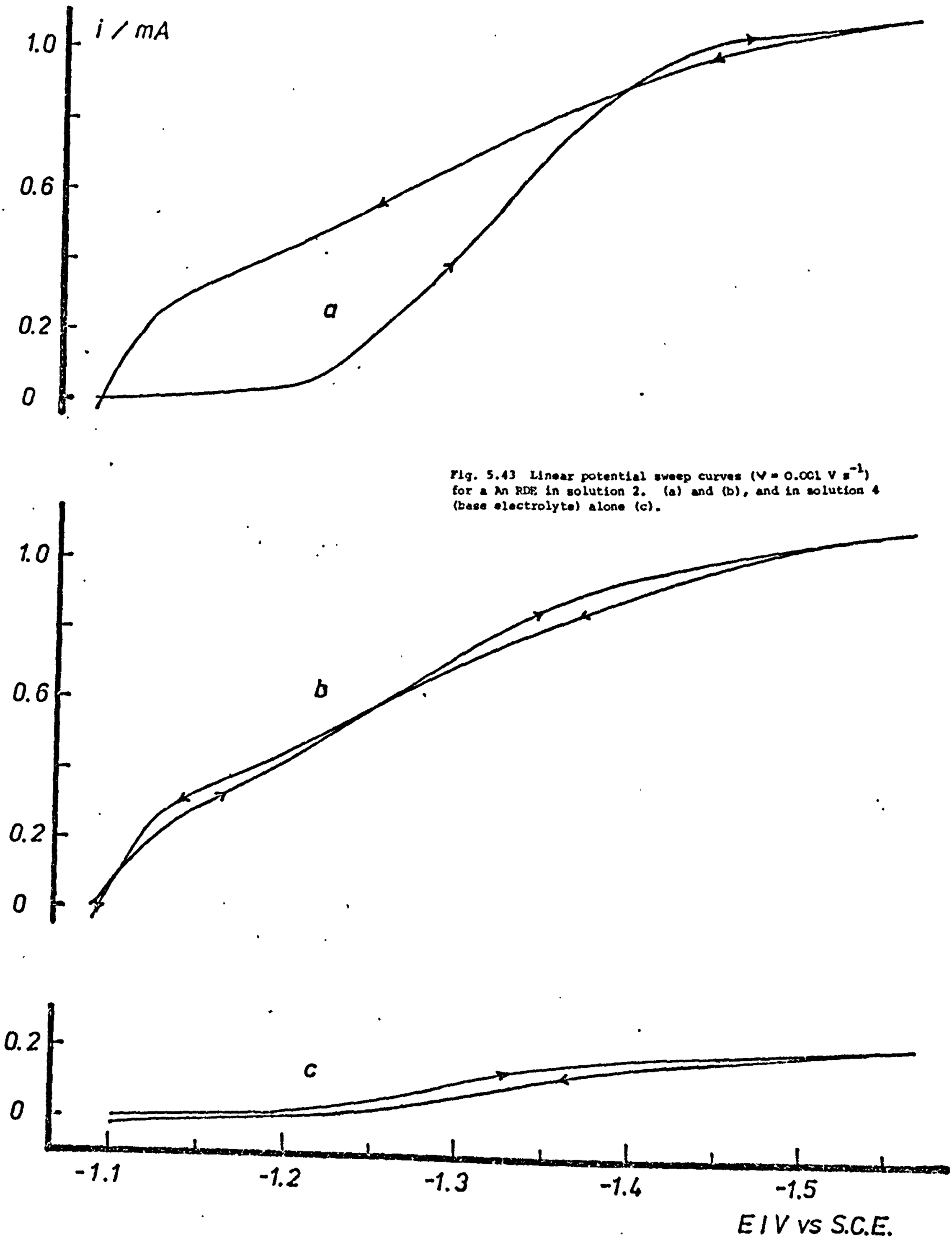

Fig. 5.43 Linear potential sweep curves ($\nu = 0.001$ V s^{-1}) for a An RDE in solution 2. (a) and (b), and in solution 4 (base electrolyte) alone (c).

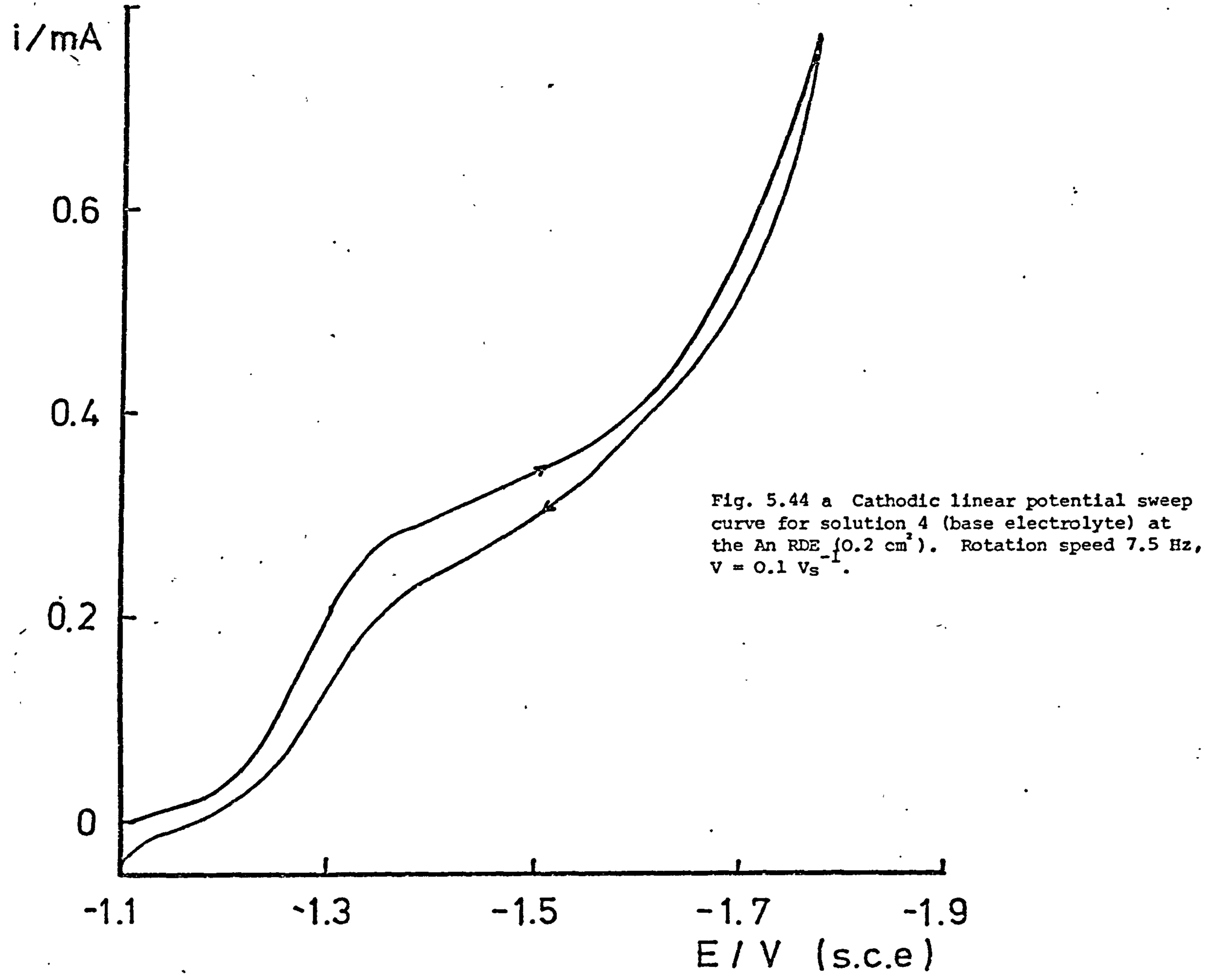

Fig. 5.44 a Cathodic linear potential sweep curve for solution 4 (base electrolyte) at the An RDE (0.2 cm^2). Rotation speed 7.5 Hz, V = 0.1 V_s^{-1}.

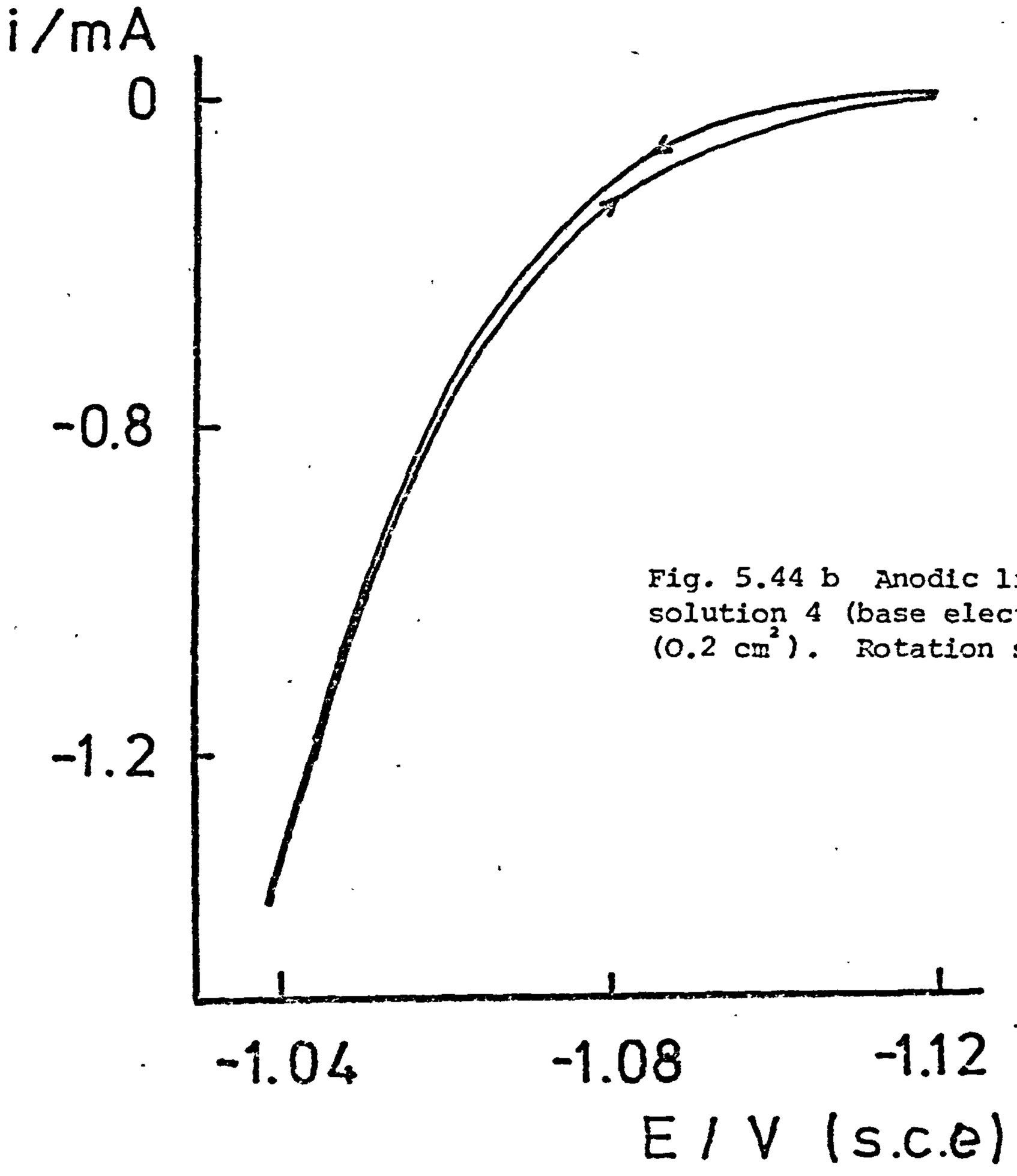

Fig. 5.44 b Anodic linear potential sweep for solution 4 (base electrolyte) at the Zn RDE ($0.2\ cm^2$). Rotation speed = 7.5 Hz, V = 0.01 V s^{-1}

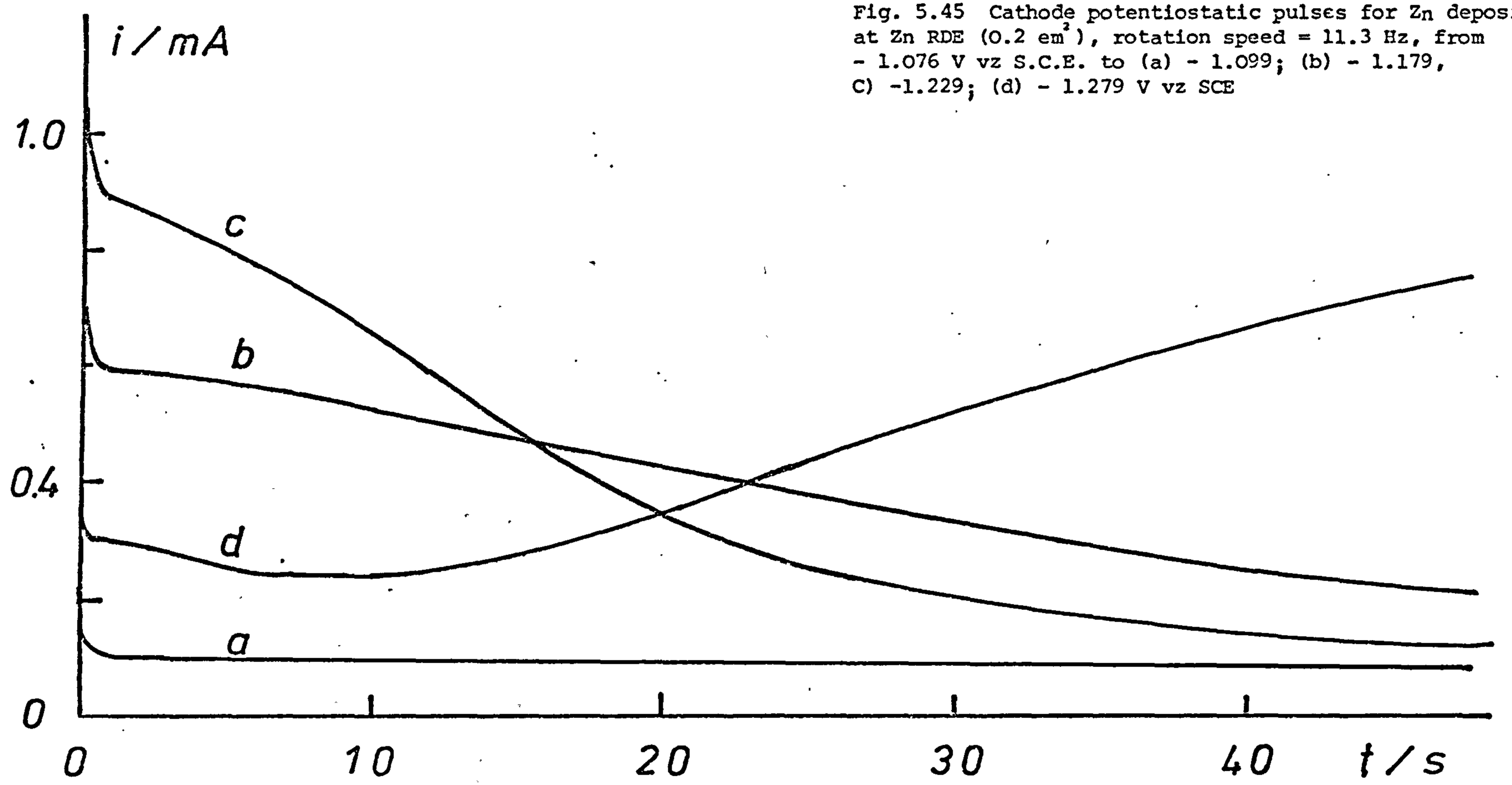

Fig. 5.45 Cathode potentiostatic pulses for Zn deposition at Zn RDE (0.2 em^2), rotation speed = 11.3 Hz, from - 1.076 V vz S.C.E. to (a) - 1.099; (b) - 1.179, C) -1.229; (d) - 1.279 V vz SCE

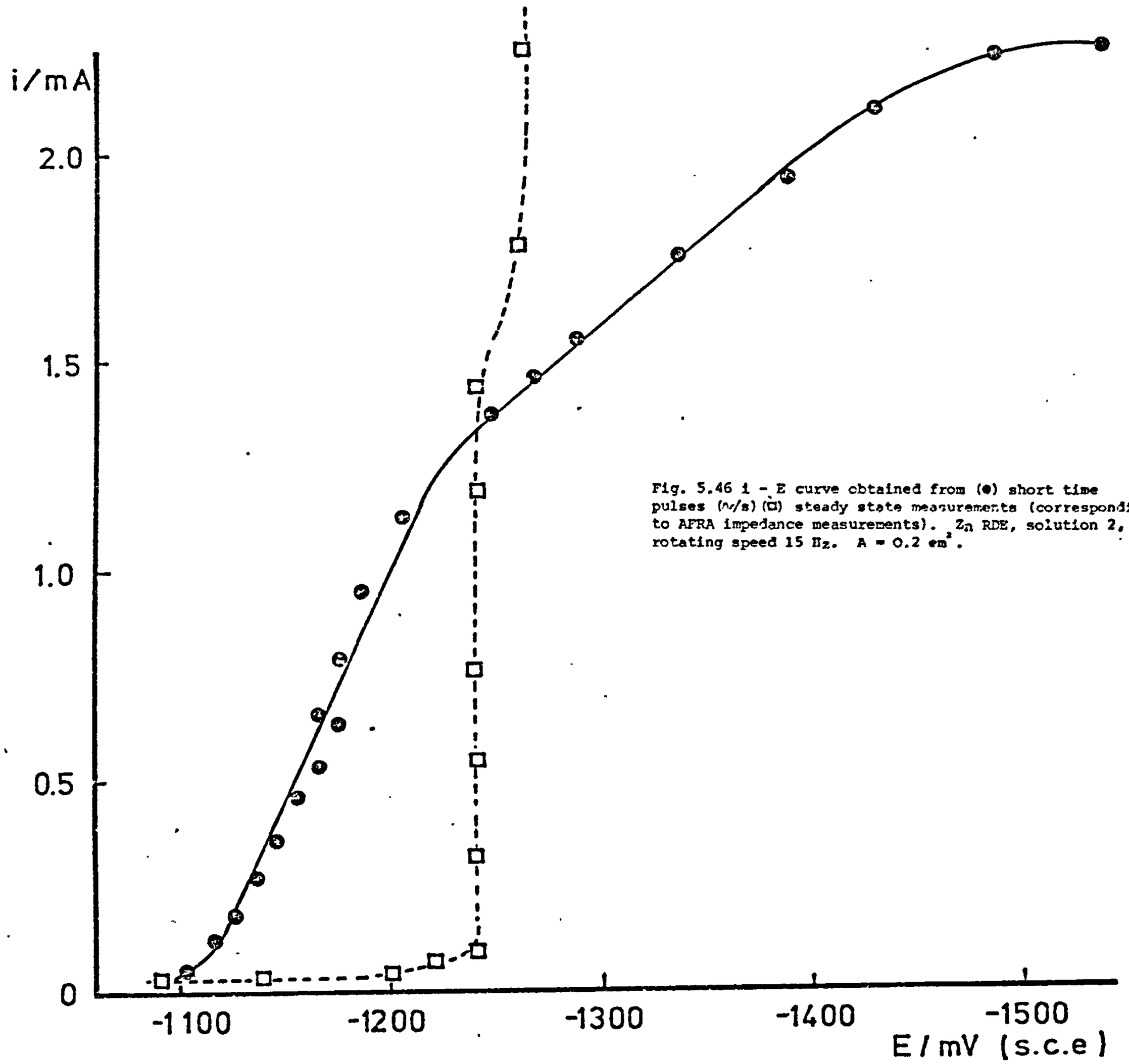

Fig. 5.46 i - E curve obtained from (●) short time pulses (∿/s) (□) steady state measurements (corresponding to AFRA impedance measurements). Zn RDE, solution 2, rotating speed 15 Hz. A = 0.2 cm^2.

ments were made at different sweep rates this has no effect and the curves are in the steady state as far as diffusion is concerned. The wave appears to split into two waves. The splitting seems to be independent of pH. Thus the effect is probably associated with the structure formed on the electrode and not with any intermediate such as Zn^{+} or probably the H^{+} reaction. It seems that at the foot of the wave the Zn^{2+} reduction is probably pseudo reversible (see a.c. section) as the slope of the curve about E_e is $\sim$ 35 Ω compared to $R_{sol} \sim 10\ \Omega$. A similar effect is observed at very slow sweeps Fig. 5.43. Fig. 5.44 shows a result of a test in the base electrolyte alone to make certain that the reduction of H^{+} did not interfere. It is clear that it is unlikely to be responsible for the wave splitting. In the same Fig. 5.44b an anodic steady state curve is shown. It is without hysteresis and when plotted log i-E has a 40 mV slope.

V.2.3. Potentiostatic pulse measurements

In view of the complicated behaviour of the i-E curves, pulse measurements were made. The hope was that it would be possible to control the initial state of the surface by the value of the starting potential. Fig. 5.45 shows a result obtained by pulsing from E = -1076 mV, which is just anodic to E_e, to the quoted potential. At shorter times, i.e. 1 pulses, the current did not have a time dependence and it was possible to build up an i-E curve by pulsing to successive potentials. An example is shown in Fig. 5.46. It is interesting to note that the curve no longer is split into two wave, although the lower portion is steep and the upper portion is much less steep. The Tafel slope of the lower portion is $\sim$120 mV and the upper portion about 200 mV. This is typical porous electrode behaviour[6] where it is expected that the Tafel slope is twice that for a planar electrode. Fig. 5.45 at longer times shows even under the steady diffusion a complex behaviour. These effects could be

caused by pH change at the electrode and formation of $Zn(OH)_2$, or inhibition by H , in addition to area changes caused by nucleation and growth. Ultimately the i-E curve (7 mins at each potential) can have the form shown in Fig. 5.46. These i-E measurements were taken simultaneously with the impedance measurements in Fig. 5.37.

V.3. Discussion

The LT measurements on pure Hg Fig. 5.11 are close to those reported in the literature[7]. The value of k_{SH} found from Fig. 5.11 is 4.9×10^{-3} cm s^{-1} and a, the cathodic Tafel slope, is 136 mV. On amalgam electrodes the TFA measurements show that in concentrated amalgams $k_{SH} = 4.6 \times 10^{-5}$ cm s^{-1} and a is possibly 100-200 mV. These new results prove that the Zn^{2+} reduction becomes slower as the amalgam approaches the Zn metal condition.

It is of interest to compare these results with those in the literature. Timmer[8] et al find the anodic Tafel slope is 40 mV. Sluyters-Rehbach[7] et al find the cathodic Tafel slope is 136 mV. Salie[9] finds that in concentrated Zn(Hg), 1M, the anodic Tafel slope is 36.8 mV going down to 100 mV in dilute amalgam. Hush et al[10] finds that the cathodic Tafel slope varies from 60 mV to 100 mV as the ionic strength is increased.

However the margin of error is fairly large in Fig. 5.11 and the Tafel slope is not definitely established from these measurements especially in view of the sweep measurements where it was deduced that the cathodic Tafel was 60-100 mV.

On solid Zn the results are less clear. As shown previously there is a large discrepancy between the TFA and AFRA results. Fig. 5.47 attempts to reduce the discrepancy by using the double layer capacity C_{dl} as a measure of the true area. Incidentally it was clear from some of the TFA results that at the long times needed to make a measurement some

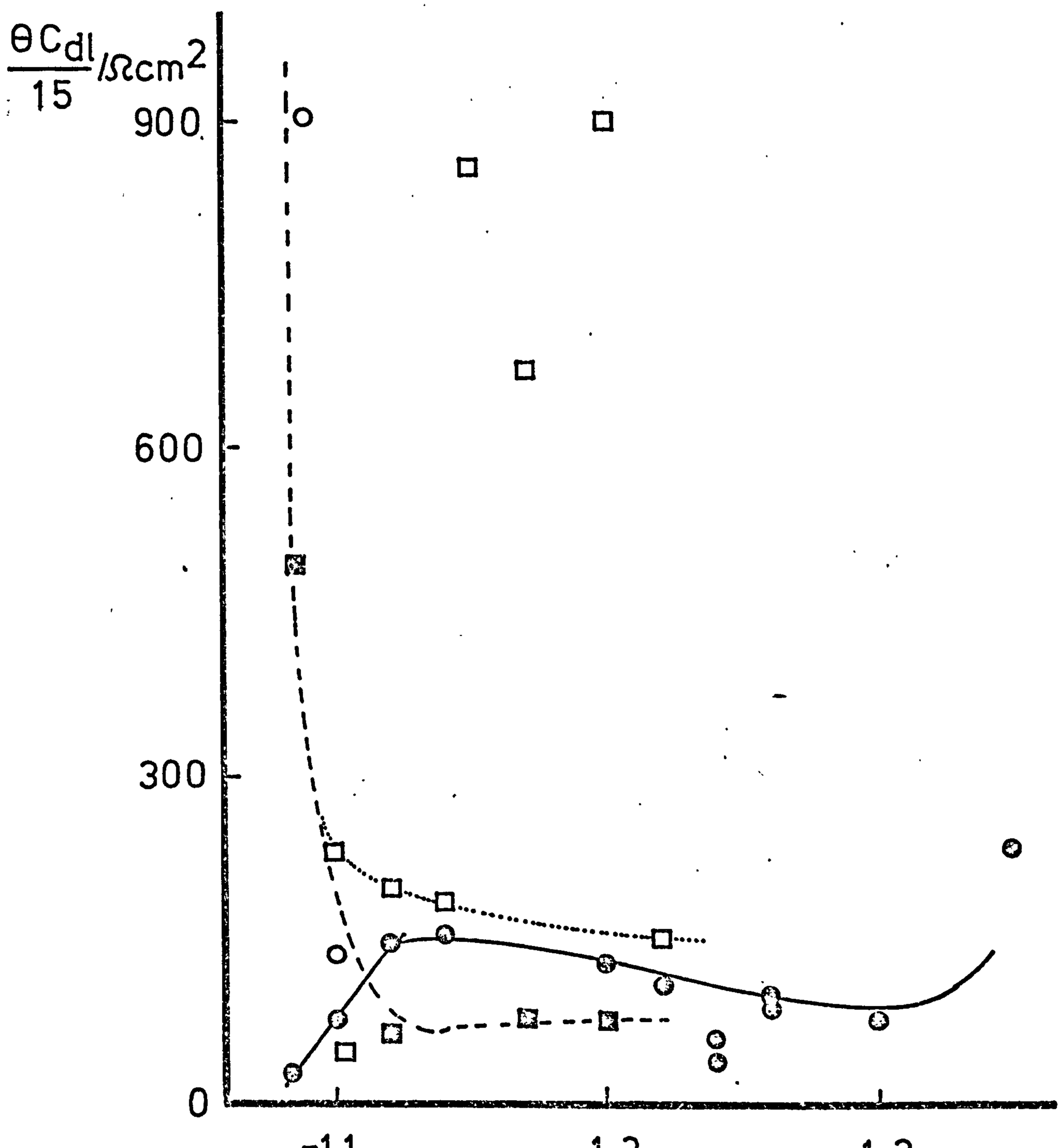

Fig. 5.47. $\theta C_{dL}/15$ vs E plot to account for electrode real area. C_{dL} obtained from frequency at the top of the complex plane impedance semicircle from ( ) AFRA, solution 2; (TFA solution 2); ( ) TFA solution 3.

of the results were flattened semicircles reminiscent of a porous structure. Only good semicircles are plotted in Fig. 5.46. It is obvious that large changes in structure on the electrode can occur. The AFRA results look as previously like a pseudo reversible reaction and the TFA results represent a falling curve under some conditions like an irreversible reaction $k_{SH} \sim 2.4 \times 10^{-7}$ cm s^{-1} or even 10^{-8} cm s^{-1} for the more irreversible curve. All these ideas agree well with previous investigations[11,12] into the Cu^{2+} reduction, which is also a 2e reduction. The mechanism in that case, in SO_4^{2-} solution, is

$$Cu^{2+} + e \longrightarrow Cu^{+}$$
$$Cu^{+} + e \rightleftharpoons Cu$$

on solid Cu giving the well known 40 mV anodic and 120 mV cathodic slope. On pure Hg the reaction is very much faster and becomes a 2e reversible reaction. The value of k_{SH} on saturated Cu/Hg is low and similar to that on solid Cu. By analogy with the Cu^{2+} reduction it seems that Zn^{2+} reduction must proceed by a similar mechanism

$$Zn^{2+} + e \longrightarrow Zn^{+}$$
$$Zn^{+} + e \rightleftharpoons Zn$$

REFERENCES

1. M. Sluyters-Rehbach, J.H. Sluyters in Electroanal. Chem. (ed. A.J. Bard) Vol. V, p.1..

2. H. Matsuda and Y. Ayabe, Z. Elektrochem. 59, 495 (1955)

3. J. Koryta, Electrochim. Acta 6, 67 (1962).

4. W.M. Schwarz and I. Shain, J. Phys. Chem. 69, 30 (1965).

5. B.K. Hovsepian and I. Shain, J. Electroanal. Chem. 14 1 (1967).

6. R de Levie, Adv. in Electrochem. Eng. 6, 1967 (ed. P. Delahay, C.W. Tobias) Interscience.

7. M. Sluyters-Rehbach, J.S.M.C. Breukel, J.H. Sluyters, J. Electroanal. Chem. 19 (1968) 85.

8. B. Timmer, M. Sluyters-Rehbach, J.H. Sluyters, J. Electroanal. Chem. 14 (1967) 181.

9. G. Salie, Z. Phys. Chem. (Leipzig) 244 (1970) 1.

10. N.S. Hush, J. Blackledge, J. Electroanal. Chem. 5 (1963) 420.

11. I.R. Burrows, K.L. Dick, J.A. Harrison, Electrochim. Acta 21 (1976) 81.

12. J.R. Burrows, J.A. Harrison, J. Thompson, J. Electroanal. Chem. 58 (1975) 241.

CHAPTER VI

SOME PROSPECTS FOR FUTURE WORK

The transform methods work quite satisfactorily and the results of $Z_{(jw)}$- w compare reasonably well with those obtained experimentally with TFA measurements. As the transform measurements are obtained in a pulse experiment they are expected to be more reliable. However as demonstrated in this thesis the transform method relies on a compromise and particularly if the electrode process is fast an appreciable error in the real component of the $Z_{(jw)}$- w diagram can result. This can be minimised by judicious selection of sampling rate and amount by which the experimental current is amplified before being fed into the analogue to digital converter. Although this method has some disadvantages it will allow rapid measurements for example for a small amplitude pulse of say 50 mS an impedance plot from 5 KHz to 20 Hz could be derived. The total pulse time would be 20.2s. The processing time from initiating the pulse would be of the order of ten minutes. This is many times better than can be achieved with the automatic frequency response analyser in which the electrode would be at the d.c. potential for $\sim$30 s. To go to lower frequencies is more favourable for the transform method for example to 1 Hz needs a 1s pulse and the AFRA needs 16 minutes.

The next stage is clearly to rationalise the present programming for faster processing. This will require programmes written in machine code. A second important development would be to programme directly an automatic bridge to make it faster. An automatic bridge would come into its own at very low frequencies 1 Hz.

The use of the transform method is very well demonstrated in the Zn^{2+} reduction kinetics. In the future the method should be applied to the reaction on solid zinc. Although an electrochemical mechanism has

been derived for the reaction a more detailed investigation of the structural changes occurring during zinc deposition should be carried out.

APPENDIX A

DERIVATION OF LAPLACE TRANSFORM ALGORITHMS FOR CALCULATION WITH A DIGITAL COMPUTER

The LT is defined by

$$\overline{f(s)} = \int_0^\infty e^{-st} F(t)\,dt \qquad (A.1)$$

where F(t) is the transient to be transformed. However in a digital computer, F(t) is represented by a finite number of points. When this transient is the digitized transient response of a cell perturbation, we must make an assumption on how two consecutive points are analytically joined in order to numerically evaluate A.1. Pilla[II(4)] assumed an exponential function. Two alternative functions will be considered here: a linear approximation to relate two consecutive points

$$F(t_i) = A + Bt_i \qquad (A.2)$$

$$F(t_{i+1}) = A + Bt_{i+1} \qquad (A.3)$$

and a quadratic approximation to relate three consecutive points

$$F(t_i) = A + Bt_i + Ct_i^2 \qquad (A.4)$$

$$F(t_{i+1}) = A + Bt_{i+1} + Ct_{i+1}^2 \qquad (A.5)$$

$$F(t_{i+2}) = A + Bt_{i+2} + Ct_{i+2}^2 \qquad (A.6)$$

It must be noted that the transform A.1 operates upon the

appropriate time-domain functions from t = 0. Since it takes a finite time to sample the first point of the current transient after the synchronous pulse simultaneous with the onset of the potential perturbation, roughly equal to half the sampling rate, it is permissible and necessary for accuracy, to include in the data a zero-time point. Pilla sets it as V(t) = 0 and I(t) = 0 because he takes into account instruments rise time, but since in the time scale of our measurements, this rise time is not significant, as shown in Fig 2.1, our zero time data will be the full potential step or zero in the case of potential sweep and for the current transient a linear extrapolation to zero based on the first couple of points sampled.

A.1) Real Axis Transform

This is defined by substituting the real σ for s in Equation (A.1), and assuming the resulting integral

$$\overline{f(\sigma)} = \int_0^\infty F(t)\, e^{-\sigma t}\, dt \qquad (A.7)$$

to exist. To ensure it converges the signal F(t) is separated into a constant and a varying part

$$F(t) = F_{var}(t) + F(t_\infty) \qquad (A.8)$$

to level $F(t_\infty)$ at the end of the transient is considered as the steady state level and subtracted from all points of the transient F(t) in order to apply the transform A.7 to the resulting variable part of the transient $F_{var}(t)$ which converges to zero. The transform of the variable part is

$$\overline{f_{var}(\sigma)} = \int_0^\infty F_{var}(t)\, e^{-\sigma t}\, dt \qquad (A.9)$$

the transform of the constant part of the current transient is a constant

also
$$\overline{f_\infty(\sigma)} = \int_0^\infty F(t_\infty) e^{-\sigma t} dt = \frac{F(t_\infty)}{\sigma} \qquad (A.10)$$

which when added to the transform of the variable part $\overline{f_{var}(t)}$, allowed by the properties of the Laplace Transform, gives the real axis transform of the whole transient

$$\overline{f(\sigma)} = \overline{f_{var}(t)} + \frac{F(t_\infty)}{\sigma} \qquad (A.11)$$

By fitting the linear or exponential approximations over successive time intervals t_i to t_{i+1} (or t_i to t_{i+2} for the quadratic approximation), from A.9 we obtain segment transforms of the varying part

$$\overline{\left[f_{var}(\sigma)\right]_i} = \int_{t_i}^{t_{i+1}} F_{var}(t) e^{-\sigma t} dt \qquad (A.12)$$

It is convenient to integrate this equation in order to derive an expression to which the different approximations can be applied.

Integrating by parts we get

$$\overline{\left[f_{var}(\sigma)\right]_i} = \left[\frac{-F_{var}(t)e^{-\sigma t}}{\sigma}\right]_{t_i}^{t_{i+1}} + \int_{t_i}^{t_{i+1}} \frac{F_{var}(t)e^{-\sigma t}dt}{\sigma} \qquad (A.13)$$

$$= \left[\frac{-F_{var}(t)e^{-\sigma t}}{\sigma} - \frac{F'_{var}(t)e^{-\sigma t}}{\sigma^2}\right]_{t_i}^{t_{i+1}} + \int_{t_i}^{t_{i+1}} \frac{F_{var}(t)e^{-\sigma t}dt}{\sigma^2} \qquad (A.14)$$

$$= \left[\frac{-F_{var}(t)e^{-\sigma t}}{\sigma} - \frac{F_{var}(t)e^{-\sigma t}}{\sigma^2} \quad \frac{F''_{var}(t)e^{-\sigma t}}{\sigma^3}\right]_{t_i}^{t_{i+1}}$$

$$+ \int_{t_i}^{t_{i+1}} \frac{F'''_{var}(t)e^{-\sigma t}dt}{\sigma^3} \qquad (A.15)$$

thus by summing the transform of the segments over all segments i and adding the transform of the constant part of the transient we get

$$\overline{f(\sigma)} = \sum_i \left[\frac{-F_{var}(t)e^{-\sigma t}}{\sigma} - \frac{F'_{var}(t)e^{-\sigma t}}{\sigma^2} - \frac{F''_{var}(t)e^{-\sigma t}}{\sigma^3} \right]_{t_i}^{t_{i+1}} + \int_{t_i}^{t_{i+1}} \frac{F'''_{var}(t)e^{-\sigma t}}{\sigma^3} dt + \frac{F(t_\infty)}{\sigma} \tag{A.16}$$

A.1.a) Linear Approximation

If two adjacent points on the transient $F_{var}(t)$ are related by

$$F_{var}(t_i) = A + Bt_i \tag{A.17}$$

$$F_{var}(t_{i+1}) = A + Bt_{i+1} \tag{A.18}$$

we can obtain B from the simultaneous solution of A.17 and A.18 as

$$B = \frac{F_{var}(t_{i+1}) - F_{var}(t_i)}{t_{i+1} - t_i} \tag{A.19}$$

Since

$$F_{var}(t) = A + B(t) \tag{A.20}$$

then

$$F'_{var}(t) = B \tag{A.21}$$

and

$$F''_{var}(t) = 0 \tag{A.22}$$

Substituting A.21 and A.22 in A.16 we obtain an algorithm with which it is possible to numerically evaluate the real axis transform, namely

$$f(\sigma) = \sum_i \left[\frac{F_{var}(t_i)e^{-\sigma t_i} - F_{var}(t_{i+1})e^{-\sigma t_{i+1}}}{\sigma} \right]$$

$$+ \frac{B}{\sigma^2}\left(e^{-\sigma t_i} - e^{-\sigma t_{i+1}}\right) + \frac{F(t_\infty)}{\sigma} \qquad \text{(A.23)}$$

A.1.b) Quadratic Approximation

In this case the points must be joined three at a time to define the constants A, B, C given by

$$F_{var}(t_i) = A + Bt_i + Ct_i^2 \qquad \text{(A.24)}$$

$$F_{var}(t_{i+1}) = A + Bt_{i+1} + Ct_{i+1}^2 \qquad \text{(A.25)}$$

$$F_{var}(t_{i+2}) = A + Bt_{i+2} + Ct_{i+2}^2 \qquad \text{(A.26)}$$

Subtracting A.24 from A.25 yields

$$B = \left(\frac{F_{var}(t_{i+}) - F_{var}(t_i)}{t_{i+1} - t_i}\right) - C\left(t_{i+1} + t_i\right) \qquad \text{(A.27)}$$

Subtracting A.25 from A.26 and substituting for B from A.27 yields

$$C = \frac{F_{var}(t_{i+1}) - F_{var}(t_i)(t_{i+2} - t_{i+1}) - F_{var}(t_{i+2}) - F_{var}(t_{i+1})(t_{i+1} - t_i)}{(t_{i+1} - t_i)(t_{i+2} - t_{i+1})(t_i -} \qquad \text{(A.28)}$$

and B may not be found by substituting for C in A.27. We now will take the derivatives of the variable part of the transient

$$F_{var}(t) = A + Bt + Ct^2 \qquad \text{(A.29)}$$

which are

$$F'_{var}(t) = B + 2Ct$$

$$F''_{var}(t) = 2C \qquad \text{(A.30)}$$

$$F'''_{var}(t) = 0 \qquad \text{(A.31)}$$

(A.32)

in order to substitute them in A.16 to give the algorithm

$$\overline{f(\sigma)} = \sum_i e^{-t_i\sigma}\left(\frac{F_{var}(t_i)}{\sigma} + \frac{B+2Ct_i}{\sigma^2} + \frac{2C}{\sigma^3}\right) - e^{-\sigma t_{i+1}}\left(\frac{F_{var}(t_{i+1})}{\sigma} + \frac{B+2Ct_{i+1}}{\sigma^2} + \frac{2C}{\sigma^3}\right) + \frac{F(t_\infty)}{\sigma} \qquad \text{(A.33)}$$

used to evaluate the real axis transform, numerically, with the quadratic approximation.

A.1.c) Exponential Approximation

For two adjacent points of the $F_{var}(t)$ transient related by

$$F_{var}(t_i) = A e^{-at_i} \qquad \text{(A.34)}$$

$$F_{var}(t_{i+1}) = A e^{-at_{i+1}} \qquad \text{(A.35)}$$

a procedure similar to the one described for the linear approximation, yields the following algorithm

$$\overline{f(\sigma)} = \sum_i \frac{\left(F_{var}(t_i)\exp(-\sigma t_i) - F_{var}(t_{i+1})e^{-\sigma t_{i+1}}\right)(t_{i+1}-t_i)}{\ln\left(F_{var}(t_i)e^{-\sigma t_{i+1}} / F_{var}(t_{i+1})\right)} \qquad \text{(A.36)}$$

A.2. Imaginary Axis Transform

This is defined by substituting the complex jw for s in A.1, to yield

$$\overline{f(jw)} = \int_0^\infty F(t) e^{-jwt}\, dt \qquad (A.37)$$

expanding e^{-jw}, A.37 can be rewritten as

$$f(jw) = \int_0^\infty F(t)\cos(wt)\,dt - j\int_0^\infty F(t)\sin(wt)\,dt \qquad (A.38)$$

where f(jw) is expressed in terms of its real and imaginary parts, making this transform very useful in the direct calculation of the real and imaginary parts of the impedance. However in order that the transforms exist the integrals in A.38 have to converge, it can be seen that for both the real and imaginary parts, multiplication of the original transient by a periodic trigonometric function is involved. Therefore A.38 will not converge unless F(t) actually becomes zero as $t \to \infty$. This is accomplished by subtracting the constant portion $F(t_\infty)$ from the remainder of the experimental curve to leave the variable portion $F_{var}(t)$ on which the transform can be performed.

The real part of this transform is given by

$$\overline{Re[f(jw)]}_{var} = \int_0^\infty F_{var}(t)\cos(wt)\,dt \qquad (A.39)$$

and the imaginary part by

$$\overline{Im[f(jw)]}_{var} = -\int_0^\infty F_{var}(t)\sin(wt)\,dt \qquad (A.40)$$

where

$$\overline{f(jw)}_{Var} = \overline{Re\left[f(jw)\right]} + j\ \overline{Im\left[f(jw)\right]}_{var} \qquad (A.41)$$

The imaginary-axis transform of the constant portion $F(t_\infty)$ is a purely imaginary constant given by

$$f_{t\infty}(jw) = -j\frac{F(t_\infty)}{w} + \frac{F(t_\infty)}{jw} \qquad (A.42)$$

which is appropriately added to $f(jw)_{var}$ to generate the complete transform

$$\overline{f(jw)} = \overline{f(jw)}_{var} + \frac{F(t_\infty)}{jw} \qquad (A.43)$$

By fitting the various approximations over successive time intervals t_i to t_{i+1} to A.39 we obtain the segment transform of the real part

$$\left[Re\right]_i = \int_{t_i}^{t_{i+1}} F_{var}(t)\ cos(wt)\ dt \qquad (A.44)$$

integrating by parts

$$\left[Re\right]_i = \left[\frac{F_{var}(t)\sin wt}{w}\right]_{t_i}^{t_{i+1}} = \int_{t_i}^{t_{i+1}} \frac{F'_{var}(t)\ sin(wt)}{w}\ dt \qquad (A.45)$$

$$= \left[\frac{F_{var}(t)\sin(wt)}{w} + \frac{F'_{var}(t)cos(wt)}{w^2}\right]_{t_i}^{t_{i+1}} - \int_{t_i}^{t_{i+1}} \frac{-\cos wt}{w^2}\ dt \qquad (A.46)$$

$$= \left[\frac{F_{var}(t)sin(wt)}{w} + \frac{F'_{var}(t)cos(wt)}{w^2} - \frac{F''_{var}(t)\sin wt}{w^3}\right]_{t_i}^{t_{i+1}} \qquad (A.47)$$

thus by summing the transform of the segments over all segments i we get

$$\overline{\text{Re}\left[f(j\omega)\right]} = \sum_i \left[\frac{F_{var}(t)\sin\omega t}{\omega} + \frac{F'_{var}(t)\cos\omega t}{\omega^2} - \frac{F''_{var}(t)\sin\omega t}{\omega^3} \right]_{t_i}^{t_{i+1}} + \int_{t_i}^{t_{i+1}} \frac{F'''_{var}\sin\omega t}{} dt \qquad (A.48)$$

In a similar fashion, from A.40 we calculate the segment transform of the imaginary part

$$[Im]_i = -\int_{t_i}^{t_{i+1}} F_{var}(t)\sin(\omega t)\, dt \qquad (A.49)$$

integrating by parts

$$[Im]_i = -\left[\frac{F_{var}(t)(-\cos\omega t)}{\omega}\right] - \int_{t_i}^{t_{i+1}} F'_{var}(t)\cos\omega t\, dt \qquad (A.50)$$

$$= \left[\frac{F_{var}(t)\cos\omega t}{\omega} - \frac{F_{var}(t)\sin\omega t}{\omega^2}\right]_{t_i}^{t_{i+1}} + \int_{t_i}^{t_{i+1}} \frac{F''_{var}(t)\sin\omega t}{\omega^2} dt$$

$$= \left[\frac{F_{var}(t)\cos\omega t}{\omega} - \frac{F'_{var}(t)\sin\omega t}{\omega^2} - \frac{F_{var}(t)\cos\omega t}{\omega^3}\right]_{t_i}^{t_{i+1}} \qquad (A.51)$$

$$+ \int_{t_i}^{t_{i+1}} \frac{F'''_{var}(t)\cos\omega t}{\omega^3} dt \qquad (A.52)$$

thus by summing the transform of the segments over all segments i and adding the transform of the constant portion we get

$$\overline{Im[f(j\omega)]} = \sum_i (Im)_i - \frac{F(t_\infty)}{\omega} \tag{A.53}$$

A.2.a) Linear Approximation

Using the values defined previously in the real axis transform, (Equations A.21 and A.22) we substitute B, $F'_{var}(t)$, and $F''_{var}(t)$ in Equation A.52, and use A.53 to give

$$\overline{Im[f(j\omega)]} = \sum_i \frac{1}{\omega}\left\{F_{var}(t_{i+1})\cos\omega t_{i+1} - F_{var}(t_i)\cos\omega t_i - \frac{B}{\omega}(\sin\omega t_{i+1} - \sin\omega t_i)\right\} - \frac{F(t_\infty)}{\omega} \tag{A.54}$$

from Equations A.21, A.22 and A.48 we obtain the algorithm for the real part of the imaginary axis transform

$$\overline{Re[f(j\omega)]} = \sum_i \frac{1}{\omega}\left\{F_{var}(t_{i+1})\sin\omega t_{i+1} - F_{var}(t_i)\sin\omega t_i + \frac{B}{\omega}(\cos\omega t_{i+1} - \cos\omega t_i)\right\} \tag{A.55}$$

A.2.b) Quadratic Approximation

Using the values defined previously in the real axis transform (Equations A.27, A.28, A.30, A.31, A.32) we obtain from A.52 and A.53 the algorithm

$$Im[f(j\omega)] = \sum_i \frac{1}{\omega}\left\{-F_{var}(t_{i+2})\cos(\omega t_{i+2}) + (B+2Ct_{i+2})\sin t_{i+2} + \frac{2C\cos(\omega t_{i+2})}{\omega^2} + F_{var}(t_i)\cos\omega t_i - \frac{B+2Ct_i}{\omega}\sin\omega t_i - \frac{2C\cos\omega t_i}{\omega^2}\right\} - \frac{F(t_\infty)}{\omega} \tag{A.56}$$

and from A.48

$$\overline{Re\left[f(j\omega)\right]} = \sum_i \frac{1}{\omega}\left\{F_{var}(t_{i+2})\sin\omega t_{i+2} + (B+2Ct_{i+2})\cos\omega t_{i+2}\right.$$

$$- \frac{2C\sin\omega t_{i+2}}{\omega^2} - F_{var}(t_i)\sin\omega t_i$$

$$\left. - \frac{(B+2Ct_i)\cos\omega t_i}{\omega} + \frac{2C\sin\omega t_i}{\omega^2}\right\} \qquad (A.57)$$

A.2.c) Exponential Approximation

In a similar fashion one can deduce the imaginary axis transform for the exponential approximation, the resulting algorithms are

$$\overline{Re(f(j\omega))} = \sum_i \frac{1}{a^2+\omega^2}\left\{F(t_{i+1})\left[-a\cos\omega t_{i+1} + \omega\sin\omega t_{i+1}\right]\right.$$

$$\left. + F(t_i)\left[a\cos\omega t_i - \omega\sin\omega t_i\right]\right\} \qquad (A.58)$$

$$\overline{Im\left[f(j\omega)\right]} = \sum_i \frac{1}{a^2+\omega^2}\left\{-F(t_{i+1})(\omega\cos\omega t_{i+1} + a\sin\omega t_i)\right.$$

$$\left. + f(t_i)(\omega\cos\omega t_i + a\sin\omega t_i)\right\} \qquad (A.59)$$

APPENDIX B.

LAPLACE TRANSFORM OF E = at AND COMPUTER PROGRAM TO CALCULATE IMPEDANCE FROM LINEAR POTENTIAL SWEEPS

The appropriate form of the function is

$$E = at \qquad t < \tau_o$$

$$E = E_K \qquad t > \tau_o$$

$$\overline{E(s)} = \int_o^{\tau} at\, e^{-st} dt + \int_{\tau_o}^{o} E_K e^{-st} dt$$

Integration by parts gives

$$\overline{E(s)} = -\frac{E_K e^{-sE_K/a}}{s} - a e^{-sE_K/a} + \frac{a}{s^2} + \frac{E_K}{s}$$

which on substituting for S = jw and splitting into the real and imaginary parts gives

$$E(Re) = \frac{a}{\omega^2} \cos\left(\frac{\omega E_K}{a}\right) + \frac{E_K}{\omega} \sin\left(\frac{\omega E_K}{a}\right) - \frac{a}{\omega^2}$$

$$E(Im) = \frac{E_K}{\omega} \cos\left(\frac{\omega E_K}{a}\right) - \frac{a}{\omega^2} \sin\left(\frac{\omega E_K}{a}\right) - \frac{E_K}{\omega}$$

This equation was then integrated into a similar programme to the pulse response and $Z_{(jw)}$ calculated by equation 2.11.

It was necessary to arrange the programme Z 10 which follows so that the Laplace procedure converged, i.e. to make currents and potential response falling functions of time as $t \longrightarrow \tau_o$.

APPENDIX C

DERIVATION OF THEORETICAL EXPRESSIONS OF THE IMPEDANCE SPECTRUM FOR SYNTHETIC TEST DATA

1) Fourier Transform of Exponential Transient

We assume that a potential pulse defined as

$$E(t) = 0 \qquad \text{for} \qquad 0 \leq t < \tau \tag{C.1}$$

causes a response

$$i(t) = 0 \qquad \text{for} \qquad 0 \leq t < \tau$$

$$i(t) = k_1 e^{-k_2(t-\tau)} \qquad \text{for} \qquad \tau \leq t \leq T \tag{C.2}$$

which when digitized can be expressed as

$$i(Rn) = 0 \qquad \text{for} \qquad 0 \leq t < \tau$$

$$i(t) = k_1 e^{-k_2(Rn-\tau)} \qquad \text{for} \qquad \tau \leq Rn < RN \tag{C.3}$$

where n = 0, 1, 2,..(1+N) and R is the sampling rate.

Applying the Fourier Transformation defined by Equation (2.3) to the current data C.2 we get

$$\overline{i(2\pi r/T)} = 0 + \frac{2}{T}\int_{\tau}^{T} k_1 e^{-k_2(t-\tau)} e^{-j2\pi rt/T} \tag{C.4}$$

where $2\pi r/T$ is the value of the frequency w set by the DAQUAD program.

Integrating C.4 we have

$$\overline{i(2\pi r/T)} = e^{k_2\tau}\frac{2}{T}\left[\frac{-k_1 e^{-(k_2 + j2\pi r/T)}}{k_2 + j2\pi r/T}\right]_{\tau}^{T} \tag{C.5}$$

$$= \frac{2e^{k_2\tau}}{T}\left[\frac{-k_1 e^{-(k_2 + j2\pi r/T)T} + k_1 e^{-(k_2 + j2\pi r/T)}}{k_2 + j2\pi r/T}\right] \qquad (C.6)$$

$$= \frac{2k_1}{T\,k_2 + j2\pi r/T}\left[e^{-j2\pi r\tau/T} - e^{-k_2(T-\tau)}\right] \qquad (C.7)$$

A simplification occurs when $e^{-k_2(T-\tau)} \longrightarrow 0$, if we also take $T = 2\tau$

Equation C.7 becomes

$$\overline{i(2\pi r/T)} = \frac{2k_1 e^{-j\pi r}}{Tk_2 + j2\pi r} \qquad (C.8)$$

since

$$e^{-j\pi r} = \cos\pi - j\sin\pi r \qquad (C.9)$$

for integral values of r the term $j \sin\pi r$ vanishes and C.8 becomes

$$\overline{i(2\pi r/T)} = \frac{-2\cos\pi r}{k_2 T + j2\pi r} \qquad (C.10)$$

$$= \frac{-2(k_2 T - j2\pi r)\cos\pi r}{k_2^2 T^2 + 4\pi^2 r^2} \qquad (C.11)$$

remembering that $T = NR$, the real and imaginary components of $i(2\pi r/T)$ derived from C.11 are

$$A_r = \frac{-2k_2 T\cos\pi r}{k_2^2 T^2 + 4\pi^2 r^2} = \frac{-2k_2 NR\cos\pi r}{k_2^2 N^2 R^2 + 4\pi^2 r^2} \qquad (C.12)$$

$$B_r = j\frac{4\pi r\cos\pi r}{k_2^2 T^2 + 4\pi^2 r^2} = j\frac{4\pi r\cos\pi r}{k_2^2 N^2 R^2 + 4\pi^2 r^2} \qquad (C.13)$$

Applying the Fourier Transformation defined by Equation 2.3 to the potential data given by C.3 we get

$$\overline{E(2\pi r/T)} = 0 + \frac{2}{T}\int_{\tau}^{T} e^{-j2\pi r t/T} E\, dt \qquad (C.14)$$

$$= \left[\frac{-E\, e^{-j2\pi r t/T}}{j\, 2\pi r/T}\right]_{\tau}^{T} \qquad (C.15)$$

$$= \frac{E}{j\pi r}\left(e^{-j2\pi r\tau/T} - 1\right) \qquad (C.16)$$

the term in parenthesis is simplified for integral values of r and $T = 2\tau$.

Equation C.16 becomes

$$\overline{E(2\pi r/T)} = j\frac{E}{\pi r}\cos(\pi r - 1) \qquad (C.17)$$

It can be seen that the real part of $E(2\pi r/T)$ is zero, i.e.

$$C_r = 0 \qquad (C.18)$$

and

$$D_r = \overline{E(2\pi r/T)} = -j\frac{E}{\pi r}\cos(\pi r - 1) \qquad (C.19)$$

or what is the same

$$D_r = 0 \quad \text{for} \quad r = 2, 4, 6, \ldots N \qquad (C.20)$$

$$D_r = j\frac{2E}{\pi r} \quad \text{for} \quad r = 1, 3, 5, \ldots N-1 \qquad (C.21)$$

The impedance frequency spectrum

$$Z(w) = \frac{\overline{E(w)}}{\overline{i(w)}} \qquad (C.22)$$

is obtained from Equations C.7 and C.16 as

$$Z(2\pi r/T) = \frac{T(k_2 + j2\pi r/T)E}{k_1\, j\, 2\pi r}\left[\frac{e^{-j2\pi r\tau/T} - 1}{e^{-j2\pi r\,\tau/T} - e^{-k_2(T-\tau)}}\right] \qquad (C.23)$$

A useful simplification of Equation C.11 occurs when

$$e^{-k_2(T-\tau)} \longrightarrow 0$$

then

$$Z(2\pi r/T) = (k_2 T + j2\pi r)E\left(\frac{1 - e^{j2\pi r\tau/T}}{j\,2\pi r\, k_1}\right) \qquad (C.24)$$

$$= \frac{E(2\pi r - jk_2 T)}{2\pi r\, k_1}\left(1 - e^{j2\pi r\tau/T}\right) \qquad (C.25)$$

With r being an integer number, the value of τ that renders more meaningful values is $\tau = 1/2T$ since with this value Equation C.25 becomes

$$Z(2\pi r/T) = \frac{2\pi r E - jk_2 T E}{2\pi r\, k_1}\left(1 - \cos\pi r\right) \qquad (C.26)$$

the term in parenthesis is zero for r = 0,2,4...N and two for r = 1,3,5... N-1. Therefore the real and imaginary parts of the impedance spectrum from Equation C.26 are

$$Z(Re) = \frac{2E}{k_1} \quad \text{for} \quad r = 1,3,5... \qquad (C.27)$$

$$Z(Im) = \frac{k_2 E T}{k_1 \pi r} \qquad (C.28)$$

where $Z(w) = Z(Re) + j\,Z(Im)$

The non-dimensional expressions of C.27 and C.28 substituting T = NR are

$$k_1 E^{-1} Z(Re) = 2 \qquad \text{for} \quad r = 1, 3, 5 \ldots \tag{C.29}$$

$$k_1 k_2^{-1} E^{-1} R^{-1} Z(Im) = \frac{-2N}{2\pi r} \tag{C.30}$$

It is interesting to observe that these values are the double of those obtained with the LT (Equations C.44 and C.45). In order to obtain the same result τ should have to be equal to T, i.e. the perturbation starting at t = 0, Equation C.23 becomes then

$$Z(2\pi r/T) = \frac{E}{k_1} - j \frac{E k_2}{k_1 2\pi r/T} \tag{C.31}$$

which is also the result obtained with the LT, unfortunately the computer program using the FFT cannot cope with the condition $T = \tau$.

2) Imaginary Axis LT of Exponential Transient

In order to test the LT software we assume that a potential pulse starting at t = 0, defined as

$$E(t) = E \qquad \text{for} \quad t \geq 0 \tag{C.32}$$

causes a response

$$i(t) = k_1 e^{-k_2 t} = k_1 e^{-k_2 R n} \qquad \text{for} \quad t \geq 0 \tag{C.33}$$

where n = 0,1,2...N and R the sampling rate; the imaginary axis transform of the current transient (from A.37) is

$$\overline{i(j\omega)} = \int_0^\infty k_1 e^{-k_2 t} e^{-j\omega t} \, dt \tag{C.34}$$

integrating

$$\overline{i(j\omega)} = \left[\frac{k_1 e^{-(-k_2 + j\omega)t}}{-(k_2 + j\omega)} \right]_0^\infty \qquad (C.35)$$

$$= \frac{k_1}{k_2 + j\omega} \qquad (C.36)$$

similarly the transform of the potential transient is

$$\overline{E(j\omega)} = \int_0^\infty E\, e^{-j\omega t}\, dt \qquad (C.37)$$

integrating

$$\overline{E(j\omega)} = \left[\frac{E}{-j\omega} e^{-j\omega t} \right]_0^\infty \qquad (C.38)$$

$$= \frac{E}{j\omega} \qquad (C.39)$$

The complex impedance is

$$Z(j\omega) = \frac{\overline{E(j\omega)}}{\overline{i(j\omega)}} \qquad (C.40)$$

Substituting C.39 and C.36 in C.40 we get

$$Z(j\omega) = \frac{E(k_2 + j\omega)}{j\omega k_1} \qquad (C.41)$$

$$= \frac{E}{k_1} - j\frac{k_2 E}{k_1 \omega} \qquad (C.42)$$

therefore

$$Z(Re) = \frac{E}{k_1} \qquad (C.43)$$

and

$$Z(Im) = \frac{-k_2 E}{k_1 \omega} \qquad (C.44)$$

where $$Z(j\omega) = Z(Re) + jZ(Im) \tag{C.45}$$

In order to make comparisons it is convenient to plot the adimensional versions of C.43 and C.44 given as

$$Z(Re)^* = Z(Re)k_1E^{-1} = 1 \tag{C.46}$$

$$Z(Im)^* = Z(Im)E^{-1}k_1k_2^{-1}R^{-1} = \frac{n}{2\pi} \tag{C.47}$$

where n is related to the frequency by

$$\omega = \frac{2\pi}{nR} = 2\pi f \tag{C.48}$$

n is now a positive rational number since the integration procedure involved in the transformation converts the digitized time domain data into a continuous signal. In this way the corresponding frequency in the non dimensional complex plane is given by fR where f is any arbitrary frequency chosen within the time scale of the time domain data.

3) <u>Imaginary Axis Laplace Transformation of $1/\sqrt{t}$ Transient</u>

The current transient defined by

$$i(t) = \frac{K}{t^{1/2}} = \frac{K}{(Rn)^{1/2}} \quad \text{for } t \geq 0, \quad n = 0, 1, 2, \ldots N \tag{C.49}$$

obtained as a response to the potential step defined by C.31, has an imaginary axis transform given by

$$i(j\omega) = \int_0^\infty Kt^{-1/2}e^{-j\omega t}\,dt \tag{C.50}$$

from tables of LT

$$\overline{i(j\omega)} = \sqrt{\frac{\pi}{j\omega}}\ K \tag{C.51}$$

Using Equation C.39 and C.40 we calculate the impedance as

$$Z(j\omega) = \frac{E}{K\sqrt{\pi j\omega}} = \frac{-E\ j^{3/2}}{K\sqrt{\pi\omega}} \tag{C.52}$$

Since $e^{j\theta} = \cos\theta + j\sin\theta$, if $\theta = \pi/2$

$$e^{j\theta/2} = j \tag{C.53}$$

substituting this result in C.52 we have

$$Z(j\omega) = \frac{E}{K\sqrt{\pi\omega}}\, e^{j(3/4)\pi} \tag{C.54}$$

$$= -\frac{E}{K\sqrt{\pi\omega}}\left(\cos[(3/4)\pi] + j\sin\left(\frac{3\pi}{4}\right)\right) \tag{C.55}$$

since $\cos(3/4)\pi = {}^{-1}/\sqrt{2}$ and $\sin\frac{3\pi}{4} = 1/\sqrt{2}$

$$Z(j\omega) = \frac{E}{K\sqrt{2\pi\omega}} - j\frac{E}{K\sqrt{2\pi\omega}} \tag{C.56}$$

$$\therefore \quad Z(Re) = \frac{E}{K\sqrt{2\pi\omega}} \tag{C.57}$$

$$Z(Im) = -\frac{E}{K\sqrt{2\pi\omega}} \tag{C.58}$$

taking the frequency as

$$\omega = 2\pi f = \frac{2\pi}{nR}$$

where n is now any rational number in the interval $0 > n \leq N$, we convert C.57 and C.58 to the adimensional forms

$$Z(Re)^{*} = Z(Re)KE^{-1}R^{-1/2} = \frac{\sqrt{n}}{2\pi} \tag{C.59}$$

$$Z(lm)^* = Z(lm)\,K\,E^{-1}\,R^{-1/2} \qquad (C.60)$$

as a function of the adimensional group fR = 1/n in order to test the LT software against this theoretical results.

APPENDIX D.

THE ESTIMATION OF R_s and $Y_w C_s$ USING THE BROOKDEAL P.S.D.

Using the circuit shown in Fig. the following four readings are taken in order.

(1) W.E. - R.E. IN PHASE (Ø)

After the phase shift on the reference unit to give

reading A = 0.0 Volts

For the next three readings the phase shift is left in position.

(2) W.E. - R.E. OUT OF PHASE ($Ø + 90^o$)

reading B = X Volts

(3) Current measuring resistor (R) IN PHASE (Ø)

reading C = Y Volts

(4) Current measuring resistor (R) OUT OF PHASE ($Ø + 90^o$)

reading D = Z Volts

From $Ø = \frac{Y}{Z}$, the phase angle Ø may be found.

$Z(w) = R \sin Ø \frac{X}{Y}$ (where R is the current measuring resistor)

$R_s = Z(w) \cos Ø$

$\frac{1}{wC_s} = Z(w) \sin Ø$

APPENDIX E.

TEST OF THE FFT SOFTWARE USING A $1/\sqrt{t}$ TRANSIENT

We examine here the impedance spectrum obtained with the FFT software for the following artificial data:

$$E(t) = 0 \quad \text{for} \quad 0 \leq t < \tau$$
$$E(t) = E \quad \text{for} \quad \tau \leq t \leq T \qquad \text{(E.1)}$$

causes the current transient

$$i(t) = 0 \quad \text{for} \quad 0 \leq t < \tau$$
$$i(t) = K(t-\tau)^{-1/2} = K R^{-1/2}(n - N)^{-1/2}$$

$$\text{for} \quad N_\tau \leq n \leq N, \quad \tau \leq t \leq T \qquad \text{(E.2)}$$

where $n = 1, 2, \ldots N$ and $\tau = RN_\tau$

There is no theoretical solution of equation 2.13 for the transient 2.44. For the exponential transient the theoretical impedance obtained with the FT, for $T = 2$, is related to the theoretical impedance obtained with the LT, for $T = \tau$ by a factor of 2. Therefore by analogy, since the shape of the current transient is similar, we employed a factor of 1.8 to fit the FFT results and compare with the theoretical impedance values obtained for the LT. In the non-dimensional form these values are given by equations 2.42 and 2.43. In Figs. E.1 to E.5 the impedance spectra in a non-dimensional form obtained with the FFT software, is compared with the above mentioned theoretical results.

As first attempt, both potential and current transients were transformed via DAQUAD program. Even when amplifying the potential step to the full range of the DAQUAD program, to improve accuracy, the resultant

impedance was only reasonably accurate in the low frequency region of the spectrum, due to the combined errors associated with the single precision rounding off errors. These results are shown in Figs. E.1 and E.2. In Fig. 2.14 an improvement of the accuracy was obtained by setting to zero the real Fourier coefficients of the potential step, Cr , as prescribed by equation C.18. In Fig. E.4 similar accuracy is obtained, substituting both Cr and Dr for its theoretical values given by equations C.18 and C.19.

By analogy with the results obtained with the exponential transient, as the transient gets flatter the accuracy in the low frequency region improves, although it deteriorates in the high frequency region of the impedance spectra. As the transient gets steeper the opposite occurs. This effect, observable in Figs. E.1 and E.2, is due to truncation errors associated with the DAQUAD program, and also with the truncation of the $K/\sqrt{t-\tau}$ transient when $t = \tau$. The maximum value that the DAQUAD program accepts in the artificial data is 2048, and this was the value of the first point of the current pulse, the rest were calculated by equation E.2 when $R \geq 0.5 \times 10^{-6}$, for the case of flatter transients more than one point at the beginning of the current pulse had to be truncated to 2048 with the consequent deterioration of the high frequency accuracy.

```
7310 GOSUB 10410
7610 V7=W(K)*V8/V9
7620 K5=COS(V7)
7630 K6=SIN(V7)
7710 V3=V9*K6/W(K)**2
7810 V4=          -V9*K5/W(K)**2+V9/W(K)**2
7910 C4=C5*C5+C3*C3
8010 R(K)=(V4*C5+V3*C3)/C4
8110 I(K)=(C5*V3-V4*C3)/C4
8210 F7=C8-C2
8310 L1=W(K)*T1
8510 L3=R(K)*Z7
8710 L4=I(K)*Z7
9010 PRINT INT(L1+0.2),L3,L4,INT(L1/6.2832+0.5)
9110 NEXT K
9120PRINT"AMPL. FACTOR (PLOT)"
9130 INPUT Z6
9210 FILEV#2:"DTA1:D.DA"
9310 FOR K=1 TO INT(N1)
9410 PRINT#2:INT(R(K)*Z6*K2+0.5);PNT(44);INT(I(K)*Z6*Z9+.5)
9510 NEXT K
9610 FOR X=0 TO 400 STEP 5
9710 PRINT#2:X;PNT(44);0
9810 NEXT X
9820 FOR Y=0 TO 6
9830 PRINT#2:05;PNT(44);Y
9840 NEXT Y
9910 FOR Y=0 TO 200 STEP 2
10010 PRINT#2:0;PNT(44);Y
10110 NEXT Y
10120 FOR X=0 TO 6
10130 PRINT#2:X;PNT(44);Q4
10140 NEXT X
10210 CLOSE#2
10310 GO TO 13710
10410 H5=0.0
10510 H6=0.0
10610 H7=0.0
10710 FOR J=2 TO P1.
10810 B8=C(J)
10910 B9=C(J-1)
11010 X1=W(K)
11110 X2=X1*X1
11210 D6=S(J)
11310 D7=S(J-1)
11410 D8=Q(J)
11510 D9=Q(J-1)
11610 E1=(B8-B9)/(X2*(T(J)-T(J-1)))
11710 E2=E1*D6-B8*D8/X1-E1*D7+B9*D9/X1
11810 E3=E1*D8+B8*D6/X1-E1*D9-B9*D7/X1
11910 E2=-E2
12010 H5=H5+E3
12110 H6=H6+E2
12210 NEXT J
13310 C5=H5
13410 C3=H6
13510 C8=H7
13610 RETURN
13710 PRINT "AGAIN? (Y FOR YES)"
13720 INPUT A$
13730 IF A$="Y" THEN 210
13800 END
```

Subroutine for program Z10 to be inserted in Z9Q, in order to analyse potential sweeps

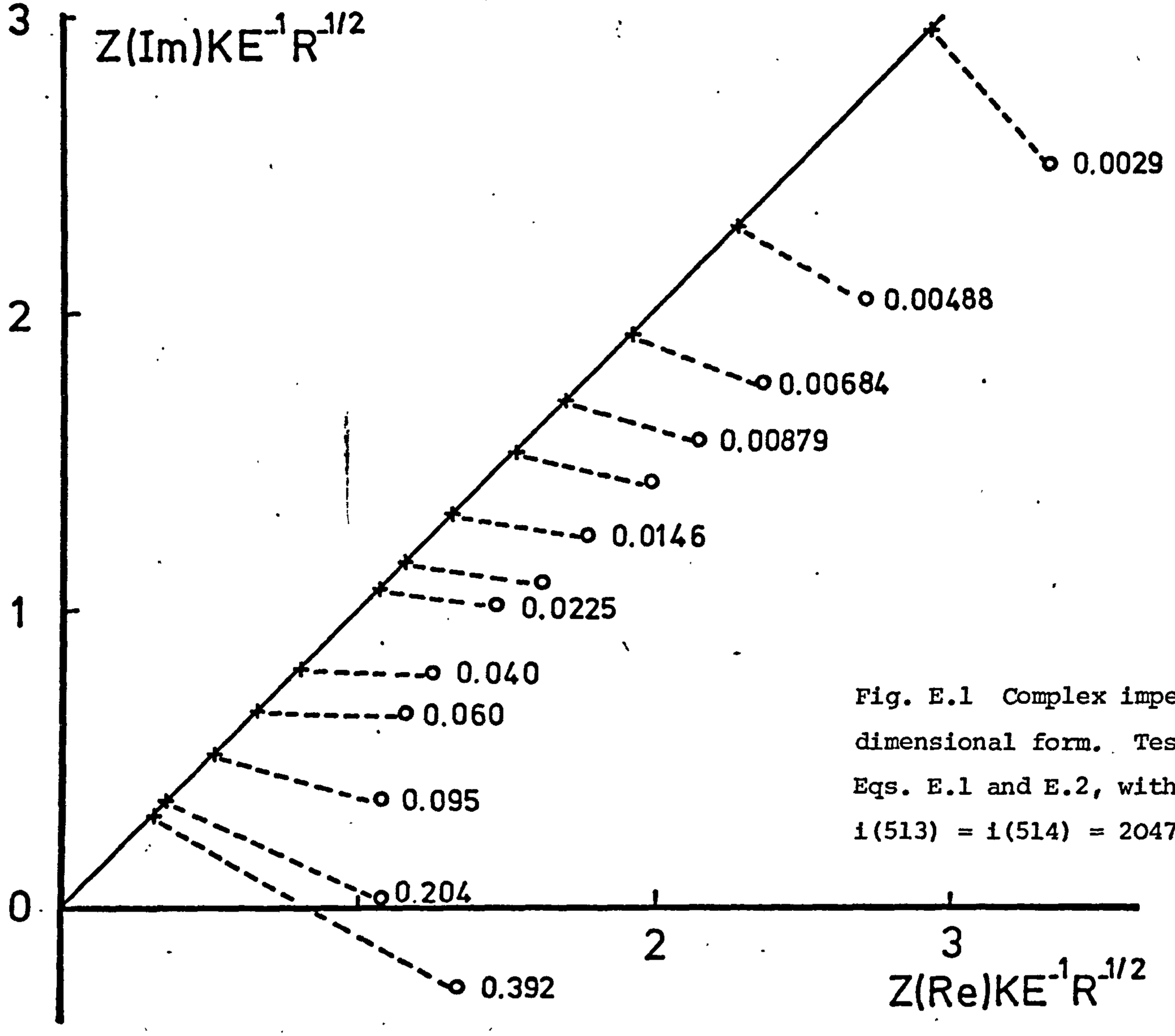

Fig. E.1 Complex impedance plane plot in non-dimensional form. Test data generated with Eqs. E.1 and E.2, with $R = 2 \times 10^{-7}$, $K = 2236$ $i(513) = i(514) = 2047$, (O) Results from FFT software with Cr and Dr machine generated. (+) Theoretical values according to 2.43. Figures on graph indicate fR value.

Fig. E.2 Complex impedance please plot in non-dimensional form. Test data generated with Eqs. E.1 and E.2 $R = 0.5 \times 10^{-6}$, K = 1414, E = 1000, N = 1024, Nτ = 512, i(513) = 2047. (O) Results from FFT software with Grand Dr machine generated values. (+) Theoretical value according to Eqs. 2.42 and 2.43.B is an expansion of graph A at high frequencies. Small figures indicate FR values.

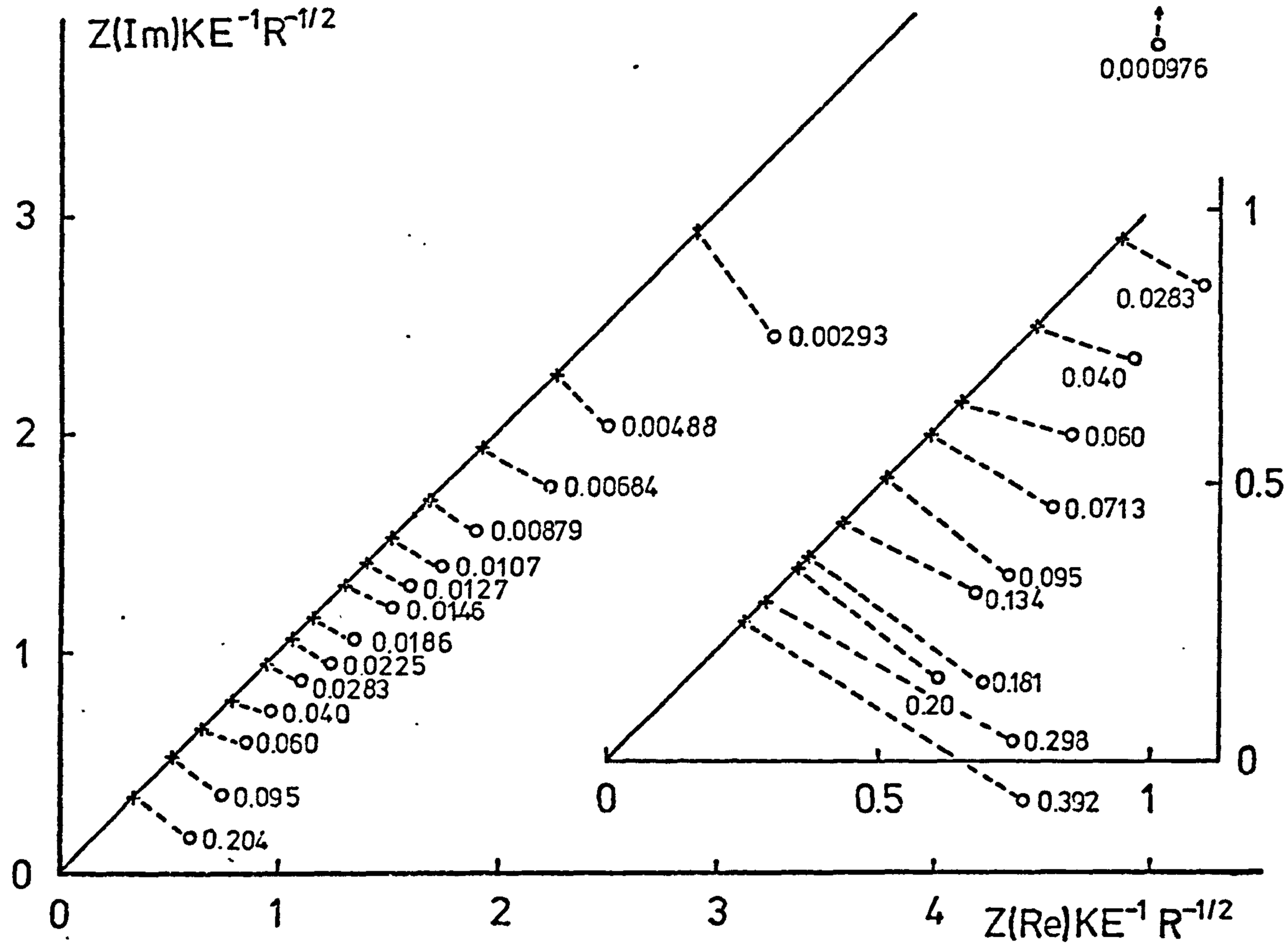

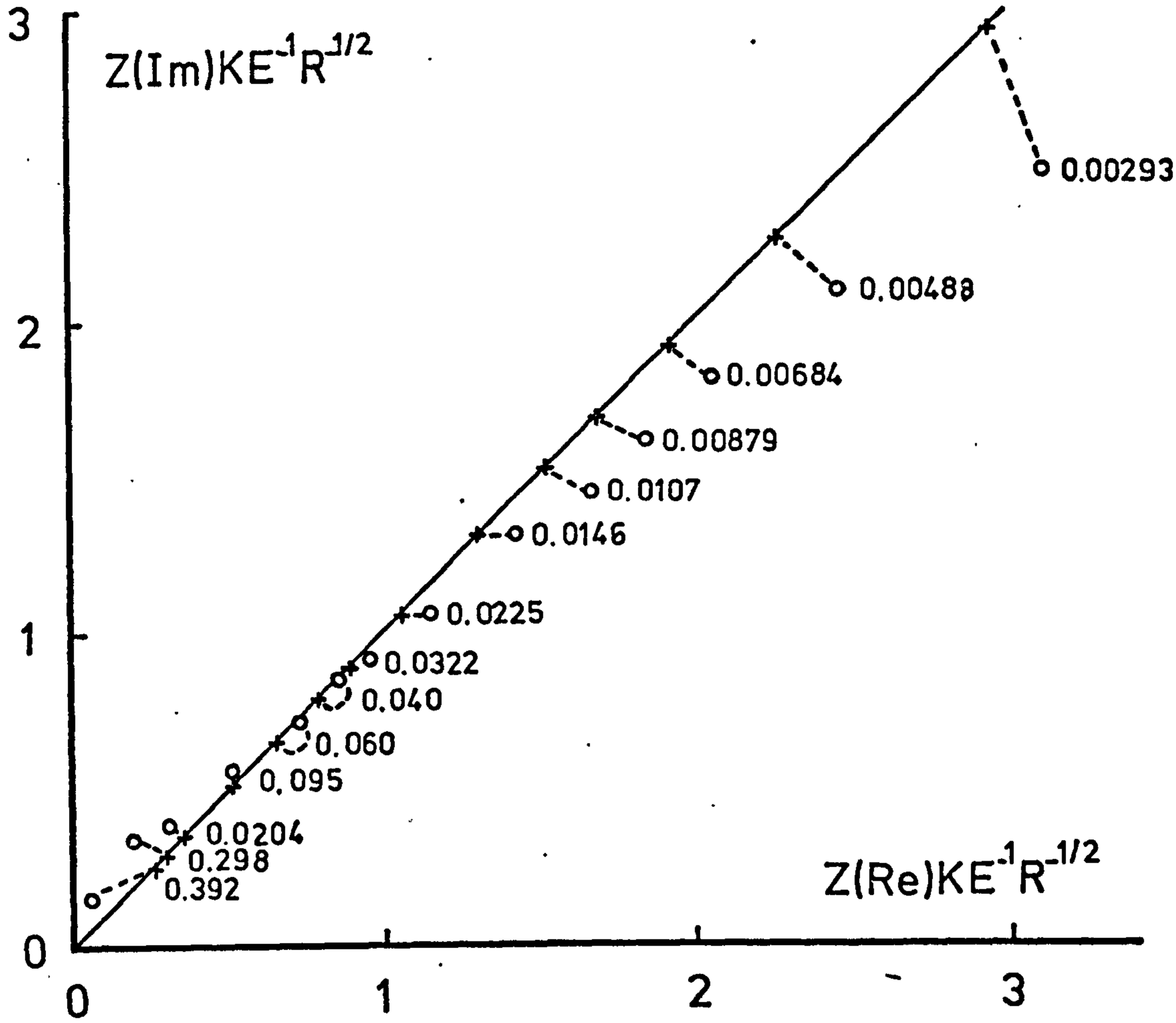

Fig. E.3 Complex impedance plane plot in non-dimensional form from test data N = 1024, Nτ = 512, R = 0.5 x 10^{-6}, K = 1414, i (513) = 2047. (O) Results of FFT software with C_r = 0. (+) Theoretical value according to Eqs. 2.42 and 2.43 Small figures on graph indicate the corresponding fR value.

Fig. E.4 Complex impedance plane plot in non-dimensional form. Test data generated by Eqs E.1 and E.2 with R = 5 x 10^{-7}, K = 1414, N_τ = 512 N = 1024, (O) Results from FFT software, Cr and Dr. generated by CD FILE program (theoretical value). Figure on graph indicate fR values.

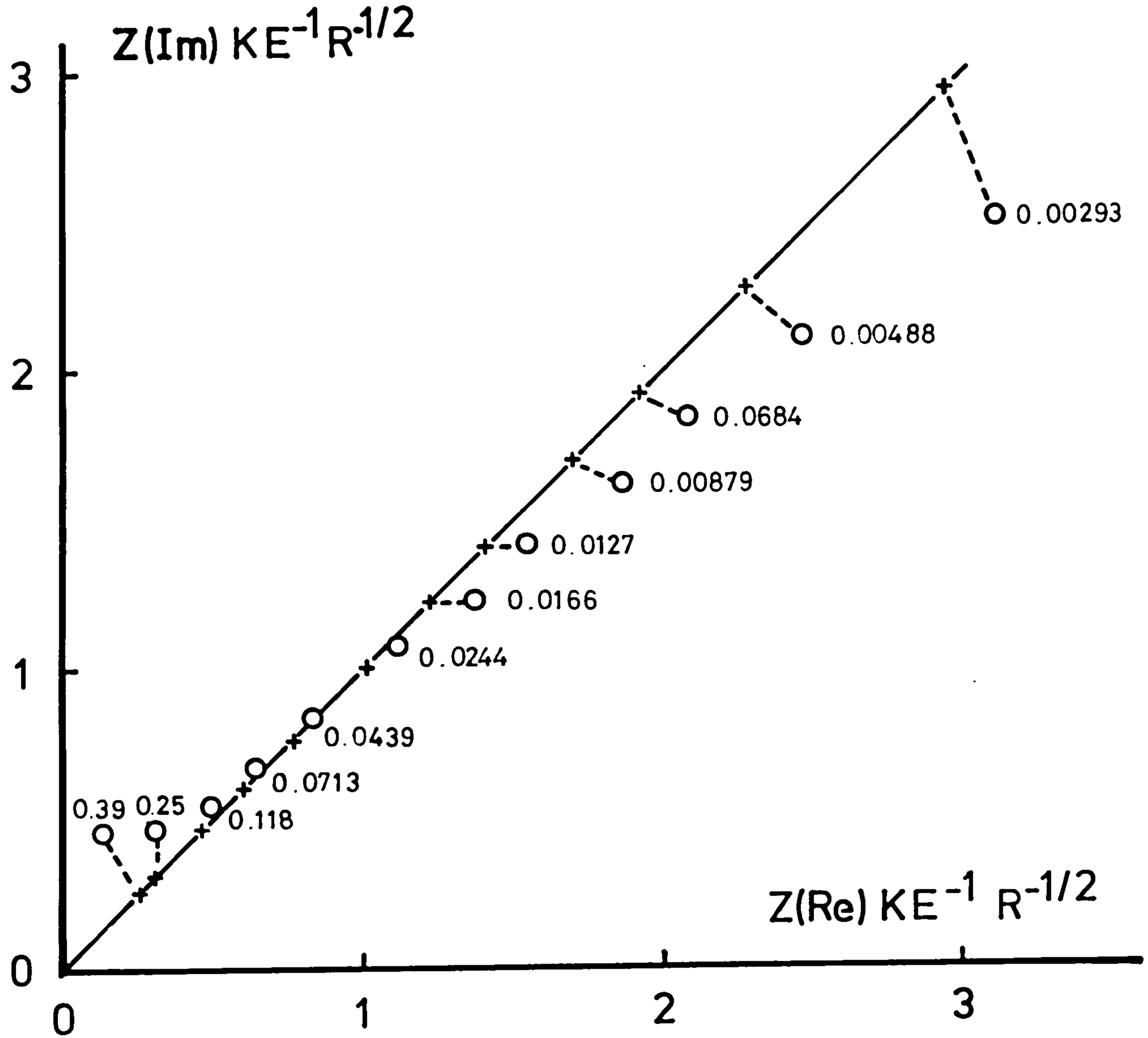
Z(Im) KE^{-1}R$^{-1/2}$
3
2
1
0
0
1
2
3
Z(Re) KE^{-1} R$^{-1/2}$
0.00293
0.00488
0.0684
0.00879
0.0127
0.0166
0.0244
0.0439
0.0713
0.118
0.39
0.25

Fig. E.4 Complex impedance plane plot in non-dimensional form. Test data generated by Eqs E.1 and E.2 with $R = 5 \times 10^{-7}$, $K = 1414$, $N_\tau = 512$ $N = 1024$, (O) Results from FFT software, Cx and Dx generated by CD FILE program (theoretical value). Figure on graph indicate fR values.

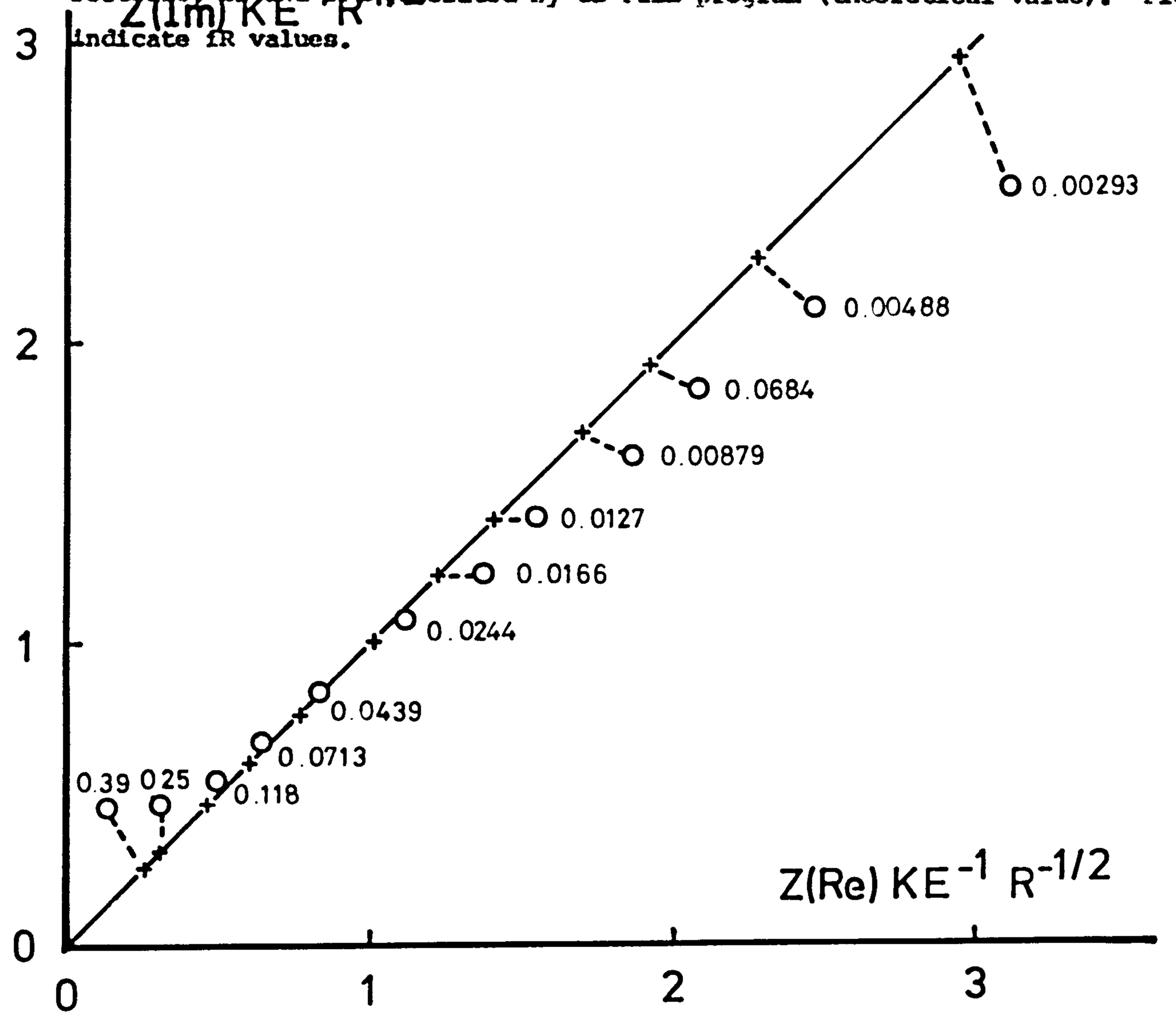

ACKNOWLEDGEMENTS

I am indebted to Dr. J.A. Harrison for his helpful advice and guidance throughout the course of my studies.

In addition I would like to thank my colleagues for many interesting discussions and direct help.

Finally I wish to express my gratitude to Conacyt (Mexico) for sponsoring this work.